BULETINUL INSTITUTULUI POLITEHNIC DIN IAŞI

F 1503/2
F F
8 000000 595171

EDITAT DE
UNIVERSITATEA TEHNICĂ „GH. ASACHI”, IAŞI

Tomul XLIII (XLVII)

Fasc. 1 - 2

Secţia II

CHIMIE şi INGINERIE CHIMICĂ

1997

BULETINUL INSTITUTULUI POLITEHNIC DIN IAŞI

ORSZÁGOS MŰSZAKI INFORMÁCIÓS KÖZPONT ÉS KÖNYVTÁR 1883

Tomul XLIII (XLVII)
Fasc. 1–2

Secţia II

CHIMIE şi INGINERIE CHIMICĂ

1997

EDITORIAL STAFF

Prof. Dr. Eng. **MIHAI GAFIŢANU** (President)
Prof. Dr. Eng. **VICTOR BULACOVSCHI** (Vice-President)
Prof. Dr. Eng. **LIVIU GROLL** (Vice-President)
Prof. Dr. Eng. **GHEORGHE ZET** (Secretary)
Prof. Dr. Doc. Eng. **ALFRED BRAIER** (Editor)
Prof. Dr. Eng. **HUGO ROSMAN** (Editor)
Prof. Dr. Eng. **MIHAIL VOICU** (Head of the Exchange Service)
Prof. Dr. Eng. **DIMITRIE ALEXA**
Prof. Dr. Eng. **ION BALASANIAN**
Prof. Dr. **AUREL BEJANCU**
Prof. Dr. Eng. **MIRCEA COZMÎNCĂ**
Prof. Dr. Eng. **SPIRIDON CREŢU**
Prof. Dr. Eng. **ION GIURMA**
Prof. Dr. Eng. **AURELIA GRIGORIU**
Prof. Dr. Eng. **CONSTANTIN PREDA**
Prof. Dr. Eng. **PAULICĂ RĂILEANU**

The **Bulletin of the Polytechnic Institute of Jassy** is edited by the **Technical University "Gh.Asachi"** (the former Polytechnic Institute), Jassy.

TEXredaction:
B. Grigoriu, A. Rotaru
Technical University of Jassy

BULETINUL INSTITUTULUI POLITEHNIC DIN IAŞI
BULLETIN OF THE POLYTECHNIC INSTITUTE OF JASSY
Tomul XLIII (XLVII), Fasc. 1-2 1997

Secţia II

CHIMIE ŞI INGINERIE CHIMICĂ

SUMAR

Pag.

IULIAN RUSU, ARIAN MAREŞ, ADRIAN CĂILEAN şi I. ROŞCA, Analiza datelor referitoare la stabilitatea termică relativă a unor polimeri utilizând o metodă de ierarhizare multicriterială (engl., rez. rom.) 7

DANIEL SUTIMAN, Influenţa concentraţiei apei asupra coroziunii oţelurilor nealiate în sistemul glicol–metanol (engl., rez. rom.) 15

GEORGETA MATZA, ŞT. IVĂŞCAN, LUCIAN GAVRILĂ şi EDUARD-EMIL IOJOIU, Unele corelaţii între structura oţelurilor şi comportarea lor la coroziune (engl., rez. rom.) 21

DOINA BEJAN şi ALINA BEJAN, Studiul pe calculator, în limbaj C, al unor factori ce influenţează solubilitatea precipitatelor (engl., rez. rom.) 27

AL. SZÉP, Utilizarea clorurii de amoniu, produs secundar al liniei de sodă modificate (engl., rez. rom.) 35

STELIAN PETRESCU şi ANA BĂCĂOANU, Transfer de masă la sublimare. Distribuţia presiunii parţiale în stratul limită de difuzie (engl., rez. rom.) 43

SAVEL IFRIM, Consideraţii asupra asociaţiilor moleculare prin legături de hidrogen (franc., rez. rom.) 53

DANIELA ŞUTEU, DOINA BÎLBĂ şi VALERIA-MARTA GORDUZA, Recuperarea coloranţilor reactivi din ape reziduale utilizând schimbători de ioni (engl., rez. rom.) 61

CRISTOFOR I. SIMIONESCU, AURELIA IOANID, GETA DAVID şi BOGDAN C. SIMIONESCU, Morfologia copolimerilor bloc cu secvenţe poli(N-acetiliminoetilenice)/polivinilice (engl., rez. rom.) 67

GH. ROZMARIN, GEORGETA CAZACU, AURELIA IOANID, GHIOCEL IOANID, C. TOMA, MIHAELA NIŢĂ, MARIUS-LIVIU CRAUS şi TH. MALUŢAN, Structura moleculară şi supermoleculară a celoligninei furfurolice de stejar (engl., rez. rom.) 77

CRISTOFOR I. SIMIONESCU, CARMEN TOPOR, GHIOCEL IOANID şi EUGEN NEAGU, Studii ESCA asupra dextranului modificat la suprafaţă (engl., rez. rom.) 91

Pag.

AUREL STANCIU, D. TIMPU, GH. STOICA şi VICTOR BULACOVSCHI, Studii privind sinteza poli(dimetilsiloxanilor) în prezenţa compuşilor cuaternari de amoniu (engl., rez. rom.) 101

DAN CAŞCAVAL, CORNELIU ONISCU, EUGEN HOROBA şi ADINA DUMITRAŞCU, Studiul separării compuşilor organici prin extracţie reactivă. IV. Modelarea matematică a procesului de separare a acidului glutamic din fază apoasă (engl., rez. rom.) 111

ABDELKRIM AZZOUZ, MOULOUD ATTOU şi MOHAMED-AMINE DIDI, Studiul spectroscopic al complecşilor bazaţi pe tributilfosfat. Efectul masei moleculei solvatate asupra legăturii P=O (engl., rez. rom.) 117

RADU VASILIU 123

GH. ROZMARIN 125

RECENZII 127

BULETINUL INSTITUTULUI POLITEHNIC DIN IAŞI
BULLETIN OF THE POLYTECHNIC INSTITUTE OF IASSY
Tome XLIII (XLVII), Fasc. 1–2 1997

Section II

CHEMISTRY and CHEMICAL ENGINEERING

CONTENTS

Pp.

IULIAN RUSU, ARIAN MAREŞ, ADRIAN CĂILEAN and I. ROŞCA, Analysis of Data concerning the Relative Thermal Stability of Some Polymers Using a Multicriterial Hierarchization Method (English, Romanian summary) 7

DANIEL SUTIMAN, The Water Influence on the Corrosive Process of Low Alloy Steels in the System Glycol–Methyl Alcohol (English, Romanian summary) 15

GEORGETA MATZA, ŞT. IVĂŞCAN, LUCIAN GAVRILĂ and EDUARD-EMIL IOJOIU, Some Correlations between Steels Structure and Corrosion Behaviour (English, Romanian summary) 21

DOINA BEJAN and ALINA BEJAN, Study on Computer, in C Language, of Some Factors Influencing the Solubility of Precipitates (English, Romanian summary) 27

AL. SZÉP, On Decomposition of Ammonium Chloride, By-product of Modified Soda Ash Manufacture, with Calcium Carbonate (English, Romanian summary) 35

STELIAN PETRESCU and ANA BĂCĂOANU, Mass Transfer at Sublimation. Partial Pressure Distribution in the Boundary Diffusion Layer (English, Romanian summary) 43

SAVEL IFRIM, Considérations sur les associations moléculaires par liaisons hydrogène (French, Romanian summary) 53

DANIELA ŞUTEU, DOINA BÎLBĂ and VALERIA-MARTA GORDUZA, Removeral of Reactive Dyes from Waste Waters Using Ion Exchangers (English, Romanian summary) 61

CRISTOFOR I. SIMIONESCU, AURELIA IOANID, GETA DAVID and BOGDAN C. SIMIONESCU, On the Morphology of Poly(N-Acetyliminoethylene)/Polyvinyl Block Copolymers (English, Romanian summary) 67

GH. ROZMARIN, GEORGETA CAZACU, AURELIA IOANID, GHIOCEL IOANID, C. TOMA, MIHAELA NIŢĂ, MARIUS-LIVIU CRAUS and TH. MALUŢAN, Molecular and Supermolecular Structure of Oak Furfural Lignocellulose (English, Romanian summary) 77

CRISTOFOR I. SIMIONESCU, CARMEN TOPOR, GHIOCEL IOANID and EUGEN NEAGU, ESCA Studies of Surface Modified Dextran (English, Romanian summary) 91

Pp.

AUREL STANCIU, D. TIMPU, GH. STOICA and VICTOR BULACOVSCHI, Studies Concerning the Synthesis of Poly(dimethylsiloxanes) in Presence of Quaternary Ammonium Compounds (English, Romanian summary) 101

DAN CAŞCAVAL, CORNELIU ONISCU, EUGEN HOROBA and ADINA DUMITRAŞCU, Study on Separation of Organic Compounds by Reactive Extraction. IV. Mathematical Modelling of the Separation Process of Glutamic Acid from Aqueous Phase (English, Romanian summary) 111

ABDELKRIM AZZOUZ, MOULOUD ATTOU and MOHAMED-AMINE DIDI, Spectroscopic Study of Complexes Based on Tributylphosphate. Effect of the Solvated Molecule Mass upon the P=O Bond (English, Romanian summary) 117

RADU VASILIU 123

GH. ROZMARIN 125

BOOK REVIEWS 127

BULETINUL INSTITUTULUI POLITEHNIC DIN IAŞI
Tomul XLIII (XLVII), Fasc. 1-2, 1997
Secţia II
CHIMIE şi INGINERIE CHIMICĂ

D.C. 541.11; 54-92

ANALYSIS OF DATA CONCERNING THE RELATIVE THERMAL STABILITY OF SOME POLYMERS USING A MULTICRITERIAL HIERARCHIZATION METHOD[1]

BY

IULIAN RUSU, ARIAN MAREŞ, ADRIAN CĂILEAN and I. ROŞCA

A way to analyse the relative thermal stabilities of some polymers, correlating two criteria of stability (the activation energy and the degradation temperature) is presented. In the first stage, the values of the reaction orders for all the studied samples are determined by means of Coats-Redfern method. With these values and with data from T and TG curves, the variations of the activation energy (E_a) and of the temperature vs. the reacted fraction (α) are determined by Levi-Reich kinetic analysis method. For a certain α value, the higher the temperature and the higher the value of E_a the higher the thermal stability of a polymer. To correlate the two criteria of stability, the ELECTRE method of multicriterial hierarchization was used on the entire studied field with a step chosen by the user. The final result is a qualitative ordering of the studied samples from the point of view of their thermal stabilities. The algorithm could be used only for those polymers (with or without additives) which respect the conditions imposed by Levi and Reich. An example of using the method for three samples of PVC suspension type (two of them containing inorganic additives) is also presented.

1. Introduction

It is known that the thermogravimetric method could be used to determine the relative thermal stabilities of polymers and copolymers which present, after degradation, changes in the sample weight. The method operates with criteria based on: a) the characteristic temperatures of the decomposing reactions; b) the weight losses; c) the kinetic parameters of the degrading process. According to the first criterion, one can compare the starting temperatures of the degrading reactions [1] or the temperatures which correspond to the maximum decomposition rate, read from the DTG curves [2]. From the point of view of the second criterion, could be compared the temperatures at which 25...50% from the amount of polymer was degraded [3], [4], the amounts of residue remained after degradation [5] or the TGA index [6]. Because the above mentioned stability criteria presented a low reproductibility, the use of the criteria based on the kinetic parameters of the degrading process were proposed. With this end in view, could be compared the values of the activation energy of the thermal degrading process estimated by means of different methods: Freeman–Carroll [7], Coats–Redfern [8], Zsako [9], Levi–Reich [10], etc. From our point of view the Levi–Reich kinetic analysis method has the advantage to determine values of the activation energy (E_a) for different values of the reacted fraction (α).

---

[1] Presented at the 14th Nordic Symposium on Thermal and Calorimetry, Oslo, Norway, June 15-17, 1994.

The aim of this paper is to present a way in which the relative thermal stabilities of polymers and also the stabilizing effect of some additives on polymers can be estimated. The analysis binds sets of data E_a vs. α (determined by means of Levi–Reich method) with sets of data temperature, T, vs. α (determined from TG and T curves).

2. Experimental

2.1. Materials

For the experimental part was used as polymer the PVC suspension type with $K = 70$, content of humidity and volatile substances of maximum 0.5%, supplied by SC OLTVIL SA (Râmnicu Vâlcea, Romania). High purity $CaCO_3$ (low in alkalies) supplied by Aldrich Chemical Company and dibasic lead phosphite ($2PbO.PbHPO_3.1/2H_2O$) supplied by SC CHIMOPAR SA (Bucharest, Romania) were used. The characteristics of the dibasic lead phosphite are presented below: a) content of $HPO_3 = 9.8...10.6\%$; b) content of $PbO = 83.8...90.1\%$; c) humidity = = maximum 0.2%.

Two mixtures were prepared combining PVC mechanically with 4% weight $CaCO_3$ (sample *2*) and 4% weight dibasic lead phosphite (sample *3*). All the samples, including the basic PVC (sample *1*), were thermal degraded.

2.2. Apparatus

The thermal analyses were performed on a MOM-Budapest derivatograph, with recording of the weight losses (TG), the derivative (DTG), the differential thermal analysis (DTA) and the temperature increases (T). The thermal curves were recorded in air at a heating rate of 10 K min^{-1}, up to 500°C. In order to obtain comparable data, the same sensitivies for TG (500 mV), DTA (1 mV), DTG (2.5 mV), T (500 mV) and a sample weight of 100 mg were used throughout.

3. Results and Discussion

The proposed way to analyse the relative thermal stabilities could be used for the polymers which respect the conditions imposed by Levi and Reich [10], namely:

1° Measurements should be made under the same conditions in all cases.

2° The TG curves should possess not more than one plateau after the degradation has commenced.

3° The TG curves should contain few, if any, irregularities.

4° The degraded material should have volatilized considerably over 50% at the final temperature.

In the first stage, for all the studied samples, should be determined by means of Coats-Redfern method the reaction orders requested by the calculation of the Levi-Reich method. Using the Levi-Reich method [10], [11] we obtain the sets of data E_a vs. α and from TG and T curves the sets of data T vs. α.

In the second stage, for all the studied samples, was followed up the determination of the maximum common interval of the reacted fractions for which exists experimentally determined values of the activation energy and of the temperature. To compare the thermal stabilities of the samples at a certain value of the reacted fraction, the sets of data E_a and T (in that point) are requested. This fact could be achieved by the interpolation of the experimental data (E_a vs. α and T vs. α) using the Cubic Spline method [12]. The entire field of α which was formerly determined is sampled with a certain step, imposed by the user, calculating equidistant values for E_a and T.

To classify the polymer samples (at a value of the reacted fraction) from the point of view of the relative thermal stabilities, a multicriterial hierarchization method is used. From flexibility grounds, the ELECTRE method [13] was used. This method could hierarchizate the studied samples using al least two criteria (in our case E_a and T). The final result is a qualitative ordering of the polymer samples from the thermal stability point of view.

The entire method was used to elaborate a computer programme written in PASCAL programmming language and tested on a HP Vectra 486/66N computer. The acquisition of the starting data could be made by the programme directly from the derivatograph by an RS232 or HPIB interface.

An example of using the method will be presented on the basis of the thermogravimetric data of the three samples mentioned above. Both additives are used on the processing of PVC: $CaCO_3$ as a filler and the dibasic lead phosphite as a thermal stabilizer.

In Figs. 1 and 2 are presented the variations α vs. T and, respectively, E_a vs. α for the studied samples.

For the three samples, the α common interval for which exists experimentally determined values of T and E_a is 0.01...0.48. The using way of the ELECTRE method will be presented for only one value of $\alpha = 0.1$.

We have three variants (three samples, $i = 3$) and two criteria (E_a and T, $j = 2$). With data obtained from the interpolation of experimental values we built the qualificatives matrix (a_{ij}). In the first column are the values of E_a (kJ mol^{-1}) and in the second the temperature values (°C):

$$(a_{ij}) = \begin{pmatrix} 238.68 & 245.1 \\ 333.74 & 251 \\ 218.7 & 256.5 \end{pmatrix}.$$

On the basis of these matrix we built the utilities matrix (u_{ij}) using the scale 0...1. The elements of the matrix are calculated with the relation:

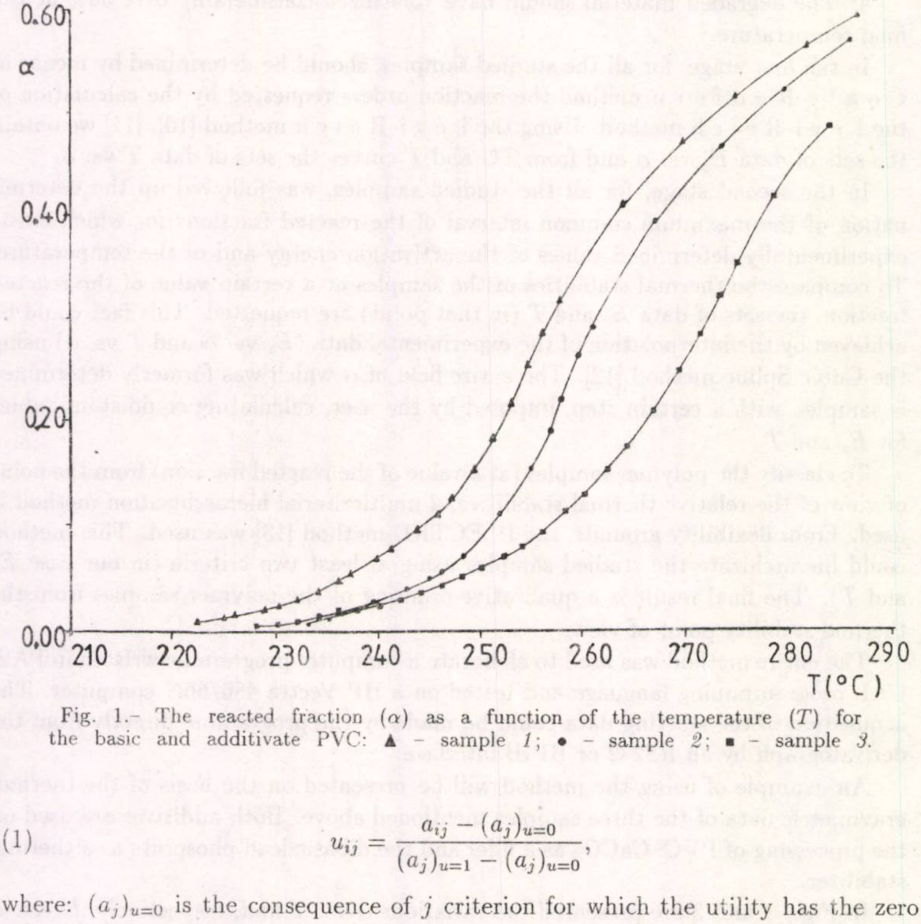

Fig. 1.– The reacted fraction (α) as a function of the temperature (T) for the basic and additivate PVC: ▲ – sample *1*; ● – sample *2*; ■ – sample *3*.

$$u_{ij} = \frac{a_{ij} - (a_j)_{u=0}}{(a_j)_{u=1} - (a_j)_{u=0}}, \tag{1}$$

where: $(a_j)_{u=0}$ is the consequence of j criterion for which the utility has the zero value; $(a_j)_{u=1}$ – the consequence of j criterion for which the utility has the value 1.

In our case $u = 1$ for the maximum value of E_a and T, $u = 0$ for the minimum value of E_a and T and consequently

$$(u_{ij}) = \begin{pmatrix} 0.174 & 0 \\ 1 & 0.518 \\ 0 & 1 \end{pmatrix}.$$

Every criterion receives an importance coefficient calculated with the relation:

$$K_j = \frac{\sum\limits_{i=1}^{m} n_{ij}}{\sum\limits_{i=1}^{m}\sum\limits_{j=1}^{n} n_{ij}}, \tag{2}$$

where n is the number of criteria, m – the number of specialists, n_{ij} – the mark granted by the i specialist for the j criterion. As it can be seen, $K_j \in [0,1]$. In

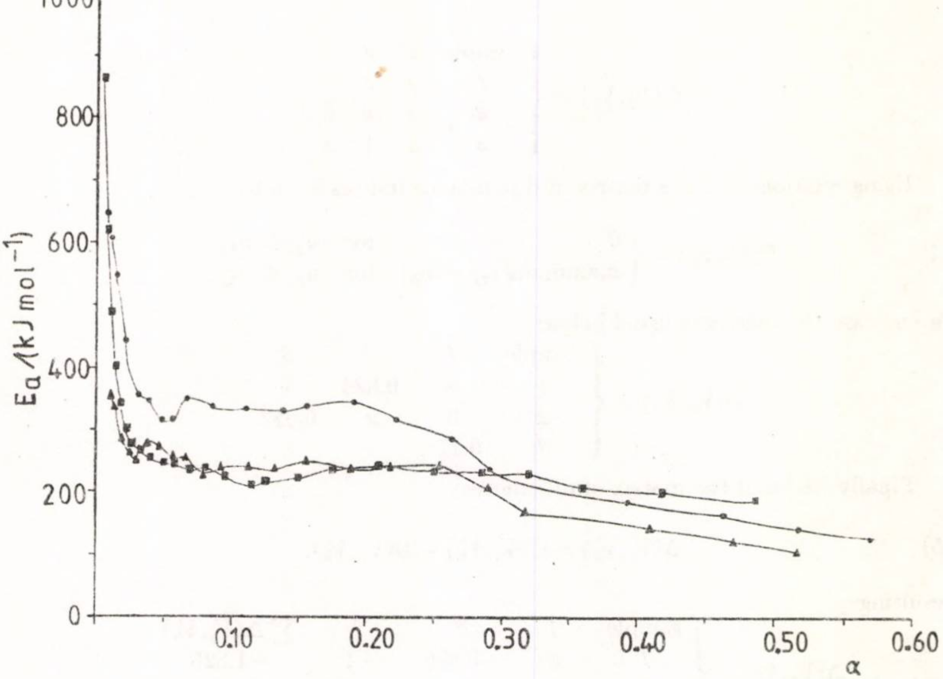

Fig. 2.- Activation energy (E_a) as a function of the reacted fraction (α) for the basic and additivate PVC: ▲ - sample *1*; ● - sample *2*; ■ - sample *3*.

literature exist many studies which can estimate the thermal stability of polymers only on the basis of the activation energy, but from the industrial point of view it does matter the temperature field in which the polymer could be processed without degradation. However, if the degradation has started, the initial temperature must be highest possible and the process rate must be very low. On these grounds the T criterion must have a much higher coefficient of importance than the E_a criterion. We propose $K_{Ea} = 0$ and $K_T = 1$.

The next step is to make up the matrix of the concordance indices, between the variants, using the relation:

$$C(V_g, V_h) = \frac{\sum\limits_j K_j}{\sum\limits_{j=1}^{n} K_j}, \tag{3}$$

where $C(V_g, V_h)$ is the index of concordance between the V_g and V_h variants. The sum $\sum\limits_j K_j$ is effected only for $u_{gj} \geq u_{hj}$ and the sum $\sum\limits_{j=1}^{n} K_j = K_{E_a} + K_T = 1$. In the studied case it results that

$$C(V_g, V_h) = \left\{\begin{array}{cccc} \text{sample} & \mathit{1} & \mathit{2} & \mathit{3} \\ \mathit{1} & x & 0 & 0 \\ \mathit{2} & 1 & x & 0 \\ \mathit{3} & 1 & 1 & x \end{array}\right. .$$

Using relations (4), the matrix of discordance indices is built:

$$D(V_g, V_h) = \begin{cases} 0 & \text{for} \quad u_{gj} > u_{hj}, \\ \text{maximum}|u_{gj} - u_{hj}| & \text{for} \quad u_{gj} \leq u_{hj}. \end{cases} \tag{4}$$

In our case the matrix is listed below:

$$D(V_g, V_h) = \left\{\begin{array}{cccc} \text{sample} & \mathit{1} & \mathit{2} & \mathit{3} \\ \mathit{1} & x & 0.826 & 1 \\ \mathit{2} & 0 & x & 0.482 \\ \mathit{3} & 0.174 & 1 & x \end{array}\right. .$$

Finally we build the matrix of differences:

$$\Delta(V_g, V_h) = C(V_g, V_h) - D(V_g, V_h), \tag{5}$$

resulting

$$\Delta(V_g, V_h) = \left\{\begin{array}{ccccc} \text{sample} & \mathit{1} & \mathit{2} & \mathit{3} & \sum \Delta(V_g, V_h) \\ \mathit{1} & x & -0.826 & -1 & -1.826 \\ \mathit{2} & 1 & x & -0.482 & 0.518 \\ \mathit{3} & 0.826 & 0 & x & 0.826 \end{array}\right. .$$

The thermal stability order is given by the increasing order of the values $\sum \Delta(V_g, V_h)$:

sample *3* > sample *2* > sample *1*.

As shown in Fig.1, for $\alpha < 2\%$, the most stable sample from the point of view of the T criterion is that one which contained $CaCO_3$, i.e. the degradation process occurred at higher temperatures (233°...238°C). For $\alpha > 2\%$, sample *3* became the most stable. However, both additives induced a stabilizing effect on PVC.

As it can be observed from Fig. 2, for $\alpha < 28\%$, sample *1* and *3* had similar behaviours ($E_a \sim 230$ kJ mol^{-1}); sample *2* had a higher value of the activation energy ($E_a \sim 340$ kJ mol^{-1}). For a higher value of the reacted fraction, sample *3* became the most stable from the point of view of E_a criterion.

The entire calculus was performed on computer, the sampling step of the reacted fraction field being of 0.01. The results are listed below.

$$\alpha = \begin{cases} 0.01...0.02 & \text{sample } \mathit{2} > \text{sample } \mathit{3} > \text{sample } \mathit{1}, \\ 0.03 & \text{sample } \mathit{3} > \text{sample } \mathit{2} > \text{sample } \mathit{1}, \\ 0.04...0.05 & \text{sample } \mathit{2} > \text{sample } \mathit{3} > \text{sample } \mathit{1}, \\ 0.06...0.48 & \text{sample } \mathit{3} > \text{sample } \mathit{2} > \text{sample } \mathit{1}. \end{cases}$$

From the above presented classification it could be observed that the dibasic lead phosphite had a larger action area as thermal stabilizer than the calcium carbonate. In all the cases samples *2* and *3* are more stable than the basic PVC (sample *1*).

4. Conclusions

The described way to analyse the data concerning the relative thermal stabilities of polymers using a multicriterial hierarchization method presents the next characteristics:

1° Could be compared from the thermal stability point of view only the polymers which are respecting the conditions imposed by the Levi–Reich method.

2° The method could supply a qualitative efficiency estimation for thermal stabilizers.

3° The method could operate with two or more criteria of thermal stability.

4° Both the values of the importance coefficients and the sampling step of the data could be chosen by the user, depending on circumstances.

5° By the computer data gathering and processing, the method supply the results in a short time.

Acknowledgements. The authors would like to thank Professor Natalia Hurduc, Professor Monica Voicu and Assistant Liviu Prună for the extremely useful discussions concerning the present paper. The authors would also like to thank the RADIX SRL, Iaşi, company (Hewlett Packard authorised dealer) for the technical support granted during the work.

Received, March 19, 1996

Technical University "Gh. Asachi", Jassy,
Department of Inorganic Chemistry
and
Department of Chemical Engineering

REFERENCES

1. Sazanov Y.N., Skvortsevich E.P., Milovskaia E.B., J. Therm. Anal., **6**, 53 (1974).
2. Vogl O., Ivansons I., Miller H.C., Williams H.W., J. Macromol. Sci., **A-2**, 175 (1968).
3. Korshak V.V., Vinogradova S.V., Danilov G.V., Beribze L.A., Salazkin S.N., Vysokomol. Soedin., **12**, 129 (1970).
4. Berlin A.A., Guerasimov B.G., Ivanov A.A., J. Polym. Sci., Part C, **40**, 183 (1973).
5. Vasile C., Călugăru E.M., Stoleriu A., Sabliovschi M., Mihai E., *Comportarea termică a polimerilor.* Ed. Acad., Bucureşti, 1980, 169.
6. Gedemer T.J., J. Macromol. Sci. Chem., Part A, **8**, 95 (1974).
7. Freeman E.S., Carroll B., J. Phys. Chem., **62**, 394 (1958).
8. Coats A.W., Redfern J.T., Nature (London), *201*, 68 (1964).
9. Zsako S., J. Phys. Chem., **66**, 1041 (1969).
10. Reich L., Levi D.W., Makromol. Chem., **66**, 102 (1963).
11. Segal E., Fătu D., *Introducere în cinetica proceselor neizoterme.* Ed. Acad., Bucureşti, 1983, 147.
12. Press W.H., Flannery B.P., Teukolsky S.A., Vetterling W.T., *Numerical Recipes. The Art of Scientific Computing.* Cambridge University Press, Cambridge, 1986, 115.
13. Andrasiu M., Baciu A., Pascu A., Puşcaş E., Tasnadi A., *Metode de decizii multicriteriale.* Ed. Tehnică, Bucureşti, 1986, 49.

ANALIZA DATELOR REFERITOARE LA STABILITATEA TERMICĂ RELATIVĂ A UNOR POLIMERI UTILIZÂND O METODĂ DE IERARHIZARE MULTICRITERIALĂ

(Rezumat)

Se prezintă o cale de a analiza stabilităţile termice relative a unor polimeri corelând două criterii de stabilitate (energia de activare şi temperatura de descompunere). În prima etapă sunt determinate cu ajutorul metodei Coats–Redfern valorile ordinelor de reacţie ale probelor studiate. Cu aceste valori şi cu datele din curbele T şi TG se determină prin intermediul metodei Levi-Reich variaţia energiei de activare (E_a) şi a temperaturii funcţie de conversie (α). Pentru o anumită valoare a lui α proba este cu atât mai stabilă cu cât temperatura şi E_a au valori mai mari. Pentru a corela cele două criterii de stabilitate pe întreg domeniul studiat s-a folosit metoda ELECTRE de ierarhizare multicriterială cu un pas impus de utilizator. Rezultatul final rezultă a fi o ordonare calitativă a probelor studiate din punctul de vedere al stabilităţii lor termice. Algoritmul poate fi folosit doar pentru acele materiale care respectă condiţiile impuse de metoda Levi–Reich. Se prezintă şi un exemplu de folosire a metodei pentru trei probe de PVC tip suspensie (două dintre ele conţinând aditivi anorganici folosiţi în prelucrarea polimerului: $CaCO_3$ şi fosfit dibazic de plumb).

BULETINUL INSTITUTULUI POLITEHNIC DIN IAŞI
Tomul XLIII (XLVII), Fasc. 1–2, 1997
Secţia II
CHIMIE şi INGINERIE CHIMICĂ

D.C. 620.193; 547.422.22

THE WATER INFLUENCE ON THE CORROSIVE PROCESS OF LOW ALLOY STEELS IN THE SYSTEM GLYCOL–METHYL ALCOHOL

BY
DANIEL SUTIMAN

The paper presents a study regarding the corrosion in anhydrous solvents as methyl–alcohol and glycol and the influence of water concentration for the corrosion.

The steels used in determinations are OL 37, OL 50 and OL 60. The corrosion products were analysed by X-ray and Mössbauer spectroscopy and a corrosion mechanism for the aggressive attack in pure glycol and glycol+water solution is proposed.

1. Introduction

The corrosion of steels in non-aqueous liquids achieved a special importance because the industrial development, being well known the corrosion of carbon-steels in liquid ammonia, the corrosion of stainless steels in anhydrous ammonia or the pitting corrosion of the same steels in dimethylformamide.

In non-aqueous solutions the water availability is very low as a consequence of both the low water bulk concentration, sometimes water being considered as an impurity, and the competitive adsorption process between water and the solvent molecules. It is well known that water, more than oxyanions such as SO_4^{-2}, CH_3COO^-, $HCOO^-$, or even the dissolved molecular oxygen, is the most effective source of oxygen and hydroxyl groups for the nucleation and growth of the acid–base passive films [1].

Beside the influence of the water content, there are other parameters which have an effect on the corrosion process, such as: chloride ions concentration, the acidity or the temperature [2],...,[9]. These parameters are dependent one another, and the water critical concentration for achieving the passive film depends on the presence of the aggressive ions.

The literature presents studies regarding the low alloy steels behaviour in methyl–alcohol solutions of sulphuric acid [10], [11], the influence of water on low alloy steels corrosion in anhydrous systems methyl–alcohol–sulphuric acid [12],...,[17] and also the corrosion process in anhydrous and aqueous systems of methyl–alcohol–halide ions [17],...,[22].

In the present paper, the corrosion of low alloy steels OL 37, OL 50 and OL 60 in anhydrous system methyl–alcohol–glycol and also the influence of water on the corrosion of these steels in methyl–alcohol and glycol are studied. The paper primarily presents the way to determine the content of the solvent or water, requested to achieve the passive film. This fact presents a highly industrial importance especially on the recovering process of the glycol in the synthetic fibres industry.

2. Experimental Part

For experiments, metallic samples with a surface of 5 cm^2 were used. Before introducing in the corrosive medium, the samples were polished with fine abrasive paper, then they were introduced into a 3% hydrochloric acid solution for 30 min., and after that introduced in boiling benzene for 15 min. The composition of steels which were corroded is presented in Table 1.

Table 1
The Composition of Steels Used in the Corrosion Process

%	C	Mn	Si	P	S
OL 37	0.20	0.8	0.4	0.06	0.06
OL 50	0.30	0.8	0.4	0.05	0.05
OL 60	0.40	0.8	0.4	0.05	0.05

The corrosive solutions were prepared from substances with highly analytical purity (merck) and bidistillated water with a conductivity of 12 μS/cm and which had no chloride ions. The solutions water content was established with the Karl–Fisher method.

For the same composition of the corrosive solution, six metallic samples from same steel were used. The samples were taken off the corrosion solution after 10, 20 days a.s.o., then introduced for 15 sec. in a solution of hydrochloric acid 3% and dryed for 10 min. at 120°C in nitrogen atmosphere. The metallic samples were entirely introduced in the solution, without direct contact with the oxygen from the air but the solutions was stirred every day.

The weight losses determined with the analytical balance were processed to penetration indices P, [mm/m^2 year], and gravimetric indices K, [mg/dm^2 day], fact that pointed out more clearly the corrosion rate variations or the formation of the passive layer.

In order to analyse the passive layer formed on the surface of the samples, the following methods were used: chemical analysis, X-ray and Mössbauer spectroscopy and also IR-spectroscopy for the solutions study.

The obtained data are presented in Tables 2,...,7.

Table 2
The Values of the P and K Indices for the Methyl–Alcohol–Water System

Solution	OL 37	OL 50	OL 60
	P/K	P/K	P/K
Methyl–alcohol	0.03/6.33	0.022/4.3	0.019/2.17
H_2O 1%	0.042/7.11	0.037/5.8	0.023/3.45
H_2O 2%	0.057/8.36	0.048/7.67	0.03/5.1
H_2O 3%	0.063/10.1	0.053/8.0	0.037/6.82
H_2O 4%	0.041/7.0	0.035/6.9	0.028/4.92
H_2O 5%	0.027/5.86	0.023/5.33	0.024/3.15

Table 3

The Values of the P and K Indices for the Glycol–Water System

Solution	OL 37 P/K	OL 50 P/K	OL 60 P/K
Glycol	0.015/3.40	0.007/0.8	0.005/0.71
H_2O 1%	0.016/3.75	0.008/0.9	0.005/0.71
H_2O 2%	0.017/4.1	0.008/0.09	0.006/0.081
H_2O 3%	0.22/5.82	0.01/0.1	0.009/0.1
H_2O 4%	0.031/6.12	0.02/0.8	0.027/0.89
H_2O 5%	0.047/8.15	0.033/1.15	0.027/0.89

Table 4

The Values of the P and K Indices for the Solutions of Methyl–Alcohol in Glycol

Solution glycol +	OL 37 P/K	OL 50 P/K	OL 60 P/K
Methyl–alcohol 5%	0.303/3.58	0.287/3.03	0.243/2.47
Methyl–alcohol 10%	0.224/2.73	0.19/2.03	0.157/1.56
Methyl–alcohol 15%	0.173/2.12	0.148/1.58	0.101/0.98

Table 5

The Values of the P and K Indices for the Solutions of Glycol in Methyl–Alcohol

Solution Methyl–alcohol +	OL 37 P/K	OL 50 P/K	OL 60 P/K
Glycol 5%	0.04/6.8	0.03/6.3	0.027/5.9
Glycol 10%	0.06/8.11	0.05/7.6	0.037/5.9
Glycol 15%	0.09/10.5	0.08/9.7	0.05/7.5

Table 6

The Values of the P and K Indices for the Solutions of 5% Methyl–Alcohol in Glycol in the Presence of Water

Glycol + methyl–alcohol 5%	OL 37 P/K	OL 50 P/K	OL 60 P/K
H_2O 1%	0.02/4.12	0.015/3.1	0.012/2.7
H_2O 2%	0.032/5.1	0.022/4.2	0.012/2.7
H_2O 3%	0.041/6.0	0.028/4.9	0.027/4.5
H_2O 4%	0.06/7.1	0.034/5.3	0.033/5.2
H_2O 5%	0.09/8.9	0.041/6.2	0.037/5.8

Table 7

The Values of the P and K Indices for the Solutions of 5% Glycol in Methyl–Alcohol in the Presence of Water

Methyl–alcohol + glycol 5%	OL 37 P/K	OL 50 P/K	OL 60 P/K
H_2O 1%	0.035/7.1	0.03/6.3	0.025/5.6
H_2O 2%	0.05/9.7	0.043/8.3	0.032/6.8
H_2O 3%	0.07/11.1	0.06/10.1	0.05/9.7
H_2O 4%	0.06/10.1	0.04/8.0	0.037/7.3
H_2O 5%	0.047/8.6	0.032/6.8	0.029/6.2

3. Results and Discussion

From the presented data one can observe that all steels are corroded even in anhydrous system, and comparing the two solvents we concluded that the methyl–alcohol is more corrosive than the glycol.

On the other hand the curves that indicate the weight losses are different; a linear curve for methyl–alcohol and a "S" shaped curve for glycol were registered (a slow increasing of the corrosion rate in the first 20 days, followed by a suddenly increasing in the next 30 days and then another slow increasing for the last days). The losses weight variation for OL 37 in pure methyl–alcohol and glycol is shown in Fig.1.

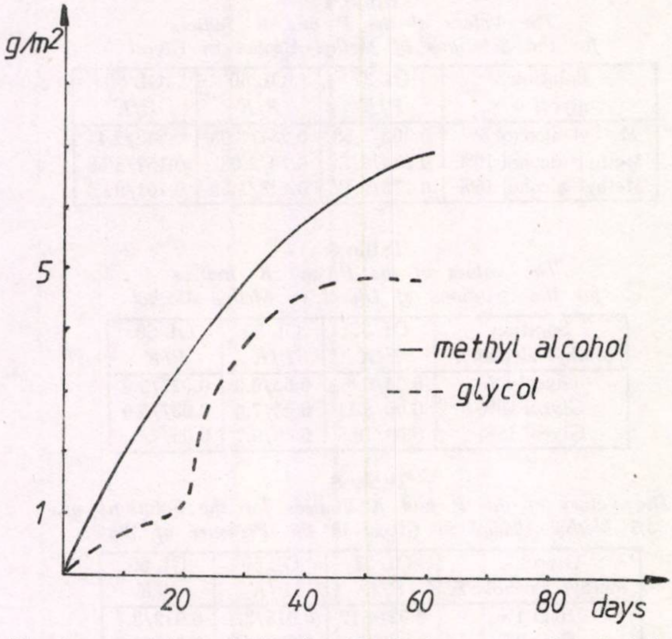

Fig. 1.– The losses weight variation for OL 37 in pure methyl–alcohol and glycol.

In anhydrous solvent system, the corrosion rate was higher for the solutions of methyl–alcohol in glycol than the solutions of glycol in methyl–alcohol. The curves that indicate the losses of weight are similar to those obtained in pure solvents.

Analysing the corrosion process in the presence of water in methyl–alcohol solutions, a decreasing of the corrosion rate for a water concentration higher than 3% was observed. We can presume that at higher concentration than 3% of water in methyl–alcohol solutions, a protection layer was formed, that stoped the further corrosion of the metal.

In glycol solutions, in the presence of water, the corrosion rate was negligible up to a concentration of 2% water. After that concentration, the corrosion rate constantly increased so that in this solvent a protection layer was not formed to stop the further corrosion.

Analysing the corrosion compounds from the system containing methyl–alcohol we conclude that the corrosion final product was Fe_3O_4 when corrosion process took place in pure methyl–alcohol, and a mixture of oxide and iron hydroxide when the corrosion process took place in the presence of water. So, the corrosion process were used with loccured the intrusion of the oxygen fron the air when pure solvent were used and both by the oxygen and the HO^- groups action in the solutions of solvents containing water.

In the system containing glycol, the corrosion final product was yellow and had the following chemical composition: Fe=24%; C=26.5%; H=5%; O=44.5%.

Studying the X-ray and Mössbauer spectra a double surronding of iron was presumed, meaning that the corrosion compound is a mixture of iron complex compounds with the coordination number 6 and 8, which are soluble in glycol [22]. From these data for the corrosion process in glycol, the following mechanism was assigned:

$$2Fe + O_2 + 2C_2H_6O_2 \longrightarrow [Fe(OH)_2(C_2H_5O_2)_2]H_2$$
$$2Fe + O_2 + 3C_2H_6O_2 \longrightarrow [Fe(OH)_2(C_2H_5O_2)_3]H_4$$

or

$$2Fe + O_2 + 2H_2O \longrightarrow 2Fe(OH)_2$$
$$Fe(OH)_2 + 2C_2H_6O_2 \longrightarrow [Fe(OH)_2(C_2H_5O_2)_2]H_2$$
$$Fe(OH)_2 + 3C_2H_6O_2 \longrightarrow [Fe(OH)_2(C_2H_5O_2)_3]H_4$$

This mechanism is also explained by a decreasing of pH-values in the corrosive solutions that contained glycol.

Analysing the composition of the steels, we conclude that the corrosion rate decreases with the increasing of the carbon content from the steel, fact that leads to the certain cast iron use of prevent the corrosion process.

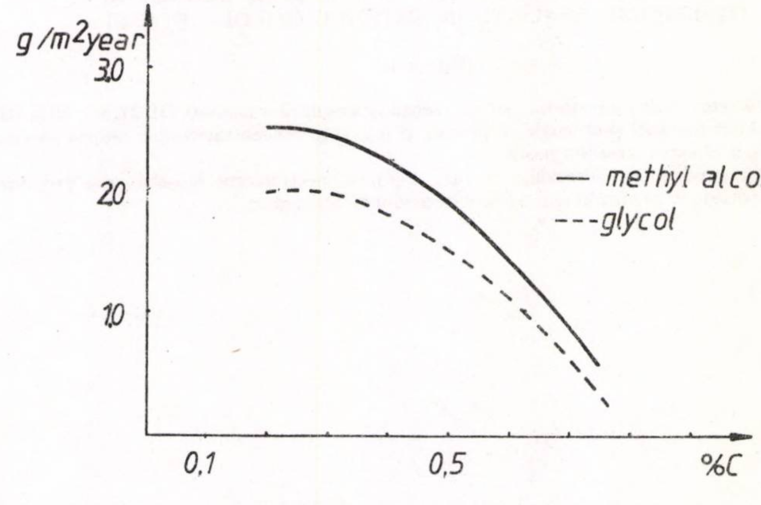

Fig. 2.- The losses weight variation depending on steel carbon concentration.

The losses weight variation depending on steel carbon concentration is shown in Fig.2.

Received, March 22, 1996

Technical University "Gh.Asachi", Jassy,
Department of Inorganic Chemistry

REFERENCES

1. Bellucci F., Caprobianco G., Corrosion Science, **4**, *28*, 371 (1988).
2. Towers O.L., Met. Construct., 479 (1984).
3. Wilde B.E., Corrosion, **37**, 131 (1981).
4. Wilde B.E., Corrosion, **38**, 168 (1982).
5. Deegan D.C., Wilde B.E., Corrosion, **32**, 139 (1976).
6. Farina C.A., Faita G., Corros. Sci., **18**, 465 (1978).
7. Farina C.A., Bazzoni B., Corros. Sci., **20**, 1101 (1980).
8. Bellucci F., Farina C.A., Mater. Chem., **5**, 185 (1980).
9. Bellucci F., Faita G., Oliviani F., J. Appl. Electrochem., **11**, 781 (1981).
10. Banas J., Electrochem. Acta, **6**, *32*, 871 (1987).
11. Banas J., Metalurgia i Oblew., **1**, *16* (1990).
12. Schwarbe K., Herman S., Proc. 4-th Int. Symp. Passivity, New Jersey, 1977, 413.
13. Eisner B., Proc. 5-th Int. Symp. Passivity, Bombones, Frances, 1979, 555.
14. Heitz E., *Advanced in Corrosion Science and Technology*. Ed. M.G. Fontana, **IV**, 1984, 149.
15. Banas J., Heitz E., J. Electrochem. Soc., **2**, *133*, 253 (1986).
16. Bellucci F., Faita G., J. Appl. Electrochem., **11**, 781 (1981).
17. Maza F., Proc. 9-th Int. Symp. Metallic Corrosion, Toronto, 1984, 102.
18. Masfeld F., J. Electrochem. Soc., *120*, 188 (1973).
19. Okamoto G., Proc. 5-th Int. Symp. Metallic Corrosion, Tokyo, 1972.
20. Banas J., Z. Phys. Chem., *262*, 1105 (1981).
21. Bellucci F., Venti P., Br. Corros. J., **2**, *25*, 133 (1990).
22. Drăgulescu C., Petrovici E., *Chimia structurală modernă*. Ed. Academiei, Bucureşti, 1977.

INFLUENŢA CONCENTRAŢIEI APEI ASUPRA COROZIUNII OŢELURILOR NEALIATE ÎN SISTEMUL GLICOL-METANOL

(Rezumat)

Se prezintă rezultatele unui studiu privind coroziunea oţelurilor nealiate OL 37, OL 50 şi OL 60 în solvenţi anhidri metanol şi etilenglicol, precum şi influenţa concentraţiei apei asupra procesului de coroziune şi realizarea stratului pasiv.

Prin analiza produşilor de coroziune cu raze X şi prin spectroscopie Mössbauer se propune un mecanism de coroziune pentru atacul agresiv în mediu de etilenglicol.

BULETINUL INSTITUTULUI POLITEHNIC DIN IAŞI
Tomul XLIII (XLVII), Fasc. 1-2, 1997
Secţia II
CHIMIE şi INGINERIE CHIMICĂ

D.C. 620.193; 669.14.018.7

SOME CORRELATIONS BETWEEN STEELS STRUCTURE AND CORROSION BEHAVIOUR

BY

GEORGETA MATZA, ŞT. IVĂŞCAN,
LUCIAN GAVRILĂ and EDUARD-EMIL IOJOIU

Stainless steel structure mainly depends on its chemical composition, especially on the content of alphageneous (Cr, Mo, W, Si, Ti, Al, Be, Nb) and gammageneous (Ni, Mn, Co, Cu, N, C) alloying elements.

The paper presents the correlations between parameters such as chemical composition and δ ferrite content of an austenitic stainless steel AISI 316L used in urea plants and the corrosion resistance of the upmentioned steel. Based on the theoretical considerations is shown that the choosed steel has an austenitic structure and it assumes to be resistant to intergranular and general corrosion. The assumption was confirmed by metallographic analysis, chemical tests for intergranular corrosion resistance and ultrasonic thickness measurements for general corrosion resistance. It has been shown that the tested steel has a good behaviour in corrosive ammonium carbamate-urea at elevated pressures and temperatures environments, being resistant both to intergranular corrosion and general corrosive attack.

1. Introduction

The structure of stainless steels mainly depends on the participation of alphageneous alloying elements: Cr, Mo, W, Si, Ti, Al, Be, Nb and of gammageneous alloying elements: Ni, Mn, Co, Cu, N, C.

In fact, the stainless steels structure is affected by the ratio between the chromium equivalent and the nickel equivalent, ratio oftenly called as "ferrite factor":

$$F = \frac{E_{\mathrm{Cr}}}{E_{\mathrm{Ni}}}. \tag{1}$$

The chromium and nickel equivalents are expressed according to equations:

$$E_{\mathrm{Cr}} = \%\mathrm{Cr} + \%\mathrm{Mo} + 1.5 \times \%\mathrm{Si} + 0.5 \times \%\mathrm{Nb}, \tag{2}$$

$$E_{\mathrm{Ni}} = \%\mathrm{Ni} + 30 \times \%\mathrm{C} + 0.5 \times \%\mathrm{Mn}. \tag{3}$$

For austenitic structures is necessary that the ferrite factor to have low values, meanwhile ferritic, austenitic-ferritic and martensitic-ferritic structures require high values for the ferrite factor [1].

Austenitic stainless steels are mainly sensitive to intergranular corrosion. To emphasize the influence of steels structure on corrosion susceptibility, an austenitic stainless steel AISI 316L (UNS S31603) produced by SANDVIK AB (Sweden) used as lining material for the urea synthesis reactor in a Stripping–Stamicarbon urea plant was studied.

2. Experimental

The urea synthesis reactor is a cylindrical vertical vessel, with a height of 25 m and an inner diameter of 2.87 m. It is designed to work up to 458 K and 15.9 MPa. The reactor is lined inside with AISI 316L stainless steel, with the chemical composition as shown in Table 1.

Table 1

Chemical Composition of AISI 316L (UNS S31603) Stainless Steel

Component	C	Mn	Ni	Cr	Mo	Si	P	S
Mass, [%]	0.02	1.67	13.14	17.16	2.24	0.34	0.016	0.007

The urea synthesis reactor consists on two semispherical bottoms (upper and lower respectively), ten cylindrical rings plated with AISI 316L rolled sheets and ten circular perforated plates made also in AISI 316L. Plate no.1 and sheet no.1 are placed at the bottom of the cylindrical body of the reactor. Through the reactor flows a mixture containing urea, ammonium carbamate, ammonia, carbon dioxide and water, at elevated pressures and temperatures.

According to the equations (1),...,(3), the ferrite factor of the AISI 316L stainless steel is:

$$F = 1.36.$$

This value indicates an austenitic structure for the steel [1]. For more accuracy, the metallographic analyse of the steel has been performed. Fig. 1 presents the micrography of the steel, that is obviously austenitic.

In order to estimate the susceptibility of this type of steel to intergranular corrosion, a chemical testing method – the Huey test [2], [3] – has been performed. This test was accepted as intergranular corrosion susceptibility testing method both by the steel producer – SANDVIK AB (Sweden), and by the urea technology licensor – STAMICARBON BV (The Netherlands).

According to Huey test, stainless steel samples previously weighted are boiled for 240 h in 65% nitric acid solution. After each boiling cycle of 48 h, the samples are weighted and the penetration index, expressed in $\mu/48$ h, is calculated. Stamicarbon specifications allow a maximum penetration index of 3.3 $\mu/48$ h; below this value the tested steel is proofed to intergranular corrosion [4]. Fig. 2 presents the results of the Huey test performed on AISI 316L samples. As it can be seen, the tested steel is proofed to intergranular corrosion.

After the Huey test, samples were metallographic examined, in order to discover possible crackings appeared after nitric boiling. No visible modifications of the structure have been reported.

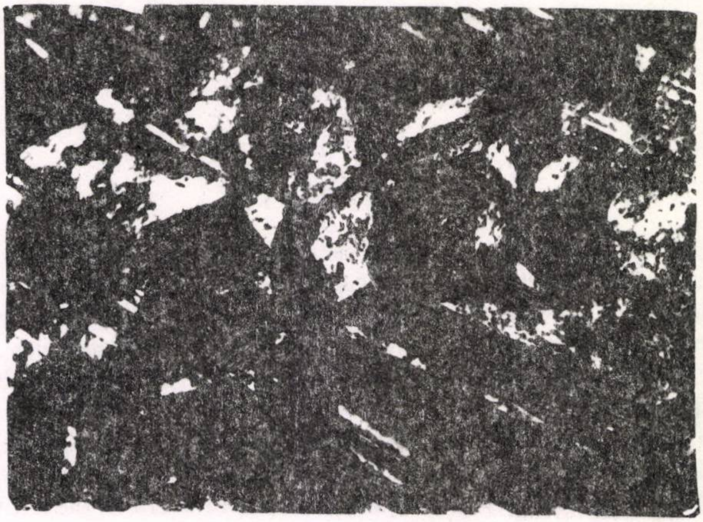

Fig. 1.– Austenitic stainless steel AISI 316L microstructure (magnitude: 220×; tackling agent: aqua regia; attack time: 10 sec.).

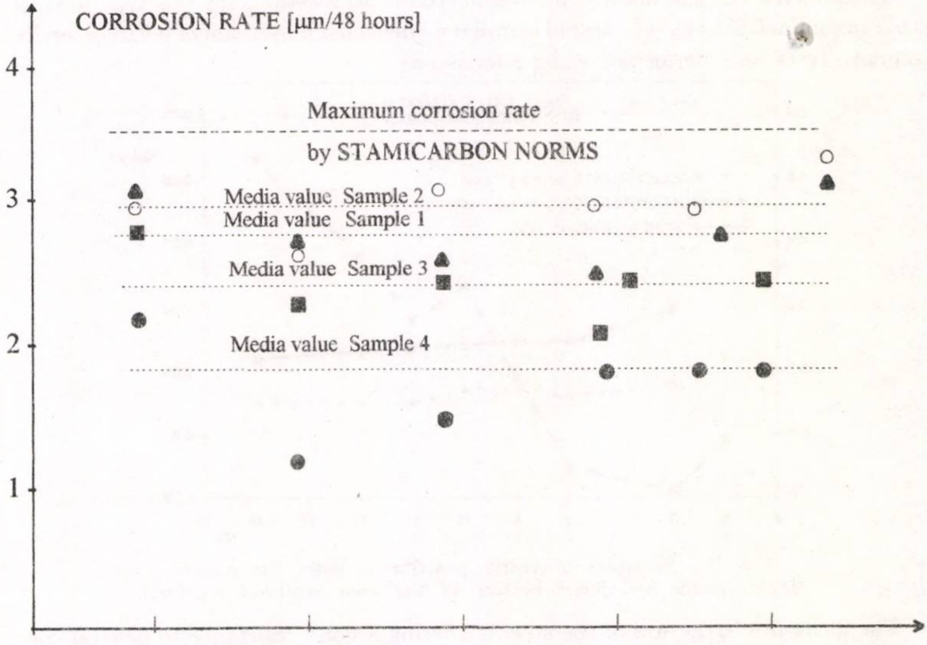

Fig. 2.– Corrosion rates – according to Huey test – for AISI 316L stainless steel samples.

A steel is not susceptible to intergranular corrosion if the condition given through equation

$$\%\mathrm{Cr} - 80 \times \%\mathrm{C} \leq 16.8 \tag{4}$$

is fulfilled [1]. For the tested steel relation (4) becomes:

$$\%\mathrm{Cr} - 80 \times \%\mathrm{C} = 15.56$$

and obviously, we may assume that it is resistant to intergranular corrosion.

An essential factor for the corrosion behaviour of austenitic stainless steels is the δ ferrite content. It has been proved that amounts of 5...20% of δ ferrite in steel structure lead to the improvement of steel resistance to stress corrosion cracking induced by chlorides [5]. These types of steels are used, with good results, in oil refineries equipments.

It has been also proved that ferrite presence in the steels used in ammonia carbamate containing environments causes growths of the selective attack of the environment against this phase [6]. It is known that between 923...1173 K, the ferritic phase tends to a precipitation one, that leads not only to material embrittlement, but due to the chromium loosses in the neighbouring areas, increases the steel sensitivity to corrosion.

The δ ferrite content allowed by Stamicarbon specifications for this type of steel is of maximum 0.6% [4]. The tested samples evidenced a maximum of 0.02% δ ferrite content. Tests were performed using a ferriscope.

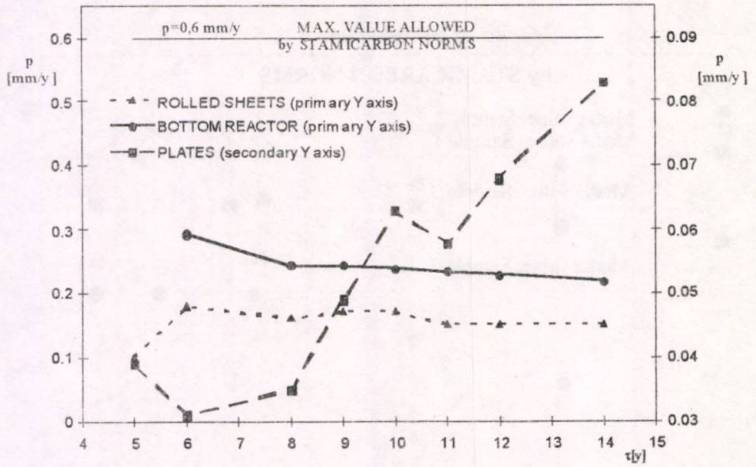

Fig. 3.- Variation of yearly penetration index for rolled sheets, plates and lower bottom of the urea synthesis reactor.

The austenitic structure of the steel is offering a good resistance to general corrosion generated by the environment from the reactor. According to Stamicarbon specifications, the maximum allowed average penetration index for AISI 316L stainless steel in carbamate–urea environments is to 0.6 mm/year. In order to obtain the yearly and average penetration index for the reactor lower bottom, rolled sheets and plates, the thickness of urea synthesis reactor lining was measured using ultrasonic measurements. Ultrasonic measurements have been performed since the urea plant became operational, in 1980, till now. Figs. 3 and 4 present the annual and average penetration index for the lower bottom of the reactor, rolled sheets and plates, during 14 years in service.

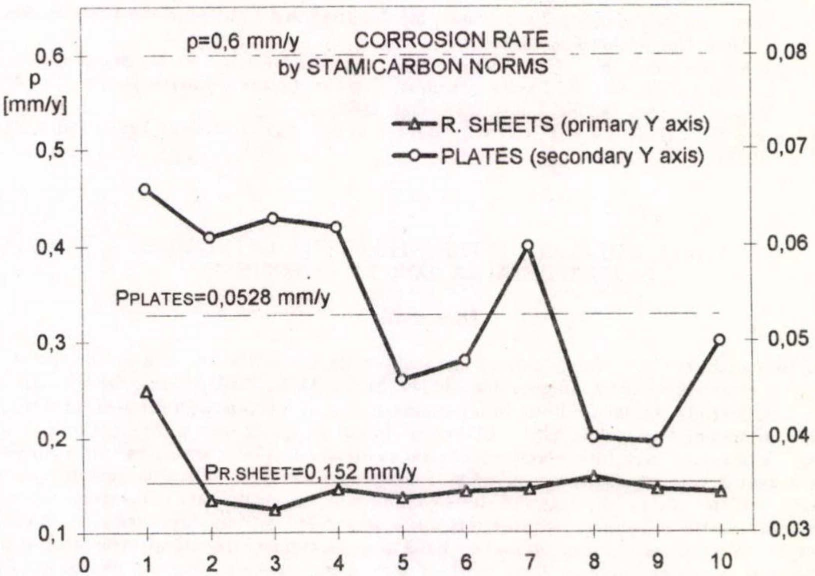

Fig. 4.- Variation of average yearly penetration index for the rolled sheets and plates from the urea synthesis reactor on the height of the reactor.

It may be observed that all measured values are below the 0.6 mm/year limit, evidencing that the lining in AISI 316L has a good behaviour to general corrosion.

3. Conclusions

The austenitic structure of AISI 316L stainless steel provided it a good resistance to intergranular and general corrosion in ammonium carbamate–urea environments at elevated pressures and temperatures.

The δ ferrite content of 0.02% from steel structure does not influence its resistance to inter- and transgranular corrosion.

Received, April 18, 1995

SOFERT S.A., Bacău,
Technical University "Gh.Asachi", Jassy,
Department of Inorganic
Chemical Technology
and
University of Bacău,
Faculty of Engineering

REFERENCES

1. Truşculescu M., Ieremia A., *Stainless Steels and Refractory Steels,* (in Romanian). Ed. Facla, Timişoara, 1983.
2. * * * Norma G~161: *Huey Test for Stainless Steels.* M.J.G. Booten.
3. * * * STAS 7114-80: *Testing Methods for Intergranular Corrosion Resistance of Austenitic Stainless Steel* (Romanian Standard).
4. Berglund G., Poschlep E., *Stainless Steels for Eliminating Chloride-Induced Corrosion in Ammonia/Urea Plants.* 5th International Conference on Urea, Hradeč - Králové, Czechoslovakia, 1988.
5. Bernhardsson S., Credsson J., Martenson C., *Stress Corrosion Cracking Resistance of Duplex Stainless Steels in Chloride Environments.* The ASM Metals Congress '82, St. Louis, USA, Oct. 1982.
6. de Jonge R., Barake F.X.C.M., Logeman J.D., Chemical Age of India, **26**, *4* (1975).

UNELE CORELAŢII ÎNTRE STRUCTURA OŢELURILOR ŞI COMPORTAREA LOR LA COROZIUNE

(Rezumat)

Structura oţelurilor inoxidabile depinde de compoziţia chimică a acestora şi, in special, de conţinutul în elemente de aliere alfagene (Cr, Mo, W, Si, Ti, Al, Be, Nb) şi gamagene (Ni, Mn, Co, Cu, N, C). Se prezintă corelaţiile dintre unii parametri, cum ar fi compoziţia chimică şi conţinutul de ferită δ, ai unui oţel austenitic AISI 316L utilizat în instalaţiile de uree şi rezistenţa acestuia la coroziune. Pe baza consideraţiilor teoretice s-a arătat că oţelul selecţionat are o structură austenitică şi este rezistent la coroziunea intergranulară şi la cea generalizată. Consideraţiile teoretice au fost confirmate de către analiza metalografică, testele chimice de susceptibilitate la coroziune intergranulară şi măsurătorile ultrasonice de grosimi realizate în vederea determinării vitezei de coroziune. S-a constatat că oţelul testat are o comportare bună în medii corozive de carbamat de amoniu-uree la temperaturi şi presiuni ridicate, fiind rezistent atât la coroziunea intergranulară, cât şi la cea generalizată.

BULETINUL INSTITUTULUI POLITEHNIC DIN IAŞI
Tomul XLIII (XLVII), Fasc. 1-2, 1997
Secţia II
CHIMIE şi INGINERIE CHIMICĂ

D.C. 541.8; 542.65

STUDY ON COMPUTER, IN C LANGUAGE, OF SOME FACTORS INFLUENCING THE SOLUBILITY OF PRECIPITATES

BY

DOINA BEJAN and ALINA BEJAN

The solubility of the precipitates is influenced by both the solid phase activity and the activity of ions in the solution.

Some factors influencing the activity of ions in the solution such as the pH, ionic strength (saline effect), precipitating agent excess (the common ion effect), presence of redox processes are studied on computer in C language.

1. Introduction

Considerations on the precipitation equilibria as well as on the factors affecting the precipitate solubility are to be found in numerous papers in the field [1],...,[3].

The solubility equilibrium may be influenced by the simultaneous presence of several equilibria within the system involving the precipitate ions which participate to the precipitation equilibrium. These equilibria are referred to as competitive. Their effect consists in the shifting of the solubility equilibrium toward the solubility increase, leading finally to the entire dissolution of the precipitates [2].

The opportunity of introduction the up-to-date calculating technique in both fundamental and applicative scientific research as well as the performance of the C programming language for these domains are presented in [4],...,[6].

2. Experimental

The programming of the above mentioned problems in the C language was carried out on a 386 SX, Packard Bell personal computer (IBM compatible).

Some operational details are given in [7].

Selections of the solutions of the problems under study, corresponding to some possible combinations, are given in the tables.

3. Results and Discussion

3.1. Programme Elaboration for Establishing pH Effect on the Solubility of B_mA_n Precipitate

The cation B^{n+} is precipitated by a precipitating agent A^{m-} and the B_mA_n precipitat is formed.

a) *Mathematical Model*

$$\alpha_{\mathrm{H}} = 1 + \frac{[\mathrm{H}^+]}{K_{a_m}} + \frac{[\mathrm{H}^+]^2}{K_{a_m}K_{a_{m-1}}} + \cdots + \frac{[\mathrm{H}^+]^m}{K_{a_m}K_{a_{m-1}}\cdots K_{a_1}},$$

where $K_{a_m}, K_{a_{m-1}}, \ldots, K_{a_1}$ are the dissociation constants of the stable species appearing in the presence of the H^+ ions [3].

$$S^{m+n} = \frac{P_s}{m^n n^n}\alpha_{\mathrm{H}}^n; \quad -\log[\mathrm{H}^+] = \mathrm{pH}.$$

Given: $m, n = 1, \ldots, 4$ (4 integer values for each); pH=0,...,14 (28 values); $P_s =$ $= 10^{-8}, \ldots, 10^{-20}$ (12 values); $K_{a_1}, \ldots, K_{a_m} = 10^{-3}, \ldots, 10^{-13}$ (4 sets of values).

Required: S^{m+n} for all sets of values given above for parameters m, n, pH, $P_s, K_{a_1}, \ldots, K_{a_m}$, and minimum value of S^{m+n}.

b) *Algorithm*

$$[H^+] = \exp\left(-\frac{\mathrm{pH}}{\log \mathrm{e}}\right).$$

The amounts $\alpha_{\mathrm{H}}, P_s, S^{m+n}$ have the known meanings.

c) *Codification*

The parameters of these problems have been symbolized as follows: MH(l) for $[\mathrm{H}^+]$; MK(l,m) for K_{a_j}; ALFAH for α_{H}; S(i,j) for S^{m+n}; i for m; j for n; S_4 for $S^{m+n}_{\min}$. Some solutions are given in Table 1.

Table 1

pH values:

0.00	0.50	1.00	1.50	2.00	2.50	3.00
3.50	4.00	4.50	5.00	5.50	6.00	6.50
7.00	7.50	8.00	8.50	9.00	9.50	10.00
10.50	11.00	11.50	12.00	12.50	13.00	14.00

Ka1,...,Kam values:

1E-05	1E-06	1E-07	1E-08	1E-09	1E-10	1E-11
1E-06	1E-07	1E-08	1E-09	1E-10	1E-11	1E-12
1E-07	1E-08	1E-09	1E-10	1E-11	1E-12	1E-13
1E-08	1E-09	1E-10	1E-11	1E-12	1E-13	1E-14

PS values:

1E-09	1E-10	1E-11	1E-12	1E-13	1E-15
1E-16	1E-17	1E-18	1E-19	1E-20	1E-21

```
n=1  l=7  k=1  j=1  i=2  Sm+n=2.433593E-05  pH=3  PS=1.0E-09
n=1  l=7  k=1  j=1  i=3  Sm+n=3.552020E-02  pH=3  PS=1.0E-09
n=1  l=7  k=1  j=1  i=4  Sm+n=3.693952E+02  pH=3  PS=1.0E-09
n=1  l=7  k=1  j=2  i=2  Sm+n=5.922377E-01  pH=3  PS=1.0E-09
n=1  l=7  k=1  j=2  i=3  Sm+n=8.516372E+06  pH=3  PS=1.0E-09
n=1  l=7  k=1  j=2  i=4  Sm+n=8.732978E+15  pH=3  PS=1.0E-09
n=1  l=7  k=1  j=3  i=2  Sm+n=8.540835E+03  pH=3  PS=1.0E-09
n=1  l=7  k=1  j=3  i=3  Sm+n=1.210013E+15  pH=3  PS=1.0E-09
n=1  l=7  k=1  j=3  i=4  Sm+n=1.223460E+29  pH=3  PS=1.0E-09
n=1  l=7  k=1  j=4  i=2  Sm+n=8.768639E+07  pH=3  PS=1.0E-09
n=1  l=7  k=1  j=4  i=3  Sm+n=1.223920E+23  pH=3  PS=1.0E-09
n=1  l=7  k=1  j=4  i=4  Sm+n=1.220239E+42  pH=3  PS=1.0E-09
n=1  l=7  k=5  j=1  i=2  Sm+n=2.433594E-09  pH=3  PS=1.0E-13
n=1  l=7  k=5  j=1  i=3  Sm+n=3.552020E-06  pH=3  PS=1.0E-13
n=1  l=7  k=5  j=1  i=4  Sm+n=3.693952E-02  pH=3  PS=1.0E-13
n=1  l=7  k=5  j=2  i=2  Sm+n=5.922377E-05  pH=3  PS=1.0E-13
n=1  l=7  k=5  j=2  i=3  Sm+n=8.516372E+02  pH=3  PS=1.0E-13
n=1  l=7  k=5  j=2  i=4  Sm+n=8.732979E+11  pH=3  PS=1.0E-13
n=1  l=7  k=5  j=3  i=2  Sm+n=8.540835E-01  pH=3  PS=1.0E-13
n=1  l=7  k=5  j=3  i=3  Sm+n=1.210013E+11  pH=3  PS=1.0E-13
n=1  l=7  k=5  j=3  i=4  Sm+n=1.223460E+25  pH=3  PS=1.0E-13
n=1  l=7  k=5  j=4  i=2  Sm+n=8.768639E+03  pH=3  PS=1.0E-13
n=1  l=7  k=5  j=4  i=3  Sm+n=1.223920E+19  pH=3  PS=1.0E-13
n=1  l=7  k=5  j=4  i=4  Sm+n=1.220239E+38  pH=3  PS=1.0E-13
Smin=2.433594E-09
```

3.2. Programme Elaboration for the Study of the Influence of Ion Charges and Solution Ionic Strength on the Precipitate Solubility

Knowing the solubility products, ion charges and solution ionic strength, the precipitate solubilities have to be estimated when these parameters are modified.

a) *Mathematical Model* [3]

$$\log S = \log S_0 - \log \gamma,$$

where: S is the solubility with a certain ionic strength; S_0 – solubility when the ionic strength is zero;

$$\log \gamma = 0.505\, z_1 z_2 \frac{\sqrt{\mu}}{1+\sqrt{\mu}}.$$

Given: $\mu = 10^{-3}, ..., 1$ (16 values); $z_1, z_2 = 1, ..., 5$ (5 integer numbers each); $S_0 = 10^{-5}, ..., 10^{-10}$ (12 values).

Required: S for all values of the above mentioned parameters, $S_{\min}$ being also estimated.

b) *Algorithm*

$$\log S = \log S_0 + 0.505\, z_1 z_2 \frac{\sqrt{\mu}}{1+\sqrt{\mu}},$$

$$S = \exp\left[\left(\log S_0 + 0.505\, z_1 z_2 \frac{\sqrt{\mu}}{1+\sqrt{\mu}}\right)\frac{1}{\log \mathrm{e}}\right].$$

c) *Codification*

S and S_0 have the same meaning as in the mathematical model.

The parameters μ, z_1, z_2 correspond in the programme with M(l), i and j, respectively; $S_{\min}$ is represented by S1.

A set of results is given in Table 2.

Table 2

```
miu values:
0.001   0.004   0.006   0.008   0.010   0.020   0.040   0.060
0.080   0.100   0.200   0.400   0.600   0.800   0.900   1.000

S0 values:
1E-05   5E-06   1E-06   5E-07   1E-07   5E-08
1E-08   5E-09   1E-09   5E-10   1E-10   5E-11


      miu=0.001   S0=1E-05   z1=1   z2=1   S=1.012506E-05
      miu=0.001   S0=1E-05   z1=1   z2=2   S=1.049322E-05
      miu=0.001   S0=1E-05   z1=1   z2=3   S=1.087477E-05
      miu=0.001   S0=1E-05   z1=1   z2=4   S=1.127019E-05
      miu=0.001   S0=1E-05   z1=1   z2=5   S=1.167999E-05
      miu=0.001   S0=1E-05   z1=2   z2=1   S=1.049322E-05
      miu=0.001   S0=1E-05   z1=2   z2=2   S=1.127019E-05
      miu=0.001   S0=1E-05   z1=2   z2=3   S=1.210470E-05
      miu=0.001   S0=1E-05   z1=2   z2=4   S=1.300099E-05
      miu=0.001   S0=1E-05   z1=2   z2=5   S=1.396365E-05
      miu=0.001   S0=1E-05   z1=3   z2=1   S=1.087477E-05
      miu=0.001   S0=1E-05   z1=3   z2=2   S=1.210470E-05
      miu=0.001   S0=1E-05   z1=3   z2=3   S=1.347373E-05
      miu=0.001   S0=1E-05   z1=3   z2=4   S=1.499760E-05
      miu=0.001   S0=1E-05   z1=3   z2=5   S=1.669381E-05
      miu=0.001   S0=1E-05   z1=4   z2=1   S=1.127019E-05
      miu=0.001   S0=1E-05   z1=4   z2=2   S=1.300099E-05
      miu=0.001   S0=1E-05   z1=4   z2=3   S=1.499760E-05
      miu=0.001   S0=1E-05   z1=4   z2=4   S=1.730083E-05
      miu=0.001   S0=1E-05   z1=4   z2=5   S=1.995777E-05
      miu=0.001   S0=1E-05   z1=5   z2=1   S=1.167999E-05
      miu=0.001   S0=1E-05   z1=5   z2=2   S=1.396365E-05
      miu=0.001   S0=1E-05   z1=5   z2=3   S=1.669381E-05
      miu=0.001   S0=1E-05   z1=5   z2=4   S=1.995777E-05
      miu=0.001   S0=1E-05   z1=5   z2=5   S=2.385989E-05
      Smin=1.012506E-05
```

3.3. Elaboration of the Programme Affording the Dependence Relation between the Solubility and the Excess of Common Ions

On this purpose a set of values of the solubility products, coefficients m and n, and concentrations of the ion in excess is considered.

a) *Mathematical Model* [3]

$$S_A^m = \frac{P_s}{m^n[A^{m-}]^n}; \quad S_B^n = \frac{P_s}{n^n[B^{n+}]^m}.$$

Given: $m, n = 1, ..., 4$ (4 integer values); $P_s = 10^{-9}, ..., 10^{-21}$ (12 values); $[A^{m-}] = 10^{-3}, ..., 5$ (16 values); $[B^{n+}] = 10^{-3}, ..., 5$ (16 values).

Required: S_A^m and S_B^n values for the variations of the above mentioned parameters over the entire definition domain, as well as their minimum values.

b) *Algorithm*

The two calculation cycles of the S_A^m and S_B^n amounts and of their minimum values are performed simultaneously, fact that decreases the execution time.

c) *Codification*

The following notations have been used: i for m; j for n; A for $[A^{m-}]$; B for $[B^{n+}]$; S for $S^m_{A\,\min}$; S$_2$ for $S^n_{B\,\min}$.

Some of the problem solutions, corresponding to a part of the possible parameter combinations, are given in Table 3.

Table 3

```
PS values:
1E-09   1E-10   1E-11   1E-12   1E-13   1E-15
1E-16   1E-17   1E-18   1E-19   1E-20   1E-21
A values:
0.001   0.005    0.01    0.05     0.1     0.5      1     1.5
  2      2.5      3       3.5      4       5     0.05   0.01

B values:
0.001   0.005    0.01    0.05     0.1     0.5      1     1.5
  2      2.5      3       3.5      4       5     0.05   0.01

PS=1E-09; A=0.001; B=0.001

m=1   n=1   SA**m=9.999999E-07        SB**n=9.999999E-07
m=1   n=2   SA**m=9.999999E-04        SB**n=2.500000E-07
m=1   n=3   SA**m=9.999998E-01        SB**n=3.703703E-08
m=1   n=4   SA**m=9.999998E+02        SB**n=3.906250E-09
m=2   n=1   SA**m=2.500000E-07        SB**n=9.999999E-04
m=2   n=2   SA**m=2.500000E-04        SB**n=2.500000E-04
m=2   n=3   SA**m=2.500000E-01        SB**n=3.703703E-05
m=2   n=4   SA**m=2.499999E+02        SB**n=3.906250E-06
m=3   n=1   SA**m=3.703703E-08        SB**n=9.999998E-01
m=3   n=2   SA**m=3.703703E-05        SB**n=2.500000E-01
m=3   n=3   SA**m=3.703703E-02        SB**n=3.703703E-02
m=3   n=4   SA**m=3.703703E+01        SB**n=3.906249E-03
m=4   n=1   SA**m=3.906250E-09        SB**n=9.999998E+02
m=4   n=2   SA**m=3.906250E-06        SB**n=2.499999E+02
m=4   n=3   SA**m=3.906249E-03        SB**n=3.703703E+01
m=4   n=4   SA**m=3.906249E+00        SB**n=3.906249E+00
SA Min=3.90625E-09 for m=4; n=1; PS=1E-09; A=0.001; B=0.001.
SB Min=3.90625E-09 for m=1; n=4; PS=1E-09; A=0.001; B=0.001.
SA^Mmin=7.812500E-12 for PS=1E-09; A=0.5; B=0.5; m=4; n=1.
SB^Mmin=7.812500E-12 for PS=1E-09; A=0.5; B=0.5; m=1; n=4.
```

3.4. Elaboration of the Programme Making Evident the Influence of the Redox Processes on the Precipitate Solubilities

Several precipitates with different solubility products and m and n coefficients, in the presence of oxidants and reducing agents which are able to give secondary reactions with the precipitate ions are taken into account.

The precipitate solubilities are calculated for different oxidants and reducing agents as a function of the standard potentials of the redox systems, the number of the electrons exchanged in the respective processes, and as well as a function of the concentrations of the considered oxidants and reducing agents.

a) *Mathematical Model* [3]

$$S^{m+n} = \frac{P_s}{m^n n^n}\left(1+\frac{[O^{s+}]10^{\frac{z(E_2^0-E_1^0)}{0.059}}}{[O^{(s-z)+}]}\right).$$

Let be: $\Delta E = E_2^0 - E_1^0$; $[O^{s+}] + [O^{(s-z)+}]$=SO.

Given: m, n=1,...,4 (4 integer values for each); P_s=10^{-9},...,10^{-21} (12 values); z=1,...,4 (4 integer values); ΔE=0.1,...,1 (10 values); $[O^{s+}]$=10^{-4},...,4 (10 values); SO=10^{-4},...,4 (10 values).

Required: Values for S_1^{m+n} and S_2^{m+n}.

b) *Algorithm*

By means of the calculation relation advanced by the mathematical model, the calculation can be made stepwise:

$$\begin{array}{ll} \text{Step } 1: \; A_1 = 10^{\frac{z(E_2^0-E_1^0)}{0.059}}; & \text{Step } 2: \; A_2 = 1+\frac{[O^{s+}]A_1}{[O^{(s-z)+}]}; \\ \text{Step } 3: \; A_3 = \frac{P_s}{m^n n^n}; & \text{Step } 4: \; S_1^{m+n} = A_3 A_2. \end{array}$$

The above calculations can be made in one stage and made it so. In other cases the stepwise variant must be applied.

c) *Codification*

The following notations have been used:

i for m; OSZ for $[O^{s+}]$; S for S^{m+n}; j for n; SOS for SO; DE for ΔE; OSZ for $[O^{(s-z)+}]$.

Some of the probleme solutions are given in Table 4.

Table 4

OS values:
0.0001 0.001 0.01 0.1 0.5 1 1.5 2 3 4

Z values:
1 2 3 4

DE values:
0.1 0.2 0.3 0.4 0.5 0.6 0.7 0.8 0.9 1

SOS values:
0.0001 0.001 0.01 0.1 0.5 1 1.5 2 3 4

PS values:
1E–09 1E–10 1E–11 1E–12 1E–13 1E–15
1E–16 1E–17 1E–18 1E–19 1E–20 1E–21
PS=1.0E–09; Z=1; DE=0.01; M=1; N=1.

```
OS=0.0001  S1m + n=1.500357E–09  SUM OS=0.01
OS=0.0010  S1m + n=6.503929E–09  SUM OS=0.01
OS=0.0001  S1m + n=1.009909E–09  SUM OS=0.50
OS=0.0010  S1m + n=1.099269E–09  SUM OS=0.50
OS=0.0100  S1m + n=2.010925E–09  SUM OS=0.50
OS=0.1000  S1m + n=1.338384E–08  SUM OS=0.50
OS=0.0001  S1m + n=1.003303E–09  SUM OS=1.50
OS=0.0010  S1m + n=1.033046E–09  SUM OS=1.50
OS=0.0100  S1m + n=1.332452E–09  SUM OS=1.50
OS=0.1000  S1m + n=4.538240E–09  SUM OS=1.50
OS=0.5000  S1m + n=2.576768E–08  SUM OS=1.50
OS=1.0000  S1m + n=1.000707E–07  SUM OS=1.50
OS=0.0001  S1m + n=1.001651E–09  SUM OS=3.00
OS=0.0010  S1m + n=1.016517E–09  SUM OS=3.00
OS=0.0100  S1m + n=1.165670E–09  SUM OS=3.00
OS=0.1000  S1m + n=2.708116E–09  SUM OS=3.00
OS=0.5000  S1m + n=1.090707E–08  SUM OS=3.00
OS=1.0000  S1m + n=2.576768E–08  SUM OS=3.00
OS=1.5000  S1m + n=5.053535E–08  SUM OS=3.00
OS=2.0000  S1m + n=1.000707E–07  SUM OS=3.00
```

4. Conclusions

The precipitate solubilities depend on several factors such as: ionic strength of the medium, presence of the common ions, presence of other equilibria along the precipitation equilibrium. The most important are: the acido-basic equilibria generally involving the precipitate anions, the complexing equilibria affecting the metallic ion concentrations and the redox equilibria which may affect the concentrations of both anions and cations.

The computer study of some factors affecting the precipitation equilibrium gives the possibility to the optimum conditions for obtaining a sparingly soluble compound.

Received, February 3, 1996

Technical University "Gh.Asachi", Jassy,
Department of Analytical Chemistry
and
"Al.I.Cuza" University, Jassy,
Computer Science Faculty

REFERENCES

1. Fişel S., Mocanu R., Sârghie I., *Chimie analitică cantitativă - Gravimetria.* EDP, Bucureşti, 1973, 54.
2. Kekedy L., *Chimie analitică calitativă.* Ed. Scrisul Românesc, Craiova, 1982, 197, 207.
3. Croitoru V., Constantinescu D.A., *Aplicaţii şi probleme de Chimie analitică.* Ed. Tehnică, Bucureşti, 1979, 212, 365.
4. Kasko A., Kasko D., *Turbo C - Tehnici de programare.* Ed. MicroInformatica, Cluj-Napoca, 1992, 5.
5. Negrescu L., *Limbajele C şi C++ pentru începători.* Vol.I, Ed. MicroInformatica, Cluj-Napoca, 1994, 13.
6. Petrovici V., Goicea F., *Programarea în limbaj C.* Ed. Tehnică, Bucureşti, 1993, 9.
7. Bejan D., Bejan A., Bul. Inst. polit., Iaşi, **XLII (XLVI)**, *3-4*, s.II (1996) (in press).

STUDIUL PE CALCULATOR, ÎN LIMBAJ C, AL UNOR FACTORI CE INFLUENŢEAZĂ SOLUBILITATEA PRECIPITATELOR

(Rezumat)

Solubilitatea precipitatelor este influenţată atât de activitatea fazei solide, cât şi de cea a ionilor în soluţie.

Se studiază, pe calculator, în limbaj C, unii factori ce influenţează activitatea ionilor în soluţie şi anume: pH-ul, tăria ionică (efectul salin), excesul de precipitant (efectul ionului comun), prezenţa proceselor redox.

BULETINUL INSTITUTULUI POLITEHNIC DIN IAŞI
Tomul XLIII (XLVII), Fasc. 1–2, 1997
Secţia II
CHIMIE şi INGINERIE CHIMICĂ

D.C. 661.521; 661.321

ON DECOMPOSITION OF AMMONIUM CHLORIDE, BY-PRODUCT OF MODIFIED SODA ASH MANUFACTURE, WITH CALCIUM CARBONATE

BY

AL. SZÉP

Industrial application of the new soda ash procedures is conditioned by the recovery and utilization of ammonium chloride. In last few years, the consumed ammonium chloride as fertilizer was little and little. In this situation, the decomposition process of the potentially waste becomes again important. In order to transformation of the recovered ammonium chloride in a required industrial product, like calcium chloride, the possibilities of its decomposition with different forms of calcium carbonate, like precipitated calcium carbonate and limestone, were developed. The experimental results obtained under isothermal conditions, at 473...673 K, in a fixed bad, discontinuously operated, tubular reactor, with different particle size (0.085...0.565 mm), showed that the process is significantly influenced by temperature and nature of calcium carbonate. The mathematical model of decomposition of the ammonium chloride with precipitated $CaCO_3$ is described by Eqs. (4).

1. Introduction

Industrial application of the procedures yielding soda ash concomitantly with ammonium chloride is conditioned, as well known, by finding some new utilization or processing domains of this solid by-product. The available information in literature as regards the processing and utilization of ammonium chloride can be divided in two groups, i.e. utilization of it as ammonium chloride and its transformation in a series of the other products such as chlorine, ammonia, hydrochloric acid, nitrogenous-phosphoric fertilizers, etc.

As regards the utilization's of ammonium chloride, the classical ores are electrotechnics, metallurgy, chemical industry and the new ores are in simple fertilizer, as component in compound fertilizers, fodder conservation, soils amelioration, etc. [1], [2].

Transformation of the ammonium chloride in other products can be achieved starting from both solid ammonium chloride and its solutions as well as from gaseous ammonium chloride. For the transformation of solid ammonium chloride different ways were developed, i.e.: obtaining ammonia and chlorine using magnesium oxide, iron oxides, cupric chloride [3], oxidation with nitric acid in the presence of manganese dioxide [4]; obtaining ammonia and hydrochloric acid using zinc chloride [5], magnesium oxide [6], sodium hydrogen sulphate [7]; obtaining chlorides and ammonia by treating with hydroxides, oxides and acid or neutral carbonates [8] or by double change reaction; obtaining ammonium salts and hydrochloric acid by treating with sulphuric acid, nitric acid or acid anhydrides [9]. Including into the above mentioned list, electrolysis of ammonium chloride solution or with gas diffusion electrode [10] we have a complete perspective of the processing possibilities of ammonium chloride.

Utilization of ammonium chloride as fertilizer for cotton field, beet growing, rice and corn crop on irrigated soils and its processing in solution producing calcium chloride solution like in the new Asahi Glass procedure [11] represents a little for the present in solving the multiple problems of soda ash manufacture. Modification of the classical Solvay procedure with yielding ammonium chloride using evaporation or salting [12], [13] represents a reliable way of the pollution diminishing, but its industrial application is conditioned by the limited possibilities of the new product utilization.

Taking into account that the 0.8...1.05 to ammonium chloride which can be obtained for each to of soda ash do not find utilization in a single branch, have been investigated, in the laboratory scale, the possibilities of its transformation in anhydrous calcium chloride by treating with calcium carbonate.

The present paper deals with the laboratory results regarding the utilization of ammonium chloride for both, natural and precipitated, calcium carbonate yielding anhydrous calcium chloride and the gases containing carbon dioxide, ammonia and water vapour.

2. Experimental

The experiments were performed using limestone, precipitated calcium carbonate from caustic soda manufacture and ammonium chloride, obtained from mother liquid by cooling and salting out with sodium chloride. The decomposition was carried out under isothermal conditions, at 473...673 K, in fixed bed discontinuously operated tubular reactor, with and without gaseous product carrying away. The particle size was 0.085...0.565 mm for both raw materials. Development of the process was expressed by means of the transformation degree variation versus time. The transformation degree was defined by relation

$$\eta_{\mathrm{CaCO_3}} = 0.9\frac{V_{[]_l}\overline{x}_{\mathrm{CaCl_2}}}{m^0_{[]_s}\overline{x}^0_{\mathrm{CaCO_3}}}, \qquad (1)$$

where: $V_{[]_l}$ is the volume of solution estimated by sample dissolution; $\overline{x}_{\mathrm{CaCl_2}}$ – calcium chloride content of the sample; $m^0_{[]_s}, \overline{x}^0_{\mathrm{CaCO_3}}$ – mass of solid and the $CaCO_3$ content of the initial sample.

3. Results and Discussion

The experimental results are presented as kinetic curves η vs. τ. The Figs. 1,...,3 show a significant influence of temperature, calcium carbonate sort and granule size (d_p) on the decomposition rate. The humidity and the granule size of ammonium chloride are a little influence on the transformation degree.

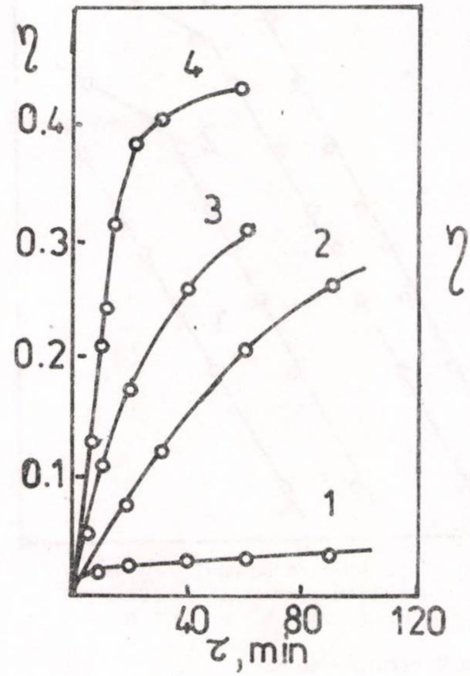

Fig. 1.- Dependence of η vs. time at different temperatures for limestone with $d_p = 0.225$ mm; *1* - 523 K; *2* - 623 K; *3* - 673 K; *4* - 773 K.

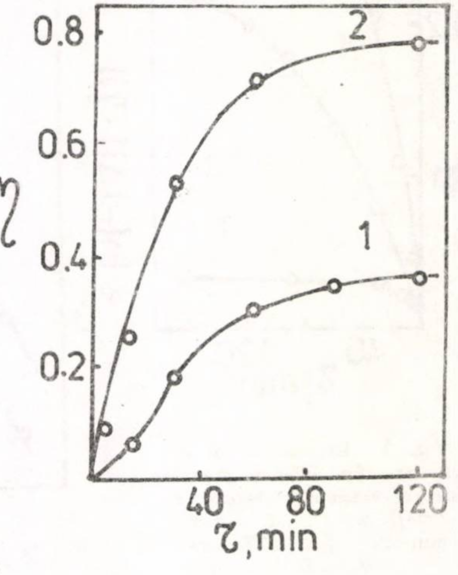

Fig. 2.- Dependence of η vs. time for different sorts of calcium carbonate at 623 K; *1* - limestone with $d_p =$ $= 0.085$ mm; *2* - precipitate calcium carbonate with $d_p = 0.085$ mm.

Processing the experimental data in the co-ordinates $-\ln\tau$ vs. $1/T$ pointed out that in the case of decomposition of limestone with $d_p < 0.085$ mm at temperatures below 623 K, the process developed according to a transformation mechanism ($E_a > 49,000$ J/mol) and over 623 K according to a combined mechanism, transformation–transfer through crust ($E_a = 12,937...16,470$ J/mol). The decomposition of limestone with large particle size, as well as the decomposition of precipitated calcium carbonate develops according to a unique transformation mechanism ($E_a = 49,822$ J/mol), but the decomposition degree of limestone does not exceed 0.2 and the decomposition of precipitated calcium carbonate is highest, about 0.75.

The information obtained from the study of parameter influence allowed to es-

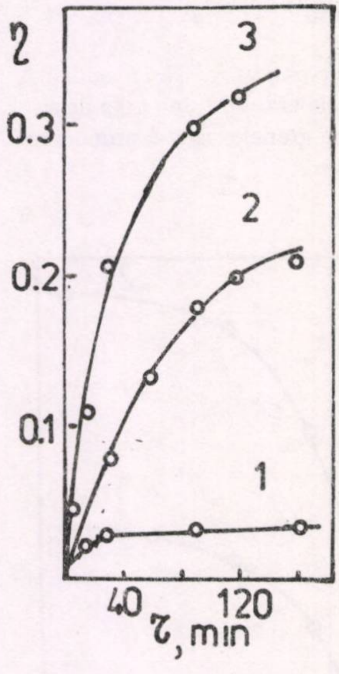

Fig. 3.- Dependence of η vs. time for different granule size of calcium carbonate at T=573 K; *1* - $d_p = 0.565$ mm; *2* - $d_p = 0.225$ mm; *3* - $d_p = 0.085$ mm.

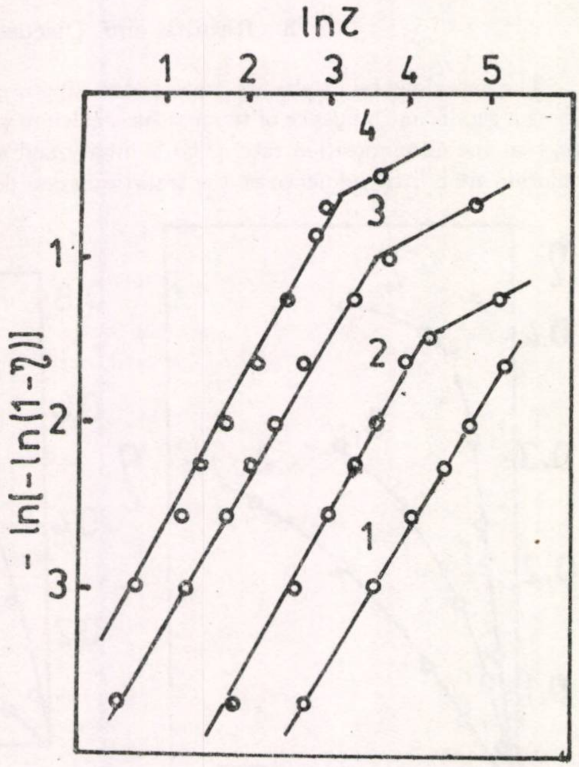

Fig. 4.- Dependence of $\ln[-\ln(1-\eta)]$ vs. $\ln\tau$ for different temperatures; *1* - 523 K; *2* - 573 K; *3* - 623 K; *4* - 673 K.

tablish the mathematical model of the macrostructural element.

For the limestone decomposition the experimental results were verified by the relations

$$\eta = 1 - \mathrm{e}^{k_1^* \tau} \quad \text{for } T < 623 \text{ K}, \tag{2}$$

$$\eta = 1 - \mathrm{e}^{-k_2^* \sqrt[4]{\tau}} \quad \text{for } T > 623 \text{ K}, \tag{3}$$

where $k_1^* = 75\,\mathrm{e}^{-51{,}037/RT}$ and $k_2^* = 10.88\,\mathrm{e}^{-21{,}478/RT}$, as can bee seen in Fig.4.

As shown in Figs. 5 and 6 the experimental results regarding the decomposition of precipitated calcium carbonate verify, with a good precision, the model described by the equation

$$\frac{\mathrm{d}\eta}{\mathrm{d}\tau} = k^*(1-\eta)^n, \quad \frac{4}{3} \le n \le \frac{5}{3}, \tag{4}$$

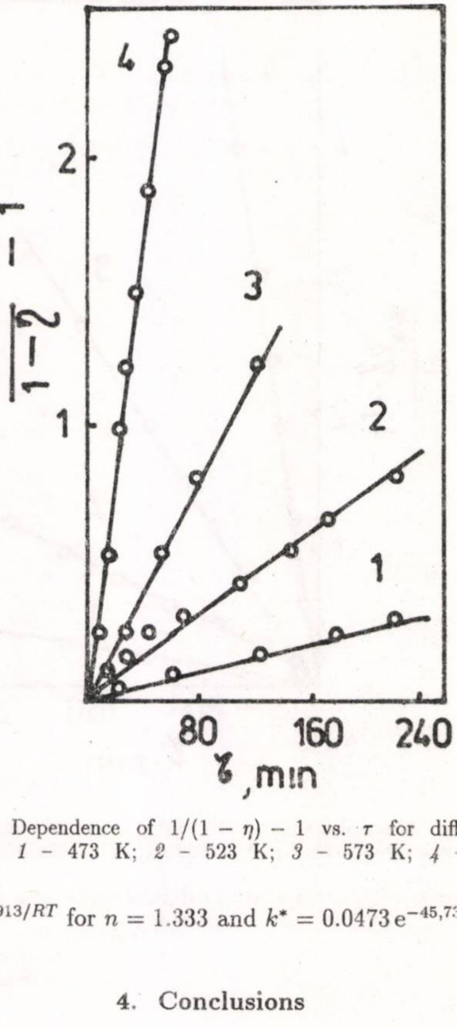

Fig. 5.- Dependence of $1/(1-\eta) - 1$ vs. τ for different temperatures; *1* - 473 K; *2* - 523 K; *3* - 573 K; *4* - 673 K.

where $k^* = 0.086\,\mathrm{e}^{-47{,}913/RT}$ for $n = 1.333$ and $k^* = 0.0473\,\mathrm{e}^{-45{,}732/RT}$ for $n = 1.666$.

4. Conclusions

The experimental results on calcium carbonate (as limestone and precipitated forms) decomposition with ammonium chloride, in fixed bed, discontinuously operated reactor, showed that the process is significantly influenced by the nature and granule size of samples and by the temperature. The transformation degree achieved for limestone, even for its granule size less than 0.085 mm, excludes the possibility of its utilization for anhydrous calcium chloride manufacture. Precipitate of calcium carbonate with adequate structure and particle size allowed to obtain transformation degree higher than 0.85 even at temperatures below than that of the calcium carbonate thermal dissociation.

On the basis of the kinetic data, the mathematical model of the decomposition

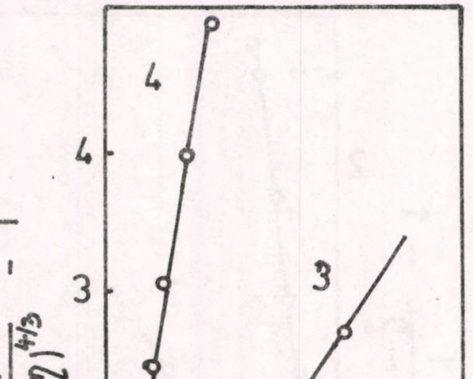

Fig. 6.- Dependence of $1/(1-\eta)^{4/3} - 1$ vs. τ for different temperatures; *1* - 473 K; *2* - 532 K; *3* - 573 K; *4* - 673 K.

of ammonium chloride with precipitated calcium carbonate have been developed.

Received, January 16, 1996

Technical University "Gh.Asachi", Jassy,
Department of Inorganic
Chemical Technology

REFERENCES

1. Calistru C., Leonte C., Hagiu C., Siminiceanu I., Popa O., *Tehnologia îngrăşămintelor minerale.* Vol. **1**, Ed. Tehnică, Bucureşti, 1984.
2. Jarzebovska I., Chemik, **20**, *12*, 448 (1967).
3. Ashboren D., Korab F., Isr. Jour. of Chem., **11**, *5*, 661 (1973).
4. * * * Patent USA, *2714550*/05.08.1955.
5. Mihailov F.K., Khim. Prom. Ukr., **3**, 8 (1966).
6. Străjescu M., Rev.Chim., **32**, *9*, 649 (1981).
7. * * * Patent Czechoslovakia, *185494*/15.09.1980.
8. * * * Patent RO, *89164*/25.05.1984.
9. * * * Patent Germany *3021254*/11.12.1980.
10. Filipescu L., *Tehnologia produselor sodice şi clorosodice.* Vol. **1**, Ed. Tehnică, Bucureşti, 1984.

11. Leszczinski S., Chemik, **37**, *1*, 8 (1984).
12. Calistru C., Ifrim L., Szép Al., Leonte C., Rev. Chim., **34**, *7*, 625 (1983).
13. Szép Al., Mihăilă Gh., Rev. Chim., **47**, *8*, 743 (1996).

UTILIZAREA CLORURII DE AMONIU, PRODUS SECUNDAR AL LINIEI DE SODĂ MODIFICATE

(Rezumat)

Implementarea industrială a variantelor tehnologice de obţinere concomitentă a sodei calcinate şi a clorurii de amoniu este condiţionată de găsirea unor domenii noi de utilizare a noului produs. Deoarece utilizarea directă ca îngrăşământ nu a rezolvat nici pe departe problema folosirii clorurii de amoniu, potenţial subprodus al unei linii de sodă modificate, s-a propus studiul experimental de transformare a sării în clorură de calciu, produs cu o piaţă oarecum mai sigură şi mai puţin pretenţioasă. În acest context se prezintă rezultatele cercetărilor experimentale, la scară de laborator, ale descompunerii clorurii de amoniu cu carbonaţi naturali şi sintetici, în condiţii izoterme, la 473...673 K, folosind particule de 0,085...0,565 mm diametru. Cercetările întreprinse arată că procesul de descompunere este influenţat semnificativ de natura carbonatului de calciu, de temperatură şi de dimensiunea particulelor de carbonat. Dintre carbonaţii utilizaţi doar cei sintetici au condus la rezultate promiţătoare, atât în ceea ce priveşte viteza procesului de descompunere, cât şi calitatea clorurii de calciu obţinute. Modelul matematic stabilit pentru acestea din urmă are forma dată de ecuaţia (4).

BULETINUL INSTITUTULUI POLITEHNIC DIN IAŞI
Tomul XLIII (XLVII), Fasc. 1-2, 1997
Secţia II
CHIMIE şi INGINERIE CHIMICĂ

D.C. 542.49; 542.63

MASS TRANSFER AT SUBLIMATION
PARTIAL PRESSURE DISTRIBUTION IN THE BOUNDARY DIFFUSION LAYER

BY

STELIAN PETRESCU and ANA BĂCĂOANU

A mathematical model of the sublimation process with a drawing agent in isothermal and stationary steady-state is proposed. The mathematical model contains only dimensionsless variables and parameters, and is used for the study of the influence of the Stanton number, of the gaseous phase velocity and of the sublimate partial pressure in the gaseous phase on the partial pressure profile in the boundary diffusion layer.

1. Introduction

Sublimation is a physical process used in technical application for the separation and purification of solid state substances. It is encountered in the drying through freezing process of solid materials.

There are many references concerning the sublimation process. Mihăilă *et al.* [1], Szép *et al.* [2] and Lombrana and Villaran [3] studied in their papers the sublimation kinetics. As for the mass transfer the present day references deal both with the theoretic and experimental study at the particle level or for a group of particles in fixed or fluidized bad, Larry *et al.* [4], Songin [5] and Halder *et al.* [6].

Jouli and Rios [7], Peng and Chen [8] dealt with the heat and mass transfer at sublimation. The theoretical study of mass transfer at sublimation is treated in the existing papers as a diffusion process of the sublimate from a solid boundary to the bulk of the gaseous phase.

In this paper a mathematical model of the sublimation process in isothermal and stationary steady-state is established. The model contains dimensionless variables and parameters. The mathematical model enables the determination of partial pressure of the sublimate in the boundary diffusion layer. The influence of the Stanton number, of the gas velocity and of the bulk gaseous phase partial pressure over the partial pressure profile in the boundary diffusion layer are analysed.

2. Mathematical Model

In order to determine the mathematical model of the sublimation process, which will be further on used to determine the partial pressure profile of the sublimate in the boundary diffusion layer, the physical model from Fig. 1 was used.

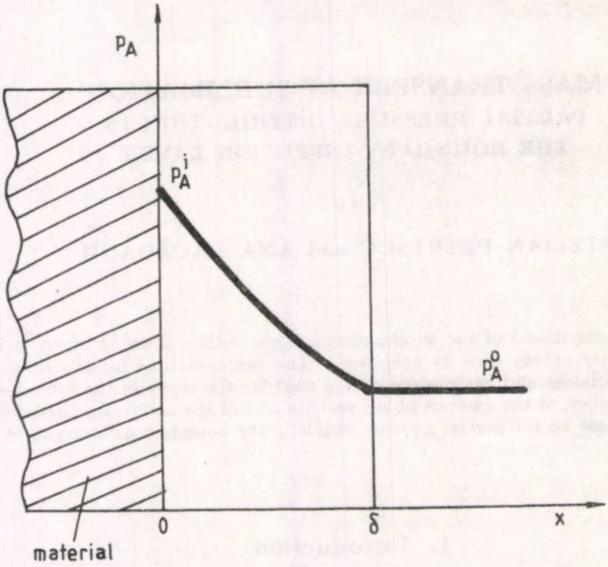

Fig. 1.- Physical model.

According to the physical model from Fig.1 the solid material that sublimate contains only one component (A). The solid material is a plate in direct contact at one side with a gaseous phase. This one is a moving perpendicularly with respect to the solid plate with the velocity v_x. In the neighborhood of the contact surface between the material and the drawing gas, a boundary diffusion layer is formed through which the component A diffuses.

The boundary diffusion layer has the thickness δ. The diffusion of component A through the boundary layer is the elementary process for sublimation which determines the process rate. Consequently the sublimation process resistance is concentrated in the boundary diffusion layer. On the contact surface between the material and the drawing agent the partial pressure of component A is p_A^i and at the extremity of the boundary layer is p_A^0. In the bulk of the gaseous phase formed by the drawing gas and by vapours of A component, the partial pressure of this component is constant (p_A^0). In the boundary layer the gaseous phase has the velocity $\overline{v}_x$. If the temperature is constant in stationary steady-state the sublimation process may be described by the convective diffusion equation:

$$D_A \frac{\mathrm{d}^2 C_A}{\mathrm{d}x^2} + \overline{v}_x \frac{\mathrm{d}C_A}{\mathrm{d}x} = 0, \tag{1}$$

where: D_A is the diffusion coefficient for component A; C_A - the molar concentration of component A.

If the gaseous phase behaves as an ideal gas then:

$$C_A \cdot = \frac{p_A}{RT}, \tag{2}$$

where: p_A is the partial pressure for component A, R - the universal gas constant, T - temperature.

Using (2), relation (1) becomes:

$$D_A \frac{\mathrm{d}^2 p_A}{\mathrm{d}x^2} + \overline{v}_x \frac{\mathrm{d}p_A}{\mathrm{d}x} = 0. \tag{3}$$

The boundary conditions are:

$$x = 0, \quad p_A = p_A^i; \qquad x = \delta, \quad p_A = p_A^0. \tag{4}$$

In order to simplify the solution of equation (3) the following dimensionless variables are introduced:

$$X = \frac{x}{\delta}, \tag{5}$$

$$P = \frac{p_A}{p_A^i}. \tag{6}$$

Substituting (5) and (6) relation (3) becomes:

$$D_A \frac{p_A^i}{\delta^2} \cdot \frac{\mathrm{d}^2 P}{\mathrm{d}X^2} + \overline{v}_x \frac{p_A}{\delta} \cdot \frac{\mathrm{d}P}{\mathrm{d}X} = 0 \tag{7}$$

or

$$\frac{\mathrm{d}^2 P}{\mathrm{d}X^2} + \overline{v}_x \frac{\delta}{D_A} \cdot \frac{\mathrm{d}P}{\mathrm{d}X} = 0. \tag{8}$$

The Stanton number for diffusion is defined by the relation:

$$\mathcal{S}t = \frac{\mathcal{S}h}{\Re e \cdot \mathcal{S}c} = \frac{k_g}{\overline{v}_x} = \frac{D_A}{\overline{v}_x \delta}, \tag{9}$$

so that equation (8) becomes:

$$\frac{\mathrm{d}^2 P}{\mathrm{d}X^2} + \frac{1}{\mathcal{S}t} \frac{\mathrm{d}P}{\mathrm{d}X} = 0. \tag{10}$$

The boundary conditions are given by:

$$X = 0, \quad P = 1; \qquad X = 1, \quad P = \frac{p_A^0}{p_A^i}. \tag{11}$$

The general solution of equation (10) is:

$$P = a + b\,e^{\frac{X}{St}}. \tag{12}$$

The constants a and b may be determined from the boundary conditions:

$$a = 1 - \frac{1 - p_A^0/p_A^i}{1 - e^{-1/St}}, \tag{13}$$

$$b = \frac{1 - p_A^0/p_A^i}{1 - e^{-1/St}}. \tag{14}$$

Substituting a and b in equation (12) we obtain:

$$P = 1 - \frac{1 - e^{-X/St}}{1 - e^{-1/St}}\left(1 - \frac{p_A^0}{p_A^i}\right). \tag{15}$$

Equation (15) enables the determination of partial pressure distribution for the A component that sublimates in the boundary diffusion layer. This equation contains only dimensionless variables and parameters. If Stanton number becomes infinitely large ($St \longrightarrow \infty$), by overriding the non-determination in equation (15) we obtain:

$$P = 1 - \left(1 - \frac{p_A^0}{p_A^i}\right) X. \tag{16}$$

Thus it may be said that for large values of Stanton number ($St \longrightarrow \infty$) the dependences $P = f(X)$ are practically linear.

3. Results and Discussion

Using equation (15) the values of the ratio $P = p_A^0/p_A^i$ were computed for the following values of the Stanton number: St=0.2, 1, 2, ∞ and of the ratio p_A^0/p_A^i=0.1, 0.3, 0.5, 0.9.

The obtained results are presented in Figs. 2,...,5. As may be seen, the ratio P and thus the partial pressure of the sublimate decreases in the boundary diffusion layer regardless of the values of the ratio p_A^0/p_A^i and of those of the Stanton number. For small values of the ratio p_A^0/p_A^i the partial pressure variation in the boundary diffusion layer is more obvious than for large values of this ratio.

For large values of the Stanton number ($St > 2$) the dependence $P = f(X)$ is practically linear. Consequently for small velocities of the gaseous phase the partial pressure profile is practically linear.

In Fig. 6 the dependence $P = f(X)$ for p_A^0/p_A^i=0.5 is plotted for several values of the Stanton number. This figure clearly show the way in which the Stanton number influences the partial pressure profile of the A sublimate. For an increasing velocity of the gaseous phase, and thus for decreasing St ($St < 1$) values the dependence $P = f(X)$ is nonlinear. The partial pressure decrease for the A component is more obvious in the first part of the boundary layer. As the Stanton number decreases the partial pressure decrease is more obvious.

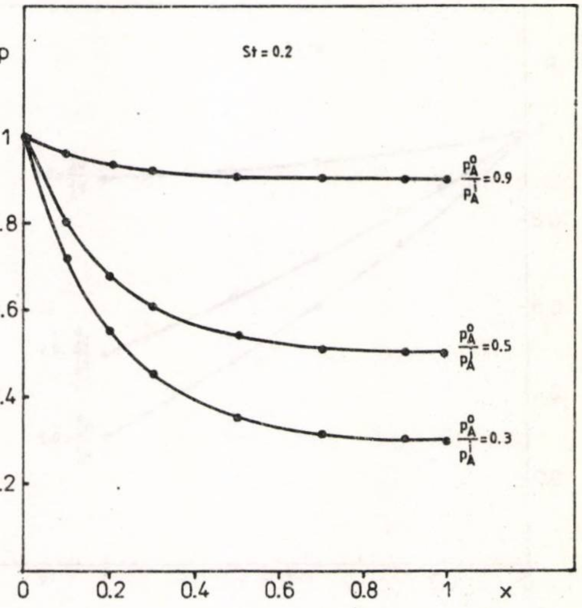

Fig. 2.- The dependence $P = f(X)$, $St=0.2$, $p_A^0/p_A^i=0.3,\ 0.5,\ 0.9$.

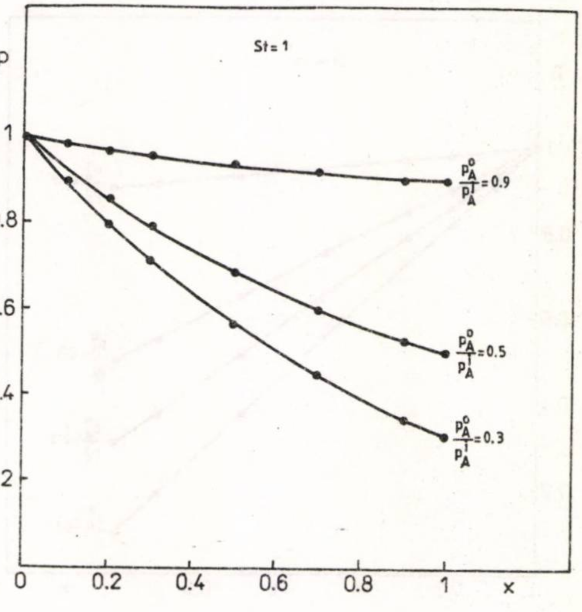

Fig. 3.- The dependence $P = f(X)$, $St=1$, $p_A^0/p_A^i=0.3,\ 0.5,\ 0.9$.

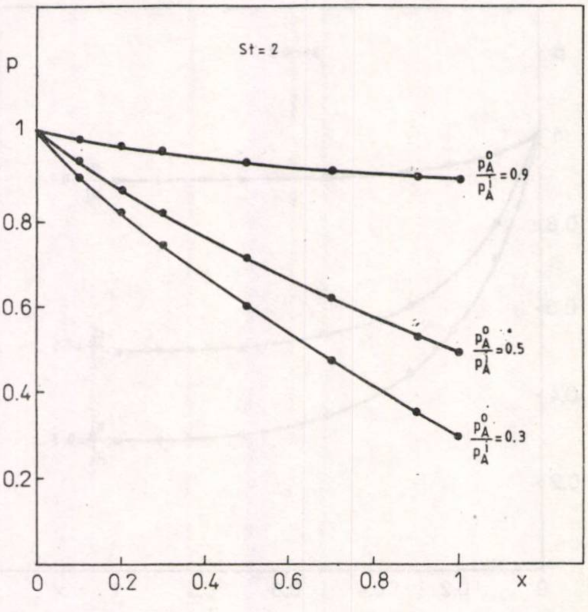

Fig. 4.- The dependence $P = f(X)$, $\mathcal{S}t=2$, p_A^0/p_A^i=0.3, 0.5, 0.9.

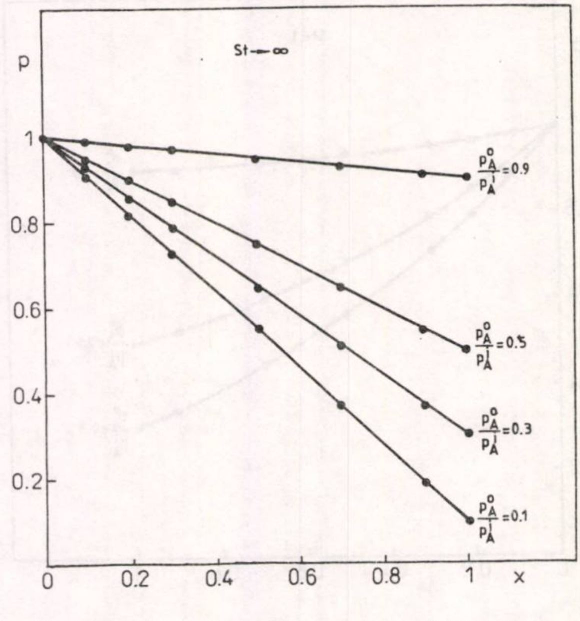

Fig. 5.- The dependence $P = f(X)$, $\mathcal{S}t=\infty$, p_A^0/p_A^i=0.1, 0.3, 0.5, 0.9.

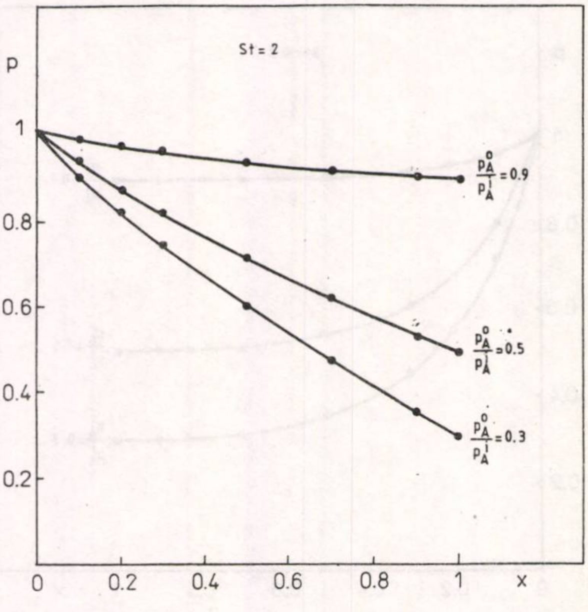

Fig. 4.- The dependence $P = f(X)$, $\mathcal{S}t=2$, $p_A^0/p_A^i=0.3,\ 0.5,\ 0.9$.

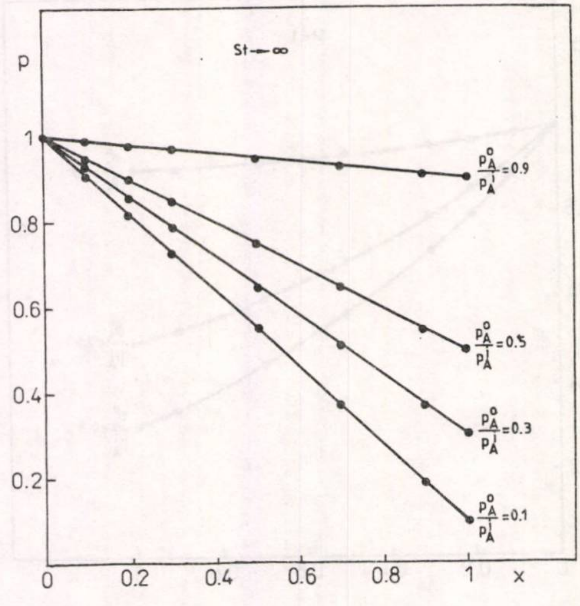

Fig. 5.- The dependence $P = f(X)$, $\mathcal{S}t=\infty$, $p_A^0/p_A^i=0.1,\ 0.3,\ 0.5,\ 0.9$.

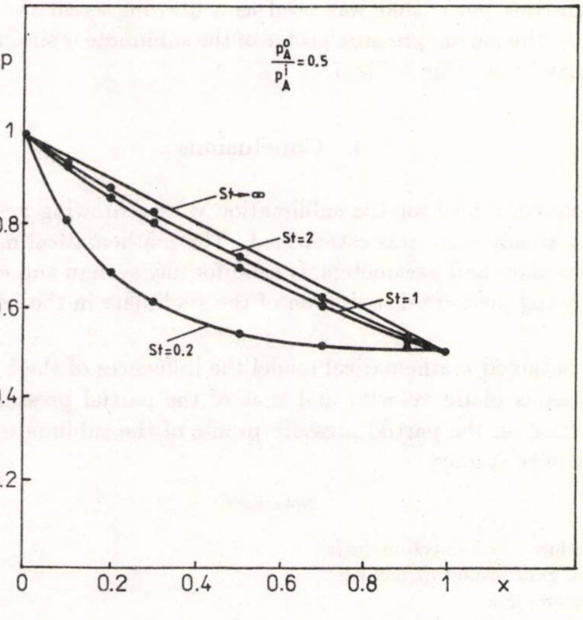

Fig. 6.– The dependence $P = f(X)$, p_A^0/p_A^i=0.5, $\mathcal{S}t$=0.2, 1, 2, ∞.

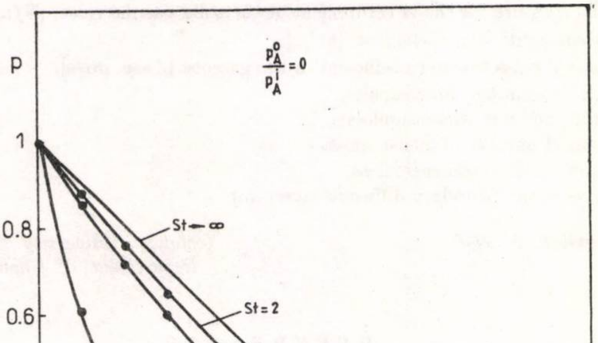

Fig. 7.– The dependence $P = f(X)$, p_A^0/p_A^i=0.2, 1, 2, ∞.

If in the gaseous phase that was used as a drawing agent the A component is missing initially, the partial pressure profile of the sublimate is similar to the previous analyses, as may be seen from Fig. 7.

4. Conclusions

A mathematical model for the sublimation with a drawing agent in isothermal and stationary steady-state was established. The mathematical model contains dimensionless variables and parameters, is valid for any system and enables the determination of partial pressure distribution of the sublimate in the boundary diffusion layer.

Using the obtained mathematical model the influences of the Stanton number, of the gaseous phase velocity and that of the partial pressure in the bulk of the gaseous phase on the partial pressure profile of the sublimate in the boundary diffusion layer were studied.

Notations

$\overline{v}_x$ – mean velocity in x direction, [m/s];
R – universal gas constant, [j/mol K];
T – temperature, [K];
C_A – molar concentration for the A component, [kmol/m^3];
p_A – partial pressure for the A component, [N/m^2];
p_A^0 – partial pressure for the A component in the bulk of the gaseous phase, [N/m^2];
p_A^i – partial pressure for the A component at the solid gas interface, [N/m^2];
D_A – molecular diffusion coefficient, [m^2/s];
k_g – individual mass transfer coefficient in the gaseous phase, [m/s];
$\Re e$ – Reynolds number, dimensionless;
Sc – Schmidt number, dimensionless;
Sh – Sherwood number, dimensionless;
St – Stanton number, dimensionless;
δ – thickness of the boundary diffusion layer, [m].

Received, November 15, 1996

Technical University "Gh.Asachi", Jassy,
Department of Chemical Engineering

REFERENCES

1. Mihăilă G., Szép Al., Calistru C., Ifrim L., J. Chim. Inst. Chem. Engn., **14**, 245-250 (1983).
2. Szép Al., Calistru C., Ifrim L., Mihăilă G., Rev. Chim., **36**, *11*, 1014-1020 (1985).
3. Lombrana J.J., Villaran M.C., J. Chem. Eng. Jpn., **26**, *4*, 389-394 (1993).
4. Larry F.W., Bruce W., William D.J., Appl. Energy., **46**, *2*, 161-169 (1993).
5. Songin H.H., J. Heat Transfer., **113**, *3*, 772-773 (1991).
6. Halder P.K., Amitava D., Proc. 12th Int. Conf. Fluid. Bed Combust., vol.**2**, 1993, 1223-1227.
7. Jouli R., Rios G.M., Drying Technol., **11**, *1*, 157-182 (1993).
8. Peng S.W., Chen G.Q., Int. Energy. Res., **17**, *3*, 193-202 (1993).

TRANSFER DE MASĂ LA SUBLIMARE
Distribuţia presiunii parţiale în stratul limită de difuzie

(Rezumat)

Se prezintă un model matematic al procesului de sublimare cu agent de antrenare, în regim izoterm şi staţionar. Modelul matematic conţine numai variabile adimensionale şi parametri, fiind utilizat pentru studiul influenţei numărului Stanton, vitezei fazei gazoase şi presiunii parţiale din volumul fazei gazoase asupra profilului presiunii parţiale în stratul limită de difuzie pentru substanţa care sublimează.

BULETINUL INSTITUTULUI POLITEHNIC DIN IAŞI
Tomul XLIII (XLVII), Fasc. 1–2, 1997
Secţia II
CHIMIE şi INGINERIE CHIMICĂ

C.D. 541.57; 546.11

CONSIDÉRATIONS SUR LES ASSOCIATIONS MOLÉCULAIRES PAR LIAISONS HYDROGÈNE

PAR

SAVEL IFRIM

On présente quelques considérations concernant la nature électrostatique des associations moléculaires par ponts hydrogène, en soulignant le fait que ces associations représentent une catégorie de liaisons spécifiques, générées par un mécanisme propre (particulier) et elles sont caractéristiques seulement pour certaines molécules.

On propose quelques principes théoriques généraux, confirmés par la pratique, qui peuvent mieux expliquer la nature des liaisons hydrogène. On introduit dans ce but la notion de „densité électronique périphérique“ des ions, en soulignant son rôle de former des associations moléculaires par ponts hydrogène.

On met en évidence, par données calculées, l'importance de la densité électronique périphérique des atomes électronégatifs, parmi lesquels se trouve l'atome d'hydrogène.

On calcule la densité électronique péripherique pour plusieurs anions de la composition de leurs hydrures et on constate que seulement les anions ayant une densité plus élevée forment de ponts hydrogène plus forts. On met en évidence l'influence de la structure chimique de la molécule toute entière sur la formation des ponts hydrogène inter- ou bien intramoléculaires.

On propose l'utilisation de la dénomination d'„association moléculaires par ponts hydrogène“ ou bien „liaisons par ponts hydrogène“, qui reflète mieux la réalité, que la dénomination d'associations par liaisons hydrogène.

1. Introduction

Associations moléculaires par liaisons hydrogène apparaissent tant pour les molécules identiques (self-association) que pour les molécules différentes (mixed-association). Associations par liaisons hydrogène se trouvent entre molécules à petites dimensions, entre molécules ayant de plus grandes dimensions et également entre les macromolécules. Les liaisons hydrogène sont du type intermoléculaire et intramoléculaire, avec la condition que la structure chimique de la molécule puisse générer ce type de liaisons.

En dépit de la nature ou des dimensions des molécules associées par liaisons hydrogène, pour la formation de ce type de liaisons, à l'exception de l'atome d'hydrogène, sont impliqués quelques atomes électronégatifs; plus fréquemment apparaît l'atome d'oxygène, ensuite l'atome d'azote, quelques atomes d'halogènes et seulement pour certaines structures chimiques on peut également trouver l'atome de soufre [1], [2].

La condition fondamentale afin d'établir des liaisons hydrogène est que cet atome, ayant les plus petites dimensions - l'hydrogène - soit placé entre ces atomes électronégatifs.

Le but de cet article est d'élaborer une explication plus générale concernant la génération des associations moléculaires par liaisons hydrogène, n'importe où ces liaisons sont formées.

2. La nature des liaisons hydrogène

Les liaisons hydrogène sont de nature électrostatique. Bien qu'il existe plusieurs atomes électronégatifs, ayant des configurations électroniques identiques sur la dernière couche, ces atomes ne sont pas toutefois tous capables d'influencer le noyau de l'atome d'hydrogène limitrophe, afin de générer des liaisons hydrogène.

Il y a des opinions selon lesquelles l'établissement des liaisons hydrogène peut être expliqué par la présence des paires d'électrons libres, nonparticipants, comme se trouvent dans le cas des atomes de fluor, d'oxygène ou de l'azote [3], dans leur combinaisons avec l'hydrogène. Si cette hypothèse réfléchiraient la réalité, il faudrait être également associées par liaisons hydrogène les molécules des autres combinaisons chimiques avec l'hydrogène, ayant des atomes électronégatifs, par exemple: l'acide bromhydrique, l'acide iodhydrique ou l'acide sulfhydrique, l'acide sélenhydrique, l'hydrogène telluré ainsi que la phosphine (H_3P) et l'arsine (H_3As). Mais, pratiquement, dans le cas de ces hydrures, les associations moléculaires par liaisons hydrogène ne sont pas mises en évidence. Par conséquent l'opinion que seulement les électrons nonparticipants sont impliqués dans la formation des liaisons hydrogène n'est pas confirmée par la pratique et, en conclusion, elle ne peut pas être généralisée.

Les liaisons hydrogène ne sont ni des liaisons covalentes, ni des liaisons de coordination, ni des liaisons ioniques non-plus. Elles représentent un type de liaisons spécifiques, totalement particulières, étant caractéristiques à certaines molécules. Ce type de liaisons est généré par un mécanisme propre.

La formation des liaisons hydrogène peut être mieux expliquée si on prend en considération les principes suivants:

1° Le rôle important pour l'établissement des liaisons hydrogène est manifesté par la densité électronique périphérique des atomes électronégatifs entre lesquels se trouve l'atome d'hydrogène.

2° Les propriétés chimiques d'un atome ne sont pas déterminées seulement par certains électrons; il faut admettre que l'atome tout entier génère ses propriétés.

3° La formation des associations moléculaires par liaisons hydrogène ne peut pas être expliquée seulement par la présence d'un atome unique ou bien d'un groupe d'atomes.

4° La structure chimique de la molécule toute entière influence l'apparition de ce type de liaisons chimiques, puisque même la densité électronique périphérique des atomes électronégatifs se trouvant dans la molécule associée est influencée par cette structure.

L'association des molécules par liaisons hydrogène n'est pas générée par la simple présence de l'atome d'hydrogène; particulièrement l'électronégativité des atomes entre lesquels se trouve l'atome d'hydrogène détermine cette association.

Ces atomes électronégatifs peuvent appartenir à la même molécule à laquelle appartient également l'hydrogène impliqué dans la formation de la liaison, mais ils peuvent appartenir aussi à des autres molécules identiques ou différentes.

La liaison covalente par laquelle l'atome d'hydrogène est lié aux atomes électronégatifs est de nature polaire et, par conséquent, son noyau, c'est-à-dire le proton, est moins écrané par une onde de très faible densité électronique, se trouvant dans l'orbitale 1 s. La présence, du point de vue géométrique, de l'autre atoms électronégatif attire un peu ce noyau. De cette manière il se fait un pont entre les deux atomes électronégatifs par l'intermédiaire de l'atome d'hydrogène. Il est donc plus correctement de nommer associations moléculaires par ponts hydrogène, ou bien liaisons par ponts hydrogène, qu'associations par liaisons hydrogène.

Mais, afin que la force électronégative puisse se manifester sur le proton, il faut exister une certaine densité électronique sur la surface de l'atome électronégatif. En prenant comme exemple les combinaison de l'hydrogène avec quelques éléments électronégatifs, à savoir: azote, phosphore, arsenic ou oxygène, soufre, sélénium, tellure et fluor, chlore, brome, iode et sachant que dans ces hydrures chaque atome électronégatif possède des paires d'électrons nonparticipants, en conditions normales de pression et température, les molécules de ces combinaisons devraient être associées par ponts hydrogène.

Mais, la pratique démontre que seulement une densité électronique plus élevée sur la surface des atomes électronégatifs génère des ponts hydrogène. Une densité électronique péripherique plus élevée existe seulement sur les atomes ayant les plus petits rayons et justement ce sont les atomes plus électronégatifs, formant les ponts hydrogène plus forts. Cette densité électronique périphérique σ peut être obtenue à l'aide de la relations:

$$\sigma = \frac{Ne}{S}, \quad \text{[coulombs]},$$

où: N est le nombre d'électrons sur la surface de l'anion; e – la charge électrique de l'électron ($1{,}602 \cdot 10^{-19}$ coulombs); S – la surface de l'anion.

Si l'on considère la forme sphérique des anions, la relation devient:

$$\sigma = \frac{Ne}{4\pi r^2};$$

ici r représente le rayon de l'anion, [Å]. A l'aide de cette relation on a calculé la densité σ pour tous les anions impliqués dans les molécules des hydrures mentionnés ci-dessus; les données obtenues sont présentées dans le Tableau 1, à côté de quelques caractéristiques des produits respectifs, en conditions normales de pression et température.

Tableau 1

Produit	Etat physique	Poids moléculaire	Point d'ébulition, [°C]	Point de fusion °C	Rayon ionique Å	σ coulombs	Molécules
HF	liquide	20,01	19,5	–83	1,36	$0{,}551 \cdot 10^{-19}$	associées
HCl	gaz	36,46	–84,9	–114,8	1,81	$0{,}311 \cdot 10^{-19}$	peu associées
HBr	gaz	80,92	–67,0	–87	1,95	$0{,}268 \cdot 10^{-19}$	nonassociées
HI	gaz	127,92	–35,7	–50,8	2,16	$0{,}218 \cdot 10^{-19}$	nonassociées
H_2O	liquide	18,01	100	0	1,40	$0{,}520 \cdot 10^{-19}$	associées
H_2S	gaz	34,07	–60,2	–83	1,84	$0{,}301 \cdot 10^{-19}$	nonassociées
H_2Se	gaz	80,98	–42,0	–64	1,98	$0{,}260 \cdot 10^{-19}$	nonassociées
H_2Te	gaz	129,63	–4,0	–51	2,21	$0{,}208 \cdot 10^{-19}$	nonassociées
H_3N	gaz	17,03	–33,3	–77,7	1,71	$0{,}348 \cdot 10^{-19}$	peu associées
H_3P	gaz	34,00	–87,4	–133	2,12	$0{,}226 \cdot 10^{-19}$	nonassociées
H_3As	gaz	77,93	–55	–119	2,22	$0{,}206 \cdot 10^{-19}$	nonassociées

Les valeurs des rayons sont celles des anions monovalents, bivalents et respectivement trivalents.

3. Discussions

Les caractéristiques physiques des produits du Tableau 1 confirment la présence des associations moléculaires pour quelques produits, bien connus. On observe que le plus petit rayon ionique se trouve chez l'anion fluor, dont la surface a la densité électronique la plus élevée. Cette densité électronique explique l'apparition des ponts hydrogène pour les molécules de l'acide fluorhydrique, ponts ayant une grande énergie, de 6,8 kcal/mol à l'état gazeux [4] et beaucoup plus grande à l'état cristallin, à savoir 23 kcal/mol. Dans le cas des molécules de l'eau, à l'état cristallin, l'énergie des ponts hydrogène est de 6,1 kcal/mol, tandis que dans le cas de l'ammoniac, à l'état cristallin, cette énergie est beaucoup plus petite, seulement de 1,3 kcal/mol. Cette diminution de l'énergie à partir de l'anion de fluor vers l'anion d'oxygène, azote et chlore, est en accord avec la diminution de la densité électronique périphérique de ces ions.

La densité électronique plus élevée sur l'anion de fluor par rapport aux autres anions des halogènes est confirmée également par les chaleurs d'hydratation des anions (kcal/mol), qui diminuent à partir de l'anion de fluor vers celui de iode [5]:

$$Q\mathrm{F}^- = 128; \quad Q\mathrm{Cl}^- = 96,9; \quad Q\mathrm{Br}^- = 92,2; \quad Q\mathrm{I}^- = 85,8.$$

L'hydratation des ions a lieu par interactions ion–dipôle, la molécule d'eau étant dipolaire. L'anion de fluor ayant une densité électronique périphérique plus grande, attire plus fortement le pôle positif de la molécule de l'eau en résultant une chaleur d'hydratation plus élevée.

Il est connu que l'ammoniac forme des ponts d'hydrogène plus forts avec l'acide fluorhydrique, ensuite avec de l'eau, qu'avec lui même [6]. Ainsi les dimères mixtes formés avec NH_3 et HF, ou bien NH_3 et H_2O sont plus stables que les dimères de l'ammoniaque. Ce fait concorde et confirme le premier principe énoncé dans cet article. En effet cette stabilité, respectivement cette énergie plus élevée des ponts hydrogène dans le cas des dimères mixtes, peut être expliquée par l'attraction plus puissante sur l'hydrogène, lié par covalence à l'azote, attraction excercée par l'atome de fluor et d'oxygène; ce sont les atomes ayant une densité électronique périphérique plus élevée. La structure de ces associations entre molécules nonidentiques doit être H_2N–H...F–H et également H_2N–H...H–O–H.

Il est bien connu que la solution aqueuse d'ammoniac contient, à côté d'ions NH_4^+ et OH^-, aussi de l'ammoniac libre; seulement celui-ci peut former d'associations par ponts hydrogène avec les molécules de l'eau. A des températures basses on a obtenu un hydrate d'ammoniac $H_3N \cdot H_2O$, à l'état cristallin, avec P.F.=–79°C. Dans ce hydrate les molécules d'ammoniac sont liées par ponts hydrogène avec les molécules de l'eau, en formant de longues chaînes [7]. Celles-ci sont réticulées avec des ponts hydrogène par l'intermédiaire des molécules d'ammoniac. Même dans ce cas ce sont les atomes d'oxygène, qui, par leur densité électronique périphérique attirent les atomes d'hydrogène de l'ammoniac.

L'apparition des ponts hydrogène est signalée aussi dans le cas des molécules d'ammoniac et HCl [8]. Sans doute dans ce cas les molécules sont parfaitement anhydres, de sorte qu'elles puissent former d'association par ponts hydrogène, selon le schéma: H_3N...H–Cl. Cette structure précède la formation du chlorure d'ammonium.

La liaison entre hydrogène et chlore dans la molécule d'acide chlorhydrique est fortement polaire; par conséquent la densité électronique sur l'atome d'hydrogène est bien diminuée et comme c'était à prévoir, la densité électronique périphérique de l'atome d'azote attire le proton et il se fait un pont d'hydrogène.

Le fait que les associations moléculaires par ponts hydrogène sont générées grâce à la densité électronique périphérique des atomes électronégatifs est soutenu également par l'association des molécules de LiF [9]; dans ce cas il apparaissent des ponts de lithium: Li–F...Li–F...Li–F.

La présence des ponts hydrogène intramoléculaires sont mises en évidence aussi dans le cas des phénols *o*-halogénés [10], mais seulement pour la configuration *cis*:

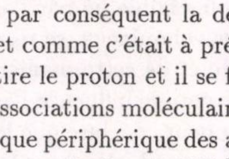

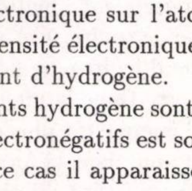

Grâce à l'effet inductif $-I$ de l'atome de chlore, effet plus fort que celui de conjugaison, la densité électronique périphérique est plus élevée sur cet atome. L'effet $-I$ du chlore est favorisé par l'effet de conjugaison des électrons nonparticipants se trouvant sur l'oxygène phénolique et pour la même raison, l'hydrogène phénolique tend vers protonisation. Cet hydrogène est attiré par la densité électronique périphérique de l'atome de chlore et il se fait un pont d'hydrogène entre les deux atomes électronégatifs. Si l'atome d'hydrogène phénolique se trouve en position *trans*, les deux atomes étant plus éloignés l'un par rapport à l'autre, l'atome de chlore ne peut plus attirer cet atome d'hydrogène et donc il n'y a pas de pont hydrogène.

Le groupement –SH, dans les molécules des thiols, ne forme pas des ponts hydrogène notables [11], mais dans le cas d'*ortho*-aminothiophénol et d'*ortho*-thioanisidine l'atome de soufre est impliqué dans la formation des ponts hydrogène. Plus encore, ces ponts d'hydrogène sont bien plus forts que ceux qui existent dans les molécules d'*ortho*-aminophénol ou d'*ortho*-anisidine [2]. Dans ce cas aussi l'apparition des ponts hydrogène est déterminée par la structure de la molécule toute entière.

Dans la molécule d'*ortho*-aminophénol l'effet de conjugaison entre le noyau aromatique et les électrons libres de l'oxygène est plus fort que dans le cas de l'atome d'azote et l'hydrogène est bien lié par l'azote.

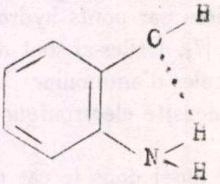

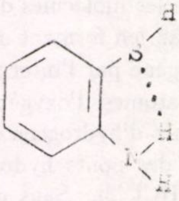

En même temps la densité électronique périphérique sur l'oxygène est plus faible et celui-ci attire moins l'hydrogène de l'azote. Pour la molécule de l'*ortho*-thiophénol, c'est l'effet de conjugaison entre le noyau aromatique et l'atome d'azote qui est le plus fort. Par conséquent l'hydrogène est plus faible lié par l'azote et il peut être attiré par l'atome de soufre. Cet atome, plus volumineux, se trouve plus proche par rapport à l'atome d'hydrogène lié sur l'azote et de cette manière il se fait un pont hydrogène plus fort. Donc la molécule toute entière influence l'apparition des ponts hydrogène dont l'énergie est plus élevée. On peut conclure que le même atome peut être impliqué, ou non, dans la formation des ponts hydrogène. Cette implication est déterminée par la structure chimique de la molécule, dans laquelle l'atome respectif se trouve lié par covalence.

4. Conclusions

On étudie et on discute la nature des liaisons hydrogène. On propose quelques principes vérifiés par la pratique, qui expliquent mieux la formation des associations intermoléculaire par liaisons hydrogène. On souligne le rôle important de la densité électronique périphérique des atomes électronégatifs afin de former des liaisons hydrogène; on calcule cette densité pour plusieurs atomes se trouvant dans la composition des molécules associées ou nonassociées et on constate que les atomes ayant une densité électronique périphérique plus élevée déterminent la formation des ponts hydrogène plus forts.

On mentionne l'importance de la structure chimique de la molécule toute entière concernant la formation des liaison hydrogène. On suggère de nommer „associations moléculaires par ponts hydrogène", ou bien „liaisons par ponts hydrogène" au lieu d'associations par liaisons hydrogène.

Reçue le 11 novembre 1996

Université Technique „Gh.Asachi“, Jassy,
Chaire de Chimie générale

BIBLIOGRAPHIE

1. Sherry A.D., Purcell K.F., J. Amer. Chem. Soc., **94**, *6*, 1848 (1972).
2. Krueger P.J., Tetrahedron, **26**, 4753 (1970).
3. Kollman A.P., J. Amer. Chem. Soc., **94**, *6*, 1837 (1972).
4. Murgulescu I.G., *Introducere în Chimia Fizică*. Vol. **I**, *1*, Ed. Acad. Române, Bucureşti, 1976, 216.
5. Negoiu D., *Tratat de Chimie Anorganică*. Vol. **II**, Ed. Tehn., Bucureşti, 1972, 86.
6. Kollman P.A., Allen L.C., J. Amer. Chem. Soc., **93**, *20*, 4991 (1971).
7. Neniţescu C.D., *Chimie Generală*. EDP, Bucureşti, 1972, 727, 901.
8. Clementi E., J. Chem. Phys., **46**, *10*, 3851 (1967).
9. Kollman A.P., Liebman J.F., Allen L.C., J. Amer. Chem. Soc., **92**, *5*, 1149 (1970).
10. Brown I., Eglinton G., Martin-Smith M., Spectrochim. Acta, **18**, *12*, 1592 (1962).
11. Roberts J.D., Caserio M.C., *Chimie Organique Moderne* (édition française). Ediscience, Paris, 1968, 544.

CONSIDERAŢII ASUPRA ASOCIAŢIILOR MOLECULARE PRIN LEGĂTURI DE HIDROGEN

(Rezumat)

Se fac câteva consideraţii privind natura electrostatică a asociaţiilor moleculare prin punţi de hidrogen, subliniindu-se faptul că acestea reprezintă o categorie de legături specifice, generate printr-un mecanism propriu şi sunt caracteristice numai anumitor molecule, organice sau anorganice.

Se propun câteva principii teoretice generale, confirmate de practică, cu ajutorul cărora se poate explica mai bine natura legăturilor de hidrogen. În acest sens se introduce noţiunea de „densitate electronică periferică a ionilor“, se subliniază rolul determinant al acesteia în formarea asociaţiilor moleculare prin punţi de hidrogen, indicându-se prin date concrete importanţa densităţii electronice periferice a atomilor electronegativi, între care se găseşte atomul de hidrogen.

Se calculează densitatea electronică periferică pentru mai mulţi anioni din componenţa hidrurilor lor şi se constată că numai anionii cu densitate electronică periferică mai ridicată formează punţi de hidrogen mai puternice.

Se scoate în evidenţă, prin exemple concrete, influenţa structurii chimice a moleculei întregi asupra stabilirii punţilor de hidrogen inter- sau intramoleculare.

Se propune folosirea denumirii de „asociaţii moleculare prin punţi de hidrogen“ sau „legături prin punţi de hidrogen“, care reflectă mai bine realitatea, decât asociaţii prin legături de hidrogen.

BULETINUL INSTITUTULUI POLITEHNIC DIN IAŞI
Tomul XLIII (XLVII), Fasc. 1–2, 1997
Secţia II
CHIMIE şi INGINERIE CHIMICĂ

D.C. 667.212; 004.86; 628.54

REMOVERAL OF REACTIVE DYES FROM WASTE WATERS USING ION EXCHANGERS

BY

DANIELA ŞUTEU, DOINA BÎLBĂ and VALERIA-MARTA GORDUZA

The ability of styrene–divinylbenzene copolymers type to remove reactive dyes from aqueous solutions was investigated. The thermodynamic sorption of the reactive dye Brilliant Red HE-3B on ion exchangers was studied using Langmuir isotherm equation at different temperatures. Other adsorption parameters studied were: initial dye concentration, the temperature and the amount of sorbent. The obtained results show that ion exchangers utilized have a relative low retention capacity for the reactive dyes from diluted solutions, the Purolite A-400 proving to be more efficient.

1. Introduction

Decontamination of the natural waters impurified with industrial effluents containing different organic substances including dyes, is an essential problem in environmental protection [1].

The literature offers limited informations concerning both dyes concentrations in natural waters and long term toxicities of the dyes [2]. Due to high number of utilized dyes and their structural diversity, a general method for elimination of residual dyes is practically impossible.

For decontamination of waste waters impurified with dyes, some methods including precipitation of the dyes with metallic salts [2], sorption on activated carbon [3],...,[5], chitin and chitosan [6],...,[8], nonconventionally celluloses sorbents [1], [9],...,[12], synthetic polymers [13], [14] and ion exchangers [15] have been proposed.

The aim of this paper is to determine the retention conditions for reactive dyes of monochlortriazinic type that could be found in waste waters by sorption on anionic resins from styrene–divinylbenzene type copolymers.

2. Experimental

The sorption experiments of monochlortriozinic bifunctional reactive dye Red Brilliant HE-3B on three types of ion exchangers (s. structure below) have been accomplished using a stock aqueous solution (1.367×10^{-2} M) from of which working solutions with $(6.835...1.367)\times10^{-5}$ M $((0.1...2)\times10^{-2}$ mg/L), concentration were prepared. Dye concentration was determined by spectrophotometric method, using a Carl Zeiss Jena spectrophotometer.

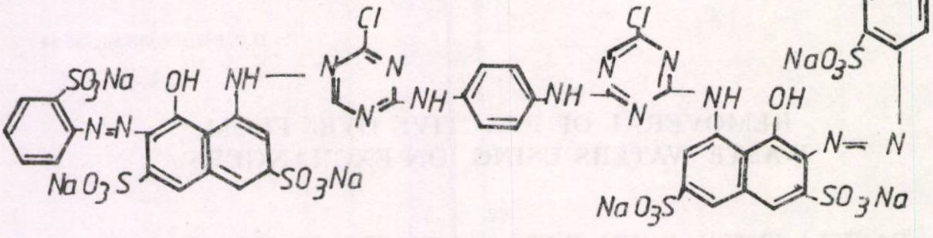

Strong basic anionites (Cl⁻ form): Vionit AT-1 and Purolite A-400 and a strong basic sorbent Amberlite IRA-401S have been used as ion exchangers. The above mentioned resins are styrene–divinylbenzene copolymers with quaternary ammonium groups (type *I*), gel structure and ionic exchange capacity of 1.1...1.3 mval/mL.

The study of Brilliant Red HE-3B dye retention on different types of resins have been carried out in static conditions, using samples of about 0.2 g sorbent and 20...100 ml solutions containing determined amounts of dye.

After a certain time of contact the phases were separated by filtration and in solution the unretained amount of dye was spectrophotometrically determinated.

3. Results and Discussion

To find the proper retention conditions for Briliant Red HE-3B dye on different anionites, the effect of pH, temperature, type and amount of sorbent, initial concentration of dye and electrolyte amount have been studied.

The amount of dye retained on anionites increased with contact time, reaching a maximum constant value after 70...80 min. (Fig. 1).

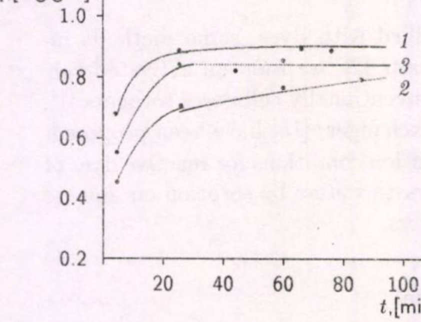

Fig. 1.– Effect of time contact on removal Brilliant Red HE-3B by: *1* – Vionit AT-1, *2* – Purolite A-400, *3* – Amberlite IRA 401-S; dye concentration, 10 mg/L.

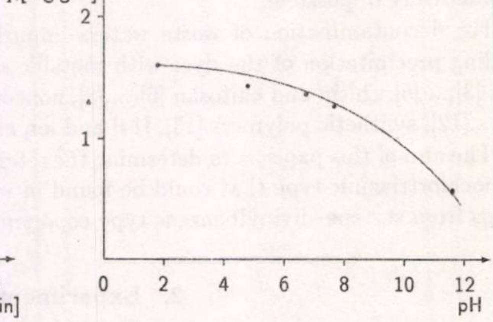

Fig. 2.– Removal of Brilliant Red HE-3B as a function of pH, on Purolite A-400 (mg dye retained per g vs. pH); dye concentration, 7 mg/L.

Due to its high molecular weight, the dye diffusion into the internal porous structure of the ion exchangers is difficult thus the equilibrium is rapid attained. In this case is prevalent the physical sorption against the ion exchange process:

$$(1)\qquad [\mathrm{Resin}^{+}]\mathrm{Cl}^{-} + \mathrm{Dye} - \mathrm{SO}_3^{(-)}\mathrm{Na}^{(+)} \longrightarrow [\mathrm{Resin}^{+}]\mathrm{SO}_3^{(-)} - \mathrm{Dye} + \mathrm{Na}^{+}\mathrm{Cl}^{-}$$

Ion exchange process has been emphasized determining the liberated chlorine by potentiometric titration with 0.02 N $AgNO_3$ solution.

The high values of dye retention in acid medium (pH=2...6) have been found (Fig. 2).

In alkaline medium the competition between hydroxyl ions from solution and dye anions for ion exchangers centers of the resin is very important.

The waste waters purification from monochlortriazinic reactive dye is less influenced by electrolytes presence (Na_2SO_4, Na_2CO_3).

The results represented in Fig. 3 show an increase of retained dye amount with temperature increase for all types of tested exchangers.

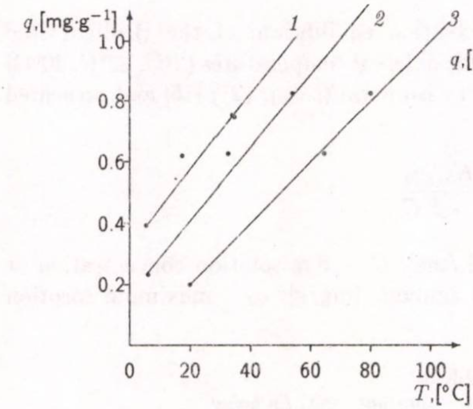

Fig. 3.– Influence of temperature at reactive dye retention on: *1* – Vionit AT-1, *2* – Purolite A-400, *3* – Amberlite IRA 401-S; dye concentration, 10 mg/L.

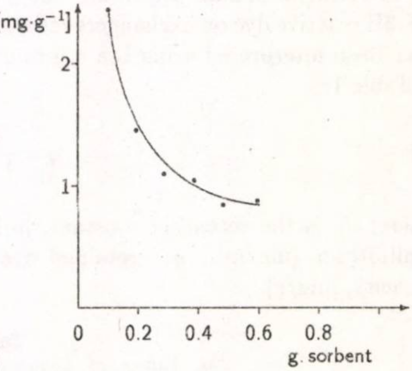

Fig. 4.– Effect of ion exchange dosage on the removal of Brilliant Red HE-3B by Purolite A-400; dye concentration, 10 mg/L.

Both the diffusion rate of dye molecules to the resin surface and retention properties of the anionites are influenced by the temperature.

The dye fixation is dependent on the resin amount utilized (Fig. 4).

Gel structure of the used ion exchange unfavours the bulky molecules penetration of the dye fact that explain the low retention obtained.

The initial concentration of the dye influences the fixation on the resin (Fig. 5). The retained amount increases with dye concentrations until maximum value corresponding to the theoretical sorption capacity of the used resin is attained.

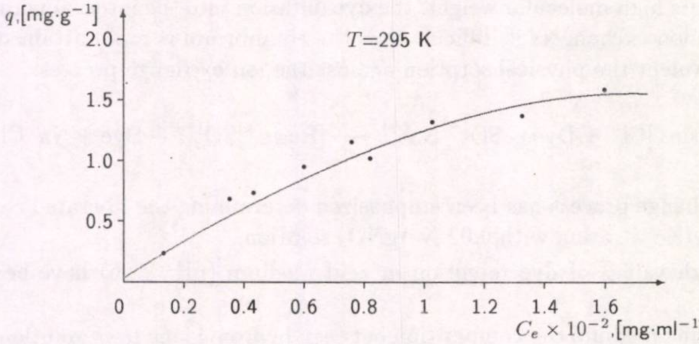

Fig. 5.– Effect of dye concentration on removal of Brilliant Red HE-3B by Purolite A-400 at a temperature of 22°C.

4. Absorption Isotherms

Experimental data regarding the retention equilibrium of the Brilliant Red HE-3B reactive dye on exchangers resins, at different temperatures (2°C, 22°C, 40°C) have been interpreted using Langmuir isotherm (s. eq. (2)) [16] and presented in Table 1:

$$q = \frac{KC_e q_0}{1 + KC_e}, \tag{2}$$

where: K is the retention constant, [mL/mg]; C_e – dye solution concentration at equilibrium, [mg/mL]; q – retained dye amount, [mg/g]; q_0 – maximum sorption capacity, [mg/g].

Table 1

The Values of Langmuir Constant and Enthalpy to Brilliant Red HE-3B Reactive Dye Removal

Sorbent	T	Langmuir constant		Enthalpy ΔH
	K	K_L L/g	q_0 mg/g	cal/mol
Vionit AT-1	275	0.148	3.08	+5,677.1
	295	0.235	4.00	
	313	0.440	8.00	
Amberlite IRA 401-S	275	0.6896	4.54	+6,620.0
	295	1.1111	4.76	
	313	1.818	5.71	
Purolite A-400	275	0.1064	2.17	+8,639.0
	295	0.1923	3.84	
	313	0.3571	6.23	

For these three types of resins, the plots $1/q$ vs. $1/C_e$ at different temperatures, allows the calculation of K and q_0 values.

Langmuir equation constant requested for some thermodynamic parameters determination has been calculated using the equation:

$$K_L = q_0 b, \tag{3}$$

where: $b = K/1000$, [L/mg]; K_L – Langmuir constant, [L/g].

The enthalpy variation (ΔH) was determined with the relation:

$$\mathrm{d} \ln K_L = -\frac{\Delta H}{R} \mathrm{d}\left(\frac{1}{T}\right). \tag{4}$$

For example, in Fig. 6 is presented the dependence $\ln K_L = f(1/T)$ for the ion exchange process: dye →IRA 401 S. The slope of the straight line, $\mathrm{tg}(\alpha) = -\Delta H/R$, allowed the exchange enthalpy evaluation.

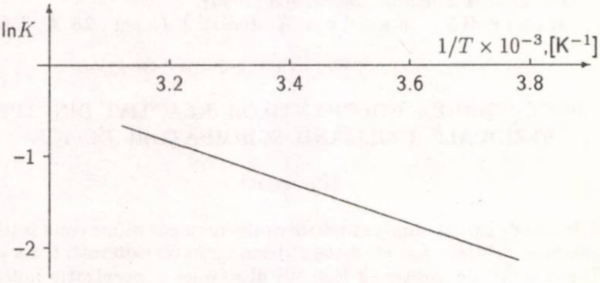

Fig. 6.– Langmuir plot for the retention of Brilliant Red HE-3B on Ambelite IRA 401-S at: *1* – 2°C, *2* – 22°C, *3* – 40°C.

The positive values of enthalpy (ΔH) demonstrate that retention processes are endotherme and the increase of temperature influences positively the fixed amount.

5. Conclusions

The sorption conditions for Brilliant Red HE-3B reactive dye of monochlortirazinic bifunctional type on ion exchangers with gel structure (Vionit AT-1, Amberlite IRA-401 S, Purolite A-400) in batch conditions have been studied.

The effect of different factors (pH, temperature, concentration, time) on sorption has been determined, the dye measurement being carried out by a spectrophotometric method.

The adsorption Langmuir isotherms at three different temperatures have been determined and the characteristic thermodynamic parameters were estimated.

Even in diluted solutions of dyes, the three types of ion exchangers with gel structure had a relative low retention capacity.

The retention capacity increases with temperature increasing the Purolite A-400 exchanger proving to be more efficient.

Received, July 26, 1996

Technical University "Gh.Asachi", Jassy,
Department of Analytical Chemistry

REFERENCES

1. Shukla S.R., Sakhardante V.D., Dyes and Pigments, **17**, 11 (1991).
2. Hou Miaolin; Dyes and Pigments, **18**, 35 (1992).
3. McKay G.J., J. Chem. Tech. Biotechnol., **32**, 759 (1982).
4. McKay G.J., J. Chem. Tech. Biotechnol., **32**, 773 (1982).
5. McKay G., Chem. Eng. Res. Des., **61**, 29 (1983).
6. McKay G., Blair H.S., Garner J.R., J. Coll. Interface Sci., **95**, 108 (1983).
7. McKay G., Blair H.S., Garner J.R., J. Appl. Polym. Sci., **29**, 1499 (1984).
8. McKay G., Blair H.S., Garner J.R., J. Appl. Polym. Sci., **30**, 4325 (1985).
9. Namasivayam C., Kanchana N., Chemosphere, **25**, 1621 (1992).
10. Shukla S.R., Sakhardante V.D., J. Appl. Polym. Sci., **42**, 829 (1991).
11. Shukla S.R., Sakhardante V.D., Dyes and Pigments, **17**, 101 (1991).
12. Low K.S., Lee C.K., Pertanika, **13**, 221 (1990).
13. Hwang M.C., Chen K.M., J. Appl. Polym. Sci., **49**, 975 (1993).
14. Hwang M.C., Chen K.M., J. Appl. Polym. Sci., **50**, 735 (1993).
15. Ignatov Iu.I., Zhur. Fiz. Khim., **54**, *2*, 406 (1980).
16. McKay G., Blair H.S., Fendon A., Indian J. Chem., **28 A**, 356 (1989).

RECUPERAREA COLORANŢILOR REACTIVI DIN APE REZIDUALE UTILIZÂND SCHIMBĂTORI DE IONI

(Rezumat)

Schimbătorii de ioni de tip copolimer stiren–divinilbenzen pot reţine coloranţi reactivi din soluţii apoase. Termodinamica sorbţiei a fost studiată utilizând ecuaţia izotermei Langmuir la diferite temperaturi. Alţi parametri de sorbţie au fost: pH-ul soluţiei, concentraţia iniţială a colorantului, timpul de contact, temperatura, cantitatea de schimbător de ioni.

S-a dovedit că schimbătorii de ioni folosiţi au o capacitate limitată de recuperare a coloranţilor reactivi monoclortriazinici din soluţii apoase diluate, Purolite A-400 dovedindu-se a fi mai eficient.

BULETINUL INSTITUTULUI POLITEHNIC DIN IAŞI
Tomul XLIII (XLVII), Fasc. 1–2, 1997
Secţia II
CHIMIE şi INGINERIE CHIMICĂ

D.C. 678.746.22

ON THE MORPHOLOGY OF POLY(N-ACETYLIMINOETHYLENE)/POLYVINYL BLOCK COPOLYMERS

BY

CRISTOFOR I. SIMIONESCU,
Member of the Romanian Academy

AURELIA IOANID, GETA DAVID and BOGDAN C. SIMIONESCU

The morphology of some block copolymers containing hydrophilic, crystallizable poly(N-acetyliminoethylene) and hydrophobic, amorphous polyvinyl (polystyrene, various polymethacrylates) sequences was studied by transmission electron microscopy technique as a function of solvent nature, rate of solvent evaporation and thermal history of the samples. Application of a thermal treatment and a careful solvent evaporation favours the obtention of thermodynamical stable morphologies.

1. Introduction

The morphology of the block copolymers is one of the most important research subjects in polymer science, since many of their useful properties, such as permeability, thermal, mechanical and rheological behaviour, strongly depend upon their microdomain structures. Considerable theoretical and experimental efforts have been devoted to the study of the microphase separation in these polymers (in melt or after solvent casting) in order to find the structure–properties relationships prerequisite to a control of their characteristics. .Several theoretical models on the morphology of block copolymers, with valuable predictive abilities, were elaborated [1],...,[3].

In block copolymers with amorphous blocks the microphase separation is essentially determined by copolymer chain composition, statistical segment lengths and the temperature dependent parameter χ (i.e., the Flory-Huggins interaction parameter). Microsphere, cylinder, lamella [6] and ordered bicontinuous double diamond structures [7] are commonly observed.

In the case of crystalline-amorphous block copolymers the additional factor of crystallizability increases the complexity of the structures. In such materials morphology formation may be the result of crystallization, microphase separation or a cooperative effect of both of them. The sample history substantially controls the final morphology [8],...,[10]. Thus, a wide range of structures have been observed and reported. A thorough review [8] of the literature data in this area led to a classification scheme of the different crystalline-amorphous block copolymers as a function of the location of the transition temperatures (T_c, T_m, T_{OD}) of the components. Two different morphologies were found to be the representative ones for the equilibrium paths, i.e. crystallization driven lamellae - composition independent, and disrupted separated microphases - composition dependent. Their formation was theoretically predicted by the Whitmore and Noolandi [2], Di Marzio, Gutmann and Hoffman [1] and, respectively, by Vilgis and Halperin [3] models.

The purpose of this study was the investigation of the morphological change of the molecular assemblies of some block copolymers with crystallizable poly(N-acetyliminoethylene) (PNAI) ($T_m \approx 150°C$) [11] and amorphous vinyl sequences, useful as nonionic surfactants [12], as a function of solvent nature and rate of solvent evaporation on casting from solution. Path dependent morphologies were observed depending if the crystallization has been avoided, or has occured prior or after microphase separation.

Transmission electron microscopy (TEM) technique was employed for the experimental investigations, considering the advantages of direct observation of the amount, size, shape and distribution of phases. Additional informations were obtained by differential scanning calorimetry.

2. Experimental

2.1. Materials

Toluene and N,N-dimethylformamide (DMF) used for solvent casting were purified by drying by appropriate methods and subsequent vacuum distillation. Nitrobenzene (comercial product) was used as received. The examined block copolymers were of BAB and $(AB)_n$ type, where the sequence A is the crystallizable one, i.e. poly(N-acetyliminoethylene) (PNAI), and the amorphous vinyl sequence B is poly(methyl methacrylate) (PMMA), poly(butyl methacrylate) (PBMA), poly[β-(N-carbazolyl ethylacrylate-co-β-(methacryloyloxy)ethyl-3,5-dinitrobenzoate) (PEDA). The block copolymers with polystyrene sequences as the vinyl ones are believed to be of predominantly multiblock type, due to the usual termination by recombination in the radical polymerization of styrene. The preparation of the studied block copolymers has been reported earlier [12]. The synthetic approach consisted in a two step combined technique, the vinyl monomer being polymerized in the presence of PNAI macroazoinitiators. These ones were syntesized by capping hydroxyl terminated PNAI of controlled molecular weight with 4,4′-azobis-4-cyanopenthanoyl chloride (ACPC). The main characteristics of the copolymers are presented in Table 1.

The composition of the block copolymers was calculated from ^{1}H-NMR and elemental analysis (N %) data and the average molecular weights were determined by gel permeation chromatography. Polymer samples were purified by reprecipitation from adequate solvents and repeated washing with selective solvents for each of the two component sequences in order to remove the unscissed macroinitiator and the eventually formed homopolymer.

Table 1
Characteristics of the Block Copolymers

No.	Sample code	DP of the PNAI sequence	Vinyl sequence type	PNAI content wt %	M_w	M_n	M_w/M_n
1	PMMA/$PNAI_{20}$	20	PMMA	16.9	21,651	14,900	1.45
2	PBMA/$PNAI_{20}$	20	PBMA	13.0	77,588	50,902	1.5
3	PSt/$PNAI_{20}$	20	PSt	15.8	83,347	33,363	2.50
4	PEDA/$PNAI_{20}$	20	PEDA	6.7	39,500	30,387	1.3

2.2. Characterization

TEM observations were carried out with a TESLA-BS 513A transmission electron microscope. Two procedures were employed to prepare the sample films. According to the first procedure the samples were obtained by casting from the solutions (1 wt %) directly dropped on the mesh plate foreseen with a thin carbon film. The solvent was allowed to slowly evaporate at room temperature or in a solvent vapour rich atmosphere over the period of a few hours.

The second method involved slow solvent evaporation over many days to weeks, the polymer solution (1...5 wt %) being deposited onto microscope slides. Following Kato's method [13] pieces of the cast films were stained by exposure to osmium tetraoxide for 48 h and then included in epoxy resin. The microtomed sections (Ultratom III LKB 8802A) were mounted on copper grids with collodion membrane and stained again in order to improve the image contrast. PNAI sequences were those selectively stained.

Glass transition and melting temperatures were determined by differential scanning calorimetry using a Mettler DSC 12E apparatus at heating rates of 5° and 20°C/min.

3. Results and Discussion

3.1. Influence of Solvent Nature

It is well known [8], [14] that the type of morphology adopted by a block copolymer with a given composition can change with the nature of the casting solvent or if a preferential solvent for one of the blocks is used. The casting solvents selected for this study were DMF, toluene and nitrobenzene. Their quality relative to each type of the component blocks can be followed in Table 2.

Even if the PNAI blocks are relatively short, all the studied polymers exhibited microphase separation, the DSC data being in agreement with the TEM images (Table 3).

An explanation may be that the microphase separation process proceeds more easily than expected as a consequence of the ability of the PNAI chains to crystallize.

Though, in several cases, we had to use the hysteresis effect to facilitate the experimental (DSC) determination/separation of the glass transition temperature of the two block components [15]. The content in PNAI being relatively small for all

Table 2

Solubility Parameters for the Block Copolymer Component Sequences and for the Used Solvents

Sequence type	Solubility parameter$^{a)}$ δ, $[(\mathrm{cal.cm^{-3}})^{1/2}]$	Solvent	Solubility parameter$^{a)}$ δ, $[(\mathrm{cal.cm^{-3}})^{1/2}]$
PMMA	10.7±2.6	DMF	12.1
	10.7±2.1	toluene	8.9
	10.7±2.1	nitrobenzene	10.0
PBMA	8.7±1.3	DMF	12.1
	9.6±1.4	toluene	8.9
	9.6±1.4	nitrobenzene	10.0
PEDA	9.0$^{b)}$	toluene	8.9
		nitrobenzene	10.0
PSt	9.0±0.6	DMF	12.1
	9.4±1.2	toluene	8.9
	9.4±1.2	nitrobenzene	10.0
PNAI	12.44$^{c)}$	DMF	12.1
		toluene	8.9
		nitrobenzene	10.0

$^{a)}$ from [20]; $^{b)}$ determined from swelling measurements; $^{c)}$ calculated [12].

Table 3

Glass Transition Temperatures of the Block Copolymers$^{a)}$

Block copolymer	T_g, [°C]
PMMA-b-PNAI-b-PMMA	$\underline{63}$, 125
PBMA-b-PNAI-b-PBMA	28, $\underline{74}$
$(\mathrm{PSt\text{-}b\text{-}PNAI})_n$	$\underline{70}$,105
EDA-b-PNAI-b-EDA	$\underline{45}$, 112
$\mathrm{PNAI_{20}}$	58

$^{a)}$the underlined value corresponds to the PNAI sequence.

studied samples, one could expect a detection of two-phase structures consisting in spherical domains of PNAI embedded in a polyvinyl matrix. This was indeed the case for the samples obtained at a moderate rate of evaporation (room temperature solvent removing during two days followed by vacuum drying for 4 h at 50°C) from toluene (δ=8.9 $(\mathrm{cal.cm^{-3}})^{1/2}$) and nitrobenzene ($\delta$=10 $(\mathrm{cal.cm^{-3}})^{1/2}$).

In most of the studied cases these solvents are selectively good for the polyvinyl blocks which have the solubility parameter in the 8.3...8.9 $(\mathrm{cal.cm^{-3}})^{1/2}$ range. The size and shape of the PNAI domains (the dark ones) are strongly influenced by the polyvinyl sequence nature (Fig. 1). Their dimensions are in the nanometer range $(1.5...8\times10^2)$ nm, the order being usually PBMA>PMMA>PSt>PEDA. Unlike the triblock copolymer with polymethacrylic end sequences which shows almost perfect spherical PNAI microdomains, for the block copolymer with PSt sequences these are deformed, tending to an ellipsoidal shape. This aspect is probably a consequence of the greater PNAI content situated at the boundary between the values usually required for the appearence of the micellar and cylindrical morphologies.

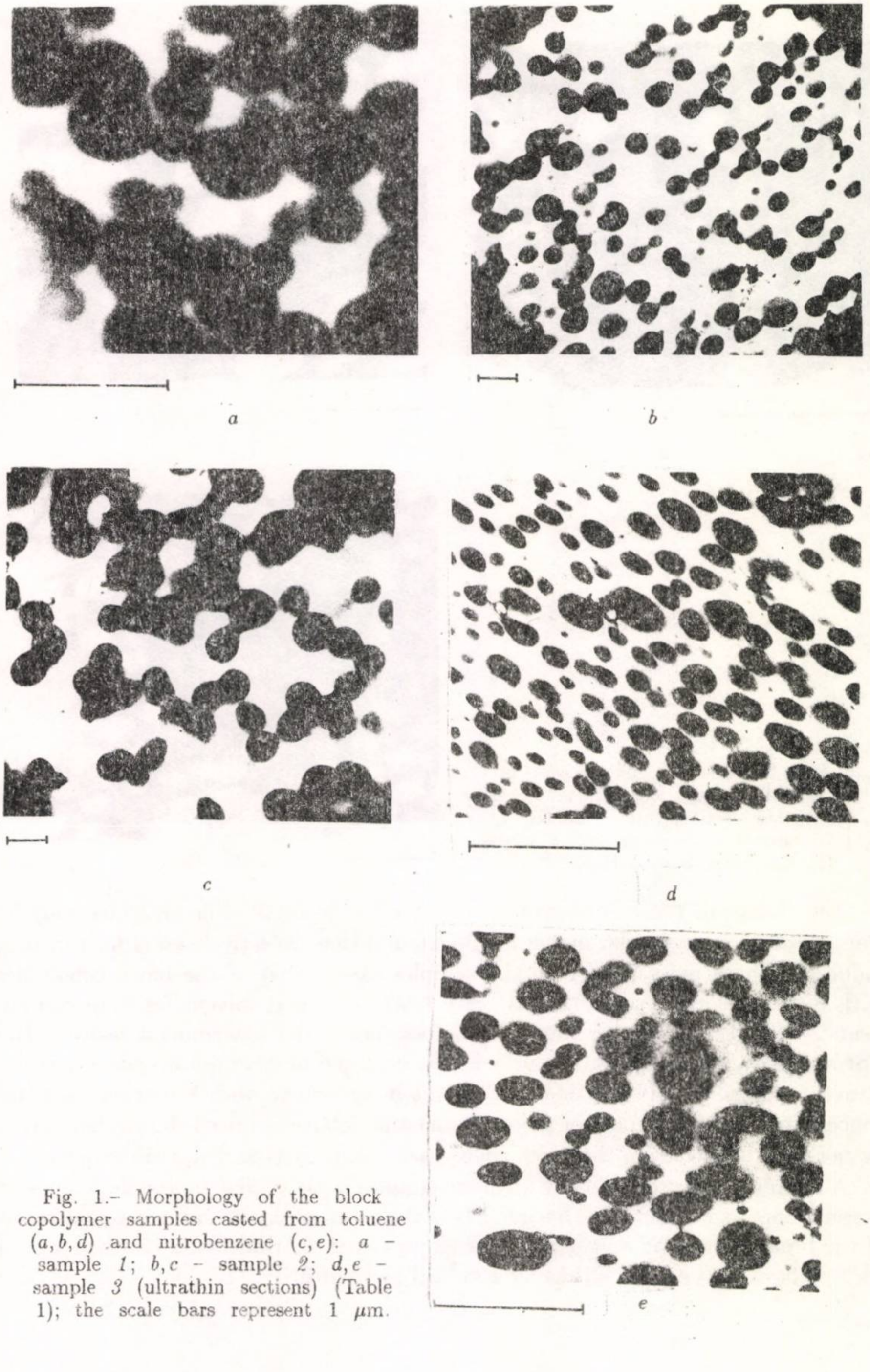

Fig. 1.– Morphology of the block copolymer samples casted from toluene (*a*, *b*, *d*) and nitrobenzene (*c*, *e*): *a* – sample *1*; *b*, *c* – sample *2*; *d*, *e* – sample *3* (ultrathin sections) (Table 1); the scale bars represent 1 μm.

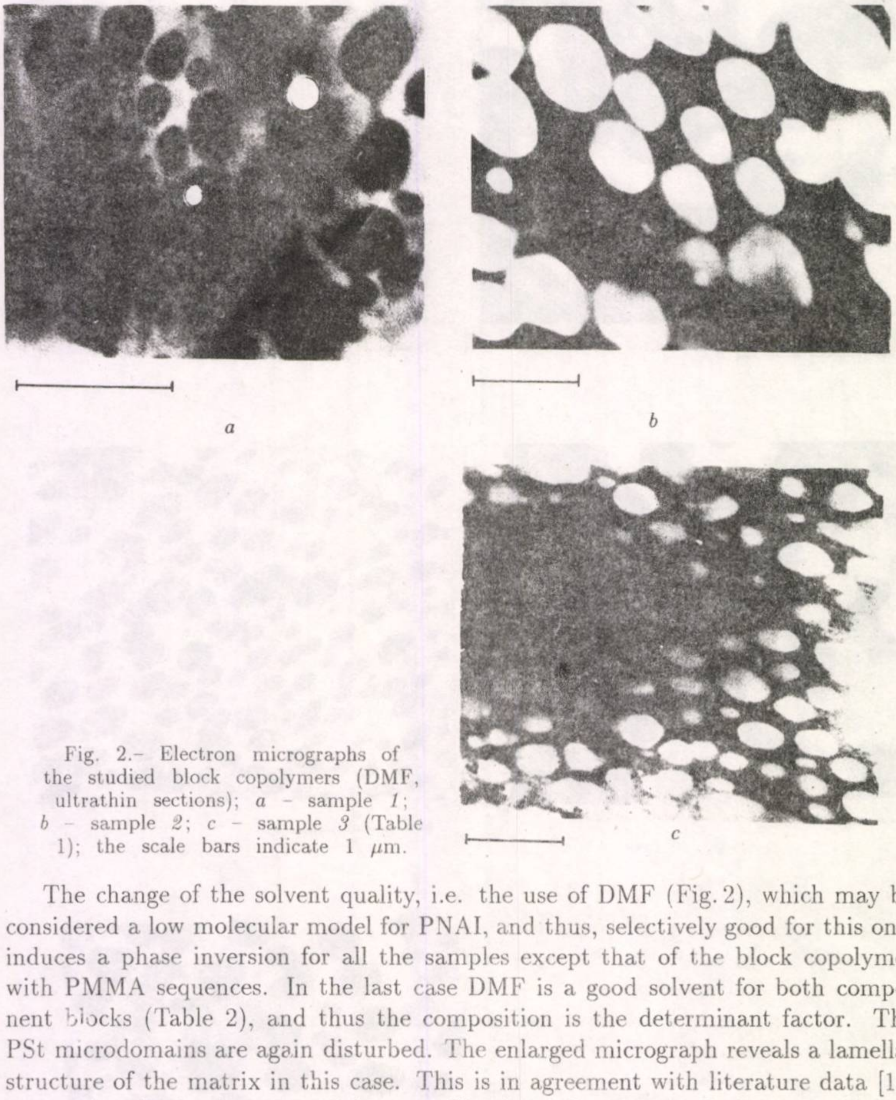

Fig. 2.– Electron micrographs of the studied block copolymers (DMF, ultrathin sections); *a* – sample *1*; *b* – sample *2*; *c* – sample *3* (Table 1); the scale bars indicate 1 μm.

The change of the solvent quality, i.e. the use of DMF (Fig. 2), which may be considered a low molecular model for PNAI, and thus, selectively good for this one, induces a phase inversion for all the samples except that of the block copolymer with PMMA sequences. In the last case DMF is a good solvent for both component blocks (Table 2), and thus the composition is the determinant factor. The PSt microdomains are again disturbed. The enlarged micrograph reveals a lamellar structure of the matrix in this case. This is in agreement with literature data [16] concerning the development of the crystallization following micelle formation during evaporation of solvent in the block copolymers with PNAI and styrene sequences.

A common feature observed in these samples is that their morphology doesn't present long range order. The irregularity of the mentioned textures may be the result of the broad molecular weight and/or compositional distribution, a disadvantage of the synthesis of the vinyl blocks by a radical mechanism.

3.2. Influence of Solvent Rate Evaporation

Assuming that the increased size of the microdomains in the samples presented here as compared to the usual one could be a non equilibrium aspect, effect of the insufficiently slow evaporation rate [17] during the sample preparation, we decided to study also the influence of this factor on sample morphology. The experiments were performed with the block copolymers having PEDA end sequences, characterized by photoconductive properties [12], [18], features certainly influenced by sample

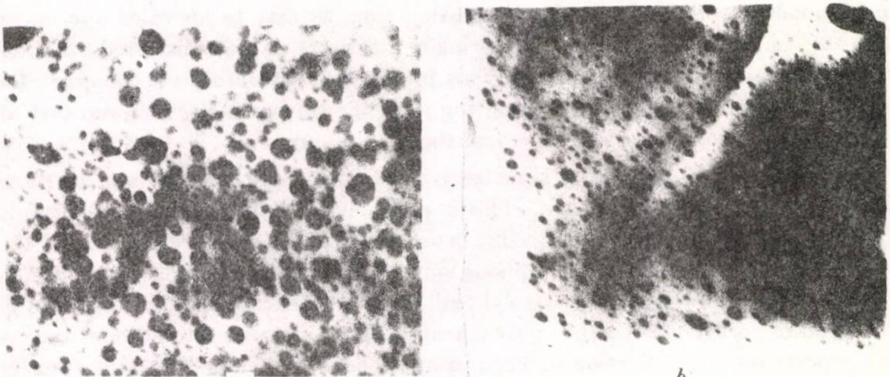

Fig. 3.- Influence of evaporation rate on the morphology of the block copolymers. Scale bars indicate 1 . μm; *a* - rapid solvent casting (direct deposition, solvent evaporation $\sim 30'$, room temperature); *b* - ultrathin section (solvent evaporation $\sim$2 days at 50°C, subsequent vacuum drying at 50°C for 24 h); *c* - direct deposition (solvent evaporation $\sim$2 days at room temperature, subsequent vacuum drying 4 h at 50°C); *d* - ultrathin section (solvent evaporation $\sim$400 h at 60°C, subsequent vacuum drying for 48 h, at 60°C, and 2 h at 70°C).

morphology. The selected solvent was nitrobenzene, which allows the variation of the evaporation rate in a large domain of values and is selectively good for the polyvinyl sequence.

As shown in Figs. 3 *a*...*d* the decrease of the rate of evaporation implies a decrease in the microdomains dimensions and an increase of the order in their arrangement.

A lamellar structure was achieved when annealing was added to the diminishing of the solvent evaporation rate (Fig. 3 *d*) (solvent evaporation at 60°C for 400 h followed by vacuum drying at 60°C for 2 days). The transformation from spherical microdomains to rippled lamellae by passing from as cast to annealed specimens proceeds via a strut morphology, consisting of a network of short distorted cylinders with a thickness of about 100 mm. This intermediate structure was observed for samples obtained by direct casting on the grid, the solvent being removed first at room temperature, during two days, and then in vacuum, at 50°C, for 4 h.

The thickness of the PEDA lamellae varies between 120 and 200 nm, as those of PNAI are of about 10...30 nm. This is probably the thermodynamically stable structure, also favoured by the specific, dense, layered, quasi-ordered texture of the PEDA blocks, induced in the amorphous vinyl polymer by the specific charge transfer interactions between the carbazolyl and 3,5-dinitrobenzoyl pendant groups [18]. This kind of "order" for PEDA is not unexpected if one takes into account the recent reports on crystallization induced in amorphous polymers by charge transfer interactions [19].

The specific structure of PEDA sequence is the main factor which determines the dimension of the corresponding lamellae [18] and is the reason of the appearence of a lamellar structure even for lower PNAI content than the theoretically predicted one (composition independent lamellar structure).

4. Conclusions

In conclusion, various morphologies were obtained for block copolymers with crystallizable (hydrophilic) PNAI and amorphous (hydrophobic) polyvinyl sequences, as a function of sample preparing conditions on casting from solution. It was found that structure modification might be thermally induced. Transmission electron microscopy (TEM) provided direct and conclusive visual evidence for the competition between crystallization and phase separation. The morphologies obtained in such conditions correspond to the theoretically predicted ones. Of course, the profile of properties exhibited by such materials will be dictated by the path preparing conditions which control the morphology of a given specimen.

Received, July 15, 1996

Technical University "Gh.Asachi", Jassy,
Department of Macromolecules
and
"P.Poni" Institute of
Macromolecular Chemistry, Jassy

REFERENCES

1. Di Marzio E.A., Guttman C.M., Hoffman J.D., Macromolecules, **13**, 1194 (1980).
2. Whitmore M.D., Noolandi J., Macromolecules, **21**, 1482 (1988).
3. Vilgils T., Halperin A., Macromolecules, **24**, 2090 (1991).
4. Leibler L., Macromolecules, **13**, 1602 (1980).
5. Helfand E., Wassermann Z.R., Macromolecules, **9**, 879 (1976).
6. Molau G.E., in *Block Polymers* (ed. S.L. Aggarwal), Plenum Press, New York, 1970.
7. Hasegawa H., Tanaka H., Yamasaki K., Hashimoto T., Macromolecules, **20**, 1651 (1987).
8. Drzewinski M.A., Polym. Prep., **35**, *1*, 660 (1994).
9. Sakurai S., Taie K., Nomura S., Shiwaku T., Hashimoto T., Polym. Prep., **35**, *1*, 594 (1994).
10. Gurovich E., Prost J., Leibler L., Polym. Prep., **35**, *1*, 93 (1994).
11. Litt M.H., Rahl F., Roldan L.G., J. Polym. Sci., Polym. Phys. Ed., **7**, 463 (1969).
12. Simionescu C.I., David G., Ioanid A., Paraschiv V., Riess G., Simionescu B.C., J. Polym. Sci., Part A, Polym. Chem., **32**, 3123 (1994); Simionescu C.I., Paraschiv V., David G., Simionescu B.C., Macromol. Reports, **A 32**, (suppl. *7*), 1095 (1995).
13. Kato K., J. Polym. Sci., **B4**, 35 (1967); Polym. Eng. Sci., **7**, 38 (1966).
14. Riess G., Hurtrez G., Bahadur P., in *Encyclopedia of Polymer Science and Engineering*, 2nd ed., vol.**2**, J. Wiley, New York, 1985, 324.
15. Gaur U., Wunderlich B., Macromolecules, **13**, 1618 (1980).
16. Ishikawa S., Fukutomi T., Eur. Polym. J., **29**, 877 (1993).
17. Cohen R.E., Bates F.S., J. Polym. Sci., Polym. Phys. Ed., **18**, 2143 (1980).
18. Simionescu C.I., David G., Ioanid A., Ioanid G., Simionescu B.C., Polym. Plast. Technol. Eng., **34**, 845 (1995).
19. Schneider H.A., private communication.
20. Burrell H., in *Polymer Handbook* (eds. Brandrup J., Immergut E.H.), 2nd ed., J. Willey & Sons, New York, 1977, IV-340.

MORFOLOGIA COPOLIMERILOR BLOC CU SECVENŢE POLI(N-ACETILIMINOETILENICE)/POLIVINILICE

(Rezumat)

Studiul electrono-microscopic al unor bloc copolimeri cu secvenţe poli(N-acetiliminoetilenice) (cristalizabile, hidrofile) şi polivinilice, de tip polistirenic sau polimetacrilic (amorfe, hidrofobe). a evidenţiat dependenţa morfologiei acestor compuşi de istoricul probei. Obţinerea unor structuri termodinamic stabile se poate realiza numai prin aplicarea unor tratamente termice şi evaporarea lentă a solventului.

BULETINUL INSTITUTULUI POLITEHNIC DIN IAŞI
Tomul XLIII (XLVII), Fasc. 1–2, 1997
Secţia II
CHIMIE şi INGINERIE CHIMICĂ

D.C. 547.458.84; 668.533; 674.031.1

MOLECULAR AND SUPERMOLECULAR STRUCTURE OF OAK FURFURAL LIGNOCELLULOSE

BY

GH. ROZMARIN, GEORGETA CAZACU, AURELIA IOANID,
GHIOCEL IOANID, C. TOMA, MIHAELA NIŢĂ,
MARIUS-LIVIU CRAUS and TH. MALUŢAN

The effect of hydrolysis process on chemical composition and anatomo-histological structure of oak wood chips has been studied. Catalytic furfural lignocellulose was subjected to some nitration reactions in the presence of sulphuric, acetic acid or ethyl alcohol. The obtained products have been characterized by IR spectroscopy, X-ray diffraction and microcalorimetry. Chemical study was completed with observations of optical and electron microscopy.

1. Introduction

Cell membrane structure of wood fibers is the result of supermolecular organization of the chemical components, with a distribution which depends on the wood species. Reactions of hydrolytic splitting of wood carbohydrates are frequently used in hydrolysis industry for producing of furfural and other compounds [1]. After conversion of pentosanes in furfural [2], a large amount of furfural lignocellulose was obtained as a by-product, mostly composed from cellulose and lignin in approximate equal proportions, chemically linked between them due to the high temperature and acid pH [3]. Modifications of chemical composition induced by hydrolysis processes are accompanied by important changes in the cytological and histological structure of wood material, determined by the swelling of fibers walls, which leads to a pronounced visible layered aspect and breaking up to libriform elements [4].

In the present paper, modifications of chemical composition of oak wood by hydrolysis processes, and of furfural lignocellulose modified by nitration, have been examined. The study have been also completed by microscopical observations on the anatomical and morphological organization of lignocellulose.

2. Experimental

2.1. Materials

Two samples of furfural lignocellulose from oak wood chips, from which the tannins were previously extracted, were used, namely; LC$_c$ – catalytic lignocellulose obtained by catalytic hydrolysis (catalysts 20% H_2SO_4) at 175°C temperature and 2 h reaction time; LC$_a$ – autocatalytic lignocellulose obtained under same conditions, the medium's acidity being assured by the COOH groups from hemicellulose's structure. Lignocelluloses were sieved on a vibratory screen, the 0.5 mm in diameter fraction being selected.

2.2. Method

Catalytic furfural lignocellulose (LC$_c$), extracted successively with an alcohol/benzen mixture and hot water, was subjected to the nitration reaction using various nitration mixtures in the conditions presented in Table 1.

Table 1

Experimental Conditions Applied in the Nitration of Catalytic Furfural Lignocellulose

Sample	HNO_3 concentration %	Reaction medium	Material/ Liquor ratio	Time h	Temperature °C
LC$_c$-*S*	12	H_2SO_4, 26%	1/10	2	35
LC$_c$-*A*	12	CH_3COOH, 66%	1/10	2	80
LC$_c$-*E*	65	C_2H_5OH, 97%	1/40	4	80

a) *Chemical and Physical Analyses*

The chemical composition of furfural lignocellulose and oak chips was determined by TAPPI standard method [5].

To characterize the structural changes appearing during nitration, IR spectra were recorded on a UNICAM SP 100 spectrophotometer, on KBr pellets. The following indices have been calculated: a) the value of hydrogen bond energy (E_{H}, [kcal]), according to relations [6]:

$$E_{\mathrm{H}} = \frac{1}{k} \cdot \frac{\nu_0 - \nu}{\nu_0},$$

where: ν_0 is the standard frequency corresponding to the free OH groups (3,650 cm^{-1}); ν – frequency corresponding to the vibration of bounded OH groups; k – constant equal to 1.6×10^{-1} kcal^{-1}); b) the asymmetry index (a/b) as a ratio between the right and left segments of the half-width of the vibration band for the OH groups [7]; c) the relative value of the IR optic density (RVOD) [8], with relation (RVOD)=$E_c(\nu_j)/E_c(\nu_s)$, where: $E_c(\nu_j)=\lg T_c(\nu_j)/T(\nu_j)$, with $T(\nu_j)$ – transmission at ν_j frequency; $T_c(\nu_j)$ – transmission at ν_j when the components content should be considered zero; ν_s – standard reference frequency (1,425 cm^{-1}).

The wetting heats were determined on a CALVET type microcalorimeter.

X-ray diffraction was performed with a DRON-20 apparatus with a Co tube. Crystallinity index (χ_c) was determined with relation $\chi_c = S_c/S_t$, where: S_c – the surface corresponding to the intensity diffused by crystalline regions; S_t – the surface corresponding to the coherent intensity diffused by sample [9]. The semi-width of the main peak (β factor) at different values for 2θ angle were also calculated from the spectrum.

b) *Anatomical Observations*

Lignocellulose was macerated in a 1/1 mixture of glycerine and alcohol at 56°C for 2 h, and rinsed with distilled water. Radial and tangential sections of 100 μm thickness were performed. The sections were coloured with aniline sulphate after a previous treatment with a NaOCl solution and immersed in a glycerine/gelatine mixture (1/1, v/v). The samples stiffened between blades and glass covers were analysed on a AMPIVAL type microscope, the figures being performed on a L-ZEISS photomicroscope equipped with projection mirror.

c) *Optical Microscopy*

Lignocellulose powder was treated with 2% NaOH solution at 25°C for 2 h and then washed to pH=7. The air dried specimens were treated with 10% phosphotungstic acid solution for 2 h at 25°C, washed and vacuum dried. The samples were immersed in alcohol and then examined on an optical IOR MC1 type microspcope.

d) *Electron Microscopy*

After treatment with 2% NaOH, the lignocellulose samples were coloured in a 2% potassium permanganate solution at room temperature for 2 h, then washed with water. The samples were dehydrated by successive treatments with a series of 20%, 40%, 60%, 80% and 100% alcohol solutions and vacuum dried on P_2O_5. Using the ultrathin sectioning method combined with the technique of replicas in two steps, the samples were examined on a TESLA SB 513A transmission electron microscopy.

3. Results and Discussion

3.1. Furfural Lignocellulose

a) *Chemical Characterization*

The data presented in Table 2 evidenced an about 20% increase of extraction substances, especially in the case of the LC_a sample (extractives in alcohol/benzen mixture and 1% NaOH). Hydrolytic splitting of etheric bonds (C–O–C bonds) [10] leads to a drastic decrease of the easy-to-hydrolyze polysaccharides, affecting the proportion of components in the lignocellulose matrix. The decrease is more marked in the case of LC_c sample due to the catalytic action of H_2SO_4. The polysaccharides remained in the furfural lignocellulose are mostly hard-to-hydrolyze polysaccharides and may take values of weight, ranging between 40% and 60%.

Due to the transformation of pentosanes in furfural by acid hydrolysis, an essential variation of the lignin/cellulose ratio from 0.58, for oak chips without tannins to 1.008, for catalytic furfural lignocellulose may be also observed.

Table 2

Chemical Composition of Furfural Lignocelluloses Compared with Oak Chips

Component	Oak wood %	Oak wood without tannins %	Autocatalytic lignocellulose %	Catalytic lignocellulose %
Extractives in:				
– alcohol/benzen mixture	6.2	6.3	19.7	6.3
– hot water	3.1	1.5	8.9	8.1
– 1% NaOH	23.5	13.4	33.4	30.8
Cellulose	43.4	40.8	45.5	43.1
Lignin	24.3	23.5	30.9	46.6
Pentosanes	15.6	16.5	13.0	2.4
Easy-to-hydrolyze polysaccharides	21.5	23.1	14.5	6.8
Hard-to-hydrolyze polysaccharides	46.8	44.3	59.2	41.2
Ash	0.2	0.7	1.4	2.8

b) *Anatomo-Histological Observations*

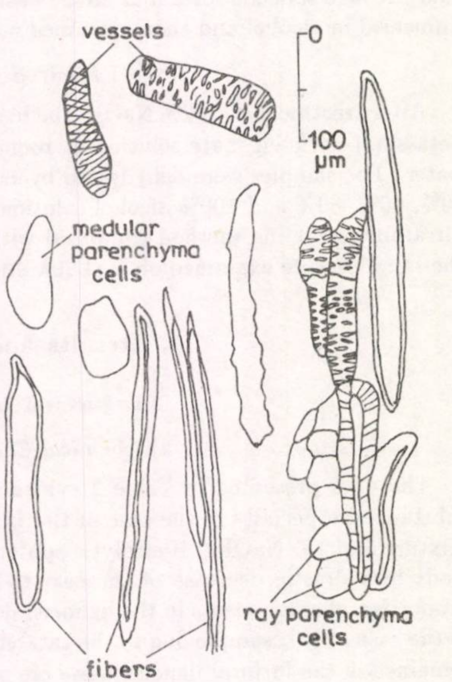

Fig. 1.– Histological elements identified in catalytic furfural lignocellulose (LC_c).

The hydrolysis reactions take place on the surface of punctuations, cavities on porosities of the cell membranes structures. The other chemical reactions occur in the liquid included in macro- and microporosities and in the hydrolysate arrounding particles, too [11]. That is why it is expected that the removal of hemicelluloses from wood will lead to changes in the cytological and histological structure of the vegetable material.

Microscopical images from Figs. 1 and 2 evidence the preservation, even if precarious, of many characteristics of the elements from the organization of vegetable tissues. Thus, wood fibers with vessels elements, the parenchyma cells, even cellular lumen distinguishing sometimes highly teased tissue fragments (Fig. 1), may be identified without any difficulty.

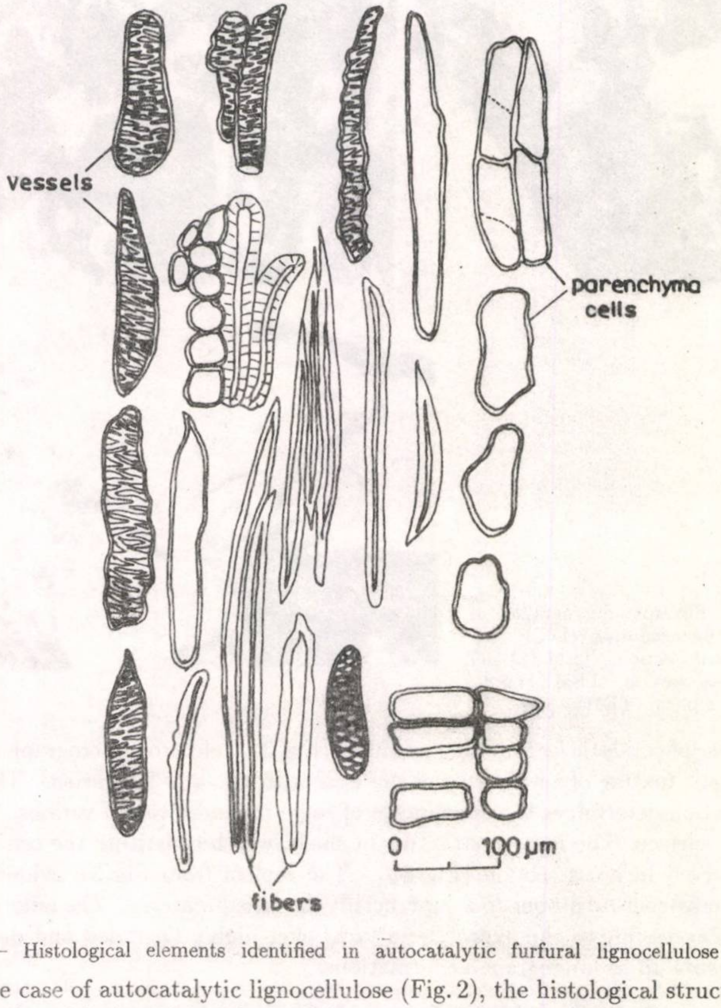

Fig. 2.- Histological elements identified in autocatalytic furfural lignocellulose (LC_a).

In the case of autocatalytic lignocellulose (Fig. 2), the histological structures are quite similar with the original form of the structural elements from oak wood tissues.

Observations on AMPIVAL microscope may be quantitative, referring to the form, aspect and size of structural elements, such as: thickness of the cell wall, inlay character on the vessel walls and disposal of punctuations. The form of the parenchyma cells changes from polygon into oval, wood vessels deform, flattering in the radial and tangential directions and forming cracks on their surfaces.

c) *Supermolecular Organization*

Electron microscopy study points out more or less marked destructions, as depending on the local organization of lignocellulose material and on the applied chemical treatment.

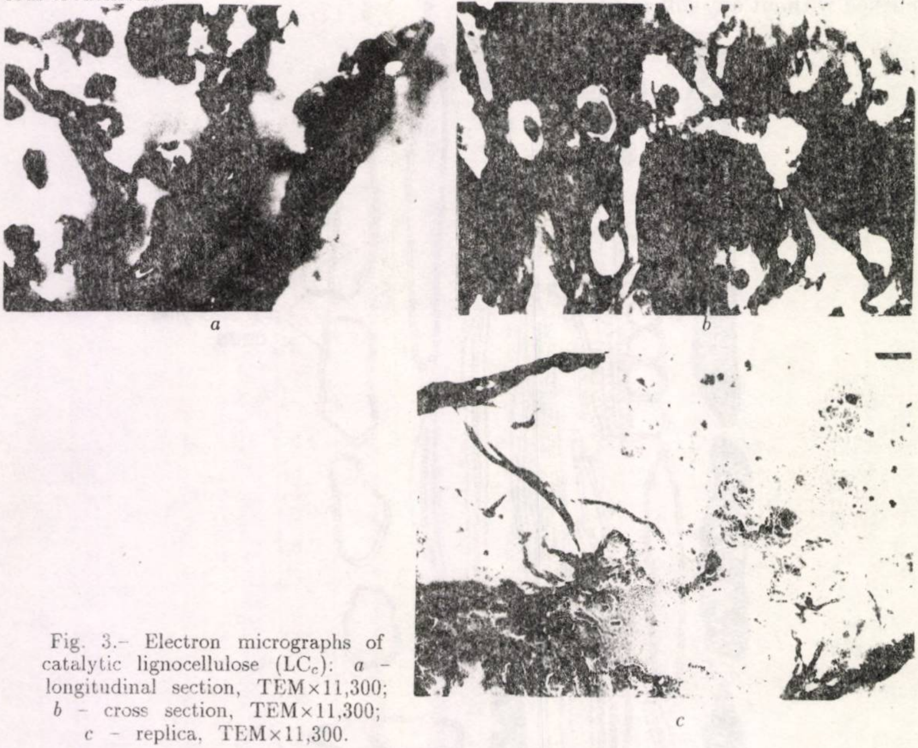

Fig. 3.– Electron micrographs of catalytic lignocellulose (LC_c): *a* – longitudinal section, TEM×11,300; *b* – cross section, TEM×11,300; *c* – replica, TEM×11,300.

In the case of catalytic furfural lignocellulose (Fig. 3 *a*), electron micrograph shows a characteristic texture of an amorphous material with granular formations. The hydrolysis reaction determines the appearance of some microcavities of various depths on the fiber surface. The layered structure of shells, which constitute the cell walls, can be observed in cross section (Fig. 3 *b*). The replica from Fig. 3 *c* evidences a granular microstructure proper to a superficially degraded material. The amorphous zones, more accessible to the hydrolytic attack, offer highly degraded and disorganized fragments up to microgranular formations.

3.2. Furfural Lignocellulose Modified by Nitration

a) *Chemical Composition*

The change of the ratio between the main components of furfural lignocellulose, due to the removal of hemicelluloses by acid hydrolysis, permits application of some specific reactions of their components.

Thus, catalytic furfural lignocellulose was subjected to nitration (specific to lignins' aromatic structure), various nitration mixtures (Table 1) being used.

Determination of the lignin and cellulose contents showed a marked decrease of the lignin percentage (Table 3), especially for LC_c-A and LC_c-E samples, due to a greater capacity of nitrolignin to be dissolved in acetic acid and alcohol respectively, and also to solvolysis reactions.

Table 3
Lignin/Cellulose Ratio from Lignocellulose Modified by Nitration

Sample	Lignin %	Cellulose %	L/C ratio
LC_c	46.6	43.1	1.081
LC_c-S	26.3	61.4	0.428
LC_c-A	2.3	90.4	0.029
LC_c-E	3.4	89.8	0.038

The lignin/cellulose ratio decreases strongly from 1.008, indicating an approximate equal proportion of the two components to the 0.038 value, a proof of the cellulosic nature of the product resulted from the reaction.

b) *IR Spectroscopy*

The detailed analysis of the IR spectra gives indications concerning the state of the OH groups and the nature of the H-bonds established between the components of lignocellulose's molecular network. One can seen from Table 4 that the decrease of the lignin content induces a slight shifting of the absorption maximum of the OH groups towards frequencies corresponding to the absorption of OH groups involved in the intense H-networks (3,650 cm^{-1}). This is confirmed by the increase of the energy of hydrogen bonds and by the statistical distribution of H-bonds strength, which becomes more homogeneous (the a/b ratio tends to 1). Increase of the asymmetrical index (a/b ratio) from 0.69 to 0.94 shows that both the intra- and the intermolecular H-bonds are broken during treatment.

Table 4
IR Characteristics and Wetting Heats Values of Lignocelluloses Modified by Nitration

Sample	Absorption band of the OH groups cm^{-1}	H-bond energy E_H kcal	Asymmetry index a/b	Wetting heat ΔH J/g
LC_c	3,460	4.28	0.69	42.9
LC_c-S	3,402	4.45	0.72	57.7
LC_c-A	3,370	4,79	0.94	65.0
LC_c-E	3,380	4.62	0.81	50.2
C_{K-H}	3,360	4.96	1.00	–

The release of an important number of OH groups from the bonds of the H-networks is also confirmed by the increase of the wetting heats of the studied samples comparatively with catalytic lignocellulose.

Increase in the energy of H-bonds, as a result of the oxidation reaction and fragmentation of lignin, leads to chemical purity and high structural order of the product, which is pointed out by LC_c-*A* and LC_c-*E* samples. For the sake of comparison, energy of the H-bonds for Kurschner–Hoffer cellulose (C_{K-H}) analytically separated from LC_c (which may serve as a reference, E_H=4.95 kcal) was determined.

For quantitative interpretations of the IR spectra the relative values of the optical density (RVOD) were calculated. Comparison of the data from Table 5 shows important changes in the vibrations corresponding to the OH and CH groups (3,400 cm^{-1}, 2,900 cm^{-1} and 1,380 cm^{-1}). High values of the optical density over the 1,090...1,080 cm^{-1} range, referring to the valence vibrations of the OH and C=O groups, also reflected a marked change of the ratio between the main components of lignocellulose.

Table 5

Relative Values of the Optical Density Calculated for Modified Lignocellulose

Position ν, [cm^{-1}]	Band origin	LC_c	LC_c-*S*	LC_c-*A*	LC_c-*E*
3,400	OH stretching (H-bonding)	1.989	2.206	2.279	2.634
2,900	OH stretching	0.799	0.922	0.716	1.033
1,730	C=O stretching (ketonic aromatic esters)	0.679	0.895	0.407	0.228
1,640...1,610	C=O stretching (aromatic aldehyde/ketones) deformation vibration of H–O–H	1.029	1.096	0.558	0.647
1,505	aromatic skeletal vibrations	0.859	0.552	0.300	0.441
1,480	CH_2 deformation vibration	1.044	0.859	–	–
1,425	CH, CH_2 deformation vibration	1.000	1.000	1.000	1.000
1,380...1,360	CH deformation vibration NO_2 valence vibration	0.991	1.069	1.156	1.269
1,320...1,310	CH deformation vibration	1.135	0.977	1.057	1.237
1,280...1,270	C–O–C valence vibration NO_2 valence vibration	1.240	1.061	1.086	1.382
1,240	C–O–C valence vibration	0.950	0.864	0.828	0.759
1,220...1,200	C=O stretching	0.919	0.796	0.867	0.741
1,165...1,160	C–O–C valence vibration	0.956	0.853	0.962	1.064
1,130...1,120	C–O–C valence vibration band asociate of OH group from cellulose and hemicellulose	1.322	1.435	1.828	2.229
1,090	C–OH stretching	1.880	1.759	2.182	2.758
1,050	C–OH stretching	2.097	2.054	3.017	3.599
1,030	C=O stretching	2.035	2.181	2.634	3.331
900	vibrations characteristic to the β glucosidic linked pyranosic ring	0.198	0.284	0.371	0.461

The LC_c-*S* sample exhibits an overlapping of the absorptions corresponding to NO_2, CH and C–O–C groups in the 1,380...1,360 cm^{-1} and 1,280...1,270 cm^{-1} ranges. The presence of NO_2 groups was confirmed by the nitrogen content (3.5%). One can also observe the high values of optical density at 1,730 cm^{-1}, 1,640...1,610 cm^{-1}

(C=O groups), indicating additional oxidation reaction during nitration.

In the case of LC_c-*A* and LC_c-*E* samples, both a decrease in the characteristic absorptions of the lignin at 1,505 cm^{-1} (aromatic ring vibrations), at 1,730 cm^{-1} and 1,640...1,630 cm^{-1} (C=O stretching aromatic aldehyde/ketones) and 1,240 cm^{-1} (valence vibrations C–O–C bonds between lignin and polysaccharides) and an increase in the absorptions corresponding to cellulose from 1,130...1,120 cm^{-1} (valence vibrations of C–O–C bond) and 900 cm^{-1} (β-glucosidic linked pyranosic ring) was observed.

Based on these data, one can assume a synergism between HNO_3 and the organic solvents (CH_3COOH and C_2H_5OH) favouring the removal of lignin from materials, which leads to an increasing of the cellulose content.

c) *X-ray Diffraction*

X-ray measurements showed the increase of the crystallinity index (Table 6) in the polymer, due to the nitration agent. This is determined by splitting the linkages between lignin, cellulose and residual hemicellulose, but also to the dissolution of lignin fragments. On the other hand, the action of the chemical factors produces a sufficient transfer of energy at molecular level to activate the cellulose macromolecules from energetic metastable (amorphous) state and to shift into a stable (crystalline) one. For these reasons, the polymer's molecular structure has been rearranged.

Table 6

Values of the Crystallinity Index and of the β Factor Calculated for Modified Lignocellulose

Sample	Crystallinity index, χ	β factor $^\circ 2\theta$
LC_c	0.639	2.862
LC_c-*S*	0.701	2.583
LC_c-*A*	0.788	2.548
LC_c-*E*	0.753	2.428

Values of the β factor suggest that the factors favouring the increase of crystalline phase content, contributes concomitantly to diminishing of the network defects and to the corresponding increase of the crystallite average sizes.

d) *Anatomo-Histological Observations*

Comparing the furfural lignocelluloses samples (LC_c – Fig. 1 and LC_a – Fig. 2, respectively), in the case of LC_c-*S* sample obtained by nitration with HNO_3 in the presence of H_2SO_4 (Fig. 4), the modifications of anatomical structure appear more pronounced. However, the outline of histological elements is preserved, permitting to recognize wood fibers, the vessels elements or the parenchyma cells.

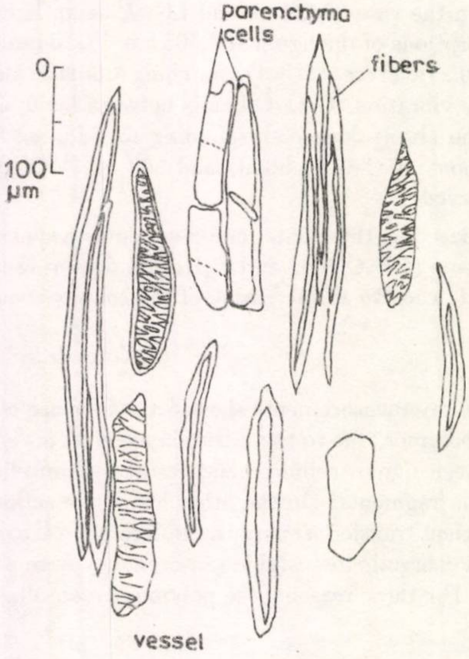

Fig. 4.- Histological elements identified in catalytic lignocellulose modified by nitration in the presence of H_2SO_4 (LC_c-S).

When lignocellulose is subjected to nitration, intense longitudinal and transversal openings of the fibrous material, from optical microscopy images, have been evidenced. One can easily observe the individual wood fibers with various lengths, with thin walls on which punctuations are visible (Fig. 5).

Treatment with phosphotungstic acid of the lignocellulose powders modified by nitration involved various steps of delignification. The observations made reveal that the nitration process is accompanied by irregularities, regions with various degrees of accessibility of the reagent being distinguished.

e) *Supermolecular Organization*

The nitration reaction, associated with oxidative and hydrolytical effects, determining more intense damages with various sizes, affects more deeply the material's organization (Figs. 6 *a* and *b*).

In the replica obtained for the LC_c-S sample (Fig. 6 *c*) regions with an irregular stratification of microfibrilar lamellas, regions with high compatibility of fibrils and regions with microglobular formations may be distinguished. This heterogeneous aspect is due to the removal of the middle lamella (ML) and also some portions of the primary wall (P) of the cell membrane.

In the case of LC_c-A (Fig. 7) and LC_c-E (Fig. 8) samples, formation of some longitudinal cracks on the fiber surface can be noticed but without affecting microfibrilar organization, a fact indicated by the absence of individual cellulose microfibrils. Var-

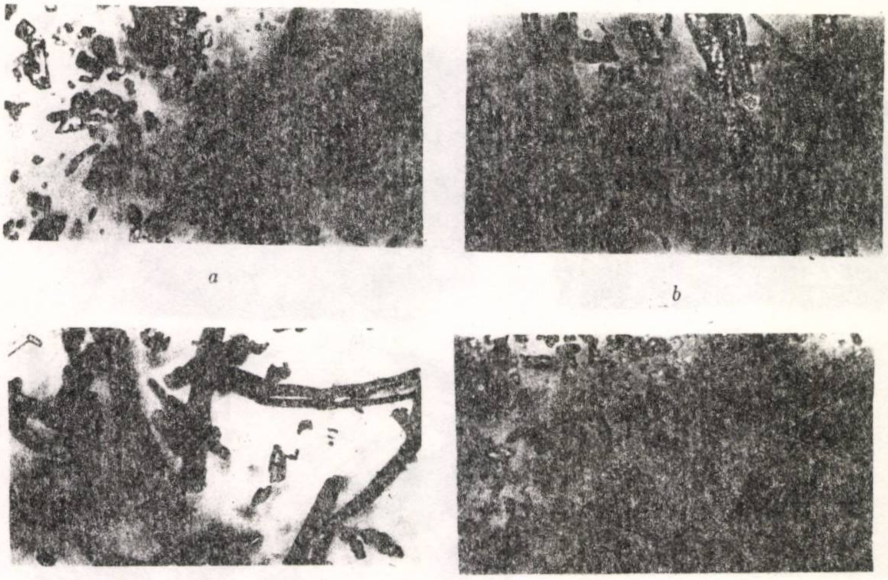

a *b*

c *d*

Fig. 5.- Optical images of the lignocelluloses modified by nitration: *a* – LC_c; *b* – LC_c-*S*; *c* – LC_c-*A*; *d* – LC_c-*E*; ×150.

ious deep destructions at the primary wall level in the lumen's direction, especially in the regions in which the primary wall appears degraded in many portions, have been observed in cross section (Fig. 7 *b*). On the background of the highly grooved replicas of the S_1 layer, rests of the primary wall may be found here and there (Fig. 7 *c*).

The deep folds localize the microfibrilar lamellar layers of the highly organized cellulose fact which is in accordance with the samples high crystallinity index. A region with a uniform aspects in which lamellas whose microfibrilar orientations change in a cross pattern can be observed (Fig. 8 *c*).

To compare the delignification degree, as a result of the nitrating agent's action, the method of staining samples with $KMnO_4$ was used. The deposition of MnO_2 occured as a result of the lignin reaction. Deposits are more opaque to the electron beams and appear as dark regions in the electron micrographs.

In the pictures of the LC_c (Fig. 3) and LC_c-*S* (Fig. 6), distribution of the black regions is heterogeneous, indicating portions with various concentrations of lignin and a small degree of delignification.

A marked diminishing of the dark regions was observed at LC_c-*A* (Fig. 7) and LC_c-*E* (Fig. 8) samples, indicating a high degree of delignification according to the results of chemical analyses.

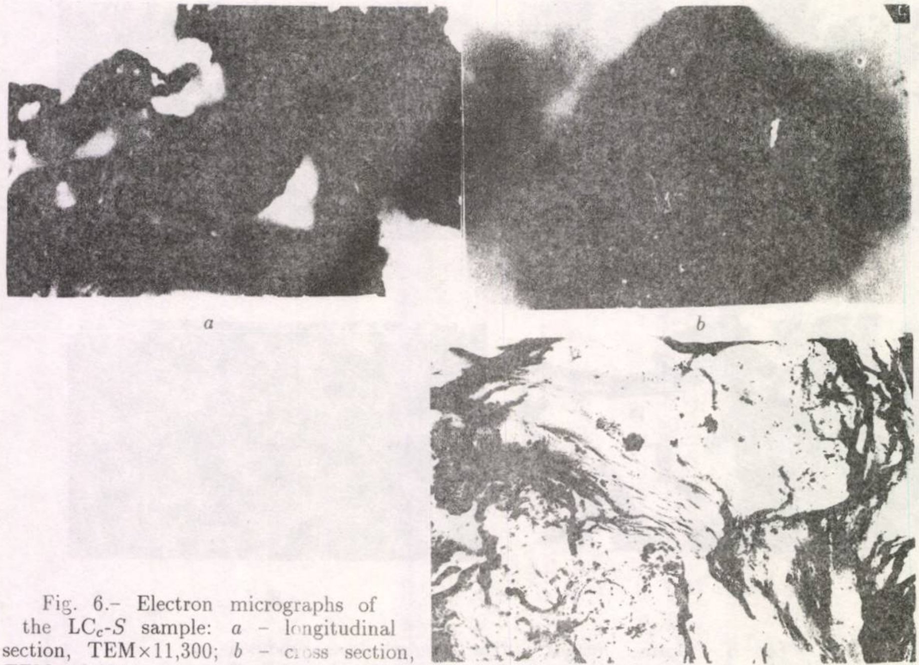

Fig. 6.– Electron micrographs of the LC_c-S sample: *a* – longitudinal section, TEM×11,300; *b* – cross section, TEM×18,000; *c* – replica, TEM×11,300.

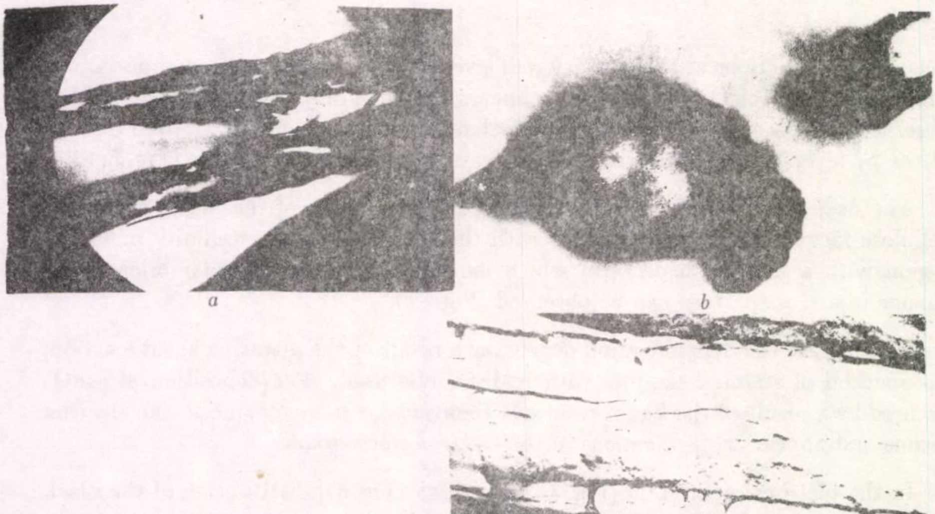

Fig. 7.– Electron micrographs of the LC_c-A sample: *a* – longitudinal section, TEM×4,200; *b* – cross section, TEM×11,300; *c* – replica, TEM×11,300.

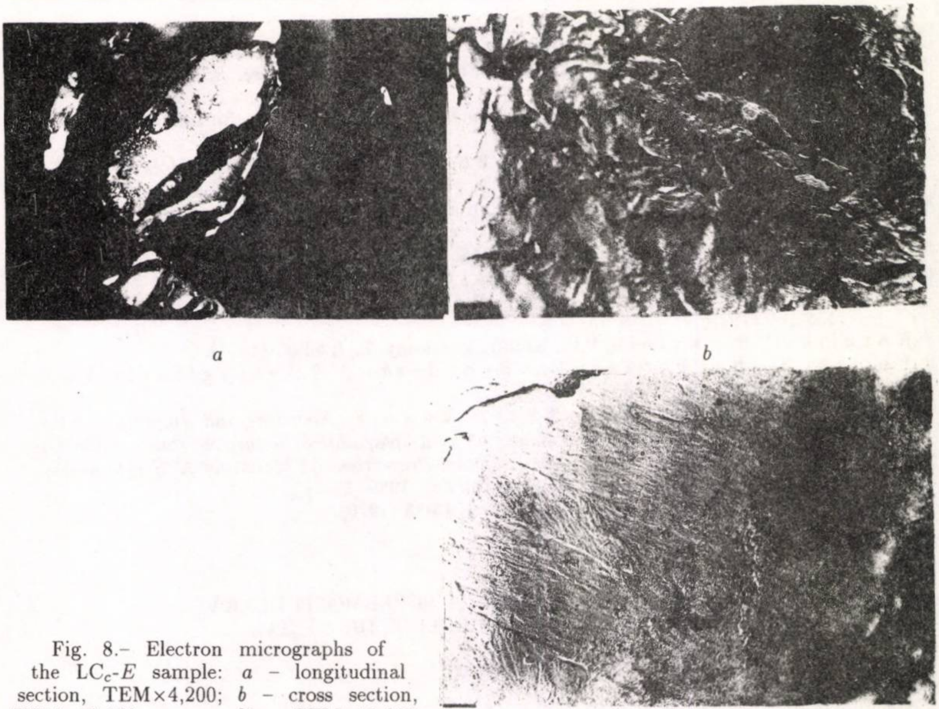

a b c

Fig. 8.– Electron micrographs of the LC_c-E sample: *a* – longitudinal section, TEM×4,200; *b* – cross section, TEM×11,300; *c* – replica, TEM×11,300.

4. Conclusions

Removal of hemicelluloses from oak wood chips by hydrolysis is accompanied by essential modifications of the chemical composition, changes in the material's cytological and histological organization, also occuring.

Chemical analyses indicated important modifications of lignin/cellulose ratio of furfural lignocellulose during nitration. Detailed analysis of the IR spectra provide informations on the stability of the hydrogen bonds between the macromolecular network's components. X-ray diffraction shows an increasing crystallinity index in the presence of organic solvents. Removal of residual hemicelluloses and lignin by nitration sensibly affects the supermolecular ordering of lignocellulose so that they are transformed into microcrystalline cellulose powders.

Received, November 25, 1996

Technical University "Gh.Asachi", Jassy,
Department of Pulp, Paper and Fibre,
"P.Poni" Institute of
Macromolecular Chemistry, Jassy,
"Al.I.Cuza" University, Jassy
and
Institute of Technical Physics, Jassy

REFERENCES

1. Fengel D., Wegener G., *Wood Chemistry, Ultrastructure, Reactions.* Walter de Gruyter, Berlin, 1984.
2. Vedernikov N.A., *The Obtaining of Furfural*, in *Hemicelluloses* (in Latvian). Zinatne, Riga, Latvia, 1991, 209-222.
3. Simionescu C.I., Rozmarin G., Popa H.J., Holzforschung und Holzverwertung, **39**, *5*, 112-116 (1987).
4. Rozmarin Gh., Bîrsan M., Toma C., Niţă M., Celuloză şi Hârtie, **41**, *1*, 6-12 (1992).
5. * * * Tappi Test Methods, Tappi Press, Atlanta, Georgia, USA, 1992-1993.
6. Struszczyk H., J. Macromol. Sci. Chem., **A 23**, *8*, 973-993 (1986).
7. Simionescu C.I., Butnaru R., Rozmarin Gh., Cell. Chem. Technol., **7**, *2*, 153-169 (1973).
8. Karklini V.B., Erinis P.P., Khimia Drevesiny, **7**, *1*, 83-93 (1971).
9. Polizzi S., Fagherazzi G., Benedetti A., Battagliarin M., J. Appl. Cryst., **23**, 359-365 (1990).
10. Koshijima T., Watanabe T., Yaku F., *Structure and Properties of the Lignincarbohydrate Complex Polymer as an Amphipathic Structure Substance*, in: W.G. Glasser, S. Sarkanen (Eds.), *Lignin. Properties and Materials.* ACS Symposium Series *397*, Am. Chem. Soc., Washington DC, 1989, 11-28.
11. Fengel D., Wood Science and Technology, **4**, 15-35 (1970).

STRUCTURA MOLECULARĂ ŞI SUPERMOLECULARĂ A CELOLIGNINEI FURFUROLICE DE STEJAR

(Rezumat)

S-a studiat influenţa procesului de hidroliză asupra compoziţiei chimice şi a structurii anatomohistologice a tocăturii din lemn de stejar. Celolignina furfurolică catalitică a fost supusă unor reacţii de nitrare în prezenţa acidului sulfuric, acidului acetic şi a alcoolului etilic. Produsele obţinute au fost caracterizate prin spectroscopie IR, difracţie de raze X şi microcalorimetrie. Studiul chimic a fost completat cu cel prin microscopie optică şi electronică.

BULETINUL INSTITUTULUI POLITEHNIC DIN IAŞI
Tomul XLIII (XLVII), Fasc. 1–2, 1997
Secţia II
CHIMIE şi INGINERIE CHIMICĂ

D.C. 547.458.1: 535-31; 539.181

ESCA STUDIES OF SURFACE MODIFIED DEXTRAN

BY

CRISTOFOR I. SIMIONESCU,
Member of the Romanian Academy

CARMEN TOPOR, GHIOCEL IOANID and EUGEN NEAGU

Dextran has been subjected, for different periods of time, to plasma (1.3, 13.56 and 27 MHz frequencies), electron beam irradiation and UV radiation. The effect of these treatments on the structure was different, as pointed out by the features appearing from the ESCA spectra in terms of observing the variation of the content in C–C and C–O linkages. The spectral results were correlated with the experimental conditions (exposure duration, frequency, radiation nature).

1. Introduction

Since many of the important physical, chemical, electrical and mechanical properties of a polymer depend on the structure, bonding and morphology in the outermost few tens of angstroms of the surface, a technique such as electron spectroscopy for chemical analysis (ESCA), able to differentiate between the surface, subsurface and bulk of a polymer, is of considerable importance. The studies of D.T. Clark, A. Dilks and their co-workers [1],...,[4], as well as those of H. Yasuda *et al.* [5] are of main interest in this direction and can be considered as fundamental in approaching the field. In a series of publications absolute and relative binding energies have been tabulated for a wide variety of structural features found in polymers [1], [6], the data representing useful tools in discussing the structure of new materials.

The knowledge of the surface composition of polymers is crucial to any rational attempt to control surface interactions, and the use of physical methods to increase the reactivity through introduction of active centers is based on this.

Natural polymers and their derivatives have been previously modified by different physical methods [7],...,[19]. The aim of this work was to investigate structural aspects of dextran which was subjected to physical stimuli.

Dextran (Fig. 1) is the name given to a large class of bacterial homoglucans composed of α-D-glucopyranosyl residues, mainly linked by $\alpha(1\rightarrow6)$ bonds, although $\alpha(1\rightarrow2)$, $\alpha(1\rightarrow3)$ and $\alpha(1\rightarrow4)$ bonds are also found [20]. It was the first microbial polysaccharide industrially produced [21] and is known to be useful as artificial blood plasma, in prevention and treatment of thrombosi [22],...,[24].

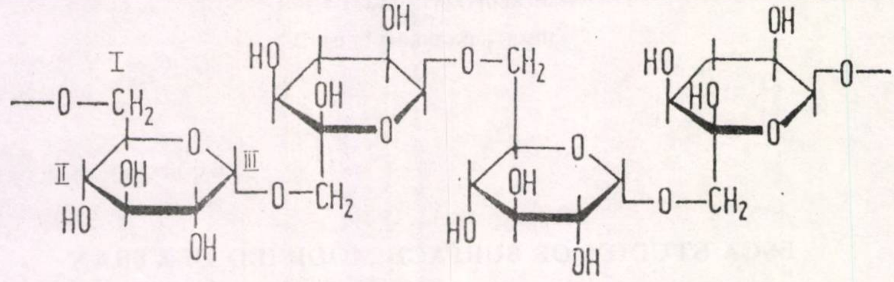

Fig. 1.- Partial structure of dextran macromolecule.

There is one branch in 1.2, 1.3 or 1.4 position [25] for each five glucosidic units. About 40% of the side chains contain only one D-glucose residue, at least 45% are two D-glucose units long, and the rest (max. 15%) are longer than two such units [26].

Films of dextran were placed in a 1.3 MHz cold plasma for different periods of time, up to 60 min. For comparison, some samples were also submitted to 27 MHz and 13.56 MHz cold plasma, to UV and electron beam, mainly for time periods which were proved to be more relevant. The resulted structures have been discussed based on ESCA spectra.

2. Experimental

Dextran with a molecular weight of 40,000 was purchased from SICOMED SA, Bucharest. The 0.2 mm thick films were obtained from water solution by evaporation, in Petri dish, at 50°C.

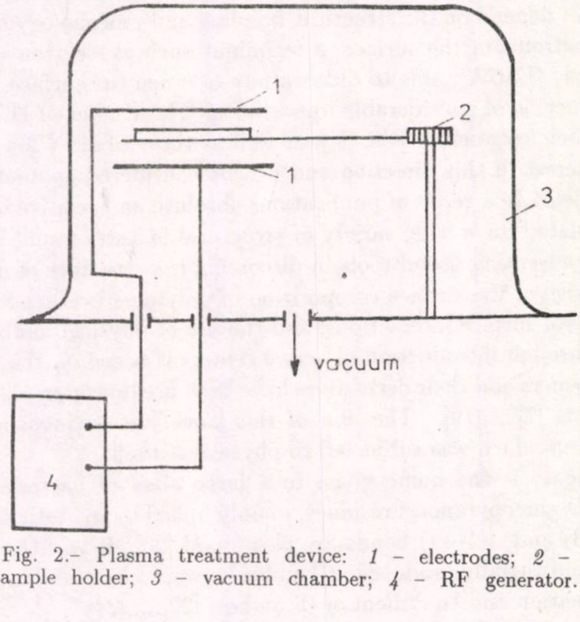

Fig. 2.- Plasma treatment device: *1* - electrodes; *2* - sample holder; *3* - vacuum chamber; *4* - RF generator.

Plasma treatment (Fig. 2) was performed for three frequencies, namely 1.3, 13.56 and 27 MHz, respectively, for the same power (40 W) and pressure (0.2 torr), with appropriate generators. A 40 W, 254 nm (main wave-length, 90%) lamp was used for the UV treatment. The films were placed at 2.5 cm from the lamp.

The electron beam was generated in the device presented in Fig. 3.

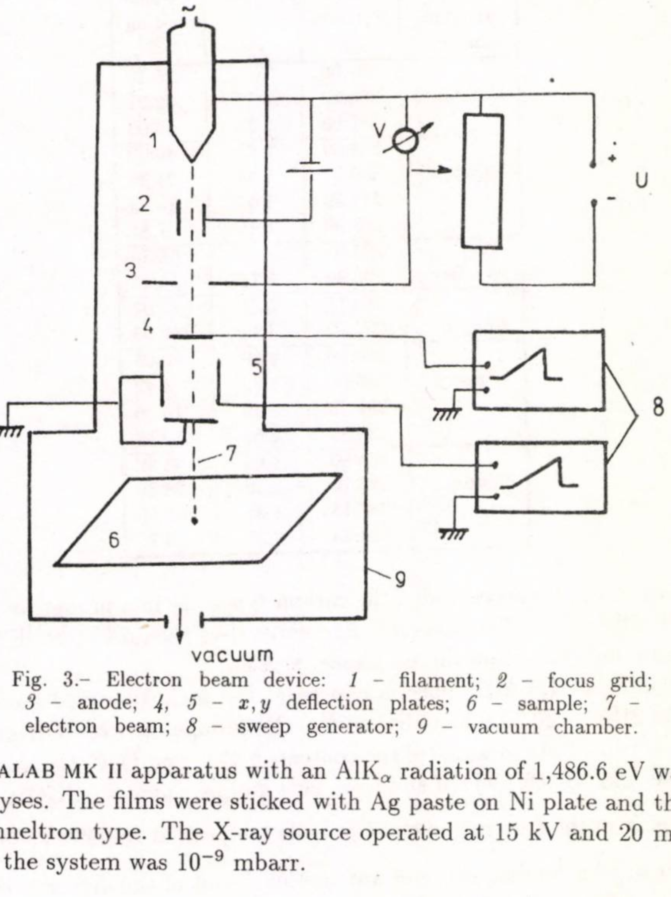

Fig. 3.– Electron beam device: *1* – filament; *2* – focus grid; *3* – anode; *4*, *5* – x, y deflection plates; *6* – sample; *7* – electron beam; *8* – sweep generator; *9* – vacuum chamber.

An ESCALAB MK II apparatus with an AlK_α radiation of 1,486.6 eV was used for ESCA analyses. The films were sticked with Ag paste on Ni plate and the detector was of channeltron type. The X-ray source operated at 15 kV and 20 mA and the pressure in the system was 10^{-9} mbarr.

3. Results and Discussion

Table 1 shows the position of $\mathrm{C_{1S}}$ peaks, full width at half maximum (FWHM) for each peak, and their contribution to the total carbon content of the sample.

The $\mathrm{O_{1S}}$ envelope spectra have the same shapes because the binding energies of the different types of oxygens are overlapping, and it was considered that a more efficient discussion should concentrate on the features of $\mathrm{C_{1S}}$ spectra.

In the following comments, for a better understanding of the involved bonds, C and O appear only with the pointed linkages, for example C–OH or O–C–O.

Table 1

Position of C_{1S} *Peaks, Full Width at Half Maximum (FWHM) and Contribution (in percents) to the Total Carbon Content* (The samples were submitted to 1.3 MHz plasma treatment)

Time of exposure min.	Peak position eV	FWHM eV	Contribution %
Untreated	285.00	1.95	28.10
	286.70	1.77	52.21
	287.90	2.38	19.69
5 min.	284.89	1.65	46.00
	286.21	1.43	20.35
	287.50	1.44	25.83
	288.90	1.41	7.81
10 min.	284.93	1.41	65.36
	285.30	2.74	34.64
30 min.	285.11	2.01	87.97
	287.49	3.14	12.03
45 min.	284.98	1.80	80.05
	286.50	1.79	4.42
	287.33	2.10	13.20
	288.60	2.62	2.33
60 min.	284.80	1.69	44.92
	286.10	2.00	24.80
	287.13	1.30	13.55
	288.23	2.38	16.73

As shown in Fig.1, theoretically, the carbon types are in a proportion of 2 I : 3 II : 1 III or 33% : 50% : 17%. The observed differences (less than 5%) from ESCA are the result of the ramifications on the backbone (s. § **1**).

After 5 min. of 1.3 MHz plasma exposure, the main observed fenomen is the loss from 52.21% to 20.35% of C linked to –OH groups, i.e., of –OH groups. The born radicals contribute to a rise of the content in C–C and O–C–O links (the peaks at 284.89 eV and 287.50 eV). In addition, new groups, such as –COOH, –COO– or 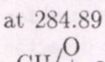 $-\mathrm{CH}\left\langle\begin{matrix}\mathrm{O}\\ |\\ \mathrm{O}\end{matrix}\right.$, appear in the system and these provide the peak at 288.90 eV. The shifts up to 0.5 eV to smaller binding energies are another result of the diminution in oxygen content, this causing a smaller influence on the binding energy value.

The 5 min. electron beam leads to a greater break in C–OH and O–C–O links with a corresponding increase in C–C content (to 67.41%) and the appearance of new oxygenated groups (11.63% at 288.90 eV). As compared to the 1.3 MHz plasma treatment, the electron beam proves to have a more dramatic effect on polymer structure (Fig.4).

Continuing the 1.3 MHz plasma exposure, for 10 min. and then for 30 min., leads to an increase in C–C links because of the break of almost all C–O bonds. After 10 min. the C–C links content (65.36%) seems to be lower than after 30 min. (87.97%) but the peak at 285.30 eV is also due to C–C links, beside some C–O bonds.

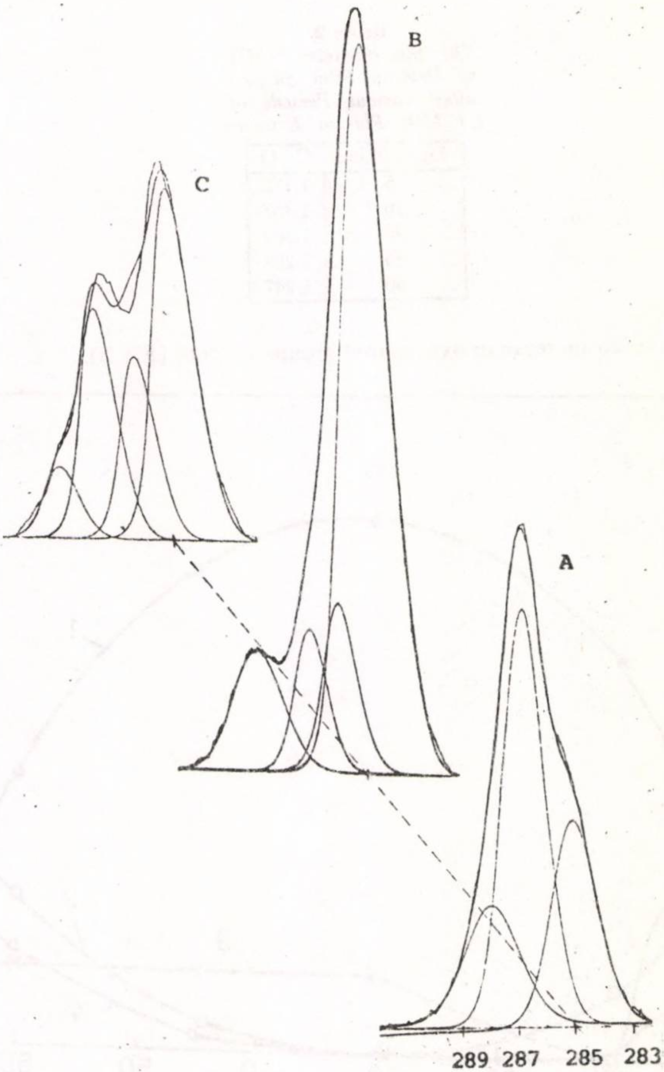

Fig. 4.- C_{1S} core level spectra of untreated dextran (*A*) and of samples obtained after 5 min. exposure to electron beam (*B*) and 1.3 MHz plasma (*C*).

From Table 2 it can be seen that, following a 10 min. discharge, the C content on surface reaches a maximum value.

The C–O bonds are further oxidated and this determines the peak at 287.49 eV. The rises in FWHM (1.74 and 3.18) indicate complex structures with many types of C–O linkages involved. Based on these, after prolonged exposure periods, the oxidation process leads to a major decrease in C–C links content (to 44.92%)

Table 2
The Stoichiometry (C:O) *of Dextran Film Surface after Various Periods of 1.3 MHz Plasma Exposure*

Time, [min.]	C : O
5	1.172
10	1.457
30	1.369
45	1.298
60	1.247

corresponding to an increase in oxygenated groups content (Fig. 5).

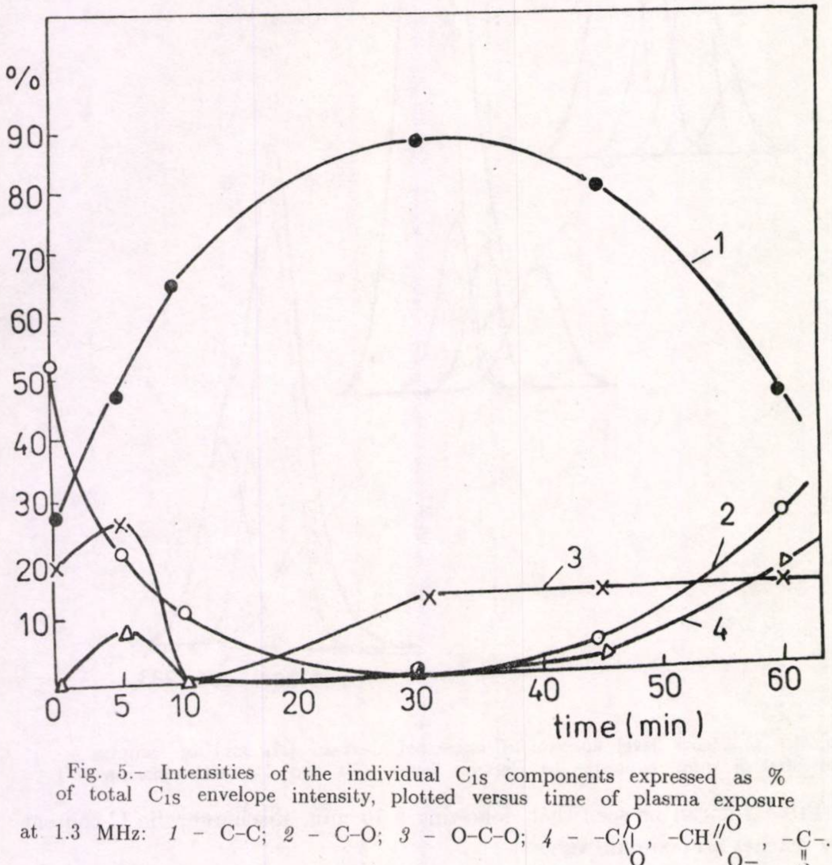

Fig. 5.– Intensities of the individual C_{1S} components expressed as % of total C_{1S} envelope intensity, plotted versus time of plasma exposure at 1.3 MHz: *1* – C–C; *2* – C–O; *3* – O–C–O; *4* – $-C\langle{}^{O}_{O}|$, $-CH\langle{}^{/\!/O}_{O-}$, $-\underset{\overset{\|}{O}}{C}-$.

At 27 MHz this increase is more evident and it goes up to 79.25% C–OH and 12.47% –COOH, –COO–, $-C\langle{}^{/\!/O}_{O-O-}$ and/or $HC\langle{}^{O}_{O}|$.

As can be seen from Fig. 5, curves *1* and *2* have an inverse variation. The loss in -OH groups leads mainly to an enreach in C–C links, but, after longer time intervals the formation of new C–O bonds from the existent C–C linkages occurs. Curves *3* and *4*, especially in the first part, have, somehow, related shapes and this indicates that these processes are going together in the way of formation and disappearance of the nominated groups.

The content of C–C links is influenced by the frequency; at higher frequencies a decrease in C–C links content is observed. After 30 min., at 13.56 MHz, it is 71.76%, and at 27 MHz it is 22.28%. Moreover, after 60 min. at 27 MHz the C–C links content is only 8.28% from all types of C linkages and O–C–O links are totally broken, leading to $\dot{\mathrm{O}}$–C and $\dot{\mathrm{C}}$–O radicals which gave rise to the previously shown oxygenated groups.

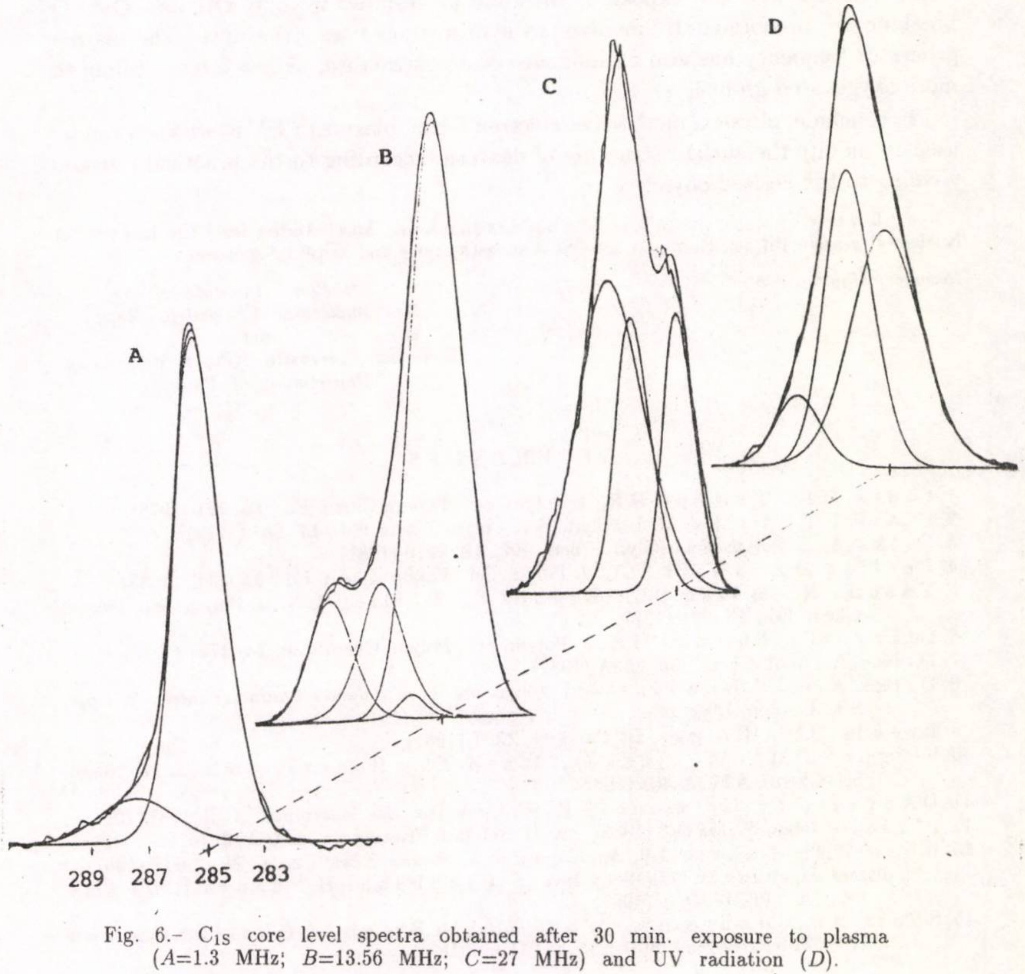

Fig. 6.– C_{1S} core level spectra obtained after 30 min. exposure to plasma (*A*=1.3 MHz; *B*=13.56 MHz; *C*=27 MHz) and UV radiation (*D*).

The UV radiation exposure for 30 min. determines the formation of more types C–C links than the other procedures (FWHM=2.97), concomitantly with a moderate loss in –OH groups and O–C–O breakage (about 10% each). Fig. 6 shows the C_{1S} core level spectra obtained after 30 min. exposure to plasma and UV radiation.

4. Conclusions

The effect of physical stimuli on the structure of dextran can be summarized as follows:

a) Exposure to 1.3 MHz plasma has a milder effect versus electron beam in terms of breaking the C–O and O–C–O links and of the variety of the resulted oxygenated groups.

b) Through the UV exposure, the radicals resulted from C–OH and O–C–O breaking are predominantly involved in hydrocarbon type structures. The plasma generator frequency has also an influence on the structure, higher values leading to more oxygenated groups.

To conclude, physical methods as electron beam, plasma or UV irradiation can be used to modify the surface structure of dextran, according to the practical purpose yielding to the desired objective.

Acknowledgements. The authors thank dr. Aurel Andrei from the Institute of Nuclear Research, Piteşti, Romania, for ESCA investigations and helpful discussions.

Received, May 6, 1996

"P.Poni" Institute of
Macromolecular Chemistry, Jassy
and
Technical University "Gh.Asachi", Jassy,
Department of Physics

REFERENCES

1. Clark D.T., Thomas H.R., J. Polym. Sci., Polym. Chem. Ed., **16**, 791 (1978).
2. Clark D.T., Dilks A., J. Polym. Sci., Polym. Chem. Ed., **17**, 957 (1979).
3. Dilks A., J. Polym. Sci., Polym. Chem. Ed., **19**, 1319 (1981).
4. Peeling D.T., Clark D.T., J. Polym. Sci., Polym. Chem. Ed., **21**, 2047 (1983).
5. Yasuda H., Marsh H.C., Brandt S., Reilley C.N., J. Polym. Sci., Polym. Chem. Ed., **15**, 991 (1977).
6. Clark D.T., Thomas H.R., J. Polym. Sci., Polym. Chem. Ed., **14**, 1701 (1976).
7. Dilks A., Anal. Chem., **53**, 802A (1981).
8. Dilks A., in J.V. Dawkins (Ed.), *Developments in Polymer Characterization*. **2**, Appl. Sci., London, 1980, 145.
9. Brewis D.M., Briggs D., Polymer, **22**, 7 (1981).
10. Soignet D.M., Hinojosa O., Ward T.L., Benerito R.R., J. Macromol. Sci.-Chem., **A17**, *3*, 403 (1982).
11. D'Angiuro L., Cremonesi P., 5th Conv. Ital. Sci. Macromol. [Atti], 1981, 402.
12. . * . Patent Japan *59,155,045* (1983), Inv.: Dainippon Printing Co.; CA, **102**, 167910s (1985).
13. Khan W.A., Labrie J.P., Mc Keown J., Radiat. Phys. Chem., **29**, *2*, 117 (1987).
14. . * . Patent Japan *61,289,175* (1986), Invs.: S. Takahashi, H. Nagata, H. Okamoto; CA, **106**, 139788p (1987).
15. Short R.D., Munro H.S., Ward R.J., Mc Briar I., Chan H.S.O., Tau K.L., Polym. Degrad. Stab., 31, *2*, 211 (1991).

16. Ito Y., Imanishi Y., Polym. Prepr., **33**, *2*, 486 (1992).
17. Kubota S., Emori K., Sen'i Gakkaishi, **50**, *8*, 343 (1994).
18. „ " „ Patent USA *104,198* (1993), Inv.: R.J. Petcavich; CA, **123**, 146031r (1995).
19. Hoecker H., Thomas H., Kuesters A., Herring J., Melliand Textilber., **75**, *6*, *E131-E133*, 506-508, 510, 512 (1994).
20. Paul F., Morin A., Monsan P., Biotech. Adv., **4**, 245 (1986).
21. Koepsell H.J., Tsuchiya H.M., J. Bacteriol., **63**, 293 (1952).
22. Bronge A., Dahlgren S., Lindquist B., Acta Chim. Scand., **137**, 29 (1971).
23. Bonar J., Walsh J., Lancet, 614 (1972).
24. Moriau M., Rodhain J., Noel H., Masure R., Vox Sang, **27**, 411 (1974).
25. Neniţescu C.D., *Chimie Organică.* Vol. **II**, Ed. Didactică şi Pedagogică, Bucureşti, 1974, 318.
26. Larm O., Lindbergand B., Svensson S., Carbohyd. Res., **20**, *1*, 39 (1971).

STUDII ESCA ASUPRA DEXTRANULUI MODIFICAT LA SUPRAFAŢĂ

(Rezumat)

Dextranul a fost supus, pentru diferite perioade de timp, acţiunii plasmei (cu frecvenţe de 1,3, 13,56 şi 27 MHz), iradierii cu fascicul de electroni şi radiaţiilor UV. Efectul acestor tratamente asupra structurii a fost diferit, aşa cum rezultă din spectrele ESCA prin analizarea variaţiei conţinutului în legături C–C şi C–O. Rezultatele spectrale au fost corelate cu condiţiile experimentale (durata expunerii, fracvenţa, natura radiaţiei).

BULETINUL INSTITUTULUI POLITEHNIC DIN IAŞI
Tomul XLIII (XLVII), Fasc. 1–2, 1997
Secţia II
CHIMIE şi INGINERIE CHIMICĂ

D.C. 665.581; 095.26

STUDIES CONCERNING THE SYNTHESIS OF POLY(DIMETHYLSILOXANES) IN PRESENCE OF QUATERNARY AMMONIUM COMPOUNDS

BY

AUREL STANCIU, D. TIMPU, GH. STOICA
and VICTOR BULACOVSCHI

The paper deals with the anionic polymerization of various mixtures of cyclosiloxanes in presence of quaternary ammonium compounds. On the example of octamethylcyclotetrasiloxane, there were established the optimum polymerization parameters using benzyltrimethylammonium hydroxide as catalyst. The influence of reaction medium, composition of cyclosiloxane mixtures and nature of the catalyst on the polymer characteristics, were also studied.

The obtained products were spectrally, thermally and viscometrically characterized.

1. Introduction

Polyorganosiloxanes are regularly named "special" polymers because of their unusual characteristics such as: stability to heat and UV radiation, low glass temperature, high gas permeability or a good lubrication. Due to their special properties, polyorganosiloxanes are used in various domains – from electric insulators and biomaterials, to part components in space ships construction [1],...,[5].

The polyorganosiloxanes are usually prepared by ring-opening polymerization of cyclosiloxanes catalyzed by acidic or basic catalysts [6]. Most of the informations are refering to the anionic polymerization of cyclic monomers, which uses the following groups of catalysts [7], [8]:

GOH; GOSi; GR; GSR,

where G denotes an alkaline metal or an ammonium or phosphonium quaternary group; R represents alkyl or trimethylsilylvinyl radicals.

Some authors consider that in such polymerizations, the active species are the free ions and ion pairs [9], so that the intermediates which determine the kinetic model should be the high ionic complexes. However, the chemistry of organoammonium and phosphonium ions does not mention such complexes [10].

Studying the polyorganosiloxane polymers our work includes the preparation of cyclodimethylsiloxane mixtures, and of asimetrical tetraorganoammonium hydroxides including their salts, which were subsequently used for the polymerization of cyclosiloxanes.

The reaction kinetics has been studied on the polymerization of octamethylcyclotetrasiloxane in presence of benzylthrimethylammoniumhydroxide. The influence of reaction medium, composition of monomer mixtures and type of the catalyst on the molecular weight of the polymers, was also analysed.

2. Experimental

2.1. Monomers

The dimethyldichlorosilane (DDS) and octamethylcyclotetrasilane (D_4) were used as received from Fluka AG. The cyclodimethylsiloxane mixtures (I D_n,...,IV D_n) were obtained by controlled hydrolysis of DDS and their characteristics are summarized in Table 1.

Table 1
The Characteristics of Cyclodimethylsiloxane Mixtures

Mixture	d^{20} g/cm^3	n^{20}	η^{20} cst.	Humidity %	Chromatographic composition, [%]					
					D_3	D_4	D_5	D_6	D_7	HMDS
I D_n	0.954	1.3968	2.7027	0.0100	2.58	85.36	10.82	1.13	0.11	0.01
II D_n	0.955	1.3962	2.5938	0.0105	2.37	86.43	9.51	1.54	0.14	0.01
III D_n	0.952	1.3965	2.6037	0.0036	2.35	87.45	9.13	0.93	0.11	–
IV D_n	0.957	1.3968	2.6126	0.0041	0.23	96.48	2.90	0.36	0.03	–

2.2. Preparation of Catalysts

The asymetrical tetraorganoammonium hydroxides were prepared as methanolic solutions and purified by usual methods. The starting materials were benzyltrimethylammonium-, benzyltrietylammonium-, and tetrabutylammonium bromides generously supplied by Merk.

The organoammonium siloxanolates were prepared from D_4 and corresponding organoammonium hydroxides in dry toluene.

The mole number of siloxanolate catalyst per gram of catalyst solution in all cases was determined by potentiometric titration with 0.1 N HCl alcoholic solution.

2.3. Synthesis of Polymers

The polyorganosiloxanes were prepared by ring-opening polymerization of cyclosiloxanes from D_n mixtures, in presence of organoammonium siloxanolates. The reaction conditions are similar to those used in kinetical studies of D_4 polymerization. Thus, D_4 (6.45×10^{-2} mole) and benzyltrimethylammonium hydroxide (BTMAH) (1.317×10^{-3} mole/l L of D_4) were charged into a reactor equipped with mechanical stirring, a reflux condenser, and a nitrogen or CO_2 inlet. The reactor was also connected to a vacuum line. The reactor was heated in a controled temperature bath, and the polymerization carried out with stirring under nitrogen atmosphere. When the reaction was completed, the catalyst was deactivated by quenching the reactor in liquid nitrogen and bubling CO_2 by one hour. Subsequently, the temperature was rised to 160°C and the unreacted monomer was removed by vacuum distilation.

Excepting the situations when kinetical measurements were necessary, after the polymerization period the transient catalyst was readily decomposed by heating the reactor at 160°C and volatile products distilled off.

2.4. Characterization

The obtained polymers were characterized by elemental and spectral analyses. The elemental composition was obtained by usual method. The IR spectra (KBr pellets) were registered on a Perkin-Elmer apparatus and the thermal analyses on a Paulik-Paulik-Erdey MOM Budapest equipment in air, between 20° and 600°C, with a heating rate of 9°C/min.

The molecular weight was viscometrically determined in toluene at 25°C using the semiempirical relation given for polydimethylsiloxane [11]:

$$[\eta] = 8.28 \times 10^{-3} M^{0.72}.$$

3. Results and Discussion

The first step in catalytic polymerization of cyclosiloxanes was the preparation of a number of cyclodimethylsiloxane mixtures designed as mD_n mixtures. They were obtained according the reaction:

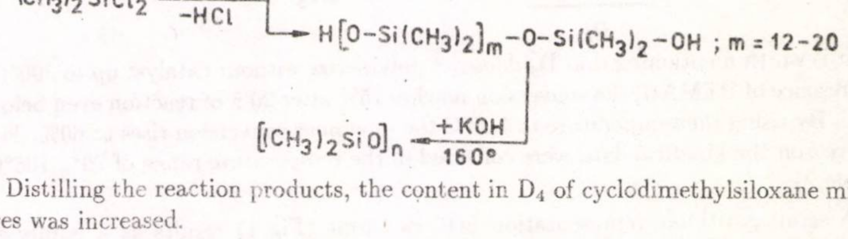

Distilling the reaction products, the content in D_4 of cyclodimethylsiloxane mixtures was increased.

The quaternary ammonium hydroxides absorbed the CO_2 from the air turning to carbonates which have no catalytic activity. For this reason they were stored as aqueous or organic solutions, but even so, after 60 days they loose their qualities.

The approach used in this study was to prepare siloxanolates by reacting the hydroxides with D_4. The quaternary ammonium siloxanolates showed a very good catalytic capacity even after one year of storage. They were prepared separately prior to the polymerization, according the reaction:

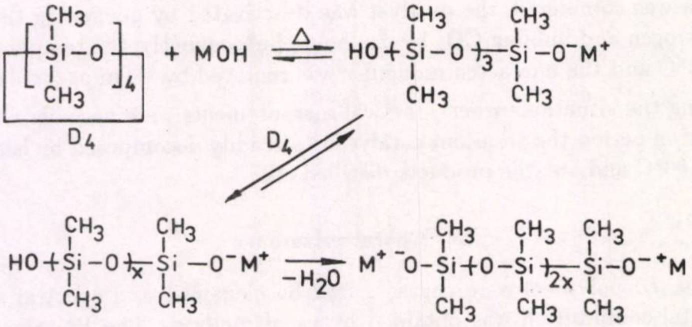

where: M^+ is $C_6H_5CH_2(CH_3)_3N^+$; $C_6H_5CH_2(C_4H_9)_3N^+$ or $(C_4H_9)_4N^+$

The studied catalysts refer to benzyltrimethylammonium siloxanolate (BTMAS), benzyltributylammonium siloxanolate (BTBAS) and tetrabutylammonium siloxanolate (TBAS). While the hydroxide salts of the quaternary ammonium bases are not readly soluble in siloxane media, their siloxanolates yield catalysts that are homogeneous from the beginning of the polymerization reaction.

Because the water and hexamethyldisiloxane, together with other chemicals with labile hydrogen, promote chain transfer reactions, some steps must be considered to eliminate these agents. By contrary, the final molecular weight of the polymers might be low.

For the kinetical purposes and to determine the optimum reaction conditions, the polymerization of D_4 in presence of BTMAH was also studied:

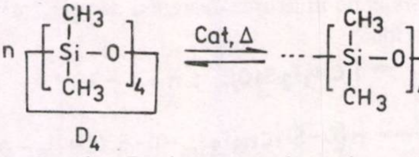

It is worth mentioning that D_4 does not polymerize without catalyst up to 300°C. In presence of BTMAH, the conversion reaches 15% after 20 h of reaction even below 60°C. By rising the temperature to 115°C the monomer conversion rises to 60%. For this reason the kinetical data were collected in the temperature range of 70°...108°C (Table 2).

A semilogarithmic representation $\ln C$ vs. time (Fig. 1) results as a family of lines, which shows that the reaction obeys a first order law. The slop (k_j) of these lines grows as the temperature rises to 105°C, dropping after, probably due to decomposition of the catalyst.

The activation energy obtained from the $\ln k$ vs. $1/T$ representation (Fig. 2) was found to be 16.44 kcal/mol.

It is worth mentioning that for an increase of 30°C in temperature, the reaction rate increases eight times.

Table 2
Experimental Data Concerning Polymerization of D_4

No.	Temp. °C	Time min.	Unreacted monomer mol×100	Polymer yield %
1	70	30	5.743	11.0
2	70	40	5.162	20.0
3	70	50	5.098	21.0
4	70	90	4.033	37.5
5	80	30	5.227	19.0
6	80	40	4.452	31.0
7	80	50	4.065	37.0
8	80	60	3.549	45.0
9	90	15	4.839	26.0
10	90	20	4.581	29.0
11	90	25	4.388	32.0
12	90	40	3.129	51.5
13	101	15	3.162	51.0
14	101	25	2.065	68.0
15	101	35	1.258	80.5
16	101	40	1.032	84.0
17	108	5	5.291	18.0
18	108	15	3.549	45.0
19	108	20	3.097	52.0

$C_0=6.453\times10^{-2}$ mole D_4;
Catalyst BTMAH – 1.317×10^{-3} mole/L of D_4.

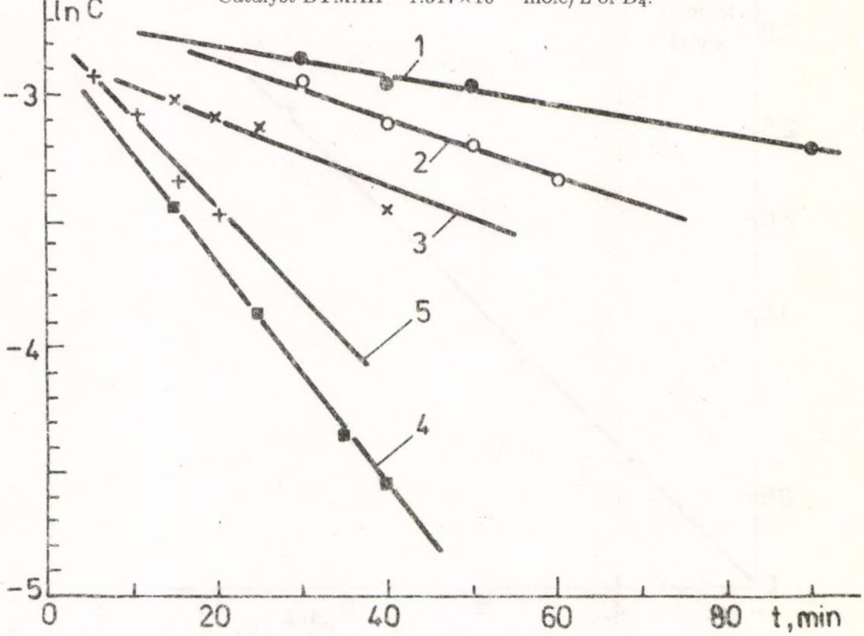

Fig. 1.– The $\ln C$ vs. time dependence at different temperatures: *1* – 70°C; *2* – 80°C; *3* – 90°C; *4* – 101°C; *5* – 108°C.

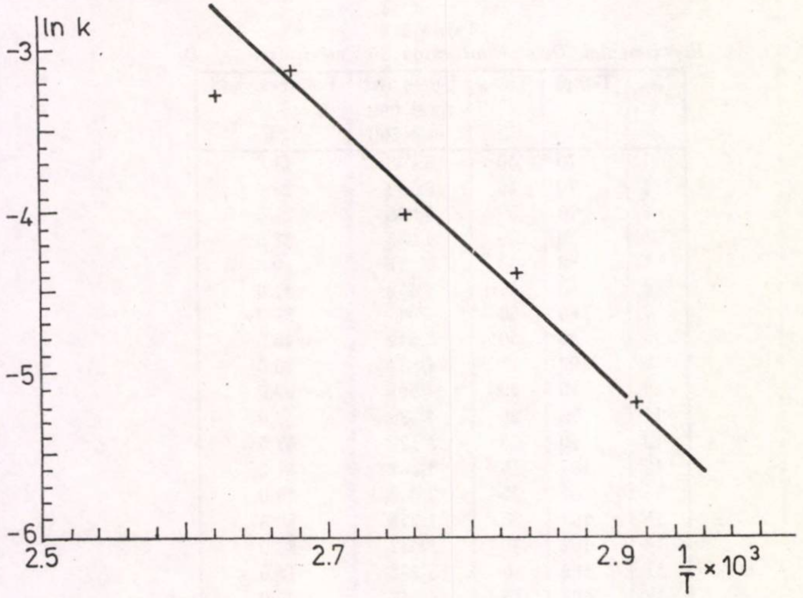

Fig. 2.- The ln k vs. $1/T$ plot for D_4 polymerization in presence of BTMAH.

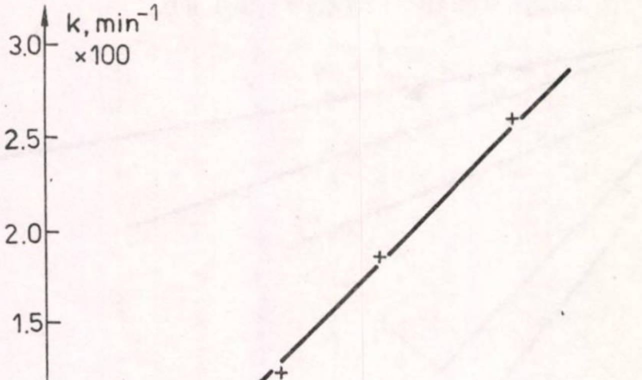

Fig. 3.- Influence of catalyst concentration (C_c) on reaction rate in D_4 polymerization.

The effect of catalyst concentration on the reaction rate is shown in Fig. 3 and one can see that the polymerization of D_4 proceeds fairly rapidly at all levels of the catalyst. The drown lines cross the origin of co-ordinates and that might be a proof that the D_4 does not polymerize in absence of catalyst.

The influence of the catalyst nature on polymerization of D_4 depends on which state it is employed. The data summarized in Table 3 show that for the same set of polymerizations, the activity of the used catalysts does not differ. In the first set the M_n and the conversion are low due to the influence of the methanol and humidity from the reaction medium. Carıying out the polymerization under nitrogen atmosphere, these characteristics rapidly improved. Similar results are obtained if one uses solide hydroxides or siloxanolates. The molecular weights are slightly higher and no catalyst deactivation will occure.

Table 3

The Influence of Nature of the Catalyst on Polymerization of D_4

	Catalyst		Polymer	
No.	State of utilization	Type	Yield, [%]	$M_n \times 10^{-5}$
1	Solution	BTMAH	70.5	0.65
2		BTMAH	84.0	1.88
3		BTBAH	65.4	0.57
4		BTBAH	80.3	2.10
5		TBAH	70.3	0.63
6		TBAH	81.0	1.76
7	Solid	BTMAH	86.0	3.39
8		BTMAH	89.5	4.10
9		BTBAH	90.2	3.95
10		BTBAH	90.4	4.05
11		TBAH	89.0	3.88
12		TBAH	90.0	3.95
13	Siloxanolate	BTMAS	87.0	3.17
14		BTMAS	91.5	4.20
15		BTBAS	90.0	3.65
16		BTBAS	90.5	4.55
17		TBAS	90.0	3.45
18		TBAS	90.6	4.12

The composition of the starting mixture also influences the conversion of monomer and the M_n, and this was followed by carrying out the polymerization of four cyclodimethylsiloxane mixtures (I D_n...IV D_n). The obtained data (Table 4) show that from I D_n and II D_n mixtures, which are rich in HMDS component, the resulted polydimethylsiloxane has poor characteristics. At the same time, the polymers prepared from IV D_4 (which contain almost 96.5% of D_4) had very close behaviours to those prepared from pure D_4.

On the other hand, the obtained results from processing of III D_4 might be explained by a high content in 3 and 5 member cyclosiloxanic rings. Such compounds show increased polymerization rates as compared to transformation of four member cyclosiloxanic units.

Table 4

The Influence of the Composition of the Starting Mixture upon Conversion and Molecular Weight

No.	Catalyst	Mixture	Polymer	
		mD_n	Yield, [%]	M_n^{-5}
1	BTMAH solution	I	76.2	1.98
2		II	81.5	2.14
3		III	86.7	2.45
4		IV	83.0	2.21
5	BTMAH solid	I	86.0	3.67
6		II	90.0	4.04
7		III	91.7	5.03
8		IV	90.3	4.19
9	BTMAS	I	88.7	3.66
10		II	90.3	4.09
11		III	91.6	4.87
12		IV	91.4	4.27

The IR-characterization of PDMS reveals strong absorbtions in the 1,090...1,020 cm^{-1} (ν_{as}Si–O–Si) and 860...800 cm^{-1} (ν_sSi–O–Si) regions, along with the specific signals for CH_3 groups: $\nu_{def}CH_3$ (1,280 cm^{-1} and 1,410 cm^{-1}), ν_sCH_3 (2,900 cm^{-1}) and $\nu_{as}CH_3$ (2,960 cm^{-1}).

It is supposed that the PDMS has a linear structure which is not influenced by the structure of the catalyst.

The elemental composition (C=30.07...32.37%; H=7.82...8.04%; Si=37.58... ...37.71%) was found to be in a good agreement with the theoretical values (C=32.43%; H=8.11%; Si=37.83%).

Interesting data were obtained from thermal analysis of PDMS polymers (Table 5). These products are stable up to 300°...330°C, but decompose over this temperature, in a strong thermo-oxidative process, when weight losses reach 78...81%. The remained rezidium (19...22%) is SiO_2.

Table 5

Thermal Stability of Polysiloxanes

Exp. no.	Destruction domain °C	Kinetical parameters		Weight losses %
		n	E_a kcal/mol	
2	295...478	1.4	41.33	78
4	308...520	1.2	40.52	81
6	307...516	1.1	35.36	80
14	328...530	1.3	42.67	79
16	330...547	1.2	40.14	80
18	325...530	1.1	36.67	81

Kinetical parameters of the thermo-oxidative destruction were calculated by Coat–Redfern method [13] and showed that the thermal degradation is an almost first order reaction (n=1.1...1.4) with an activation energy of 35.36...42.64 kcal/mol.

4. Conclusions

The polymerization of D_4 with BTMAH obeys a first order kinetics with $k^0_{101}=$ $=0.046\ \text{min}^{-1}$. That means it is three times faster than the polymerization of D_4 at 140°C in presence of KOM as catalyst. The optimum parameters for polymerization were found to be $T=100°C$, reaction time – 40 min., $C_k=1.37\times10^{-3}$ mol/1L of D_4.

It is worth mentioning that the polymerization is faster when siloxanolates are used as catalysts.

The quaternary ammonium compounds (BTMAH, BTBAH and TBAH) have a catalytic activity similar to TMAH, therefore, they can be used with good results in anionic ring-opening polymerizations.

The products obtained in polymerization of D_n mixtures are similar to those obtained starting from D_4. This might constitute a technological advantage since one can overpass the step of isolation individual cyclosiloxanes.

The employed procedure gives linear and neutral poly(dimethylsiloxanes) since the catalyst decomposes in nonactive products and it might be conceived as a continuous process which might represent an important direction in poly(organosiloxane) fabrication.

Received, November 5, 1996

Technical University "Gh.Asachi", Jassy,
Department of Macromolecular
Chemistry and Technology

REFERENCES

1. Zeigler J.M., Gordon F.W. (Eds.), *Silicon-Based Polymer Science. A Comprehensive Resource.* Advances in Chemistry Series, **224**, Amer. Chem. Soc., Washington DC, 1990, 45.
2. Rochow E.G., *Silicon and Silicones.* Springer-Verlag, Berlin, 1987.
3. Heimenz P.C., *Polymer Chemistry: The Basic Concepts.* M. Dekker, New York, 1984.
4. Masuda T., Isobe E., Higashimura T., Takada K., J. Am. Chem. Soc., **105**, 7473 (1983).
5. Voronkov M.G., Mileshkevich V.P., Yuzhelevski Yu.A., *The Siloxane Bond – Physical Properties and Chemical Transformations.* M. Dekker, New York, London, 1978.
6. Chojnowski J., J. Inorganic and Organometallic Polym., **1**, 299 (1991).
7. Kendrick T.C., Parbhoo B., White I.W., *Siloxane Polymers and Copolymers* in Patai S., Rappaport Z. (Eds.), *The Chemistry of Organic Silicon Compounds.* Vol. **2**, John Wiley & Sons, New York, 1989.
8. Saam I.C., *Silicon-Based Polymer Science.* Edited by I.M. Zeigler and F.W. Gordon, Amer. Chem. Soc., Washington DC, 1990.
9. Sigwalt P., Actual. Chim., **3**, 45 (1986).
10. Kopylov V.M., Prohodko P.L., Koviazin V.A., Vysokomol. Soed., **A24**, 1751 (1982).
11. Hang A., Meyerhoff G., Makromol. Chem., **53**, 91 (1962).
12. Smith-Lee A., *The Analytical Chemistry of Silicones.* John Wiley, New York, 1991, 305.
13. Coats A.W., Redfern J.P., Nature, **201**, 68 (1964).

STUDII PRIVIND SINTEZA POLI(DIMETILSILOXANILOR) ÎN PREZENŢA COMPUŞILOR CUATERNARI DE AMONIU

(Rezumat)

Se studiază polimerizarea anionică a diferitelor amestecuri de ciclosiloxani în prezenţa compuşilor cuaternari de amoniu. Pe exemplul octametilciclotetrasiloxanului s-au stabilit parametrii optimi de polimerizare folosind hidroxidul de benziltrimetilamoniu drept catalizator.

S-a studiat, de asemenea, influenţa mediului de reacţie, a compoziţiei amestecurilor ciclosiloxanice, cât şi a naturii catalizatorului asupra caracteristicilor polimerului.

Produsele obţinute au fost caracterizate din punct de vedere spectral, termic şi viscozimetric.

BULETINUL INSTITUTULUI POLITEHNIC DIN IAŞI
Tomul XLIII (XLVII), Fasc. 1–2, 1997
Secţia II
CHIMIE şi INGINERIE CHIMICĂ

D.C. 66.022; 621.928; 547.466.1

STUDY ON SEPARATION OF ORGANIC COMPOUNDS BY REACTIVE EXTRACTION

IV. MATHEMATICAL MODELLING OF THE SEPARATION PROCESS OF GLUTAMIC ACID FROM AQUEOUS PHASE

BY

DAN CAŞCAVAL, CORNELIU ONISCU,
EUGEN HOROBA and ADINA DUMITRAŞCU

A correlation between the reactive extraction yield of Glutamic Acid from the aqueous phase with Amberlite LA-2 in butyl acetate and the parameters significantly influencing the process (the pH-value, the concentration of extractant, and the extraction time) is settled. These parameters influence the separation process in a 99.9% extent and their optimum values were determined.

1. Introduction

The Glutamic Acid (GA) is one of the most important amino acid from the viewpoint of its using in medicine or food industries. The annual production of GA is about 400,000 t. This amino acid is obtained by fermentation. The recovery of GA from the fermentation broth is achieved industrially through a lot of laborious stages, with very high materials and energy consumption [1], [2]. To eliminate this technological disadvantages, in the previous works the authors proposed the GA separation from the aqueous phase by reactive extraction with Amberlite LA-2 in butyl acetate as extractant [3].

This paper is aimed to settle a relationship between the reactive extraction yield and the factors influencing decisively this process, namely the pH-value, the extractant concentration in butyl acetate, and the extraction time. In this purpose the statistical analysis was used, with the planning of experiments, the mathematical model describing the reactive extraction of the GA with Amberlite LA-2 being developed on this basis. The parameters significantly influencing the separation have been settled by the Fisher test and confirmed by the study on the yield variation.

2. Materials and Method

2.1. Extraction Equipment

The extraction used equipment consists of a glass column (*1*) of 56 mm inner diameter and 180 mm height, provided with a jacket (*2*) through which passes the thermosetting agent, namely water maintained at 25°C by means of the thermostat (*3*) (Fig.1). The two phases were mixed together by a vibratory mixer (*4*) consisting from a perforated disk of 45 mm diameter having a 17% free section. The vibration had a amplitude of 3.5 mm and a frequency of 50 Hz. The emulsion was evacuated through the valve (*5*) and separated in a centrifugal separator.

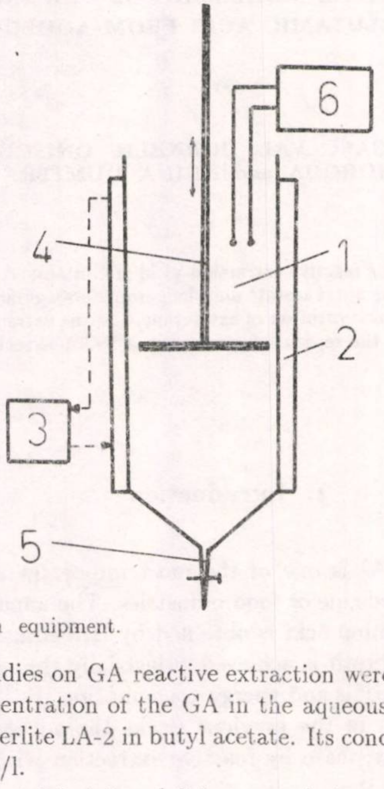

Fig. 1.– The extraction equipment.

The experimental studies on GA reactive extraction were carried out in a batch system. The initial concentration of the GA in the aqueous phase was of 3.10 g/l. The extractant was Amberlite LA-2 in butyl acetate. Its concentration in the solvent was of 46, 106 and 166 g/l.

The pH adjustement at 0.5, 1.5 and 2.5 was made by means of a 5% sulphuric acid solution added to the initial aqueous solution as a function of the prescribed pH-value measured by a digital pH-meter (*6*).

The mixing time (extraction time) was 15, 45 and 75 s.

The volume ratio between the aqueous phase and the organic phase was of 2 : 1 (50 ml organic phase).

The process development was followed up dosing the GA concentration in the initial aqueous phase and in the refined, by the spectrophotometric method, reading the absorbtion of ninhydrin – amino acid complex at 570 nm [4].

2.2. Process Modelling

The reactive extraction yield was calculated by the relationship:

$$Y = \left(1 - \frac{C_1}{C_0}\right) 100, \quad [\%], \tag{1}$$

where: C_0 is the initial concentration of GA in the aqueous solution, [g/l]; C_1 – the concentration of GA in the refined, [g/l].

In this paper, the influence of the pH, the extraction time and the extractant concentration in butyl acetate on the reactive extraction yield was followed up. Thus, real values of the process variables were arbitrarily chosen, their limits and coding being given in Table 1.

Table 1
The Limits and Coding of Process Variables

Variable	Code	Variable level			Step
		–1	0	1	
pH	x_1	0.5	1.5	2.5	1
τ, [s]	x_2	15	45	75	30
C_A, [g/l]	x_3	46	106	166	40

C_A – the concentration of Amberlite LA-2 in butyl acetate, [g/l].

In order to settle the correlation between the obtained extraction yield and the above parameters, the following model has been proposed:

$$Y = b_0 + b_1x_1 + b_2x_2 + b_3x_3 + b_{12}x_1x_2 + b_{13}x_1x_3 + b_{23}x_2x_3. \tag{2}$$

The experimental matrix is given in Table 2.

Table 2
The Experimental Matrix

Exp.no.	x_1	x_2	x_3	Y_{exp}, [%]	Y_{calc}, [%]
1	–1	–1	–1	79.29	78.83
2	–1	–1	1	81.48	81.94
3	–1	1	–1	82.52	82.98
4	–1	1	1	99.13	98.67
5	1	1	1	81.33	81.79
6	1	–1	–1	50.12	50.58
7	1	1	–1	57.53	57.07
8	1	–1	1	63.18	62.72
9	0	0	0	91.93	–
10	0	0	0	92.44	–
11	0	0	0	93.81	–
12	0	0	0	92.60	–

By means of the obtained data the regression coefficients b_j, the sum of the regression coefficients squares $\mathrm{SP}(b_j)$ and the experimental error S_r^2 have been calculated according to literature [5] using the following relations:

$$(3)\qquad b_0 = \overline{Y},\ \ b_j = \frac{\sum\limits_{i=1}^{8} x_{ji} Y_i}{\sum\limits_{i=1}^{8} x_{ji}^2},\ \ b_{jk} = \frac{\sum\limits_{i=1}^{8} x_{ji} k_{ki} Y_i}{\sum\limits_{i=1}^{8} x_{ji}^2 k_{ki}^2},\ \ (j = 1, ..., 3;\ k = 1, ..., 3),$$

$$(4)\qquad \begin{gathered} \mathrm{SP}(b_0) = \sum_{i=1}^{8} Y_i^2, \qquad \mathrm{SP}(b_j) = b_j \sum_{i=1}^{8} x_{ji} Y_i - \frac{\left(\sum\limits_{i=1}^{8} x_{ji}\right)\left(\sum\limits_{i=1}^{8} Y_i\right)}{8}, \\ S_r^2 = \frac{\sum\limits_{i=1}^{n} \left(Y_i - \overline{Y}\right)^2}{n-1}, \qquad n = 4. \end{gathered}$$

The experimental error was estimated based on the results of the 9...12 runs in the programme centre:

$$S_r^2 = 0.634.$$

The obtained values are listed in Table 3.

Table 3

The Obtained Values for the Regression Coefficients

Regression coefficient	Value
b_0	74.32
b_1	-11.28
b_2	5.805
b_3	6.958
b_{12}	0.585
b_{13}	3.145
b_{23}	2.258

Table 4

The Values of the Function F

Function F	Value
F_0	7.254×10^6
F_1	1.605×10^3
F_2	0.425×10^3
F_3	0.611×10^3
F_{12}	4.319
F_{13}	64.337
F_{23}	0.125×10^3

The standard deviation is:

$$S_{Yxxx} = 0.649.$$

For checking the normal results obtained in the programme centre the Q-test was used. Thus, the calculated Q value is [5]:

$$(5)\qquad Q = \frac{|a_1 - a_2|}{R} = 0.643,$$

where: a_1 is the uncertain value (93.81%); a_2 – the closest to the uncertain value (92.60%); R – the amplitude (difference between the most distant values).

From literature [5], for a certain threshold of 0.05, Q=0.77 was found. Since the calculated value of 0.643 is lower than the tabulated one (of 0.77) it follows that the uncertain value of 93.81% is also a normal value, so that the four yields values obtained in the programme centre were taken for calculation.

To settle the factors which are influencing decisively the separation process the Fisher test was used. The values of the Fisher function were calculated with the following relation and compared with the tabulated values [5]:

$$F = \frac{\mathrm{SP}(b_j)}{S_r^2}. \tag{6}$$

For a confidence level of 0.05 and for three and seven freedom degrees values, it was found from [5] that F=4.35. All the values of the F function greather than the tabulated one indicate that these factors significantly influence the reactive extraction of the GA with Amberlite LA-2.

Hence, the regression equation may be written as:

$$Y = 74.32 - 11.28x_1 + 5.805x_2 + 6.958x_3 + 0.585x_1x_2 + 2.258x_1x_3 + 3.145x_2x_3. \tag{7}$$

The calculated values of the reactive extraction yield were listed in the Table 2. The experimental yield values varried around the calculated ones:

$$Y_{i\mathrm{exp}} = Y_{i\mathrm{calc}} \pm tS_{Yx_1x_2x_3}. \tag{8}$$

The t values are to be found in the tables for Student distribution [5], for a confidence threshold of 0.05 and seven degrees of freedom namely:

$$t = 2.365 \qquad \text{and} \qquad Y_{i\mathrm{exp}} = Y_{i\mathrm{calc}} \pm 1.535.$$

The overall influence of the factors under consideration is estimated by means of the value of the multiple correlation coefficient, r_{Yxxx}:

$$r_{Yx_1x_2x_3} = \sqrt{1 - \frac{S^2_{Yx_1x_2x_3}}{S_Y^2}}, \tag{9}$$

where:

$$S_Y^2 = \frac{\sum\limits_{i=1}^{n}(Y_i - \overline{Y})^2}{n - (k-1)}, \qquad n = 1,\ k = 3, \tag{10}$$

denotes the dispersion of the individual values, Y_i, around the mean value for the 12 runs. The value of r_{Yxxx}=0.9993, resulting by calculation, would suggest a good correlation between the experimental values and the regression equation. In fact, this conclusion was substantiated by the tabulated values of the experimental and calculated reactive extraction yields (Table 2).

3. Determination of Optimum Values of the Parameters under Consideration

To determine the optimum values of the parameters which are decisively influencing the reactive extraction of the GA from the aqueous phase an optimization calculation of regressive equation previously derived has been performed. Thus, the gradient method [6] and the following restrictions were taken into account:

$$-1 \leq x_1 \leq 1, \quad -1 \leq x_2 \leq 1, \quad -1 \leq x_3 \leq 1, \quad Y \leq 100\%. \tag{11}$$

The optimum was found on the boundary, the optimum values of these parameters being in this case:

$$x_1 = -1, \quad x_2 = 1, \quad x_3 = 1.$$

With these values the parameter decoding was made and the following values resulted:

$$\text{pH} = 0.5, \quad \tau = 75 \text{ s}, \quad C_A = 166 \text{ g/l}$$

for a maximum yield of 98.67%.

4. Conclusions

The separation of Glutamic acid from aqueous solution by reactive extraction with Amberlite LA-2 in butyl acetate was studied and an empirical mathematical model describing this process was derived. With this aim the influence of pH-value, the extractant concentration in organic phase and the mixing time was followed up. The conclusion was that these parameters influence the separation in a 99.9% extent and their determined optimum values are:

$$\text{pH} = 0.5, \quad \tau = 75 \text{ s}, \quad C_A = 166 \text{ g/l}.$$

Received, May 15, 1995

Technical University "Gh.Asachi", Jassy,
Department of Organic Industries

REFERENCES

1. Oniscu C., *Tehnologia produselor de biosinteză.* Ed. Tehnică, Bucureşti, 1978.
2. Raicu P., *Biotehnologii moderne.* Ed. Tehnică, Bucureşti, 1990.
3. Caşcaval D., Oniscu C., Tudose R., Bul. Inst. polit., Iaşi, **XLII (XLVI)**, *1-2*, s.II (1996).
4. Magearu V., *Controlul analitic al proceselor biotehnologice.* Ed. Tehnică, Bucureşti, 1988.
5. Gluck A., *Metode matematice în industria chimică.* Ed. Tehnică, Bucureşti, 1971.
6. Curievici I., *Optimizări în industria chimică.* EDP, Bucureşti, 1980.

STUDIUL SEPARĂRII COMPUŞILOR ORGANICI PRIN EXTRACŢIE REACTIVĂ
IV. Modelarea matematică a procesului de separare a acidului glutamic din fază apoasă

(Rezumat)

Se stabileşte o corelaţie între randamentul procesului de extracţie reactivă a acidului glutamic cu Amberlite LA-2 şi parametrii care influenţează semnificativ procesul, respectiv valoarea pH-ului, concentraţia agentului de extracţie în solvent şi timpul de extracţie. Calculele au evidenţiat faptul că aceşti parametri determină în proporţie de 99,9% procesul, obţinându-se valorile optime ale acestora.

BULETINUL INSTITUTULUI POLITEHNIC DIN IAŞI
Tomul XLIII (XLVII), Fasc. 1–2, 1997
Secţia II
CHIMIE şi INGINERIE CHIMICĂ

D.C. 621.384.3; 661.8...455

SPECTROSCOPIC STUDY OF COMPLEXES BASED ON TRIBUTYLPHOSPHATE

EFFECT OF THE SOLVATED MOLECULE MASS UPON THE P=O BOND

BY

ABDELKRIM AZZOUZ, MOULOUD ATTOU and MOHAMED-AMINE DIDI

The infrared study of TBP and its related metal complexes was undertaken. The complexes [TBP-Metal nitrates] were prepared by contacting equal volumes (10 ml) of a 40% TBP solution in kerozene with saturated aqueous solutions of nitrates of cobalt, uranyl, thorium and nitric acid. The IR spectra were recorded using a Philips-Pye Unicam SP-300 and a Perkin-Elmer spectrometer. Quantitative IR spectroscopy suggests a $UO_2(NO_3)_2TBP_3$ formula with a monodendate nitrate ion. By complexation, only the P=O bond stretching of the complex is altered, whereas the P–O–C band stretching of TBP does not seem to be affected.

1. Introduction

The organic esters of *o*-phosphoric acid are well known as being complexing agents in hydrometallurgy. Tributylphosphate (TBP) is one of the most powerfull extracting agent and its use is of a great interest, especially in the recovery of lanthanides or actinides from aqueous leaching solutions resulting from ores treatments. The TBP complexation ability with metal salts is due to its P=O bond.

The infrared spectra of alkyl esters have been already reported [1] and also suggested the correlations for the P=O, P–H and P–O bonds [2], [3]. Attempts for studying the complexes of TBP, mostly with uranyl nitrate, were also made [4], [5]. The main difficulty arises from the fact that the data resulting from IR investigations are strongly dependent on the operating conditions, e.g., the purity, the pH value and the concentrations of the contacted solutions. In this context, the main aim of this paper consists in examining the behaviour of the P=O bond in some combinations of tri-*n*-butylphosphate with compounds such as nitrate salts or acids using saturated solutions.

2. Experimental

TBP and the nitrates salts used in the present investigations were supplied by Merck and were of puriss grade. The complexes were prepared by contacting equal volumes (10 ml) of a 40% TBP solution in kerozene with saturated aqueous solutions of nitrates of cobalt, uranyl, thorium and nitric acid.

The IR spectra were recorded using a Philips-Pye Unicam SP-300 spectrometer. Liquid samples were examined as films between KBr plates having a 4 mm thickness. Air is used as reference. For further correlation, spectra of some substances have also been measured by a Perkin-Elmer spectrometer using NaCl and Servofrax plates.

3. Results and Discussion

3.1. Infrared Spectroscopy of Pure TBP

According to the authors, the infrared spectra for TBP are different, and until now no standard spectra were available. Thus, in the present investigations, there has been performed three spectra using NaCl, KBr and Servofrax on two different instruments. The results are summarized in Table 1. These correlations are in good agreement with those reported by Bellamy and Beecher [6].

Table 1

Main Infrared Bands of Pure TBP

Bands	Pye-Unicam	Perkin Elmer	
	KBr	NaCl	Servofrax
C–H stretching	2,960	2,980	2,910
CH_2 stretching shoulder	2,875	2,890	2,880
P=O stretching	1,280	1,275	1,270
CH_2 bending	1,460	1,468	1,463
P–O–C stretching	1,030	1,028	1,000
C–H rocking	910	908	900
CH_3 symmetric stretching	1,380	1,380	1,381

Characteristic IR bands of TBP are attributed essentially to stretching vibrations of C–H (2,960 cm^{-1}), P=O (1,280 cm^{-1}) bonds and to P–O–C (1,030 cm^{-1}) group. The presence of the aliphatic group is revealed by the $-CH_2$ shoulder at 2,875 cm^{-1}, the angle deformation between both C–H bonds (1,460 cm^{-1}) and the swinging of the P–O–C (1,030 cm^{-1}) group.

a) *The P=O bond*

It was early observed [2], [7] that if compared phosphoric acid esters and phosphine oxide, the P=O frequency shifted unidirectionally. The position of the P=O band seems to depend on the electronegative effects of the attached groups [8]. In this molecule, there are two competitive trends: (i) oxygen is more electronegative than phosphorus and attracts the electron; (ii) nevertheless, the neighbouring electronegative alkoxy groups tend to reduce this electron delocalisation. It results a stronger P=O band and the corresponding band position is shifted to higher frequency. In some alkylphosphates the absorption of P=O band is weak, and this can be explained by the presence of an $O-C_2H_5$ vibration close to that of the P=O bond.

b) *The P–O–C (Aliphatic) Bond*

The observation of the spectra shows that in all cases the P–O–C (aliphatic) bond intensively absorbs between 1,000 and 1,050 cm^{-1}. Such a squeletal vibration generally occurs in a narrow range. Moreover, only slights shifts appear to be produced by the substitution of the alkyl group by ethyl, buthyl or 2-ethylhexyl radicals.

3.2. Infrared Spectroscopy of Complexed TBP

a) *The Shift of the P=O Bond*

Practically, the TBP molecule is rarely free being often complexed with water, acids, solvents and any other impurities present in TBP. The change between a complex and another one is strongly dependent on the media features, e.g.: pH, concentration.

As previously quoted, only the P=O band can be altered by the presence of solvated species in TBP or by the solvant nature, as further examined. For instance, addition of water to TBP until saturation shifts the absorption band from 1,250 to 1,260 cm^{-1} [9]. When nitric acid was used, this band appears at 1,208 cm^{-1}, as illustrated in Table 2.

Table 2

Positions of P=O Band in TBP Complexes

Mixture	Mass of solvated molecule g/mole	P=O band cm^{-1}
TBP	0	1,280
TBP/H_2O	18	1,260
TBP/HNO_3	63	1,208
TBP/$UO_2(NO_3)$	394	1,194
TBP/$UO_2(NO_3)_2$ (in HNO_3)^a	457	1,188
$UO_2(ClO_4)_2$ (in CCl_4)^b	468.9	1,183
$Th(NO_3)_4$	480	1,182
$Th(NO_3)_4$ (in HNO_3)^a	543	1,170

[a] one assumed that a molecule of nitric acid and a molecule of uranyl nitrate are simultaneously extracted into the same $UO_2(NO_3)_2$–TBP_3–HNO_3 complexe;

[b] one considers that this non polar solvent is not complexed to TBP.

The P=O stretching band of TBP is observed at 1,275...1,280 cm^{-1}. During the complexes formation, the P=O stretching band is generally shifted towards lower wavelengths. Katzin [9] asserts that the weight of the solvated molecule is probably the predominant factor of the P=O band shifting. This assertion is in good agreement with our results, as illustrated by Fig. 1. The data presented in this figure take into account that each molecule of TBP is complexed only with one mole of solvated molecules.

Thus, it can be easily observed that increasing the mass of the solvated molecules, a shift of the $\nu_{P=O}$ to the small value by comparison with pure TBP was induced. The solvatation effect may also depend on the cationic charge and on the nature and the strength of the attraction force between TBP and the solvated molecule.

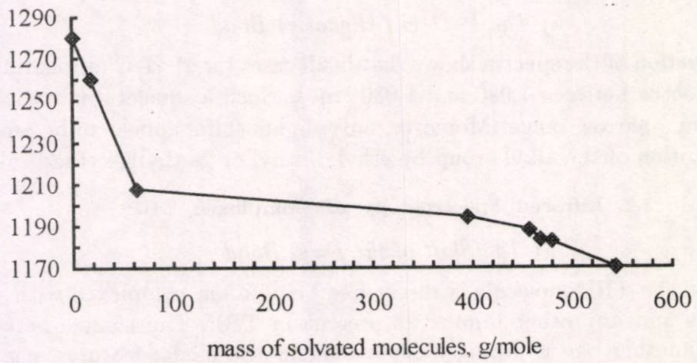

Fig. 1.– Effect of the mass of the complexed molecules upon the $\nu_{P=O}$ value.

b) *Other Features of the TBP Complexes*

The compounds which bear a metal atom and a nitrate group is also characterized by IR bands laying in the regions of 1,530...1,480 cm^{-1} and 1,290...1,253 cm^{-1}. These bands indicate in some extent that the nitrate group is co-ordinated to the metal atom by means of an oxygen atom (Table 3). The P=O band related to water saturated TBP shows a 10 cm^{-1} shift; this fact can explain the band that appears between water and the oxygen of the phosphoryl group [10].

Table 3

Characteristic Bands of the Molecules Solvated by TBP

Band	$UO_2(NO_3)_2$	$Th(NO_3)_4$	$Th(NO_3)_4$	$UO_2(ClO_4)_2$	$UO_2(NO_3)$	$Th(NO_3)_4$
Medium	HNO_3	water	HNO_3	CCl_4	water	water
NO_3 sym.stret.	1,275	1,280	1,310	–	1,275	1,275
NO sym.stret.	1,510	1,522	1,664	–	1,516	1,503
OH bending	–	–	–	–	1,640	–
Uranyl group	930	–	–	–	930	–

In this case, one can observe that the broad OH bonded region at 3,430 cm^{-1} disappeared. In addition, there appears no free OH band in this complex and therefore the complex of TBP is probably bonded to hydrogen atom of nitric acid. Moreover, one must point out that the infrared spectrum of HNO_3 in TBP shows three bands that decrease in absorbance as the concentration of TBP is decreased by displacement with HNO_3 (~820, 800 and ~1,300 cm^{-1}). One can also observe a shift toward longer wavelength [11], for the hydrogen bonded phosphoryl group by decreasing the TBP concentration. However, this particular shift is independent upon the medium and is rather a result of the formation of the complexe involving HNO_3 and TBP. Some vibrations bands attributed to nitrate groups are listed for TBP–HNO_3 complex in the region of 1,500...1,600 cm^{-1} (NO_2 antisymmetric stretching vibration). Absorption bands of the NO_3^- ion are not observed.

c) *Effect of the Concentrations*

In such complexes, the concentration of uranyl nitrate is a determinant factor. An increase of this concentration is accompanied by some qualitative changes in IR spectra. Concerning the $TBP/UO_2(NO_3)_2/HNO_3$ system, an increase of uranyl nitrate concentration deals to the increase of the intensity of the band observed at 1,190...1,195 cm^{-1} attributed to the P=O bond vibration.

Another increase was observed for the intensity of the IR bands in the 930 and 1,520 cm^{-1} regions corresponding respectively to the uranyl ion and to the NO_2 antisymmetric stretching vibrations. Moreover, the intensity band of the 1,275 cm^{-1} region, related to the NO_2 symmetric stretching, decreases. At saturation, the region listed at 1,280 cm^{-1} represents itself completely the NO_2 symmetric stretching.

Maintaining constant the $UO_2(NO_3)_2$ concentration and decreasing that of the nitric acid, the 930 and 1,275 cm^{-1} bands, related to symmetric stretching vibrations of the uranyl ion and of the NO_2 group, remained constant. The large P=O band is shifted toward 1,185 cm^{-1}.

d) *The Complexes Stoichiometry*

A special interest must be devoted to the IR spectra of $[UO_2(NO_3)_2TBP]$ complex. It is generally well accepted that uranyle nitrate is extracted by TBP into the $[UO_2(NO_3)_2TBP_2]$ form, such a complex containing two bidendate ions. Quantitative IR spectroscopy has already allowed the determination of a third TBP molecule in the considered complex suggesting, thereby, a $[UO_2(NO_3)_2TBP_3]$ formula with a monodendate nitrate ion.

It is also assumed that the oxygen atom of the nitrate ion is shifted from the six coordination sites of the uranyl ion and the vacant place is then occupied by an oxygen atom of the P=O groups. The difference between the two complexes is materialized by the occurrency of three P=O bonds and three -N=O bonds instead of two in the complex containing three molecules of TBP (Table 3).

The stability of a given TBP complex is dependent upon the importance of the shifting. When the latter is important, the stability of the complex is better. This fact can be due to the covalent nitrate bonding. As it is known, covalent nitrate bonding in TBP solutions of nitric acid and metal nitrates shifts the nitrate absorption band to lower wavelength [12].

4. Conclusions

IR spectroscopy study of complexes of TBP shows that only the P=O bond stretching of the complex is altered. A certain linearity between the frequency shifting of P=O band stretching and the covalence capacity of nitrates in given solvents was observed. This correlation is in agreement with the fact that the ionic potential relative to the P=O band shifting is directly dependent on the covalence capacity of the compound. It can be concluded that covalent species are much more extracted than ionic ones. The P-O-C band stretching of TBP does not seem to be affected, fact that signifies that the oxygen of the butyl group is not implied in the complex formation.

Received, April 26, 1995

Centre de Développement
des Matériaux, Alger
et
Université de Tlemcen, Algérie

REFERENCES

1. Meyrick C.I., Thompson H.W., J. Chem. Soc., 225 (1950).
2. Daasch L.W., Smith D.C., Anal. Chem., **23**, 853 (1951).
3. Gore T.C., Disc. Faraday Soc., **9**, 138 (1950).
4. Ferraro J.R., J. Inorg. Nucl. Chem., **10**, *3/4*, 319 (1959).
5. Ohwada K., Ishihara T., J. Inorg. Nucl. Chem., **28**, *10*, 2343 (1966).
6. Bellamy L.J., Beecher L., J. Chem. Soc., **83**, 475 (1952).
7. Bell J.V., Heisler J., Tannenbaum H., Goldenson J., J. Am. Chem. Soc., **76**, 5185 (1954).
8. Thomas L.C., *Interpretation of the Infrared Spectra of Organophosphorus Compounds.* Heyden, London, 1974.
9. Katzin L.I., Mason G.W., Peppard D.F., Spectrochimica Acta, **34A**, 57-61 (1978).
10. Afonin A.A., Komarov E.V., Smirnov A.V., Zhur. Strukt. Khim., **30**, *6* (1978).
11. Shuler W.E., *Nitric Acid Species in Tri-n-butylphosphate Solutions.* AEC Research and Development Report, 1960.
12. Woodhead J.L., J. Inorg. Nucl. Chem., **27**, *5*, 1111 (1965).

STUDIUL SPECTROSCOPIC AL COMPLECŞILOR BAZAŢI PE TRIBUTILFOSFAT

Efectul masei moleculei solvatate asupra legăturii P=O

(Rezumat)

A fost întreprins studiul, prin spectroscopie IR, al tributilfosfatului (TBP) şi al complecşilor săi. Complecşii TBP-azotaţi metalici au fost preparaţi prin contactarea, la volum egal (10 ml), a unei soluţii 40% TBP în kerosen cu o soluţie apoasă saturată de azotat de cobalt, uranil, toriu şi de acid azotic. Spectrele IR au fost înregistrate cu două spectrofotometre: Philips-Pye Unicam SP-300 şi Perkin-Elmer. Prin studiul cantitativ IR s-a stabilit formula complexului cu azotat de uranil ca fiind $UO_2(NO_3)_2TBP_3$, având o structură monodentată. Prin complexare numai frecvenţa la întindere a legăturii P=O este influenţată, în timp ce frecvenţa legăturii P–O–C a TBP-ului nu pare a fi afectată.

BULETINUL INSTITUTULUI POLITEHNIC DIN IAŞI
Tomul XLIII (XLVII), Fasc. 1-2, 1997
Secţia II
CHIMIE şi INGINERIE CHIMICĂ

RADU VASILIU
1920 – 1997

On January 14-th 1997, passed away professor dr.eng. Radu Vasiliu, at the 77 years of age, distinguished scientist and professor, outstanding personality of the Faculty of Industrial Chemistry, former head of the Engineering Chemistry and Physical Chemistry Departments.

Professor Radu Vasiliu has bean born in Jassy, in 1920, in a middle-class family. He performed his medium schooling at the well-known "National Lyceum" where, under a beneficial education, he plenary could enhance his natural propensity for the study of physics, chemistry and technology.

In 1939 he enrolled for Faculty of Industrial Chemistry, one of the most important to belong to Polytechnic School "Gh. Asachi". Here, Radu Vasiliu accomplished his engineering grounding in industrial chemistry and graduated in 1944 with an excellent record from the professorial staff.

As a student, Radu Vasiliu clearly proved to be very determined to became a good engineer in the branch of industrial chemistry and its excellent results entailed the esteem and appreciation of his professors. Therefore, after graduation Radu Vasiliu was recommended to be a member of the teaching staff of the Faculty.

His universitary career begun in 1944, firstly as assistant at Electrochemistry and Metallurgy Department, under the professional guidance of professor Ioan Ciochină. At the same time, Radu Vasiliu took the advantage to make extra-studies with academician professor Ştefan Procopiu, afterwards with professor Teofil Vescan.

In this way he acquired an excellent experience in Electricity and Magnetism, Radioactivity, Applied Physics and several other related domains.

For eight years (1960-1968), Radu Vasiliu was in charge of the Radioactive Isotopes Department, part of the Institute of Physics.

As a recognition of his scientific merits, in 1979 professor Radu Vasiliu has been accredited by the Ministry of Education as Ph.D. supervisor in the domain of Electrochemistry.

Inside of scientific community, professor Radu Vasiliu is to be known for his remarkable contributions in the realm of theoretical and applied Electrochemistry, Radiochemistry, Radioactive isotopes (especially for establishing the rates and mechanism of the chemical transformations). His entire scientific work has been materialised in numerous scientific papers, patents, research projects, scientific contracts, public conferences in different scientific meetings, etc.

For the use of his students, professor Radu Vasiliu wrote several textbooks in Electrochemistry, still consulted.

Peoples just like professor Radu Vasiliu that sort of peoples, are now more in more of rare accuracy; he was strongly devoted to his profession, sincerely attached to the scientific community, open-hearted with his colleagues and his students, conscientious, tactful, earnest and helpful.

Professor Radu Vasiliu was not only a typical specialist in chemical engineering but a highly cultivated person, disposed toward the subtle analyses and syntheses, to history and philosophy, to the great culture on the whole. He often was enough concerned by subtle anxieties such as the limits of the human knowledge.

On January 14-th, 1997, the scientific community of our University suffered an irremediable lost.

Technical University "Gh.Asachi", Jassy,
Department of Physical Chemistry

BULETINUL INSTITUTULUI POLITEHNIC DIN IAŞI
Tomul XLIII (XLVII), Fasc. 1–2, 1997
Secţia II
CHIMIE şi INGINERIE CHIMICĂ

GHEORGHE ROZMARIN
1928 – 1997

Professor Gheoreghe Rozmarin was born on April 17, 1928, in the village of Zubreşti, the district of Lăpuşna, Bessarabia.

In 1951 he graduated the Faculty of Industrial Chemistry, at the Polytechnic Institute of Jassy. Between 1952-1955 he is assistant at the Departments of Russian language, Mathematics and Analytical Chemistry and, starting with 1955, he becomes lecturer in the Department of Cellulose, Paper and Artificial Yarns, this year representing the beginning of his long-life didactic and scientific career. The first results of the investigations developed are already recognized by the prize awarded to his team by the Ministry of Education (1958). As assistant (1957-1962), he specializes himself in the technology of artificial yarns and chemistry of wood, bringing important contributions to the laboratories' organization and preparation of highly qualitative laboratory works for students. As member of a team deeply involved in settling in Romania a new domain of scientific research, the efforts made for the realization of such ambitious objectives are crowned in 1963, when he defends his Ph.D. thesis and becomes a doctor in the chemistry and technology of cellulose.

He attends several specialization stages abroad and is actively present in most of the scientific manifestations organized both in Romania and in countries with a rich scientific tradition.

Between 1962-1965, Gh. Rozmarin is lecturer, teaching Wood Chemistry and Technology of Hydrolytic Preparations. In parallels, he becomes chief of laboratory at the "P. Poni" Institute of Macromolecular Chemistry of Jassy (1964-1974) – another opportunity for extending his main scientific concerns.

In 1965 he becomes assistant professor and in 1972 – full professor in the Department of Cellulose, Paper and Artificial Yarns.

The didactic and scientific endowments of professor Gh. Rozmarin have been unanimously recognized, both in Romania and abroad.

Thus, between 1969-1970 he is associate professor at the Faculty of Sciences of the University of Grenoble (France), and between 1974-1975 – professor at the University Mohamed V of Rabat (Morocco).

In 1984, he is elected member of the International Academy for Wood Science (IAWS) and from 1979 he is a Ph.D. supervisor in the domain of wood, cellulose and lignin chemistry.

In parallels with all these activities, professor Gh. Rozmarin was also member of various diploma boards of examiners, didactic degrees certification, and organizer of the international symposia on cellulose held in Jassy starting with 1966. Special mention should be made of his contributions as a member of the Editorial board of the international journal, issued in Jassy, *Cellulose Chemistry and Technology* (1967-1997). His didactic activity involved teaching of wood chemistry, chemistry of macromolecular compounds, technology of hydrolytic preparations, polymer rheology, physical and organic chemistry; lured by the desire of a continuous improvement of the teaching level, he published 7 courses and laboratory guide books for students, candidates for a doctor's degree and independent researchers.

The results of his investigations have been materialized in the realization – within a collaboration project – of two important monographs: *The Chemistry of Reed* (1966) and *The Chemistry of Wood in Romania. The Popular and the Willow* (1973) – which remain as remarkable contributions brought to the field, world widely recognized.

In 1984, professor Rozmarin publishes the monograph entitled *Macromolecular Bases of Wood Chemistry* – a highly original study, both by its conception and manner in which the genuine results of the Romanian school of cellulose and paper had been inserted among the international ones.

Professor Rozmarin wrote about 220 scientific studies, presenting essential information of annual plants, hardwood species, hydrolytic and fermentative treatments, chemical modification of lignin, hydrolysis, analytical methods in wood chemistry, cellulose structure.

Professor Rozmarin used to impress everybody around him – colleagues, students, co-workers – by his profound and sincere attachment to school, to which he dedicated his whole activity. His name remains as a reference in the evolution of wood chemistry – a domain to which his contributions will always remain.

Today, when he is absent – no more among us – we came to realize he was a model of teacher, wholly engaged in serving school, and the very numerous promotions of engineers he formed.

He will be always remembered.

Technical University "Gh.Asachi", Jassy
Department of Cellulose, Paper and Yarns

BULETINUL INSTITUTULUI POLITEHNIC DIN IAŞI
Tomul XLIII (XLVII), Fasc. 1–2, 1997
Secţia II
CHIMIE şi INGINERIE CHIMICĂ

RECENZII BOOK REVIEWS

BERNÉ F., CORDONNIER J., *Traitement des eaux. Épuration des eaux résiduaires de raffinage. Conditionnement des eaux de réfrigération.* Editions TECHNIP, Paris, 1996, 306 pp., ISBN 2.7108-0613-4.

„L'ouvrage de MM. François Berné et Jean Cordonnier s'inscrit dans la collection des enseignements du Centre d'Études Supérieures Raffinage, Pétrochimie et Ingénierie de l'École Nationale Supérieure du Pétrole et des Moteurs.

En effet, le traitement des eaux résiduaires et des eaux de réfrigération produites par l'activité industrielle est devenu la préoccupation quotidienne des exploitants d'Usines et, particulièrement, de raffineries de pétrole et d'installations pétrochimiques.

La lutte contre la pollution, le souci permanent de limiter la consomation de l'eau, devenue rare ces dernières années, constituent pour les industriels des problèmes essentiels et les installations de traitement reçoivent autant de soin et d'attention que les unités de production.

Cet ouvrage constitue un bilan des sources de pollution et une synthèse des techniques les plus récentes utilisées en antipollution et restera un document de base pour les ingénieurs de nos usines."

(M. Verwaerde - Avant-propos)

Chapitre 1: *Chimie des eaux naturelles et des eaux résiduaire industrielles*; 1. Composition Minérale des eaux; 2. Impuretés des eaux naturelles; 3. Caractérisation des eaux de réfrigération atmosphérique; 4. Caractérisation des eaux résiduaires dans l'industrie du pétrole; 5. Interprétation des analyses d'eaux; 6. Principales réactions développées lors des traitements chimiques; Chapitre 2: *Les effluents du raffinage et leur épuration primaire*: 1. Les sources d'Er au raffinage et au vapocraquage; 2. Legislation; 3. Définition et organisation des traitements; 4. Prétraitement des condensats „acides"; 5. Prédeshuilage; 6. L'épuration physico-chimique des effluents prédeshuilés; Chapitre 3: *Epuration biologique aérobie et traitements tertiaires des effluents du raffinage et de la pétrochimie*; 1. Systèmes d'épuration biologique aérobie; 2. Réalisations des épurations biologiques par boues activées; 3. Traitements tertiaires; Chapitre 4: *Traitement des soudes usées*; 1. Origine et composition des SU; 2. Désulfuration des SU; 3. Déphénolage des SU; Chapitre 5; *Traitements des effluents de la pétrochimie*; 1. Originalités des effluents de la pétrochimie; 2. Notion de „Polluants toxiques"; 3. Influence de la salinité et de certains composés; 4. Traitements particuliers; 5. Production de styrène; 6. Production d'oxyde de propylène; 7. Production de polypropylène; 8. Production de polystyrène; 9. Production de nylon-6; Chapitre 6; *Chaines de traitement. Contrôle de l'épuration et disposition des boues*; 1. Mobil oil Française. Raffinerie de Gravenchon; 2. ELF. Raffinerie de Grandpuits; 3. Société des pétroles Shell. Raffinerie du Petit-Couronne; 4. ESSO SAF. Port-Jérome; 5. Complexe Shell de Berre; 6. Disposition des boues; 7. Contrôle des chaines d'épuration; Chapitre 7: *Le conditionnement de l'eau des circuits de refroidissement*; 1. Rappel des différents types de circuits rencontrés; 2. Principales caractéristiques d'un circuit sémi-ouvert sur refrigérant atmosphérique; 3. Inconvénients rencontrés et origines; 4. Protection contre les salissures et les développements biologiques; 5. Protection contre les risques d'entartrage et de corrosion; 6. Recherches d'économie d'eau; 7. Mise en oeuvre de la protection; 8. Contrôles et efficacité; 9. Cas des circuits ouverts (à un seul passage); 10. Cas des circuits fermés; 11. Circuits d'eaux de mer; 12. Conclusion; Abréviations et sigles.

ARMAREGO W.L.E., PERRIN D.D., *Purification of Laboratory Chemicals*. Fourth Edition, Butterworth Heinemann, Oxford, 1996, 529 pp., ISBN 0-7506-2839-1.

The purpose of this book is to help chemists, biochemists and other scientists to purify the chemical reagents which they use in their work. Despite the fact that commercially available chemicals are often of a very high quality, and quite satisfactory for some applications within science and technology, it is becoming almost as important to know impurities are present and make allowance for them so as to remove them completely. This book will show you how.

The main chapters describe processes taken from the literature, for purifying over 4,000 organic and 750 inorganic and organometallic commercially available chemicals. Further chapters describe the methods and techniques currently used for purification in laboratories and prescribed in the text.

Methods for purifying classes of chemicals where specific compounds are not treated individually in the text are dealt with in a separate chapter. This considerably expanded and revised fourth edition includes much new material dealing with modern reagents for natural products chemistry, protein biochemistry and molecular biology. It also includes many individual compounds not previously covered, and more information is given for most entries, including melting and boiling points, molecular weights, refractive indexes, densities and CAS registry numbers, as well as likely contaminants and storage conditions in appropriate cases.

Contents. *Chapter 1. Common Physical Techniques used in Purification*: General Remarks; Distillation; Vacuum Distillation; Steam Distillation; Azeotropic Distillation; Isopiestic or Isothermal Distillation; Sublimation; Recrystallisation; Drying; Chromatography; Solvent Extraction and Distribution; Molecular Sieves; Some Hazards of Chemical Manipulation in Purification and Recovery From Residues; Tables; Bibliography; *Chapter 2. Chemical Methods used in Publication*: General Remarks; Removal of Traces of Metals from Reagents; Use of Metal Hydrides; Purification via Derivates; General Methods for the Purification of Classes of Compounds; General Procedures for the Purification of some Classes of Organic Compounds; Bibliography; *Chapter 3. Purification of Organic Chemicals; Chapter 4. Purification of Inorganic and Metal-Organic Chemicals; Chapter 5. Purification of Biochemicals and Related Products; Index.*

ZOEBELEIN H. (Ed.), *Dictionary of Renewable Resources*. VCH, Weinheim, Germany, 1997, 320 S., ISBN 3-527-30075-9.

This dictionary provides profound information on renewable resources. Topics are all relevant plant and animal sources and the substances derived thereof, the standard technologies of isolation and derivatization, and the major fields of application, with regard to economic aspects and future developments. In addition to the "classical" use as raw materials of the chemical industry, the fields of energy/fuels, practical applications, e.g. as construction and insulation materials, the most important pharmaceutical agents, raw materials of cosmetics and toiletries as well as fragrances are treated. Not only modern methods are taken into account but also older, almost forgotten fields that stimulate new considerations.

Well written and carefully structured, the dictionary is a very usable tool for a broad spectrum of users in different fields of profession, e.g. in public institutions, science and teaching of industry, in agriculture and ecology.

Data apariţiei: martie 1998, Comanda: 66
Coli tipar: 8,4, Tiraj: 325 exemplare

UNIVERSITATEA TEHNICA „GH. ASACHI"
IASI
TIPOGRAFIA

Str. Lascăr Catargi Nr. 38

ORSZÁGOS MŰSZAKI INFORMÁCIÓS KÖZPONT ÉS KÖNYVTÁR
1883

ISSN 0254-7104

BULETINUL INSTITUTULUI POLITEHNIC DIN IAŞI

F 1503/2
FF
8 000000 595164

EDITAT DE
UNIVERSITATEA TEHNICĂ „GH. ASACHI”, IAŞI

Tomul XLIII (XLVII)

Fasc. 3 - 4

Secţia II

CHIMIE şi INGINERIE CHIMICĂ

1997

BULETINUL INSTITUTULUI POLITEHNIC DIN IAŞI

ORSZÁGOS MŰSZAKI INFORMÁCIÓS KÖZPONT ÉS KÖNYVTÁR 1883

Tomul XLIII (XLVII)
Fasc. 3–4

Secţia II

CHIMIE şi INGINERIE CHIMICĂ

1997

EDITORIAL STAFF

Prof. Dr. Eng. **MIHAI GAFIŢANU** (President)
Prof. Dr. Eng. **VICTOR BULACOVSCHI** (Vice-President)
Prof. Dr. Eng. **LIVIU GROLL** (Vice-President)
Prof. Dr. Eng. **GHEORGHE ZET** (Secretary)
Prof. Dr. Doc. Eng. **ALFRED BRAIER** (Editor)
Prof. Dr. Eng. **HUGO ROSMAN** (Editor)
Prof. Dr. Eng. **MIHAIL VOICU** (Head of the Exchange Service)
Prof. Dr. Eng. **DIMITRIE ALEXA**
Prof. Dr. Eng. **ION BALASANIAN**
Prof. Dr. **AUREL BEJANCU**
Prof. Dr. Eng. **MIRCEA COZMÎNCĂ**
Prof. Dr. Eng. **SPIRIDON CREŢU**
Prof. Dr. Eng. **ION GIURMA**
Prof. Dr. Eng. **AURELIA GRIGORIU**
Prof. Dr. Eng. **CONSTANTIN PREDA**
Prof. Dr. Eng. **PAULICĂ RĂILEANU**

The **Bulletin of the Polytechnic Institute of Jassy** is edited by
the **Technical University "Gh.Asachi"** (the former Polytechnic Institute), Jassy.

This issue was published in 1998

TEXredaction:
B. Grigoriu, A. Rotaru
Technical University of Jassy

BULETINUL INSTITUTULUI POLITEHNIC DIN IAŞI
BULLETIN OF THE POLYTECHNIC INSTITUTE OF JASSY
Tomul XLIII (XLVII), Fasc. 3–4 1997

Secţia II

CHIMIE ŞI INGINERIE CHIMICĂ

SUMAR

Pag.

AL. DUCA şi LAVINIA COJOCARIU, Analiza ionilor din serul uman. II. Determinarea polarografică a sodiului, potasiului şi caracterizarea voltametrică a serului uman (engl., rez. rom.) 7

ALEXANDRA RALUCA IORDAN, CHARLES KAPPENSTEIN, MOHAMED I. ZAKI şi CLAUDINE GERON, Influenţa potasiului asupra catalizatorului de rodiu/alumină în atmosfera de CO. Studiu prin spectroscopie în infraroşu *in situ* (franc., rez. rom.) 17

DOINA BÎLBĂ şi LAURENŢIU CIOCHINĂ, Determinarea concentraţiilor urme de cobalt prin spectrometrie în fază solidă (engl., rez. rom.) 27

I. ROŞCA, MIHAELA VIZITIU, DOINA SIBIESCU, DANIEL SUTIMAN şi ADRIAN CĂILEAN, Sinteza şi studiul polimerilor de coordinaţie ai Zr(IV) cu liganzi derivaţi de la acizii 2,8-dimetilfenoxifosfinic şi dihexilfosfinic (engl., rez. rom.) 33

ANA ONU, CRISTINA COSTIN şi N. AELENEI, Caracterizarea polidispersităţii maselor moleculare la polisulfone (engl., rez. rom.) 37

MARIANA NEAMŢU şi I. SIMINICEANU, Determinarea produşilor de reacţie la fotodegradarea bisfenolului-A din apă prin procedeul UV-peroxid de hidrogen (engl., rez. rom.) 43

GEORGETA MATZA, ŞT. IVĂŞCAN, LUCIAN GAVRILĂ, DANIELA GAVRILĂ şi N. APOSTOLESCU, Metode neconvenţionale utilizate pentru măsurarea vitezei de coroziune a sistemelor metalice (engl., rez. rom.) 51

AL. SZÉP, CAROLINA HAGIU şi GH. MIHĂILĂ, Obţinerea sulfatului de amoniu prin sinteza directă. I. Stabilirea regimului tehnologic (engl., rez. rom.) 59

VALERIU NAGACEVSCHI, MATEI MACOVEANU şi N. PEIU, Model pentru dispersia unui poluant în atmosferă (engl., rez. rom.) 71

CRISTINA VLASE, CORNELIU ONISCU, EUGEN DIACONU şi AUREL VLASE, Cercetări privind sinteza şi purificarea sulbactamei-pivoxil (franc., rez. rom.) ... 77

Pag.

VALERIA HARABAGIU, MARIANA PINTEALĂ, CORNELIA COTZUR, CRISTINA IOJOIU şi BOGDAN C. SIMIONESCU, Polisilani. 1. Reacţia de cuplare a diclormetilfenilsilanului în prezenţa sistemelor metale alcaline/eter coroană (engl., rez. rom.) 83

MIRCEA CONSTANTINESCU, VICTOR BULACOVSCHI şi SILVIA CURTEANU, Polimerizarea radicală a stirenului. Modelare şi simulare (engl., rez. rom.) 91

Z. BENCHEIKH, B. BELAZOUZ şi I. RABIA, Distribuţia dimensiunii particulelor de copolimeri stiren–divinilbenzen preparaţi prin polimerizare în suspensie (engl., rez. rom.) 105

CARMEN-CĂTĂLINA IOAN, Criteriile tehnicilor de anchetă psihosocială (franc., rez. rom.) 115

Profesorul Alexandru Duca la a optzecea aniversare 119

RECENZII 121

BULETINUL INSTITUTULUI POLITEHNIC DIN IAŞI
BULLETIN OF THE POLYTECHNIC INSTITUTE OF JASSY
Tome XLIII (XLVII), Fasc. 3–4 1997

Section II

CHEMISTRY and CHEMICAL ENGINEERING

CONTENTS

Pp.

AL. DUCA and LAVINIA COJOCARIU, Analysis of the Human Serum Ions. II. Polarographic Determination of Sodium, Potassium and Voltammetric Characterization of Human Serum (English, Romanian summary) 7

ALEXANDRA RALUCA IORDAN, CHARLES KAPPENSTEIN, MOHAMED I. ZAKI et CLAUDINE GERON, Influence du potassium sur le catalyseur rhodium/alumine en atmosphère de CO. Etude par spectroscopie infrarouge *in-situ* (French, Romanian summary) 17

DOINA BÎLBĂ and LAURENŢIU CIOCHINĂ, Determination of the Trace Amounts of Cobalt by Solid-Phase Spectrophotometry (English, Romanian summary).... 27

I. ROŞCA, MIHAELA VIZITIU, DOINA SIBIESCU, DANIEL SUTIMAN and ADRIAN CĂILEAN, Synthesis and Study of Some Co-ordination Polymers of Zr(IV) with 2,8-Dimethyl-Phenoxiphosphinic and Dihexylphosphinic Acids as Ligands (English, Romanian summary) 33

ANA ONU, CRISTINA COSTIN and N. AELENEI, Characterization of the Molecular Weight Distribution of Polysulfones (English, Romanian summary) 37

MARIANA NEAMŢU and I. SIMINICEANU, Determination of the Reaction Products of the Bisphenol-A Photodegradation in Water by Ultraviolet Catalysed Oxidation with Hydrogen Peroxide (English, Romanian summary) 43

GEORGETA MATZA, ŞT. IVĂŞCAN, LUCIAN GAVRILĂ, DANIELA GAVRILĂ and N. APOSTOLESCU, Unconventional Methods Used for Corrosion Rate of Metallic Systems Measurement (English, Romanian summary) 51

AL. SZÉP, CAROLINA HAGIU and GH. MIHĂILĂ, On Ammonium Sulfate Manufacture. I. Operating Parameters of the Technological Process (English, Romanian summary) 59

VALERIU NAGACEVSCHI, MATEI MACOVEANU and N. PEIU, Model for the Air Dispersion of a Pollutant (English, Romanian summary) 71

CRISTINA VLASE, CORNELIU ONISCU, EUGEN DIACONU et AUREL VLASE, Recherches concernant la synthèse et la purification du sulbactame-pivoxyle (French, Romanian summary) 77

Pp.

VALERIA HARABAGIU, MARIANA PINTEALĂ, CORNELIA COTZUR, CRISTINA IOJOIU and BOGDAN C. SIMIONESCU, Polysilanes. 1. Coupling Reaction of Dichloromethylphenylsilane in the Presence of Alkali Metal/Crown Ether Systems (English, Romanian summary) 83

MIRCEA CONSTANTINESCU, VICTOR BULACOVSCHI and SILVIA CURTEANU, Free Radical Polymerization of Styrene. Modelling and Simulation (English, Romanian summary) 91

Z. BENCHEIKH, B. BELAZOUZ and I. RABIA, On Particle Size Distribution of Styrene–Divinylbenzene Copolymers Prepared by Suspension Polymerization (English, Romanian summary) 105

CARMEN-CĂTĂLINA IOAN, Les critères des techniques d'investigation psycho-sociale (French, Romanian summary) 115

Professor Alexandru Duca at His Eighties 119

BOOK REVIEWS 121

BULETINUL INSTITUTULUI POLITEHNIC DIN IAŞI
Tomul XLIII (XLVII), Fasc. 3–4, 1997
Secţia II
CHIMIE şi INGINERIE CHIMICĂ

D.C. 541.132; 615.361; 545.33; 537.741.3

ANALYSIS OF THE HUMAN SERUM IONS

II. POLAROGRAPHIC DETERMINATION OF SODIUM, POTASSIUM AND VOLTAMMETRIC CHARACTERIZATION OF HUMAN SERUM

BY

AL. DUCA and LAVINIA COJOCARIU

Normal polarography ($i - E$) permits the determination of sodium and potassium ions sum, dissolved oxygen and some organic substances in the human serum. Using the modified electrodes voltammetry, alkaline metals can be indirectly determined. The principle of three alternatives in the literature is presented [2],...,[4] and also an original alternative with polymeric films modified electrodes.

1. Introduction

The sum of sodium and potassium ions ($Na^+ + K^+$) can be determined by polarographic method in LiOH solution or $(CH_3)_4N-OH$ solution (as supporting electrolyte) using the normal polarography ($i - E$); the ionic ratio $Na^+/K^+ = 10/1...15/1$ can be established using the derivative polarography ($di/dE - E$) [1].

Voltammetrically, the concentration of alkaline metals (Li^+, Na^+, K^+, Rb^+, Cs^+) can be established using many indirect alternatives with different modified electrodes. We mention in what follows three of these methods [2],...,[4].

The silvers ions Ag^+ from a modified zeolit membrane AgY can be substituted by alkaline ions. The alkaline ions concentration can be established by voltammetric determination of silver ions.

Another possibility is based on the modification of voltammograms shape and characteristics in the presence of alkaline ions, using a modified electrode Ni – $[NiFe(CN)_6]^{2+}$ [3].

The voltametric determination principle for nonelectroactive cations is proceeded from the redox characteristic of a cupric hexacyanoferrate electrode (CuHCF):

$$Cu_3^{II}(Fe^{III}(CN)_6)_3 + 2e^- + 2K^+ = K_2Cu_3^{II}(Fe^{II}(CN)_6)_2 \tag{1}$$

The determination of K^+ (and so on) is based on the cathodic peaks due to CuHCF reduction when the sample containing cations passed the electrode surface ($E = +0.45$ V). In the case of a complex sample containing cations, their separation can be realised in a flow system [4].

A voltammogram made in a large potential range (+2.0...–1.0 V), would characterise a human serum type (ions and organic molecules). The human serum can be characterized by the apparent normal redox potential, E^0, and by shape and characteristics modifications of the polymeric films voltammograms.

2. Experimental

Polarographic measurements were performed on the Czechoslovack Polarograph LP7. A dropping mercury electrode DME was used. The DME cappilary has the following characteristics: m=2.65 mg/s; t=3.125 s, determined at -1.00 V; Hg column height H=65 cm. The sensibility of the polarograph was established between $S=10^{-9}...2\times10^{-7}$ A/div, compensation coarse between 0.5...50 μA/V, damping D=2, the sweeping rate was 200 and 400 mV/min. The potential range was between -1.4 and -2.4 V.

The supporting electrolyte was LiOH 0.1 M. The experiments were realised with serum standard and human serum, diluted 1/50 with bidistilled water. The sample volume was 5 mL. Determinations were carried out with and without oxygen elimination (with N_2).

For calibration procedures, solutions obtained by dilution with bidistilled water from the initial standards of NaCl and KCl 0.1 M were used. The salts were of analytical grade and were dried for one hour at about 110°C. The solutions were prepared using bidistilled water.

The potentiometric determinations of E^0 were performed on a pH/pX meter PYA, model 78. The working electrode was a platinum wire vs. a saturated calomel electrode (SCE). Both were imersed in a one compartiment cell, magnetically stirred.

The voltammetric determinations were carried out on Polarograph Radelkis OH 102. For the electrodeposing of the polymeric films, one compartiment cell with three electrodes was used. The working electrode was a platinum wire, the reference electrode was a SCE and a platinum auxiliary electrode. For electrodeposing, the potential was maintained constant at +0.7 (+0.8) V a specified time, between 5...30 min. The oxygen from the system was eliminated before producing the modified polymeric film electrode.

The aniline and pyrrole were purified by distilation and the 0.1 M solutions were in bidistilled water.

3. Results and Discussions

3.1. Polarographic Determination of Na^+ and K^+ in the Human Serun

In the case of alkaline ions Na^+, K^+, because of a small difference between their reduction potentials $(E_{1/2})_{Na}$=-2.11 V and $(E_{1/2})_{K}$=-2.13 V; $\Delta E_{1/2}$=0.02 V), using the polarographic method (the normal alternative i - E, N) only their sum can be determined.

Using the derivative alternative of the polarographic method ($\mathrm{d}i/\mathrm{d}E - E$, D) the ratio Na^+/K^+ can be established until 10/1,...,15/1, without their separation.

The principle of this method is based on the fact that for the same concentration of Na^+ and K^+ the peak current response has different hights (h) and depths (a) – we refere to derivative response –, as it is indicated in Fig. 1. From the calibration graph, measuring h_{Na}, h_K and a_{Na}, a_K we can simply infere the Na^+/K^+ ratio [1]. The correspondence between h, a and the cations concentrations is indicated in Fig. 2.

Normal and derivative curves obtained at two different scan rates are comparatively represented in Fig. 3. The DME was immersed in a serum solution, diluted 1/50. The scan rates were 200 mV/min and 100 mV/min.

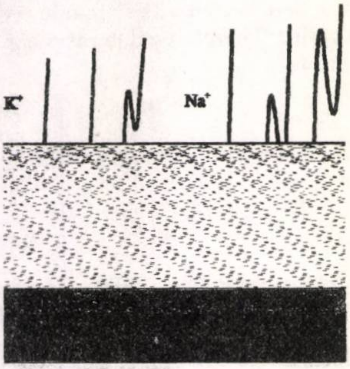

Fig. 1.- Derivative polarographic curves of Na^+ and K^+; cation concentrations are identical for curves *1, 2, 3*.

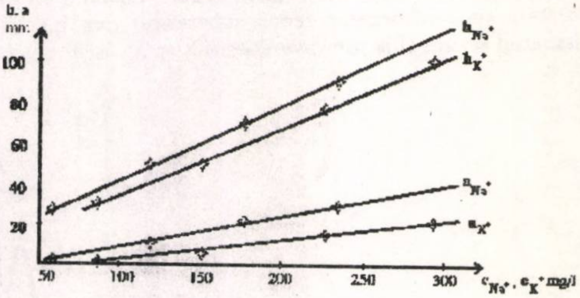

Fig. 2.- Calibration graphs; the correspondence between the hight (h) and the depth (a) of the polarographic derivative curves and cations concentration.

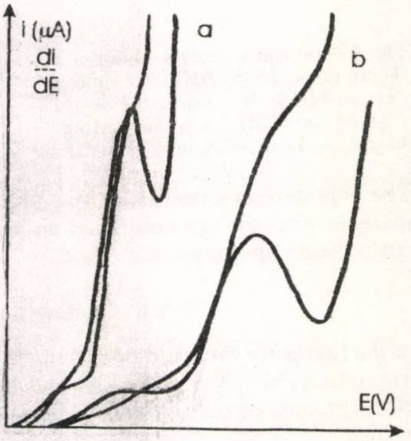

Fig. 3.- Normal and derivative curves, DME, human serum (1/50) in LiOH 0.1 M supporting electrolyte: a - N, R_s=50, D=2, v=200 mV/min; D, R_s=1; b - N, R_s=50, D=2, v=100 mV/min; D, R_s=1.

If the recording starts from 0.0 V without oxygen elimination from the solution (with N_2), two reduction steps for oxygen can be observed (Fig. 4). This way can be estimated the dissolved oxygen content in the human serum, compared with the oxygen content in the supporting electrolyte (without serum). On the other side, it is known that between the organic redox substances and the oxygen exists a well specified ratio. Therefore, this ratio can be used as an important indicator for the human serum.

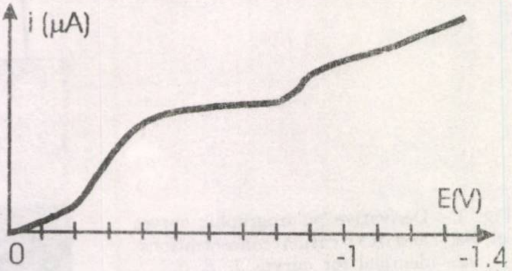

Fig. 4.– Normal curve (N), DME, human serum (1/50) in LiOH 0.1 M supporting electrolyte; without oxygen elimination; R_s=10.

Another important observation is the "alkaline prewave" that shows a report for a certain class of organic redox substances existing in the human serum. In the calcinated serum this prewave does not exist as it can be seen in Fig. 5.

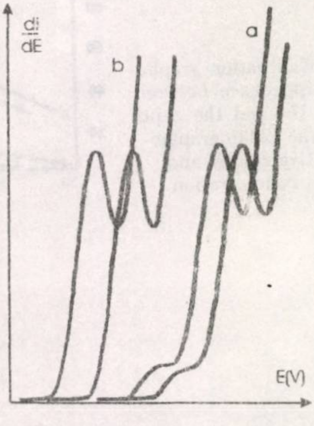

Fig. 5.– Derivative curves obtained on Polarograph LP-7, DME: *a* – human serum (1/50); *b* – calcinated serum (1/50) in LiOH 0.1 M supporting electrolyte; D, R_s=0.5, v=200 mV/min.

The polarographic results for the alkaline ions in fresh and calcinated serum are comparable with the ones obtained on standard serum and with the ones obtained using the flame photometric method.

3.2. Alkaline Ions Voltammetry

In the literature there are many papers refering to the possibilities of alkaline ions determination (Li^+, Na^+, K^+, Cs^+ and NH_4^+). The indicated methods are voltammetric techniques or combinated methods (liquid cromatography with amperometric detection).

Among these methods we selected three alternatives and briefly display them:

1° The principle for the determination of alkaline metal traces using zeolite modified electrodes [2] consists in the substitution of silver ions from the zeolite (type AgY) in methanol, as it can be seen in Fig. 6.

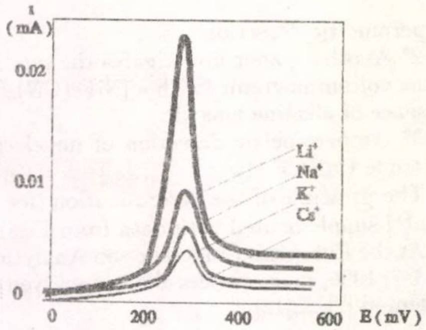

Fig. 6.– Anodic stripping voltammograms of AgY in methanol; the majority of supporting electrolyte was 0.1 M tetrabutylammonium perchlorate (TBAP); the solution also contained 10 ppm of the following cations: Li^+, K^+, Na^+, Cs^+; sweep rate 10 mV/s.

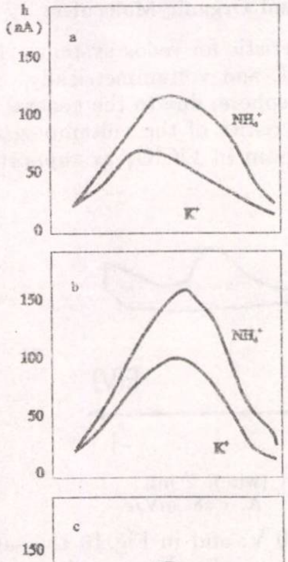

Fig. 7.– Hydrodynamic voltammograms for 1×10^{-4} M K^+ and 1×10^{-4} M NH_4^+ at the CuHCF electrode: mobile phases: *a* – 0.1 M HNO_3; *b* – 0.02 M HNO_3; *c* – 0.005 M HNO_3; flow rate 2.0 mL/min [4].

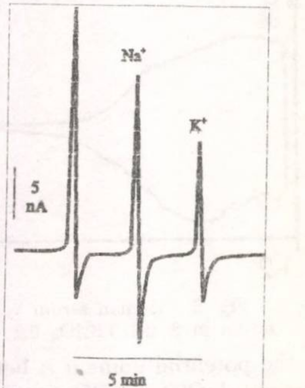

Fig. 8.– Liquid chromatogram of a mixture containing 1×10^{-3} M Na^+ and 5×10^{-5} M K^+; mobile phase 0.0025 M HNO_3; potential +0.45 V; flow rate 2.0 mL/min [4].

It can be observed from Fig. 6 that method sensibility is reverse to ionic weight. The peaks appear at the same potential value (E_p=271.4 mV). The method is sensitive but not selective. It can be applied with liquid chromatography coupled with amperometric detection.

2° Another paper investigates the modifications of the shape and characteristics of the voltammograms (with a $[NiFe(CN)_6]^{2-/-}$ – derivatized nickel electrode) in the presence of alkaline ions [3].

3° Amperometric detection of nonelectroactive cations in flow systems, at an electrode CuHCF [4].

The principle of the determination (for example K^+) is based on the redox reaction [1] supplemented with data from Figs. 7 and 8.

At the European Conference on Analytical Chemistry in Bologna (Italy), September 1-7, 1996, many papers about modifyed electrodes, as amperometric sensors, were presented [7],...,[12].

3.3. The Human Serum Voltammetry (Ions and Organic Molecules)

It is well known that the value of E^0 is a characteristic for redox systems. This value can be determined potentiometrically EPt/SCE and voltammetrically. The voltammetric determination has a larger informative sphere, due to the general appearance in a large potential range and the characteristics of the voltammogram. In Fig. 9 it is presented a human serum voltammogram in $LiClO_4$ as supporting electrolyte; the potential domain is between +2.0...1.0 V; and in Fig. 10 the same voltammogram in $LiClO_4+LiOH$ as supporting electrolyte, after oxygen elimination (with N_2).

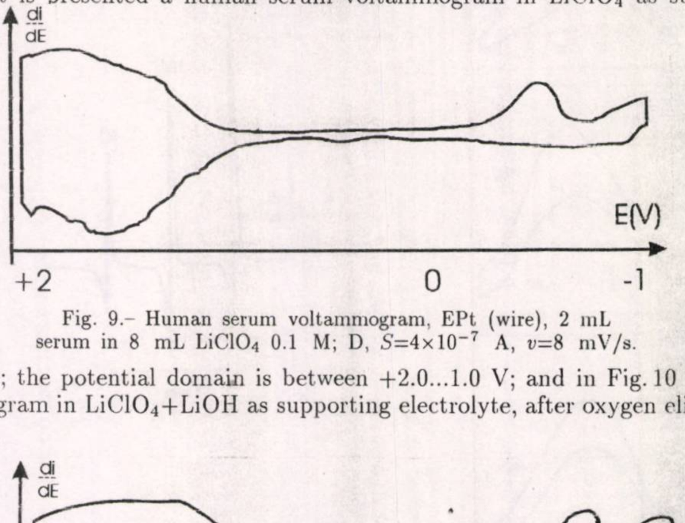

Fig. 9.– Human serum voltammogram, EPt (wire), 2 mL serum in 8 mL $LiClO_4$ 0.1 M; D, $S=4\times10^{-7}$ A, $v=8$ mV/s.

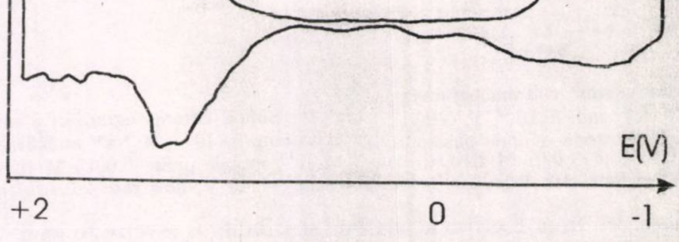

Fig. 10.– Human serum voltammogram, EPt (wire), 2 mL serum in 7 mL $LiClO_4$ 0.1 M and 1 mL LiOH 1 M; D, $S=4\times10^{-7}$ A, $v=8$ mV/s.

It can be observed from Fig. 9 the existance of two redox domains between +1.0 V and +2.0 V (E_{pa}=+1.7 V), virtually reversible and between 0.0 V and -1.0 V (E_{pc}=−0.3 V), virtually irreversible.

In the two redox domains (Fig. 10) the between +0.8...2.0 V first anodic process prevails (E_{pa_1}=+1.25 V and E_{pa_2}=+1.35 V) and in the second, between 0.0,...,1.0 V, the catodic process prevails (E_{pc}=−0.45 V).

Using the potentiometric method, E^0 values were determined on a series of human serum, noted from *1* to *4*. The numeric data E^0 were performed in aqueous solutions and in phosphate buffer pH=7 solutions. The serum was diluted 1/5. For these serum samples we established the rH values also. The results are listed in Table 1.

Table 1
Potentiometric Determinations of E^0 in Serum

Serum Samples	Aqueous solutions		Phosphate buffer solutions (pH=7)		
	pH	E^0	pH	E^0	rH
1	8.55	125	7.08	260	22.97
2	8.40	130	7.07	261	22.98
3	8.35	135	7.06	270	23.27
4	7.90	160	7.04	275	23.40

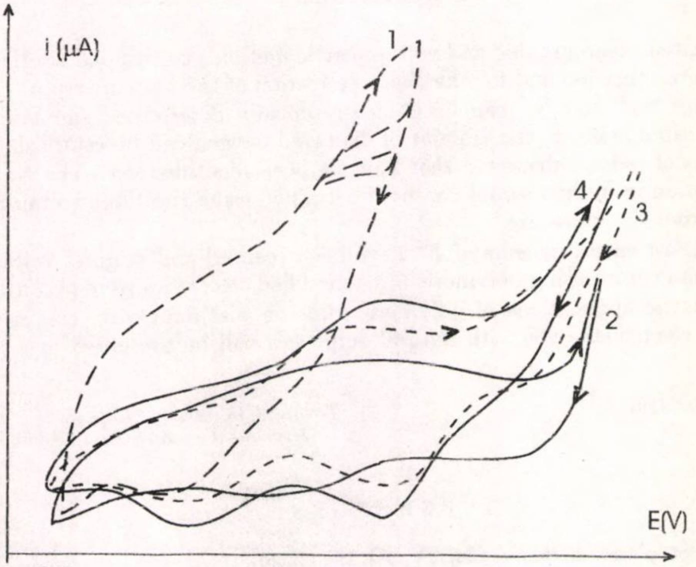

Fig. 11.– EPt (wire) PP(H_2SO_4) in: 10 mL H_2SO_4 0.1 N (*1*); 10 mL NaCl 0.1 M (*2*); 8 mL NaCl 0.1 M +2 mL EDTA 0.1 M (*3*); 6 mL NaCl 0.1 M +2 mL EDTA 0.1 M (pH=4.94) +2 mL serum (*4*); N, $S=16\times10^{-7}$ A, v=8 mV/s.

The rH, another important characteristic of a redox system, can be calculated knowing E^0 and pH. In the case of biological fluids, whose composition is very complex, rH represents the redox capability of the system in its totality, being a resultant of all redox processes that take place. The rH describes the dynamics of primary and secondary methabolism, conditioning the whole activity of the living cell.

In the literature and from our experience in the field of electronic conductor polymers of over ten years, it is well known that dopped polymeric films are very sensible in different supporting electrolytes and nonelectrolytes, in the studied potential ·ange (+0.8,...,-1.0 V).

In Fig. 11 can be observed the shape and characteristics of a polypyrrole film PP(H_2SO_4) voltammogram in: H_2SO_4 0.1 N, NaCl 0.1 M, 8 mL NaCl 0.1 M +2 mL EDTA 0.1 M, 6 mL NaCl 0.1 M +2 mL serum +2 mL EDTA 0.1 M. The film PP(H_2SO_4) was deposited on a platinum wire, in a mixture of 5 mL H_2SO_4 2 N and 5 mL pyrrole 0.1 M at E=+0.70 V, for 10 min.

In the same conditions polyaniline films PA(HCl) can be obtained. The results are comparable with the ones obtained with films PP(H_2SO_4).

The PA(HCl) was deposited on a platinum wire, in a mixture of 5 mL HCl 2 M and 5 mL aniline 0.1 M at E=+0.70 V, for 30 min.

Such voltammograms for the human serum can serve as fingerprints for a specified serum.

4. Conclusions

The presented polarographic and voltammetric methods correspond for the alkaline metals determination and for the characterization of the human serum.

The sum of Na^+ and K^+ can be polarographically determined and also their ratio. In the same manner, the amount of dissolved oxygen can be established and a certain class of redox substances that hansn't been identified yet. The Na^+ and K^+ concentration in human serum can be determined using the three voltammetric alternatives from the literature.

Potentiometric measurements of E^0 have been realised and original voltammograms of human serum using polymeric films modified electrodes were performed.

Potentiometric applications of polymeric films on platinum wire, compared to paste carbon electrodes PCE with natural sulphures will be presented in a future paper.

Received, May 12, 1997

Technical University "Gh.Asachi", Jassy,
Department of Analytical Chemistry

REFERENCES

1. Duca Al., St. şi cerc. de chimie, Cluj, **IV**, *3-4*, 130 (1956).
2. Baker M.D., Sanaratne C., Anal. Chem., **64**, 697 (1992).
3. Amos L.J., Duggel A., Mirsky E.J., Ragonesy P., Bocarsly A.B., Anal. Chem., **60**, 245 (1988).
4. Thomsen K.N., Baldwin R.P., Anal. Chem.,**61**, 2594 (1989).
5. Duca Al., Gaburici M., Ivănoiu M., *Electroanaliza cu electrozi modificaţi pe suprafeţe diferite* (in print).
6. Biryukova I.V., Klyuev S.A., Europ. Conf. on Analyt. Chem., Euroanalys, Sept. 1-7, 1996, Bologna, Italy, Book of Abstracts, Mo P 143.

7. Brainina M., Ivanova A., Sarayeva S., Zaboyeva N., Europ. Conf. on Analyt. Chem., Euroanalys, Sept. 1-7, 1996, Bologna, Italy, Book of Abstracts, We P 93.
8. Daniele S., Baldo M.A., Mazzocchin G.A., Europ. Conf. on Analyt. Chem., Euroanalys, Sept. 1-7, 1996, Bologna, Italy, Book of Abstracts, We L 14.
9. Bilewicz R., Europ. Conf. on Analyt. Chem., Euroanalys, Sept. 1-7, 1996, Bologna, Italy, Book of Abstracts, We L 10.
10. Muszalska E., Bilewicz R., Europ. Conf. on Analyt. Chem., Euroanalys, Sept. 1-7, 1996, Bologna, Italy, Book of Abstracts, We P 76.
11. Michalska A., Europ. Conf. on Analyt. Chem., Euroanalys, Sept. 1-7, 1996, Bologna, Italy, Book of Abstracts, Fr L 32.
12. Karyakin A.A., Bobrova O.A., Lukachova L.V., Karyakina E.E., Europ. Conf. on Analyt. Chem., Euroanalys, Sept. 1-7, 1996, Bologna, Italy, Book of Abstracts, Fr P 20.

ANALIZA IONILOR DIN SERUL UMAN

II. Determinarea polarografică a sodiului, potasiului şi caracterizarea voltametrică a serului uman

(Rezumat)

Polarografia normală (i–E) permite determinarea concentraţiei sumei Na^+ şi K^+, a oxigenului dizolvat şi a unei clase de substanţe organice redox în serul uman. Folosind voltametria cu electrozi modificaţi se pot determina indirect metalele alcaline. În acest sens s-au prezentat trei variante din literatură şi, de asemenea, o variantă originală cu electrozi modificaţi cu filme polimetrice.

BULETINUL INSTITUTULUI POLITEHNIC DIN IAŞI
Tomul XLIII (XLVII), Fasc. 3–4, 1997
Secţia II
CHIMIE şi INGINERIE CHIMICĂ

C.D. 546.32; 541.128; 661.897 · 35.333

INFLUENCE DU POTASSIUM SUR LE CATALYSEUR RHODIUM/ALUMINE EN ATMOSPHÈRE DE CO

ETUDE PAR SPECTROSCOPIE INFRAROUGE *IN-SITU*

PAR

ALEXANDRA RALUCA IORDAN, *CHARLES KAPPENSTEIN, **MOHAMED I. ZAKI et *CLAUDINE GERON

On a étudié le rôle du potassium sur le catalyseur de rhodium déposé sur alumine en atmosphère de monoxyde de carbone. Les supports utilisés ont été l'alumine et l'alumine modifiée avec des ions de potassium calcinés à 700°C. Comme technique d'analyse a été utilisée la spectroscopie en infrarouge à transformée de Fourier. Les mesures ont été réalisées *in situ*. Les spectres IR indiquent une bonne dispersion du rhodium à la surface du catalyseur et une bonne interdispersion du rhodium et du potassium. Les spectres obtenus mettent en évidence que la présence des ions K^+ empêche le processus d'oxydation du rhodium en atmosphère de monoxyde de carbone.

1. Introduction

Les métaux de transition catalysent une large gamme de processus industriels dans l'industrie chimique. L'utilisation des catalyseurs métalliques massiques n'est pas vraiment intéressante car l'efficacité du métal (activité par unité de masse de matière active) est loin d'être optimisée. Elle coûte par le fait même très cher dans le cas des métaux précieux. De plus, ces catalyseurs présentent une faible stabilité thermique qui se caractérise par une diminution de leur surface métallique par frittage. Pour contrecarrer ceci les métaux nobles sont supportés sur des matrices de haute surface spécifique (exemple: les oxydes inorganiques refractaires). Cette opération contribue à augmenter l'efficacité du catalyseur par un maximum de surface spécifique, à accentuer la stabilité thermique, donc la durée de vie et aussi à accroître la sélectivité [1].

L'alcalinisation des supports tels que l'oxyde d'aluminium fournit un moyen efficace de contrôler l'acidité de surface. Cette acidité de surface représente un facteur important de l'activité catalytique [2],...,[4]. Certains ions alcalins au alcalino-terreux peuvent réduire les dépôts de coke sur les catalyseurs Rh/Al_2O_3 utilisés en reformage [5]. De plus, l'alcalinisation de Rh/Al_2O_3 augmente notablement la conversion catalytique de l'éthanol ou du méthanol en alcools supérieurs primaires linéaires [6].

2. Partie expérimentale

2.1. Réactifs

Alumine Al_2O_3 (Aluminium oxid C, Degussa), Carbonate de potassium K_2CO_3 anhydre p.a. (Labosi), Hydrogénocarbonate de potassium $KHCO_3$ p.a. (Merck), Chlorure de rhodium (III) hydraté, $RhCl_3.nH_2O$ (Johnson Matthey), Hydrogène N55 (Air Liquide), Monoxyde de carbone CO N47 (Air Liquide).

2.2. Préparation *ex-situ* des échantillons

a) Al_2O_3–R: alumine de référence. L'alumine a été immergée dans l'eau (20 ml H_2O/g Al_2O_3), agitée mécaniquement pendant 30 min., puis laissée reposer durant une heure. La suspension est séchée 24 heures à l'étuve à 120°C, ensuite elle est broyée.

b) Al_2O_3(700): alumine de référence calcinée à 700°C dans un four moufle en atmosphère statique d'air pendant 3 heures.

c) Al_2O_3/K_2CO_3: Al_2O_3–R est immergée dans une solution de K_2CO_3 0.0407 M (20 ml/g Al_2O_3), puis agitée, laissée reposer, séchée dans les mêmes conditions que l'alumine de référence et finalement broyée. La masse de potassium est de 0.063 g pour 1 g alumine.

d) K–Al_2O_3(700): l'échantillon Al_2O_3/K_2CO_3 calciné à 700°C.

e) Rh/Al_2O_3(NR): une solution aqueuse de $RhCl_3$ 0,0196 M a été ajoutée goutte à goutte sur Al_2O_3(700) (5 ml solution/g Al_2O_3(700), soit 0.01 g Rh/g support). Après agitation pendant 30 min. dans un bain à ultrasons, la suspension a été séché 24 h à 120°C.

f) Rh/K–Al_2O_3(NR): échantillon obtenu de la même manière et en utilisant les mêmes quantités que pour Rh/Al_2O_3(NR).

2.3. Technique d'analyse. Spectroscopie infrarouge *in situ*

L'état de surface du catalyseur a été étudié à l'aide du monoxyde de carbone comme molécule sonde. Les mesures *in situ* ont été réalisées sur des échantillons autosupportés pastillés à 5 *t* (25±2 mg/cm^2) et placés dans une cellule d'analyse IR en pyrex, équipée avec des fenêtres en CaF_2 qui permettent de travailler dans le domaine de 4 000...1 000 cm^{-1}. Cette cellule facilite le chauffage *in situ* et le dégazage de la pastille. Le banc de vide est conçu pour obtenir un vide propre sans huile (pression de 10^{-5} Torr, (1 Torr = 133,2 Pa)) et équipé avec un manomètre Baratron et une jauge de pression Pirani/Penning. La pression au niveau de la pastille est estimée à $5{\cdot}10^{-5}$ Torr. Le chauffage a été réalisé avec un four extérieur équipé par un contrôle électronique et un thermocouple chromel–alumel situé dans le voisinage immédiat de la pastille. La montée en température est de 10°C/min. La pression de dégazage est de l'ordre de 5.10^{-5} Torr.

Les spectres ont été enregistrés après refroidissement, à la température du faisceau en atmosphère statique. Le refroidissement est obtenu sous vide en régime dynamique.

Pour chaque échantillon, le premier traitement est le dégazage à température ambiante sous vide, suivi d'un dégazage de 2 heures à 200°C.

Le schéma ci-dessous résume le protocole opératoire utilisé.

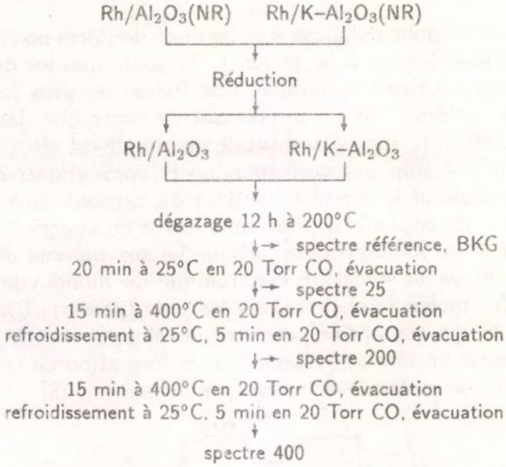
Rh/Al2O3(NR)
Rh/K-Al2O3(NR)
Réduction
Rh/Al2O3
Rh/K-Al2O3
dégazage 12 h à 200°C
spectre référence, BKG
20 min à 25°C en 20 Torr CO, évacuation
spectre 25
15 min à 400°C en 20 Torr CO, évacuation
refroidissement à 25°C, 5 min en 20 Torr CO, évacuation
spectre 200
15 min à 400°C en 20 Torr CO, évacuation
refroidissement à 25°C, 5 min en 20 Torr CO, évacuation
spectre 400

Protocole opératoire

L'admission des gaz se réalise toujours à la température ambiante. La réduction des échantillons est effectuée sous une pression de 200 Torr d'hydrogène à 200°C en deux étapes de 30 min. chacune. Après chaque étape il y a une période de dégazage de 30 min. à 200°C. L'admission d'hydrogène est effectuée à température ambiante.

3. Résultats et discussions

L'adsorption de CO présente un intérêt considérable dans la connaissance des surfaces. La grande inertie chimique du monoxyde de carbone due à son énergie de liaison, de l'ordre de 1 070 kJ mol^{-1}, représente la raison première de l'utilisation de cette molécule dans les études fondamentales d'adsorption sur les métaux de transition, dans la compréhension des problèmes complexes d'adsorption rencontrés dans la catalyse hétérogène.

3.1. Structure électronique de la molécule CO

La construction des orbitales moléculaires du monoxyde de carbone est présentée dans la Fig.1 [7]. L'orbitale la plus basse, 3σ, principalement développée sur l'oxygène (atome le plus électronégatif), est liante entre C et O. Dans l'orbitale 4σ, il y a un mélange s/p important sur l'oxygène de telle sorte que le gros lobe pointe du côté opposé au carbone. L'orbitale 5σ présente quant à elle une contribution p sur l'oxygène et un mélange des orbitales s et p sur le carbone tel que l'amplitude de cette fonction, principalement développée sur le carbone, est augmentée vers l'extérieur de la molécule. Enfin, dans l'orbitale moléculaire antiliante la plus haute, 6σ, il y a un mélange des quatre orbitales de fragment de telle sorte que tous les recouvrements sont antiliants. Cette orbitale est plus développée sur l'atome le moins électronégatif (C). Il y a dix électrons de valence dans CO, si bien que, dans la configuration électronique fondamentale, les cinq orbitales moléculaires les plus basses sont occupées: $(3\sigma)^2(4\sigma)^2(1\pi)^4(5\sigma)^2$. La plus haute orbitale occupée est une orbitale de type σ, pratiquement non liante. Si on essaie d'établir une analogie entre cette description et celle fournie par le modèle de Lewis, $|^{(-)}C\equiv O^{(+)}|$, on peut faire correspondre deux liaisons de type π aux orbitales liantes 1π. L'ensemble des trois orbitales σ occupées décrit donc la liaison σ et les deux doublets non liants. L'orbitale 3σ est celle qui contribue le plus à la liaison C–O, alors que les deux orbitales 4σ et 5σ paraissent mieux décrire les doublets non liants; les gros lobes sont dirigés vers l'extérieur de la molécule. Il est intéressant de noter que dans la plus haute orbitale occupée (HOMO), la zone d'amplitude maximale est située sur le carbone, ce qui conduit souvent à établir une correspondance (approximative) entre les deux électrons de cette orbitale et le doublet nonliant du carbone dans la structure de Lewis. La présence de ce doublet non liant, „haut en énergie", est responsable du caractère donneur-σ du monoxyde de carbone lié aux métaux de transition. Un autre aspect important de la structure électronique de monoxyde de carbone est la nature des orbitales moléculaires vacantes les plus basses (LUMO): ce sont les orbitales antiliantes 2π qui sont principalement développées sur le carbone. Cette caractéristique joue aussi un rôle important dans la formation de la liaison entre un métal de transition et une molécule de monoxyde de carbone [8].

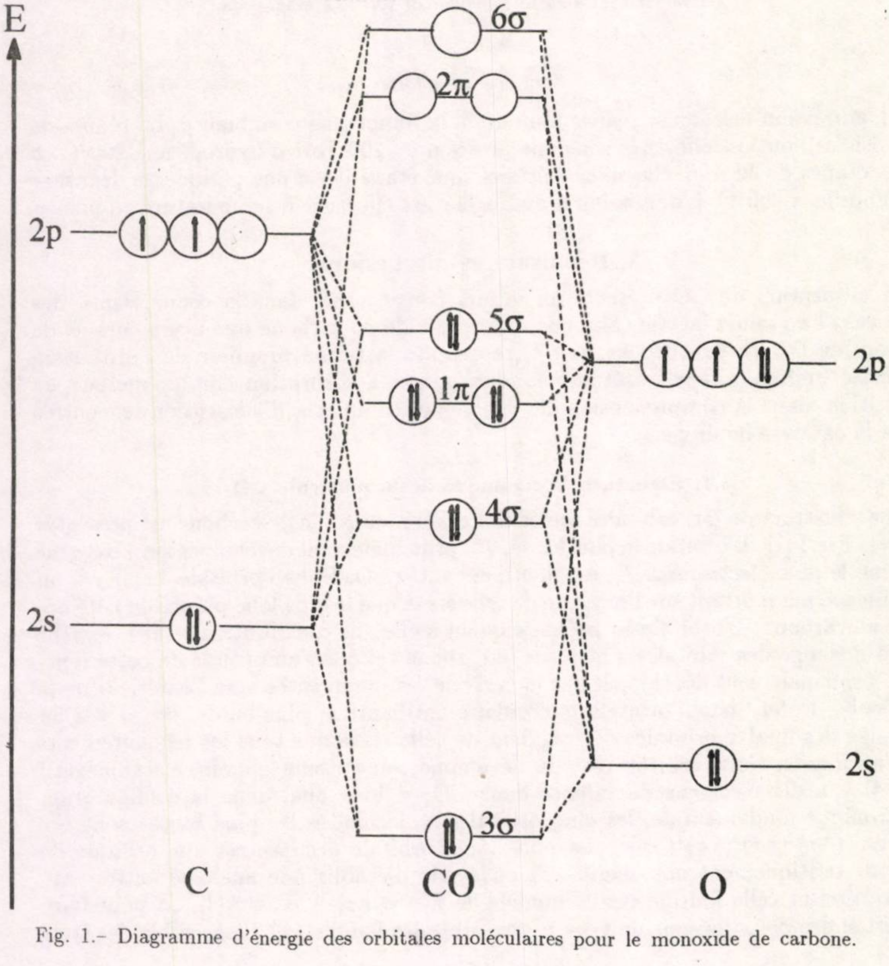

Fig. 1.- Diagramme d'énergie des orbitales moléculaires pour le monoxide de carbone.

Le monoxyde de carbone s'adsorbe facilement et la vibration d'élongation ν_{CO} présente un coefficient d'extinction relativement important lorsque CO est chimisorbé sur le rhodium. Les chercheures ont identifié trois types de bandes ainsi que les structures les plus probables responsables de celles-ci [9]. Dans le Tableau 1 sont présentées les espèces formées par l'adsorption sur rhodium. L'attribution des bandes a été réalisée en accord avec les données de la littérature de spécialité [10].

L'espèce nommée „gem dicarbonyl“ apparaît surtout sur des catalyseurs totalement réduits, bien dispersés. Les espèces „linéaire“ et „ponté“ apparaissent davantage sur les catalyseurs peu dispersés formés de grosses particules bien réduites. La coordination du rhodium est alors multiple et désignée par Rh_x. Les sites de distribution ressemblent à ceux trouvés sur des monocristaux (plans 111).

Tableau 1
Caractérisation des espèces formées après adsorption de CO sur rhodium

Domaine de nombre d'onde cm^{-1}	Structure proposée	Dénomination attribuée	Etat d'oxydation du métal
2 090...2 105 (vibration symétrique) 2 022...2 076 (vibration antisymétrique)	CO Rh CO espèce I	gem dicarbonyl	(+1)
2 040...2 076	Rh–CO espèce II	linéaire	(0)
1 845...1 920	O OC C CO Rh Rh et/ou Rh C=O Rh espèce III	pontée	(0)

3.2. Etude du catalyseur Rh/AL_2O_3 après chauffage en atmosphère de CO

La Fig. 2 présente la région 2 200...1 600 cm^{-1} des spectres IR qui correspond à la vibration ν_{CO} du monoxyde de carbone et traduit l'état de la surface du catalyseur Rh/Al_2O_3 traité en atmosphère de CO à une température de 25...400°C.

Après 20 min. à la temperature ambiante, sous 20 Torr de CO, apparaissent deux bandes fortes à 2 104 et 2 034 cm^{-1} et une bande large et mal définie, centrée sur 1 835 cm^{-1}. Sur l'échantillon traité à 200°C on constate une forte diminution des bandes à 2 104 et 2 034 cm^{-1} et une faible diminution de l'intensité de celle à 1 835 cm^{-1}. Si à 25°C la bande à 2 104 cm^{-1} a une intensité plus importante que celle à 2 034 cm^{-1}, à 200°C, elles deviennent égales. Un épaulement apparaît à 2 050 cm^{-1}. A 400°C l'intensité de la bande 2 100 cm^{-1} diminue encore alors que l'épaulement précédent à 2 000 cm^{-1} devient le pic le plus intense du spectre et se déplace à 2 044 cm^{-1}; la bande à 2 034 cm^{-1} disparaît ou bien est masquée par le pic large à 2 044 cm^{-1}. Le maximum à 1 835 cm^{-1} se déplace à 1 860 cm^{-1} et une autre bande large et faible apparaît à 1 925 cm^{-1}.

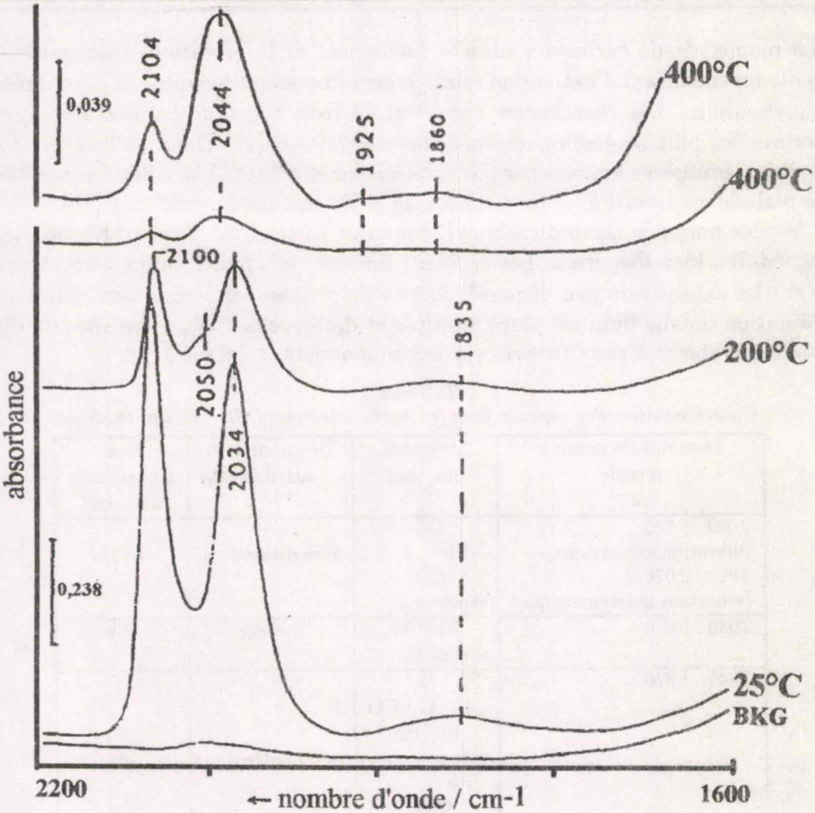

Fig. 2.- Spectres IR de CO adsorbé à 25°C sur Rh/AL_2O_3 après chauffage sous CO.

La formation de l'espèce I ($Rh^I(CO)_2$: 2 104, 2 034 cm^{-1}) diminue avec l'augmentation de la température. La présence majoritaire de l'espèce I dans l'échantillon à 25°C indique une très bonne dispersion de Rh à la surface.

Les espèces pontées (1 840...1 860 cm^{-1}), apparues à 25°C, semblent être les moins influencées par la température des traitements. A 400°C apparait un pic nouveau à 1 925 cm^{-1}, qui coexiste avec celui à 1 860 cm^{-1}. Le premier peut être attribué au CO dans un centre de coordination double [11] et le deuxième au CO dans un centre triple de coordination.

L'adsorption de CO à 25°C sur l'échantillon chauffé sous CO à 200°C indique l'apparition de CO lié linéairement à des atomes de Rh(0) (espèce II: ν_{CO}=2 040...2 076 cm^{-1}, $Rh^0(CO)$). Cette espèce devient majoritaire après traitement à 400°C. La présence de l'espèce I dans le spectre à 25°C indique une grande dispersion du Rh en surface.

L'apparition de l'espèce II linéaire à une température plus élevée peut indiquer l'abondance soit des sites Rh(0) fortement dispersés, soit des agrégats importants couverts avec charbon [12]. L'apparition de la bande due aux espèces linéaires peut s'expliquer par le fait que le CO adsorbé augmente la mobilité du Rh en surface [13].

3.3. Etude du catalyseur Rh/K–Al_2O_3 après chauffage en atmosphère de CO

La même technique que celle précédente a été utilisée. La Fig. 3 présente les spectres IR après adsorption à température ambiante de CO sur l'échantillon Rh/K–Al_2O_3 traité en atmosphère de CO de 25°...400°C. Le spectre de référence BKG présente dans cette région un pic faible et large à 2 042 cm^{-1}, dû, probablement, à une pollution de l'échantillon. A 25°C apparaissent des bandes larges à 2 037, 1 945 et 1 799 cm^{-1}. Après traitement à 200°C ces bandes se déplacent à 2 020 cm^{-1} (avec diminution de l'intensité), 1 900 cm^{-1} et 1 758 cm^{-1} (avec augmentation de l'intensité). A 400°C se produit un nouveau déplacement des pics à 2 033, 1 929 et 1 767 cm^{-1}. Le pic à 1 929 cm^{-1} diminue, alors que les autres pics augmentent et un nouvel épaulement apparaît à 2 063 cm^{-1}.

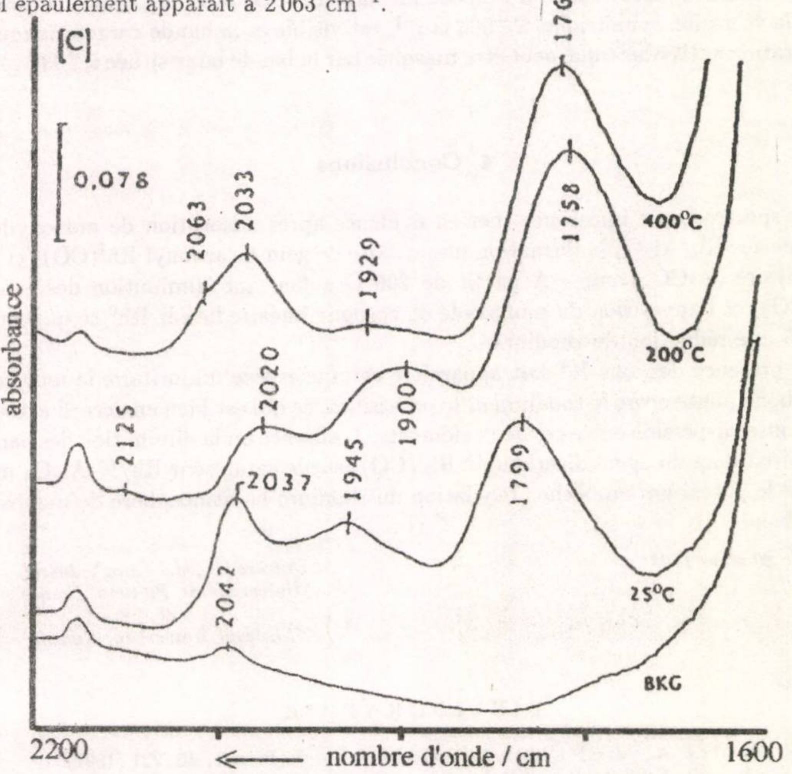

Fig. 3.– Spectres IR de CO adsorbé à 25°C sur Rh/K–Al_2O_3 après chauffage sous CO.

L'introduction de potassium entraîne des modifications importantes dans les spectres. L'apparition d'une nouvelle bande à 1 799 cm^{-1} peut être expliquée soit comme un déplacement d'une ancienne bande, soit comme une bande liée à la présence de K^+. Dans le cas des solides Ni–K/SiO_2, l'apparition d'une bande à 1 780 cm^{-1} a été attribuée, par G.A. Martin [14], à la formation d'une espèce CO pontée entre deux atomes de nickel; cette bande est observée à 1 930 cm^{-1} dans le cas de Ni/SiO_2; le déplacement de fréquence dû à la présence des ions K^+ peut s'expliquer par un enrichissement du métal en électrons sans que l'hypothèse d'une interaction directe puisse être rejetée [15].

L'hypothèse de la formation d'une espèce Rh – C = O ... K [16] semble être raisonnable. L'adsorption de CO sur les métaux est réalisée selon un schéma σ–π dans lequel la molécule CO est liée au métal par l'atome de carbone.

Les autres pics (à 2 063, 2 037, 2 033, 2 020, 1 945, 1 929 et 1 900 cm^{-1}) peuvent être attribués aux autre espèces où CO est lié au Rh(0); on peut expliquer les petites différences par la présence de K^+. Les espèces „gem dicarbonyle“ n'ont pas été mises en évidence dans le spectre.

Tenant compte de l'effet donneur du potassium on peut faire les attributions suivantes: 2 033...2 037 cm^{-1} à l'espèce linéaire Rh–CO; pour le „gem dicarbonyl“, seule la vibration symétrique, à 2 063 cm^{-1}, est visible et la bande caractéristique de la vibration antisymétrique peut être masquée par la bande large située à 2 033...2 037 cm^{-1}.

4. Conclusions

La spectroscopie infrarouge met en évidence après adsorption de monoxyde de carbone sur Rh/Al_2O_3 la formation majoritaire de gem dicarbonyl $Rh^I(CO)_2$ et très minoritaire de CO ponté. A partir de 200°C a lieu une diminution des espèces $Rh^I(CO)_2$ et l'apparition du monoxyde de carbone linéaire lié sur Rh^0 ce qui correspond à une réduction du rhodium.

La présence des ions K^+ fait apparaître comme espèce majoritaire le monoxyde de carbone ponté entre le rhodium et le potassium, ce qui est bien en accord avec une bonne interdispersion entre ces deux éléments. L'absence ou la diminution des bandes caractéristiques du „gem dicarbonyl“ $Rh^I(CO)_2$ sur le catalyseur $Rh/K–Al_2O_3$ montre que le potassium empèche l'oxydation du rhodium en atmosphère de monoxyde de carbone.

Reçue le 20 mars 1997

Université „Al.I Cuza“, Jassy,
** Université de Poitiers, France*
et
*** Kuwait University, Kuwait*

BIBLIOGRAPHIE

1. Rochefort A., LePeltier F., Rev. Inst. Fr. du Pétrole, **46**, 221 (1991).
2. Tanabe K., *Solid Acids and Bases: Their Catalytic Properties.* Academic Press, London, New York, 1970.
3. Boehm H.P., Knözinger H., dans *Catalysis – Science and Technology*, par Anderson J.R. et Boudart M. (Eds.), Springer-Verlag, Berlin, Vol. **4**, 1983, 39.
4. Knözinger H., dans *Catalysis by Acids and Bases*, par Imelic B. *et al.* (Eds.), Elsevier, Amsterdam, 1985.
5. Davies P., Stone C.M., Patent USA 3,271,325, Sept. 6, 1966; Appl. 221,898; Sept 6, 1962.

6. Clark R.T., Patent USA 3, 972,952, Aug. 3, 1976; Appl. 558,524; Mar. 14, 1975.
7. Jolly W.L., *Modern Inorganic Chemistry*. McGraw-Hill, New York, 1985, 107.
8. Volatron F., Jean Y., *Les orbitales moléculaires en chimie. Introduction et applications*. McGraw-Hill, Paris, 1991, 98.
9. Yang A.C., Garland C.W., J. Phys. Chem., **61**, 1504 (1967).
10. Yao H.C., Rothschild W.G., J. Chem. Phys., **68**, 4774 (1978); Primet M.J., Chem. Farad. Trans. I., **74**, 2570 (1978); Primet M., Védrine J.C., Naccache C., J. Mol., Catal., **4**, 411 (1978); Yates D.J., Murrel L.L., Prestridge E.B., J. Catal., **57**, 41 (1979); Solymosi F., Pasztor M., J. Chem. Phys., **84**, 4789 (1985); Solymosi F., Rasko J., J. Mol. Catal., **15**, 107 (1989).
11. Sheppard H., Nguyen T.T., Adv. Infrared Raman Spectrosc., **5**, 67 (1978).
12. Zachi M.I., Kunzmann G., Yates B.C., Knözinger H., J. Phys. Chem., **91**, 1486 (1987).
13. Yates D.J.C., Murrel L.L., J. Catal., **71**, 3908 (1979).
14. Martin G.A., Rev. Phys. Appl., **16**, 181 (1981).
15. Praliaud H., Primet M., Martin G.A., Bull. Soc. Chim. Fr., **5**, 79 (1986).
16. Kiennemann A., Breault R., Hindermann J.P., Laurin M., J. Chem. Soc., Faraday Trans., **83**, 2119 (1987).

INFLUENŢA POTASIULUI ASUPRA CATALIZATORULUI DE RODIU/ALUMINĂ ÎN ATMOSFERA DE CO

Studiu prin spectroscopie în infraroşu *in situ*

(Rezumat)

S-a studiat rolul potasiului în comportarea unui catalizator de rodiu depus pe alumină în atmosferă de monoxid de carbon. Suporturile utilizate au fost alumina şi alumina promotată cu ioni de potasiu calcinate la 700°C. Tehnica de analiză utilizată a fost spectroscopia în infraroşu cu transformată Fourier. Măsurătorile au fost realizate *in situ*. Spectrele IR indică o bună dispersie a rodiului pe suprafaţa catalizatorului. S-a evidenţiat o bună interdispersie a rodiului şi potasiului. Studiul spectrelor obţinute indică faptul că prezenţa potasiului diminuează procesul de oxidare a rodiului în atmosferă de monoxid de carbon.

BULETINUL INSTITUTULUI POLITEHNIC DIN IAŞI
Tomul XLIII (XLVII), Fasc. 3–4, 1997
Secţia II
CHIMIE şi INGINERIE CHIMICĂ

D.C. 546.73; 535.243

DETERMINATION OF THE TRACE AMOUNTS OF COBALT BY SOLID-PHASE SPECTROPHOTOMETRY

BY
DOINA BÎLBĂ and LAURENŢIU CIOCHINĂ

A method for the determination of trace amounts of cobalt with Nitroso-R salt reagent by solid phase spectrophotometry is presented. The red colour complex [Co(II): reagent= =1:3] is sorbed and concentrated on an anionic resin, the absorbance of resin phase being measured directly into 1 mm cells at $\lambda = 520$ and 700 nm. Cobalt may be determined in concentration range of 15...250 μg.l^{-1} with a relative standard deviation of 3.44%, the sensitivity of the method, expressed as molar absorptivity being of 1.5×10^6. The method can be applied to cobalt determination from natural waters and industrial effluents.

1. Introduction

The influence of the cobalt on the important biological processes is well known by specialists and imposes a rigorous control of the cobalt content from natural waters. Many determination methods of the trace amounts of cobalt (10^{-7}...10^{-6} %) include the group preconcentration by coprecipitation [1], solvent extraction [2], [3], sorption [4],...,[6], flotation [7]. A special importance is payed to the immobilized reagents on different kind supports which made possible the cobalt determination directly on the sorbent phase by several instrumental methods such as: solid-phase spectrophotometry [8], diffuse reflectance spectrometry [9], [10], absorption voltammetry [11].

The solid-phase spectrophotometry (SPS) is a technique that uses a solid matrix, usually an ion exchanger, for preconcentration of the species of interest with the aid of a chromogenic reagent, the absorbance of the coloured resin beads being directly measured [12]. The SPS method allows simultaneously preconcentration and development of the colours, having an increased sensitivity than that of conventional colorimetry.

In the present paper a determination method of the trace amounts of cobalt (II) with the aid of Nitroso-R salt reagent (NRS), by solid-phase spectrophotometry, has been developed.

2. Experimental

2.1. Reagents and Apparatus

The chloride form of a strongly basic anion exchanger Dowex 1×8 (100...200 mesh) has been used. The resin was pretreated with 2M HCl, washed with doubly-distilled water until the washings were free from chloride and then air-dried.

The stock solution of cobalt of 1×10^{-2} M, prepared by dissolution of $Co(NO_3)_2\cdot6H_2O$, has been complexonometrically standardized.

The Nitroso-R-salt (the disodic salt of the 1-nitroso-2-hydroxynaphtalene-3,6-disulfonic acid) (pK=7.5) in aqueous solution of 5×10^{-3} M form has been used as chromogenic reagent.

The medium acidity was carried out with solutions of CH_3COONa, HCl, NaOH and was checked up by pH-metric measurements.

For spectral measurements, a Specol spectrophotometer with 1 mm cells has been used.

2.2. Absorbance Measurements

The mixture of analyte and proper reagents was equilibrated with the solid phase by mechanical shaking. The coloured resin was then collected by filtration and filled together with a small volume of filtrate by means of a pipette into a 1 mm cell.

The absorbance of the complex sorbed on the solid phase is measured against a cell filled with the blank resin at the maximum wavelength $\lambda_{\max}$ (corresponding to the absorption maximum of the complex) and at another wavelength (within the 700...800 nm range) where only the solid phase causes attenuation of radiation. Thus, the errors due to variation of filling of the resin beads into cells (the change in path-length or scattering) are eliminated.

The net absorbance A_{RC} of the complex species sorbed on the resin is obtained using Yoshimura's equation [13]:

$$A_{RC} = \Delta A - \Delta A^*,$$

where:

$$\Delta A = (A_{\max} - A_{700})_{\text{sample}}, \quad \Delta A^* = (A_{\max} - A_{700})_{\text{blank}}.$$

3. Results and Discussion

Due to the sulfonic groups which are strongly dissociated, Nitroso-R salt reagent is fixed on the anionic resin by a ion-exchange mechanism giving a yellow-orange colour with an absorption maximum at $\lambda \simeq 400$ nm.

In aqueous weak acidic solutions the Nitroso-R salt reacts with cobalt (II) [14], forming a 1:3 red colour complex that is sorbed on anionite and showed two absorption maxima at $\lambda_1=415$ nm and $\lambda_2=500...550$ nm. The electronic spectra of the reagent and his complex with cobalt in resin phase, shown in Fig. 1, have a

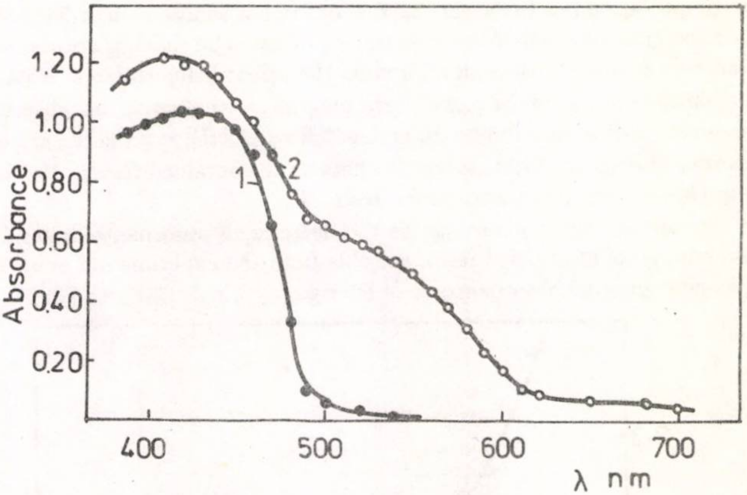

Fig. 1.- Absorption spectra in Dowex 1×8 resin phase: *1* - Nitroso-R salt, $C_{\mathrm{NRS}} = 2.5\times10^{-5}$ M; *2* - Cobalt-Nitroso-R salt, $C_{\mathrm{Co}} = 5\times10^{-6}$ M, $C_{\mathrm{NRS}} = 2.5\times10^{-5}$ M.

similar shape to that of corresponding solutions spectra, the slight displacement of absorption bands being explained by the molecules deformation in sorbent phase.

Since at $\lambda \simeq 520$ nm the influence of the colour of free reagent (sorbed on anionite) on complex species colour may be neglected, the subsequent measurements will be carried out at this wavelength, against a cell with resin as blank.

The optimum pH value of cobalt-Nitroso-R salt formation and fixation on anionite falls in the range 5...6 and coincides with that recommended for spectrophotometric determinations in acetic solutions (Fig. 2).

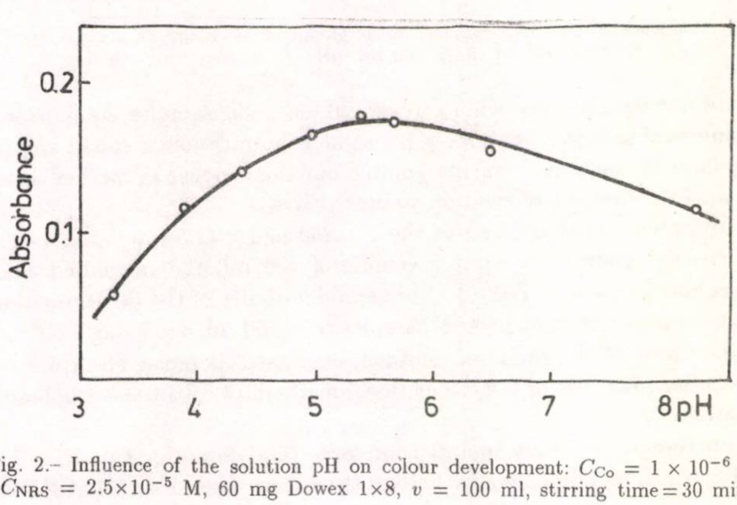

Fig. 2.- Influence of the solution pH on colour development: $C_{\mathrm{Co}} = 1\times10^{-6}$ M, $C_{\mathrm{NRS}} = 2.5\times10^{-5}$ M, 60 mg Dowex 1×8, v = 100 ml, stirring time = 30 min.

The complexation reactions were carried out in hot solutions in order to decrease the formation time of cobalt-Nitroso-R salt complex. The shaking optimum time of 100 ml analyte solution with resin is 30 min., the colour being stable at least 90 min.

The influence study of Nitroso-R salt reagent concentration on absorbance of cobalt complex indicated a minimum molar [NRS]/[Co(II)] ratio necessary of 10 : 1.

The order of reagents addition has no effect on the obtained results, the following one being chosen: cobalt–reagent-buffer–resin.

The increase of resin amount causes the decrease of absorbance values (Fig. 3). The minimum amount of dried resin, suitable from the experimental point of view, leading to enough large absorbance, is of 60 mg.

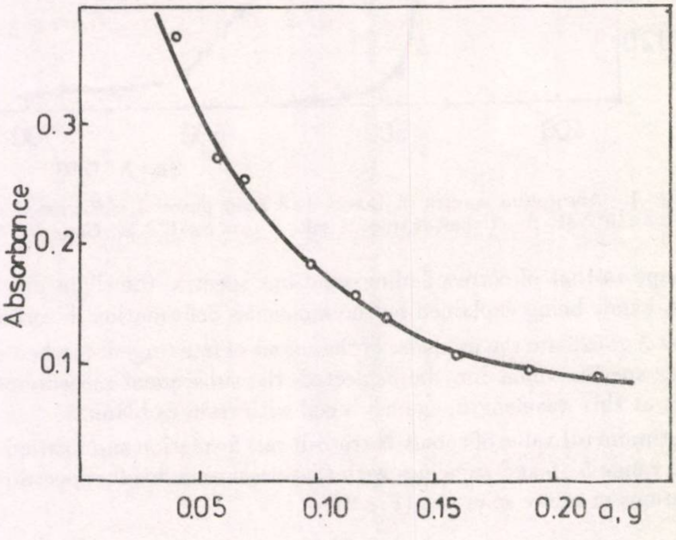

Fig. 3.- Influence of the resin amount on development of colour: $C_{\mathrm{Co}} = 1 \times 10^{-6}$ M, $C_{\mathrm{NRS}} = 2.5\times10^{-5}$ M, $v = 100$ ml, pH = 5, stirring time = 30 min.

The absorbance measurements carried out on resin samples equilibrated with varied volumes of solutions containing the same concentration of cobalt and proportional amounts of the other reagents pointed out the increase of method sensitivity together with the increase of solution volume (Fig. 4).

The calibration curve is linear in the 15...250 μg.l^{-1} (2.5×10^{-7} M...4×10^{-6} M) range of concentration for a sample volume of 100 ml, the calculated analytical parameters being shown in Table 1. The reproductibility of the determinations was verified on a number of eight parallel samples ($v = 100$ ml, $c = 59$ μg Co.l^{-1}) [15].

The sensitivity of the proposed method, expressed as molar absorptivity, is of 100 times larger than that of the conventional methods of cobalt spectrophotometric determinations.

The interference of heavy metals complexes (Cu, Mn, Zn, Cd, Ni, Pb) with Nitroso-R salt can be eliminated by boiling the coloured resin with 1 M HNO_3.

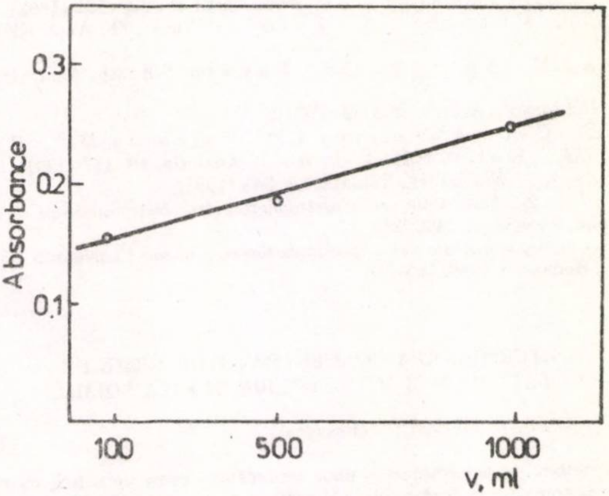

Fig. 4.- Influence of the sample volume on colour development: $C_{Co} = 1\times10^{-6}$ M, $C_{NRS} = 2.5\times10^{-5}$ M, 60 mg Dowex 1×8, pH = 5, stirring time = 30 min.

Table 1
Analytical Parameters

Parameter	Value
Intercept	0.015
Slope, $[l.\mu g^{-1}]$	0.0025
Linear dynamic range, $[\mu g.l^{-1}]$	15...250
Relative standard deviation (RSD), [%]	3.44
Detection limit (K=3), $[\mu g.l^{-1}]$	0.78
Determination limit (K=10), $[\mu g.l^{-1}]$	2.6
Molar absorptivity	1.5×10^{6}

The proposed method can be applied for cobalt determination in natural waters samples and in industrial effluents.

Received, April 4, 1996

Technical University "Gh.Asachi", Jassy,
Department of Analytical Chemistry

REFERENCES

1. Akatsuka K., Nobuiama N., Atsuya I., Anal. Sci., **5**, *4*, 475 (1989).
2. Sran R., Baul T., Srinivas P., Khathing D., Anal. Lett., **25**, *8*, 1545 (1992).
3. Granzhan A., Charikov A., Vest. Leningr. Univ., **4**, 107 (1990).
4. Ohzawa K., Uchiyama K., Yoshimura Y., Imaeda K., Anal. Sci., **7**, *3*, 499 (1991).
5. Panteleev G., Tsizin G., Formanovski A., Starsshinov N., Sdeykh E., Kuzmin N., Zolotov Yu., Zh. Anal. Khim., **46**, *2*, 355 (1991).
6. Chambaz D., Haerdi W., J. Chromatogr., **600**, *2*, 203 (1992).
7. Cabezon L.M., Cabellero M., Diaz J.M., Analusis, **19**, *4*, 123 (1991).
8. Fernandez-deCordova M.L., Molina-Diaz A., Pascual-Reguera

M.I., Capitan-Valvey L.F., Anal. Lett., **25**, *10*, 1961 (1992).

9. Ivanov V.M., Morozko S.A., Zolotov Yu.A., Zh. Anal. Khim., **48**, *8*, 1389 (1993).
10. Trutneva L.M., Shvoeva O.P., Savvin S.B., Zh. Anal. Khim., **49**, *5*, 473 (1994).
11. Zhang Z., Mikrochim. Acta, **1**, *1-2*, 89 (1991).
12. Capitan F., Capitan-Vallvey L.F., Valencia M.C., Bosque-Sendra J.M., Molima F., de Orbe J., Analusis, **19**, 177 (1991).
13. Yoshimura K., Waki H., Talanta, **32**, 345 (1985).
14. Marczenko Z., *Separation and Spectrophotometric Determination of Elements*. Ellis Harwood, New York, 1986, 243.
15. Sommer L., *Analytical Absorption Spectrophotometry in the Visible and Ultraviolet*. Akad. Kiadó, Budapest, 1989, 105-110.

DETERMINAREA CONCENTRAŢIILOR URME DE COBALT PRIN SPECTROMETRIE ÎN FAZĂ SOLIDĂ

(Rezumat)

Se prezintă o metodă de determinare a unor concentraţii urme de cobalt cu reactiv sare R-nitrozo prin spectrofotometrie în fază solidă. Complexul de culoare roşie [Co(II) : reactiv = 1 : 3] este sorbit şi concentrat pe o răşină anionică, absorbanţa fazei de răşină fiind măsurată direct în cuve de 1 mm la $\lambda = 520$ şi 700 nm. Cobaltul poate fi determinat în domeniul de concentraţie de 15...250 µg/l cu o eroare standard relativă de 3,44%, sensibilitatea metodei exprimată ca absorptivitate molară fiind de $1{,}5 \cdot 10^6$. Metoda poate fi aplicată la determinarea cobaltului din probe de ape naturale şi efluenţi industriali.

BULETINUL INSTITUTULUI POLITEHNIC DIN IAŞI
Tomul XLIII (XLVII), Fasc. 3–4, 1997
Secţia II
CHIMIE şi INGINERIE CHIMICĂ

D.C. 661.883.1. 54-92

SYNTHESIS AND STUDY OF SOME CO-ORDINATION POLYMERS OF Zr(IV) WITH 2,8-DIMETHYL-PHENOXIPHOSPHINIC AND DIHEXYLPHOSPHINIC ACIDS AS LIGANDS

BY

I. ROŞCA, MIHAELA VIZITIU, DOINA SIBIESCU,
DANIEL SUTIMAN and ADRIAN CĂILEAN

The optimal conditions of the synthesis of some co-ordination polymers derived from the interaction of acetyl-acetonate of Zr(IV) and 2,8-dimethylphenoxiphosphinic acid and dihexylphosphinic acid are presented.

Chemical analysis, the IR-absorption spectra, the X-ray diffraction and determination of the kinetic parameters of the thermal decomposition reactions were the methods applied for the research.

1. Introduction

Wishing to obtain new compounds in the field of the co-ordination polymers with organophosphinic acids as ligands, some polymers of Zr(IV) derived from the interaction between acetylacetonate of Zr(IV) and one of the acids: 2,8-dimethylphenoxiphosphinic and dihexylphosphinic were synthesized and studied. The methods used for the study of the new polymers were: chemical analysis, the IR-absorption spectroscopy, the X-ray diffraction, derivatography and the determination of the kinetics parameters for the thermal decomposition reactions. The study of the presented compounds is a continuation of previous works of the authors in the field of co-ordination polymers with ligands derived from organophosphinic acids and some metallic cations [1],...,[9].

2. Experimental

2.1. Synthesis and Determinations of Chemical Composition and of the Molecular Weight

The co-ordination compounds here presented were obtained in melting mixtures and by reagent in organic solvents.

With this purpose, stoichiometric quantities of the reagents were used; 1 mole of Zr(IV) acetylacetate and 4 moles of 2,8-dimethylphenoxiphosphinic acid or of dihexylphosphinic acid were maintained for three hours at the melting temperature of the acid or the same quantities were maintained under reflux in one of the next solvents: ethanol, benzene or toluene.

After three hours, when the reaction between the reactants was accomplished, the obtained products were separated and washed with distilled water; then they were maintained in to an oven at a temperature of 105°C till constant weight. The obtained products were white friable solids. The yield of the syntheses presented values of at least 98%. The results of the chemical analysis and of the molecular weight determined for the benzene soluble fractions are presented in Table 1. The cryoscopic method was used for molecular weight determination, method also used by other authors for the same type of compounds [1],...,[9].

Table 1
Chemical Composition, [%] and Molecular Weight (M) of the Synthesized Compounds

Compound	Zr(IV)	C	H	O	P	*M*
	calc.	calc.	calc.	calc.	calc.	
	exp.	exp.	exp.	exp.	exp.	
Zr-I	8.09	59.62	4.26	17.03	11.00	7.950
	8.26	59.36	4.39	17.20	11.16	
Zr-II	8.91	56.30	10.16	12.51	12.12	8.200
	9.98	56.50	10.31	12.71	12.21	

From the reactants rate and the results of the chemical analysis, the following chemical reactions were established for the syntheses of the compounds:

$$n\mathrm{Zr(Acac)_4} + 4n(\mathrm{CH_3C_6H_3OC_6H_3CH_3})\mathrm{PO_2H} \longrightarrow [\mathrm{Zr(CH_3C_6H_3OC_6H_3CH_3PO_2)_4}]_n + 4n\mathrm{HAcac}$$

$$n\mathrm{Zr(Acac)_4} + 4n(\mathrm{C_6H_{13}})_2\mathrm{PO_2H} \longrightarrow \{\mathrm{Zr}[(\mathrm{C_6H_{13}})_2\mathrm{PO_2}]_4\}_n + 4n\mathrm{HAcac}$$

For an easier writing the compounds were noted as follows:

$$[\mathrm{Zr(CH_3C_6H_3OC_6H_3CH_3PO_2)_4}]_n \overset{\text{not}}{=} \text{Zr-I and } \{\mathrm{Zr}[(\mathrm{C_6H_{13}})_2\mathrm{PO_2}]_4\}_n \overset{\text{not}}{=} \text{Zr-II}.$$

2.2. Derivatographic Analysis and Determination of the Kinetics Parameters of the Thermal Decomposition Reactions

A Paulik-Paulik-Erdey derivatograph was used for the derivatographic analysis; 50 mg samples of polymer were heated at a heating rate of 10°C/min, in the temperature range 20°...700°C.

Studying the registered curves it was shown that the thermal destruction occurred releasing gaseous products derived from the organic radicals of the organophosphinic acids. The final solid product is the one with the empirical formula: $\mathrm{Zr(PO_3)_4}$, or $\mathrm{ZrO_2.2P_2O_5}$.

It was shown that the co-ordination polymer derived from the 2,8-dimethylphenoxiphosphinic acid presented a higher thermal stability in comparison with that derived from the other acid, fact which confirmed the hypothesis that the benzene nucleus brings a thermal stabilization in the structure of the synthesized compounds.

The Freeman - Carrol method [10] was used for the reaction order and activation energy determinations. In Table 2 the values of the reaction order and of the activation energy in the two stages of the thermal decomposition of the synthesized compounds are presented.

Table 2

The Two Stages of the Thermal Decomposition, the Values of the Reaction Order and of the Activation Energy, [kJ/mol]

Compound	Stage 1, [°C]		Stage 2, [°C]		Reaction order	Activation energy
	Start	End	Start	End	$\frac{\text{Stage 1}}{\text{Stage 2}}$	$\frac{\text{Stage 1}}{\text{Stage 2}}$
Zr-I	325	405	405	560	$\frac{0.82}{0.90}$	$\frac{178}{190}$
Zr-II	290	395	395	530	$\frac{0.85}{0.93}$	$\frac{154}{180}$

2.3. IR-Absorption Spectra

The IR-absorption spectra were registered using a model III Leitz-Weithler spectrometer with a frequency band of 400...4,000 cm^{-1}.

Generally, the IR-absorption spectra of the co-ordination polymers are similar with those of the free acids from which they are derived. The differences arise only in the field of $>PO_2$ groups absorption due to the co-ordination of these ones to the central atom Zr(IV).

Literature indications [1],...,[9] present the characteristics absorption range for the $>PO_2$ group, between the values 950...1,360 cm^{-1}. The absorption band with the maximum value 1,175 cm^{-1}, which is characteristic to the P=O group from the free acids, turns into two maxim values at 1,190 and 1,130 cm^{-1} in the co-ordination compounds derived from the same acids, having Zr(IV) as central atom. This spectrum is characteristic for the formation of the complex combinations of organophosphinic acids with metallic cations [1],...,[9], [11],...,[15].

If the vibration frequencies characteristic for the $>PO_2$ group from the free acid and from the co-ordination compounds are noted ν and, respectively, ν', the following equation:

$$\Delta\nu = \frac{\nu - \nu'}{\nu} \cdot 100$$

represents the percent modifications of the vibration frequencies of the $>PO_2$ group when it is engaged in co-ordination bound:

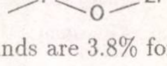

The $\Delta\nu$ values of the compounds are 3.8% for Zr-I and 2.2% for Zr-II.

2.4. X-Ray Diffraction Spectra

The X-ray diffraction spectra for the synthesized compounds were registered using a Kristalloflex Siemens instrument that has a Röntgen tube with $\text{Cu}(\text{K}_\alpha)$ radiations filtred through Ni. The anode voltage is 35 kV and the intensity is 12 mA. The irradiation technique consists in transmission using continuous exploration of the diffraction spectra with Geiger–Müller counter situated on texture goniometer. The diffraction-field was of $2\theta = 10°...45°$. From the X-ray diffraction spectra, the crystallinity degree was determined using the equation:

$$X_c = \frac{F_c}{F_c + F_a} \cdot 100,$$

where F_c represents the crystalline halo area and F_a – the amorphous one.

All the synthesized compounds had a bi-phase structure: one characteristic for the amorphous state and the second with diffraction lines characteristic for the crystalline one. The crystallinity degree for the synthesized compounds is relatively small having the values: 8% for Zr-I and 23% for Zr-II.

Received, April 10, 1997

Technical University "Gh.Asachi", Jassy,
Department of Inorganic Chemistry

REFERENCES

1. Block P.B., Simkin J., Ocone R.L., J. Am. Chem. Soc., **84**, 1749 (1962).
2. Stone A., Graham G.A.W., *Inorganic Polymers*. Acad. Press, London, 1962.
3. Korsak V.V., Krukovski P.C., Vysomolek. Soed., **A69**, 583 (1967).
4. Golgoţiu T., Roşca I., Makromolek. Chem., *160*, 59 (1972).
5. Roşca I., Vysomolek. Soed., **B.1**, 34 (1985).
6. Roşca I., Vysomolek. Soed., **B.10**, 735 (1985).
7. Silvestru C., Haiduc I., J. Organomet. Chem., *365*, 83 (1989).
8. Silvestru C., Haiduc I., Caruso F., Rossi M., J. Organomet. Chem., *448*, 75 (1993).
9. Roşca I., Sutiman D., Căilean A., Vizitiu M., Rusu I., Sibiescu D., Thermochim. Acta, *269/270*, 295 (1995).
10. Freeman S., Carrol B., J. Phys. Chem., **62**, 394 (1958).
11. Kossler I., *Methoden der Infrarot Spectroscopie in der Chemischen Analyse*. Akad. Verlag, Leipzig, 1961.
12. Nakamoto K., *Infrared Spectra of Inorganic and Co-ordination Compounds*. John Wiley & Sons, New York – London, 1963.
13. Okaya A., *Paramagnetic Resonance*. Acad. Press, New York, 1963.
14. Lewis J., Wilkins R.G., *Modern Co-ordination Chemistry*. Academic Press, London – New York, 1988.
15. Brezeanu M., Spacu P., *Chimia combinaţiilor complexe*. Ed. Did. şi Ped., Bucureşti, 1986.

SINTEZA ŞI STUDIUL POLIMERILOR DE COORDINAŢIE AI ZR(IV) CU LIGANZI DERIVAŢI DE LA ACIZII 2,8-DIMETILFENOXIFOSFINIC ŞI DIHEXILFOSFINIC

(Rezumat)

Se stabilesc condiţiile optime de sinteză ale polimerilor de coordinaţie obţinuţi din interacţiunea acetilacetonatului de Zr(IV) cu acizii: 2,8-dimetil-fenoxi-fosfinic şi dihexil-fosfinic.

Metodele aplicate pentru cercetarea compuşilor sintetizaţi sunt: analiza chimică, spectrele de absorbţie în IR şi spectrele de raze X, determinarea parametrilor cinetici ai reacţiilor de descompunere termică.

BULETINUL INSTITUTULUI POLITEHNIC DIN IAŞI
Tomul XLIII (XLVII), Fasc. 3–4, 1997
Secţia II
CHIMIE şi INGINERIE CHIMICĂ

D.C. 547.544; 539.2

CHARACTERIZATION OF THE MOLECULAR WEIGHT DISTRIBUTION OF POLYSULFONES

BY
*ANA ONU, *CRISTINA COSTIN and N. AELENEI

The most favourable conditions of the turbidimetric titration have been established in order to obtain the molecular weight distribution curves of some polysulfones based on bisphenol A. The chloroform/ethanol solvent/nonsolvent system has been used, working with a nonsolvent adding rate of 1.08 ml/min and the initial concentration of polymer solution of 0.06 g/dl. The standardization of the method was made with samples of known molecular weights between 17,900 and 180,000 g/mole. The method was used to obtain the molecular weight distribution curve of an industrial polysulfone.

1. Introduction

Polysulfones are macromolecular compounds containing SO_2 groups and hydrocarbonated rests in the main polymer chain. The aromatic polysulfones are characterized by an excellent thermal stability and oxidation resistance, which are principally due to aryl-sulfonics groups, highly resonant, as well as to the sulphur – which is in the highest state of oxidation. The most polysulfones are clear, rigid, with high modulus of elasticity and rigidity, and with glass-transition temperatures between 180° and 250°C. Among the aromatic polysulfones, very important are the poly(ether-sulfones) and especially the polysulfone obtained by polycondensation of 4,4-diclorodiphenil sulfone with the sodium salt of 2,2-bis(4-hydroxyphenylpropane) (bisphenol A):

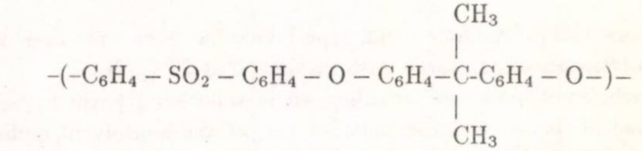

$$-(-C_6H_4-SO_2-C_6H_4-O-C_6H_4-\underset{\substack{|\\ CH_3}}{\overset{\substack{CH_3\\ |}}{C}}-C_6H_4-O-)-$$

This polysulfone is clear, rigid, thermoplastic, with good electroinsulating and mechanical properties. These properties are appreciably maintained in the –100°... +150°C temperature range. This polysulfone has many applications in electrotechnics and electronics, in medical technique, for drug and food packings resisting to physical and chemical agents [1].

The polymer properties and its operating parameters on processing depend, principally, both on molecular weight and polydispersity. The determination of polydispersity involves the quantitative fractionation of the macromolecular products, the characterization of the fractions regarding molecular weight and the plotting of the molecular weight distribution curves. Since these methods require complicated operations, a long time and large quantities of solvents and nonsolvents, for a rapid check of the quality of the polymeric products, searches were made in order to obtain a quick image of their heterogeneity. Thus, appeared the analytical methods of fractionation as: ultracentrifugation, gel permeation chromatography and turbidimetric titration.

Among the analytical methods of fractionation, turbidimetric titration is the most used, offering a simple and enough precisely alternative to obtain the distribution curves. However, to use this method it is necessary a preliminary standardization for a certain polymer. This involves the utilization of a relatively monodisperse fraction series, of known molecular weight, the adequate selection of solvent/nonsolvent pair,establishing of the best concentration domain for measurements and of the titration rate, so that convenient titration curves could be obtained in order to explain quantitative data. Once established the work conditions and standardization curve, it is sufficiently only to obtain the turbidimetric titration curve for getting the distribution curves of a certain polydisperse polymer.

Turbidimetric titration can be used both to obtain molecular weight distribution of the polymers, copolymers and polymer mixtures, and to obtain some information on the thermodynamic behaviour of the studied polymer/solvent/nonsolvent system [2]. The classic procedure, proposed by Morey and Tamblyn [3], has been continuously improved, both as work techniques and interpretation manner of data [4], [5].

In this work, the best conditions of turbidimetric titration were established in order to obtain the molecular weight distribution of polysulfones based on bisphenol A. Having as a start point Virskii [4] and Geczy [5] method for experimental data interpretation we have proposed a rapid procedure which may be used in this purpose.

2. Experimental

A commercial polysulfone UDEL type P3500 has been fractioned by gradual precipitation from tetrahydrofuran with methanol, at 20°C [6].

For turbidimetric curves recording an installation [7] which permits the thermostatation of the system, the constant rate of the nonsolvent adding, an efficient stirring of the solution and the automatic record of the transmitted light has been used.

Some solvent/nonsolvent pairs were tested. Tests concerning nonsolvent adding rate and the moving rate of the paper on the recording apparatus has also been done. The initial solution concentration domain has been established, so that the titration curves could be easily and correctly interpreted. Thus, the following optimal conditions has been found: the solvent/nonsolvent system–chloroform/ethanol, the nonsolvent adding rate – 1 ml/min; temperature – 20°C; the initial concentration of the solutions – 0.06 g/dl.

The standardisation of the method has been done with polysulfone fractions of molecular weight between 17,900 and 180,000 g/mole. The number average molecular weights were obtained with a Hewlett-Packard model 502 membrane osmometer, in chloroform, using the cellophane 600 membranes.

3. Results and Discussion

The number-average molecular weights of the unfractioned polysulfone and of the fractions were:

Sample	NF	Fr.I	Fr.II	Fr.III	Fr.IV	Fr.V	Fr.VI
M_n, [g/mole]	162,000	17,900	35,200	53,100	55,400	61,800	180,000

The recorded turbidimetric curves of various fractions, used for standardization, showed that the differences between molecular weights are reflected in some characteristics of the titration curves as follows: the nonsolvent volume necessary for the appearance of the first precipitate amount, V_0, and the maximum of the curve, which is proportional with maximum optical density, D_M.

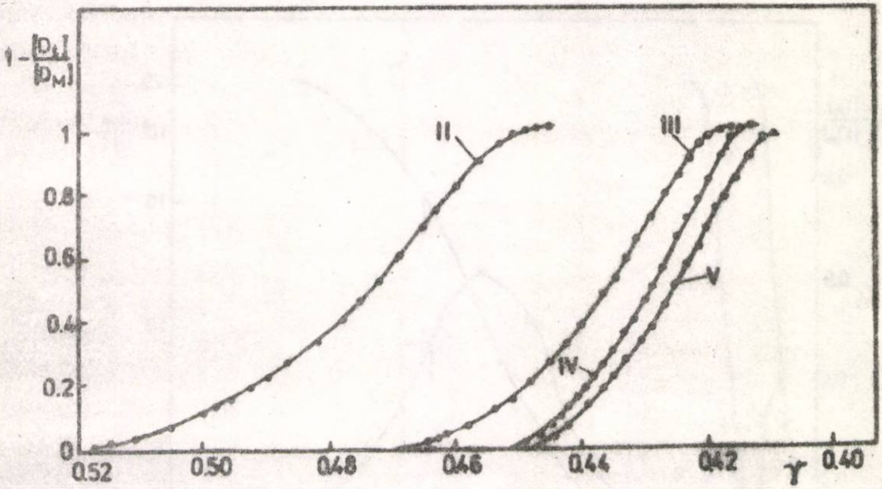

Fig. 1.– The normalized turbidimetric curves of the fractions II, III, IV and V.

For the calculus, the normalized turbidimetric curves or equations are necessary [2]. The optical density at different moments of the titration, D_t, is corrected for dilution, according to the relationship:

$$[D_t] = \frac{D_t}{1-\gamma}, \tag{1}$$

where $[D_t]$ is normalized optical density and γ – the volume fraction of nonsolvent:

$$\gamma = \frac{V_{NS}}{V_S + V_{NS}}, \tag{2}$$

with V_S – the volume of the polymer solution and V_{NS} – the added nonsolvent volume at the respective time. According with the standard procedure, the $[D_t]$ vs. γ dependence was plotted for each polysulfone fraction and then the normalised turbidimetric curves, in $(1 - [D_t]/[D_M]) - \gamma$ co-ordinates (Fig. 1), where $(1 - [D_t]/[D_M])$ is just the gravimetric fraction (w) used in the preparative fractionation [4].

With a view to obtain the integral molecular weight distribution curves, $w = f(M)$, one firstly found the γ vs. M dependence, using for this the narrow fractions of known molecular weights. It has been admitted that, at the end of the titration, the whole polymer quantity has been taken out from solution, i.e.: $[D_t] = [D_M]$ for $w = 0$ and $[D_t] = 0$ for $w = 1$. It was also considered that, for each fraction, the value of optical density corresponding to the precipitation of half of the polymer quantity, $[D_t]_{1/2}$, and the respective $\gamma_{1/2}$, from $[D_t]$ vs. γ dependence, were characteristic. For the given system, the following dependence has been obtained:

$$M_n = \frac{4545.45}{\gamma - 0.35}. \tag{3}$$

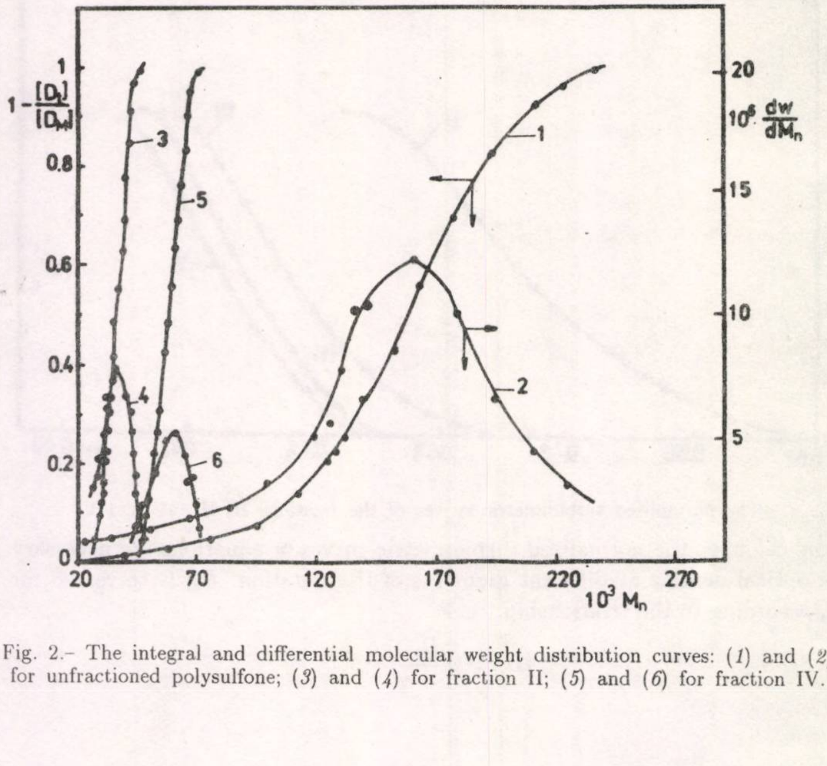

Fig. 2.– The integral and differential molecular weight distribution curves: (*1*) and (*2*) for unfractioned polysulfone; (*3*) and (*4*) for fraction II; (*5*) and (*6*) for fraction IV.

The relation (3) permits the calculus of the M_n value for a given γ. Thus, graphs like those shown in Fig. 1, in $w-\gamma$ co-ordinates, can be turned into graphs that show the dependence w vs. M, (the integral molecular weight distribution curves). By derivation of the integral curves the differential molecular weight distribution curves could be obtained.

The integral and differential distribution curves for the unfractioned sample and for the two fractions with narrow distribution are presented in Fig. 2. It is notable that the number average molecular weight corresponding to the maximum of the curves are in a satisfactory agreement with the experimental data.

4. Conclusions

a) The best conditions for the turbidimetric titration in order to obtain the molecular weight distribution curves for some polysulfone based on bisphenol A were established. These conditions were: solvent/nonsolvent system – chloroform/ethanol, the initial concentration of polymer solution – 0.06 g/dl, the nonsolvent adding rate – 1 ml/min, the work temperature – 20°C.

b) For the standardization of the method six polysulfone fractions obtained by gradual precipitation in tetrahydrofuran/methanol system were used. The number averages molecular weights have been determined by osmotic measurements; they were between 17,900 and 180,000 g/mole.

c) On the basis of the normalized turbidimetric curves and of the standardization equation, the data requested to obtain the molecular weight distribution curves of some sample with narrow distribution and of an industrial polysulfone sample were calculated. The maximums of the distribution curves are in accordance with the number average molecular weight values obtained from osmotic measurements, both for the fractions and for unfractioned polymer.

Received, March 3, 1997

* *"Al.I.Cuza" University, Jassy,*
Department of Physical Chemistry
and
Technical University "Gh.Asachi", Jassy,
Department of Physical Chemistry

REFERENCES

1. Johnson R.N., *Polysulfones, Encyclopedia of Polymer Science and Technology.* Vol. **11**, Ed. Bikales N.M., Intersci. Publ., John Wiley and Sons, 1969.
2. Onu A., Beldie C., Mat. plastice, **21**, *2*, 97 (1984).
3. Morey D.R., Tamblyn J.W., J. Appl. Physics, **16**, 419 (1945).
4. Virskii P.I., Klapovskaia A.O., Adrianeva N.N., Alkaeva F.O., Vysokomol. Soed., **A10**, 1688 (1968).
5. Geczy I., Gyarmathy-Tamas A., Acta Polymerica, **31**, *4*, 225 (1980).
6. Aelenei N., Rusu M., Nagacevschi V., Mat. plastice, **23**, *4*, 197 (1986).
7. Schneider I.A., Onu A., Vasile C., Toader M., Pat. Romania No. *28455* (1975).

CARACTERIZAREA POLIDISPERSITĂŢII MASELOR MOLECULARE LA POLISULFONE

(Rezumat)

S-au stabilit condiţiile optime de titrare turbidimetrică pentru obţinerea curbelor de distribuţie a maselor molare a unor polisulfone pe bază de bisfenol A. S-a utilizat sistemul solvent/nesolvent cloroform/alcool etilic, lucrându-se la o viteză de adăugare a nesolventului de 1,08 ml/min, concentraţia iniţială a polimerului în soluţie fiind de 0,06 g/dl. Pentru etalonarea metodei s-au utilizat fracţiuni cu masa molară medie numerică cuprinsă între 17 900 şi 180 000 g/mol. Metoda s-a utilizat atât pentru obţinerea curbelor de distribuţie pentru fracţiuni cu distribuţie îngustă, cât şi pentru o probă tehnică, polidispersă.

BULETINUL INSTITUTULUI POLITEHNIC DIN IAŞI
Tomul XLIII (XLVII), Fasc. 3–4, 1997
Secţia II
CHIMIE şi INGINERIE CHIMICĂ

D.C. 547.562; 621.384.4; 546-39

DETERMINATION OF THE REACTION PRODUCTS OF THE BISPHENOL-A PHOTODEGRADATION IN WATER BY ULTRAVIOLET CATALYSED OXIDATION WITH HYDROGEN PEROXIDE

BY

MARIANA NEAMŢU and I. SIMINICEANU

Model aqueous solutions containing 0.52 mmol L^{-1} bisphenol-A (BPA) and different doses of hydrogen peroxide, prepared from pure substances, have been irradiated with a UV low-pressure mercury lamp immersed in a batch cylindrical photoreactor, at constant temperature. A number of 160 samples have been analysed by HPLC in order to determine the concentrations of primary degradation products vs. irradiation time and initial H_2O_2 added. Three main primary products have been identified: phenol (PH), 1,4-dihydroxybenzene (DHB), and 1,4-benzoquinone (BQ). The anionic products were identified by high performance ion chromatography-exclusion (HPICE) with a Dionex system for a sample taken after 40 min. of irradiation in the presence of 0.2453 mmol L^{-1} H_2O_2. The main anions identified were oxalate, acetate, glycolate, formate, lactate, malate, and succinate. A material balance of total organic carbon (TOC) in solution, based on the concentrations measured after 40 min. irradiation with 0.2453 mmol L^{-1} H_2O_2, results in a mineralization degree of 80.6936%. Hence the process investigated can be applied as an effective procedure for water treatment. The investigations must be continued in order to elucidate the photodegradation mechanisms as well as to optimize the operating parameters.

1. Introduction

Many toxic and hazardous compounds are often present in water at low concentration levels, which can make their removal difficult and costly by conventional biological, physical and chemical wastewater treatment methods. Biological processes are used commonly to remove organic compounds from waste water but a large number of toxic compounds are only partially degraded by these processes. These toxic compounds have been called *biorefractory compounds*. Tertiary treatment processes, such as carbon adsorption, also have limitations in removing many toxic and biorefractory compounds. Activated carbon has very low adsorbtive capacity for certain polar aliphatic compounds and must be replaced or regenerated when its adsorbtive capacity is reached.

A newer method for treating hazardous and biorefractory organic wastes is the advanced oxidation process with hydrogen peroxide catalysed by ultraviolet light.

Although hydrogen peroxide has many advantages in UV catalysed oxidations, few studies of this oxidizing agent have been reported [1]. The combination of hydrogen peroxide and ultraviolet light has been applied mainly for acetates, organic acids, explosives and pesticides removal from water. In addition, H_2O_2 plus UV has been used to remove naturally present organics from tap water and boiler feed water.

Bisphenol-A (BPA) has been recently identified as environmental pollutant with estrogenic effects [2] and a controversial biodegradability [3]. Our results on the degradation of BPA in water by UV-activated hydrogen peroxide oxidation have been presented in a previous paper [4]. We have found that after only 20 min. of UV-254 nm irradiation in the presence of 0.4907 mmol L^{-1} H_2O_2 the conversion of BPA was over 98%. However, the almost complete destruction of the contaminant is only a necessary condition for the process application but not a sufficient one. The process is practically effective only if the final products are nontoxic compounds, mainly carbon dioxide and water. The aim of this study was to identify the reaction products formed in the photodegradation of BPA in water by UV-activated hydrogen peroxide.

2. Experimental

2.1. Materials

The aqueous BPA solutions of 0.52 mmol L^{-1} have been prepared with double distilled deionised water (conductivity 0.056 μS) and pure BPA supplied by Fluka AG. The mixture was stirred at 298 K for 48 hours, then passed thought a MN 640d filter. To aqueous solution, nearly saturated in BPA, hydrogen peroxide of 30% H_2O_2 from Merck has been added at three levels so that its initial molar concentration was of 0.245, 0.368, and 0.490 mmol L^{-1}, respectively.

2.2. Photolysis Procedure

The aqueous solutions, prepared as above, were irradiated with a UV low-pressure mercury lamp (Heraeus/Hanau) whose spectrum is rich in 254 nm line, immersed in a batch cylindrical photoreactor. The experimental equipment has been minutely described in a previous paper [5].

2.3. Analytical Methods

The concentration of BPA unconverted during irradiation, as well as the concentrations of the primary products (phenol (PH), 1,4-dihydroxylbenzen (DHB) and 1,4-benzoquinone (BQ)) were measured by HPLC analysis, using a Lichrosper RP-18 column of 4.6×250 mm. The mobile phase was of 50% acetonitrile and 50% water at flow rate of 0.8 mL min^{-1}. The injection volume was of 10 μL, at 311 K. The chromatograph was LC 1090 (Hewlett-Packard Co.) with a diode array detector (DAD) and a computer for data processing. The peaks were identified by the retention time and spectra matching.

The determination of anions, formed as secondary degradation products (oxalic, glycolic, lactic, acetic, formic, etc.) was performed with a Dionex high performance ion chromatography-exclusion (HPICE) system [6],...,[9]. The HPICE system has hydrophobic functional groups within the resin structure which promote adsorption and hydrogen bonding with steric repulsion effects [8]. These two additional retention mechanisms allow resolution of organic acids which are poorly solved by Donnan exclusion alone.

The separation was performed on an AS6 column (250×9 mm ID) packed with 8 μm particles of styrene/acrylate/divinylbenzene, with 8% cross-linking, working at 60°C. The eluent was a 0.4 mmol L^{-1} solution of heptafluorbutyric acid with a pH = 3.3 and a flow rate of 1 mL min^{-1}. A conductivity detector was used for the ion identification [5].

3. Results and Discussion

The 160 experimental runs representing the concentrations of the four primary compounds (BPA, PH, DHB and BQ) vs. irradiation time have been plotted for a given dose of hydrogen peroxide (Figs. 1,...,4), at constant temperature (298 K).

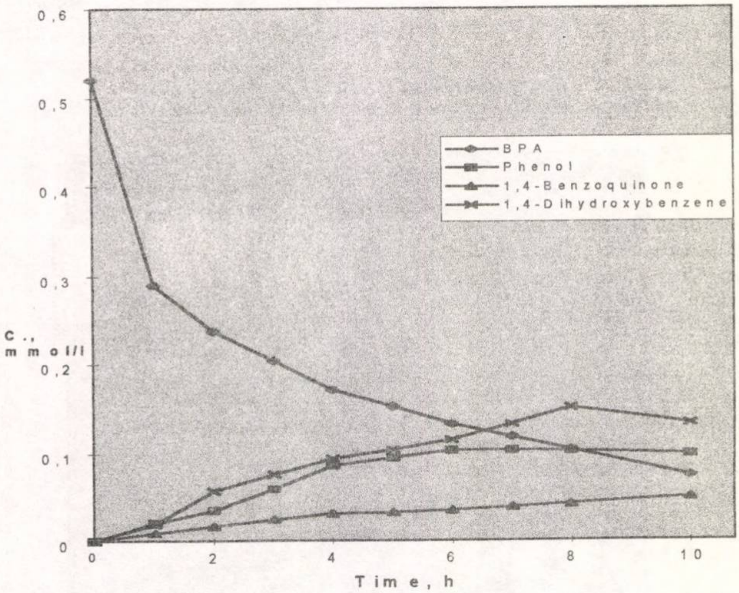

Fig. 1.- Photodegradation of BPA with UV only, at 298 K.

The anionic products, formed at the BPA photodegradation with UV and 0.245 mmol L^{-1} H_2O_2, irradiated for 40 min. have been identified by means of the chromatogram presented in Fig. 5.

The retention times (t_R) and the concentration of the identified acids are given in Table 1.

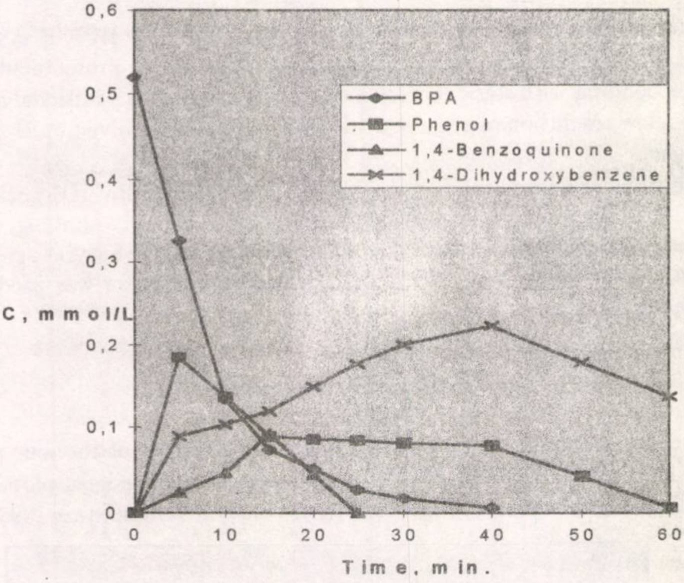

Fig. 2.- Photodegradation of BPA with UV-activated hydrogen peroxide at 298 K and 0.2453 mmol L^{-1} H_2O_2.

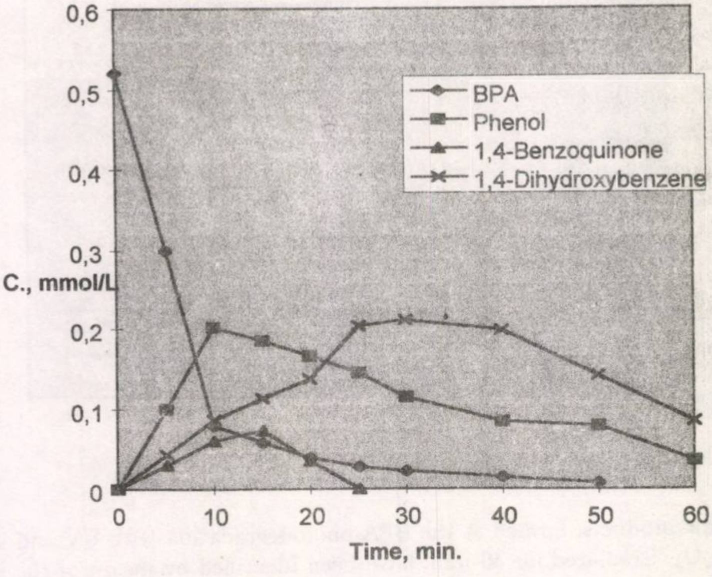

Fig. 3.- Photodegradation of BPA with UV-activated hydrogen peroxide at 298 K and 0.368 mmol L^{-1} H_2O_2.

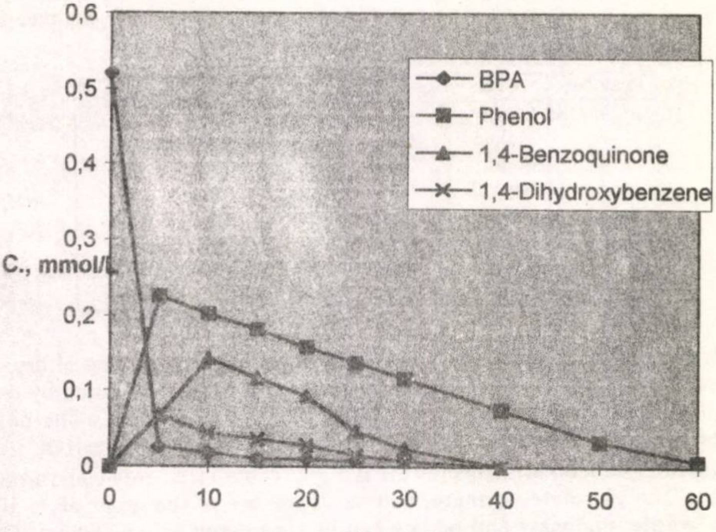

Fig. 4.– Photodegradation of BPA with UV-activated hydrogen peroxide at 298 K and 0.4907 mmol L^{-1} H_2O_2.

By comparing the kinetic curves in Fig. 1 to those in Figs. 2,...,4 the synergetic effects of H_2O_2 plus UV light on the degradation of BPA in water must be noticed. It is also easy to observe that the decomposition degree is grown by increasing the initial hydrogen peroxide concentration. Almost complete degradation (98.13%) was

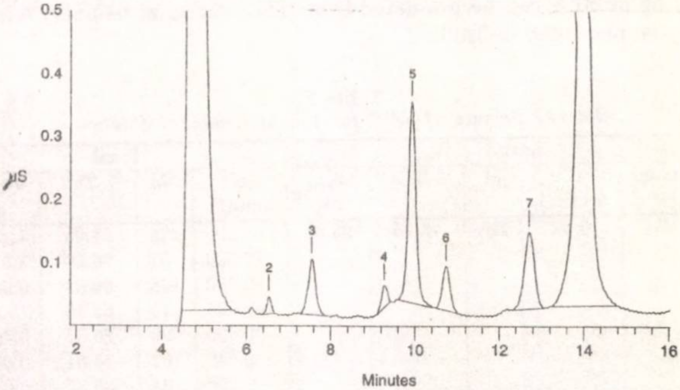

Fig. 5.– Conductivity chromatogram: decomposition of BPA with UV plus 0.2453 mmol L^{-1} H_2O_2, 40 min. irradiation time (for identification of peaks, s. Table 1).

attained after 20 min. irradiation with an initial H_2O_2 concentration of 0.4907 mmol L^{-1} for the aqueous solution of 0.52 mmol L^{-1} BPA. The three primary products of degradation (PH, DHB and BQ) have a maximum of concentration which shifts to shorter time by increasing the initial dose of hydrogen peroxide. The phenol (PH)

Table 1
HPICE Results: Identified Anions, Retention Times and Concentrations

Peak No.	Anion	t_R, [min]	Concentration, [μmol L^{-1}]
1	Oxalic	4.72	20.43
2	Malonic	6.53	0.0492
3	Malic	7.55	0.336
4	Glycolic	9.27	1.100
5	Formic	9.93	1.300
6	Lactic	10.73	0.745
7	Succinic	12.72	1.200
8	Acetic	13.98	24.100

is the first that reaches its maximum. This shows that the first step of degradation is the decomposition of BPA to PH and C_1-C_3 acid fragments, formed by oxidation with hydroxyl radicals generated in the H_2O_2 photolysis reaction. The next steps are the oxidation of PH to DHB followed by the equilibrium DHB⇔HQ.

The anionic products, identified by HPICE (s. Table 1), mainly consist of acetate and oxalate. The glycolate, formate, and succinate are of the order of 1×10^{-6} mol L^{-1} whilst lactate, malonate and malate can be considered only as traces. Our data on anionic products, obtained at fixed time, are not sufficient for the elucidation of the photodegradation mechanisms. In fact, this was not the main goal of our work. Nevertheless, at least qualitatively, the anions that we have found correspond to those identified in the photodegradation of phenol [6]. By analogy with PH degradation we may further assume that the oxalate and acetate fragments are rapidly oxidated to formate and finally to carbon dioxide [7]. Therefore, for practical purposes, we consider the degree of mineralization of the total organic carbon (TOC) as the most important effectiveness criterion of the degradation process. The degree of mineralization of BPA can be evaluated from TOC material balance, based on our measurements, presented in Table 2.

Table 2
Material Balance of TOC for 1 L of Irradiated Solution

	Initial				Final			
Compound	C^0 mmol/L	M	% TOC	m^0_{TOC} mg	C μmol/L	M	% TOC	m_{TOC} mg
BPA	0.52	228	78.95	93.60	6.200	228	78.95	1.116
PH					77.000	94	76.59	5.543
BQ					0.000	108	66.67	0.000
DHB					142.000	110	65.45	10.223
Oxalic					20.430	90	26.67	0.490
Malonic					0.049	104	34.61	0.0018
Malic					0.336	134	35.82	0.016
Glycolic					1.100	76	31.58	0.0026
Formic					1.300	46	26.09	0.0156
Lactic					0.745	90	40.00	0.0268
Succinic					1.200	118	40.68	0.0576
Acetic					24.100	60	40.00	0.05784
Total Organic Carbon				93.60				18.0708

The data in Table 2 show that from initial 93.6 mg TOC in BPA after 40 min. of UV irradiation in the presence of 0.2453 mmol L^{-1} H_2O_2 only 18.0708 mg TOC remained. The rest has been mineralized (volatilized, as CO_2). This corresponds to a mineralization degree of 80.6936%. With a greater concentration of hydrogen peroxide the mineralization will be, obviously, enhanced.

4. Conclusions

In order to estimate the effectiveness of the water treatment by the UV/H_2O_2 oxidative process, investigations have been made concerning the degradation rates and degradation products of BPA aqueous model solution. The unconverted BPA, as well as the primary degradation products (PH, DHB and BQ) have been determined by the HPLC method. The anionic products were identified by the HPICE method. A material balance of the total organic carbon (TOC) in solution, based on our measured concentrations for 40 min. irradiation in the presence of 0.2453 mmol L^{-1} H_2O_2, leads to a mineralization degree of 80.6936%. In these conditions the residual TOC mainly consists of DHB (56.57%), phenol (30.67%), and unconverted BPA (6.17%). The anionic products have lower shares in TOC: acetic (3.2%), oxalic (2.71%), succinic (0.32%), lactic (0.148%), glycolic (0.014%), malic (0.09%), formic (0.09%), malonic (0.01%). With an increased concentration of hydrogen peroxide the degree of mineralization expected will be much greater. Hence oxidative treatment with UV/H_2O_2 results in an effective detoxification of polluted water.

Acknowledgements. This research, performed in the IOC laboratories directed by Professor A. Kettrup, has been financially supported by a grant from the German Academic Exchange Service – DAAD.

Notations

C^0, C – initial and final concentration, [mmol L^{-1}];
M – molar weight, [kg $kmol^{-1}$];
m_{TOC} – mass of total organic carbon, [mg].

Received, February 3, 1997

State University of Moldova, Kishinew
and
Technical University "Gh. Asachi", Jassy,
Department of Inorganic
Chemical Technology

REFERENCES

1. Legrini O., Oliveros E., Braum A.M., Chem. Rev., **93**, 671 (1993).
2. Safe H.S., Environmental Health Perspectives, **103**, *4*, 347 (1995).
3. Dorn B.P., Chou C.S., Gentempo J.J., Chemospere, **16**, 1501 (1987).
4. Siminiceanu I., Neamţu M., Bul. Inst. polit., Iaşi (submitted).
5. Neamţu M., Siminiceanu I., Rev. Chim., **48** (1997) (in print).
6. Scheck K.C., Frimmel H.F., Wat. Res., **29**, 2346 (1995).
7. Scheur Cl. *et al.*, J. of Chromatography A, **706**, 253 (1995).
8. Weiss J., *Ionenchromatographie.* VCH, Wenheim, 1991, 215.
9. Neamţu M., Siminiceanu I., An. Şt. Univ. „Al. I. Cuza", Iaşi, **4**, s. Chim., 177 (1996).

DETERMINAREA PRODUŞILOR DE REACŢIE LA FOTODEGRADAREA BISFENOLULUI-A DIN APĂ PRIN PROCEDEUL UV-PEROXID DE HIDROGEN

(Rezumat)

Soluţii model cu 0.52 mmol L^{-1} bisfenol-A (BPA) şi diferite doze de peroxid de hidrogen, preparate din substanţe pure, au fost iradiate cu o lampă UV cu mercur la joasă presiune, imersată intr-un fotoreactor discontinuu cu amestecare perfectă, de formă cilindrică, la temperatură constantă (298 K). Cele 160 probe de soluţie au fost analizate cromatografic (HPLC) pentru a determina concentraţia produşilor primari ai fotodegradării în funcţie de timpul de iradiere şi doza de H_2O_2. Pe lângă BPA netransformat au fost identificaţi trei produşi primari: fenolul (PH), 1,4-dihidrobenzenul (DHB) şi 1,4-benzochinona (BQ). Produşii anionici au fost identificaţi prin ion-cromatografie de înaltă performanţă (HPICE), pe un sistem DIONEX, pentru probe luate la intervale de 40 min. în prezenţa unei doze iniţiale de 0,2453 mmol L^{-1} H_2O_2. Principalii acizi identificaţi au fost: oxalic, acetic, glicolic, formic, lactic, malic şi succinic. Pe baza acestor rezultate se poate schiţa un mecanism al procesului de fotodegradare începând cu etapa de formare a fenolului din bisfenol până la oxidarea finală a acidului formic la dioxid de carbon şi apă. Deoarece în practica purificării apei conţinutul de carbon organic (TOC) este un indicator esenţial, s-a efectuat un bilanţ de masă al TOC din apă, pe baza concentraţiilor măsurate prin HPLC şi HPICE. S-a găsit că, după 40 min. iradiere cu 0,2453 mmol L^{-1} H_2O_2, din 93,6 mg carbon conţinut într-un litru de apă sub formă de bisfenol-A au mai rămas doar 18,07 mg carbon organic. Restul (80,69%) s-a mineralizat sub formă de dioxid de carbon care intră în circuitul natural al carbonului. Această constatare arată că procesul studiat, cu unele perfecţionări, poate sta la baza unui procedeu eficace de tratare a apelor poluate cu substanţe organice periculoase.

BULETINUL INSTITUTULUI POLITEHNIC DIN IAŞI
Tomul XLIII (XLVII), Fasc. 3–4, 1997
Secţia II
CHIMIE şi INGINERIE CHIMICĂ

D.C. 620.193.28

UNCONVENTIONAL METHODS USED FOR CORROSION RATE OF METALLIC SYSTEMS MEASUREMENT

BY

***GEORGETA MATZA, ŞT. IVĂŞCAN, **LUCIAN GAVRILĂ,**
***DANIELA GAVRILĂ and N. APOSTOLESCU**

The results of corrosion rate measurements performed on the lining made in W1.4435.2 stainless steel of the synthesis reactor from a Stripping – Stamicarbon urea plant are presented. The ultrasonic measurements pointed out that corrosion rate is greater at the reactor bottom, where thermal and hydrodynamic conditions are more toughly. Reactor lining is more attacked than the afferent plates, due to the supplementary errosion that occurs more conspicuous in the peripherical areas.

The measured corrosion rate was not constant; there were maximal values corresponding with the periods when plant operation has not been performed in the most proper way.

1. Introduction

The main purpose of corrosion control in chemical industry processes is to ensure a continuous manufacturing of the products without accidentally shut-downs, causing damages of equipments because the corrosion actions of the chemicals involved in the process. Production and benefits are closely linked to the economical selection of materials, to the corrosion control measurements and to the availability of production equipments.

The conventional methods used for the corrosion rate measurements may be classified in: gravimetric, volumetric, physical, electrochemical and chemical methods. All these methods are widely used in laboratories. Because into an industrial plant the corrosion intensity is influenced by a wide range of factors: environment composition, temperature, pressure, hydrodynamic conditions, etc., the corrosion rate may be accelerated by changings in manufacturing technology or by modifying the output of the plant, making it greater or less than the designed output. Hence, it results that a periodical measurement of the corrosion rate would be advantageous for preventing the premature failure of equipments and installations. Also, the monitoring of corrosion rate allows a right estimation of the influence of technological decisions on the corrosion induced damages.

The corrosion rate measurement methods used in industrial plants are faster than the laboratory ones, and they include undestructive methods, also called *unconventional methods.* Their main advantage is that measurements can be performed directly on the equipments that work in corrosive environments, being needless to gather up material samples from equipments.

By these methods, internal and/or external discontinuities of the metallic framework, generated by corrosion processes, may be detected. There are also limits in applying undestructive methods, mainly due the shape and dimensions of parts, the nature and orientation of faults, accesibility of tested surfaces, as well as the nature of the construction material. For best efficiency in evidencing faults, the use of different undestructive testing methods at the same time is recommended [1].

Among undestructive testing methods we can count: the visual examination, penetrant liquids techniques, magnetic powders techniques, penetrant radiation techniques and ultrasonic techniques.

2. Experimental

Corrosion rate measurements using undestructive ultrasonic techniques were performed on the protective lining of an urea synthesis reactor from a Stripping – Stamicarbon urea plant located at S.C. SOFERT S.A., Bacău, a major Romanian fertilizers producer.

As protective material for the reactor, an austenitic stainless steel AISI 316L Urea Grade (W1.4435.2) made by SANDVIK INTERNATIONAL AB (Sweden), is used. The chemical composition of the steel is presented in Table 1 [2].

Table 1
Chemical Composition of AISI 316L U.G. Stainless Steel

Component	Mass percent
Carbon*)	0.020
Silicon	0.400
Manganese	1.700
Phosphorum*)	0.015
Sulphur*)	0.010
Chromium	17.500
Nickel	14.000
Molybdenum	2.600
Iron	balance

*) maximal values.

The synthesis reactor shown in Fig. 1 has a 165 m^3 capacity, a height of 25 m and an inner diameter of 2.87 m. It is designed for temperatures up to 456 K and pressures up to 15.9 MPa.

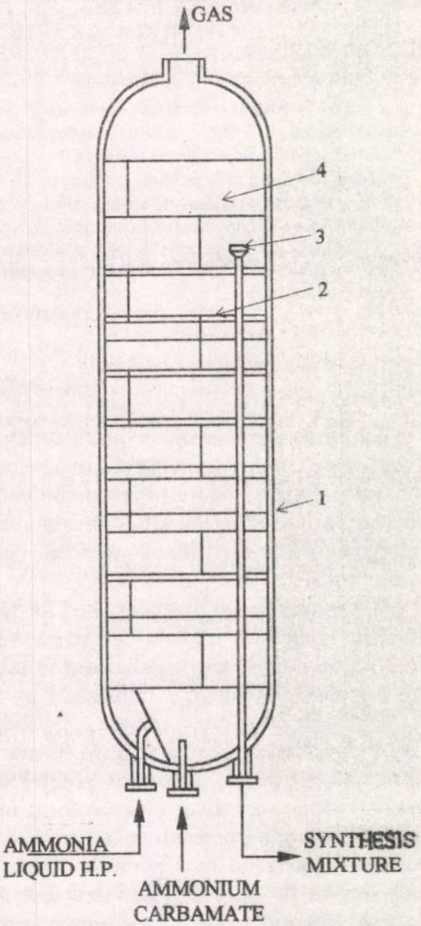

Fig. 1.– Stripping – Stamicarbon urea synthesis reactor: *1* – body; *2* – plates; *3* – overflow; *4* – anticorrosive protection rolled sheets.

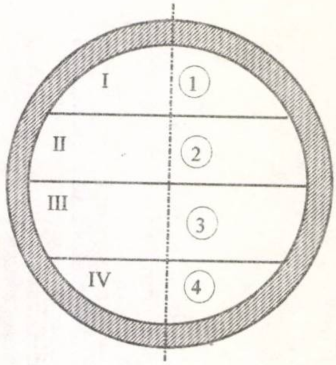

Fig. 2.– Orifice plate from the urea systhesis reactor.

The reactor is equipped with ten internal perforated plates (with plate no. 1 at the lower part of the reactor) placed at 1.76 m one from another. The plates are made from 316L U.G. stainless steel with an initial thickness of 6 mm. Each plate consists of four segments as shown in Fig. 2.

The reactor body is protected against corrosion with AISI 316L U.G. stainless steel rolled sheets, with an initial thickness of 12 mm. The cylindrical part of the reactor is plated with ten rolled sheets (with no. 1 sheet at the lower part), each having 2.5 m height. The upper and lower semispherical bottoms of the reactor are also plated in AISI 316L U.G., with the initial lining thickness of 12 mm.

The urea plant was started up in 1980 and the first thickness measurements of the anticorrosive lining were done in 1985 and after that, yearly. Thickness measurements were performed for plates, rolled sheets and lower bottom, using a digital ultrasonic device equipped with double crystal sensing device (emission – reception) with a 4 MHz frequency. The measurement points were located as follows: i) on the reactor rolled sheets, at the middle of each one, in four points; ii) on the reactor plates, at the middle of each plate segment (points *1,...,4* according to Fig. 2); iii) on the lower bottom of the reactor, on each petal at 100 mm left and right from the welding seams.

Dividing the thickness difference measured in two consecutively years by the time elapsed between measurements, the corrosion rate, expressed as the penetration index p, [mm/year], is obtained. Also, an average penetration index, p_{med}, may be estimated with the expression:

$$p_{\text{med}} = \frac{d^0 - d}{t}, \quad [\text{mm/year}],$$

where d^0 denotes the initial thickness of the metallic material, [mm], d – the actual thickness ultrasonic measured, [mm], and t – the operating time, [years], of the material in the corrosive environment.

3. Results and Discussions

The values of the yearly performed thickness measurements are presented in Figs. 3 and 4, for the reactor rolled sheets and plates respectively. Time variation of the penetration index for the reactor lower bottom is represented in Fig. 5.

As shown in Figs. 3 and 4, the thickness decrease is not uniform neither in time, neither on the reactor height. Measurements performed at the lower bottom reveal that there are areas with accentuated attacks and the corrosion attack is nonuniform, as shown in Fig. 5.

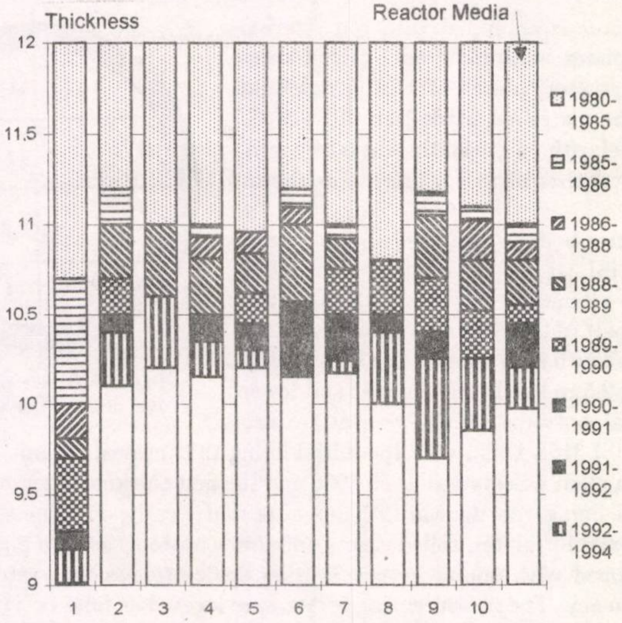

Fig. 3.- Thickness decreasing of the reactor rolled sheets between 1980–1994.

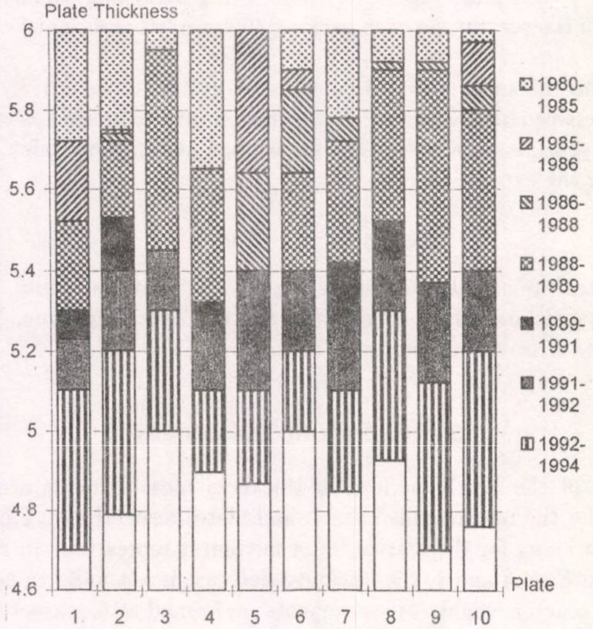

Fig. 4.- Thickness decreasing of the reactor plates between 1980–1994.

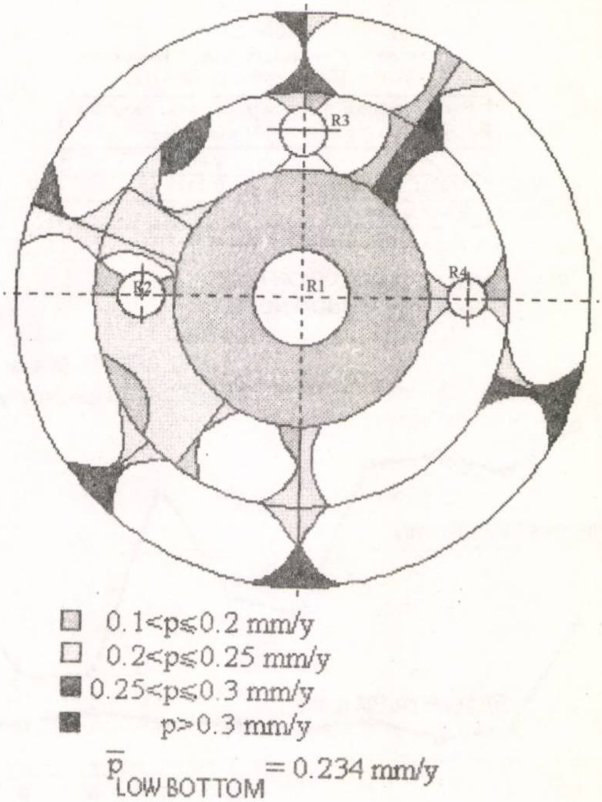

Fig. 5.- Variation of average penetration index on the protection lining of the lower bottom of the urea synthesis reactor between 1980–1994.

The average penetration index values for plates, rolled sheets and lower bottom are shown in Table 2. Comparing the values from Table 2 with the maximal penetration index of 0.6 mm/year allowed for 316L U.G. stainless steels by STAMICARBON B.V. (The Netherlands) – the licensor of the urea plant – for ammonium carbamate – urea environments [3] it is observed that all the corrosion rates are beyond this limit.

The variation of the average penetration index on the height of the reactor, for plates and rolled sheets, is shown in Fig. 6.

An advanced corrosion rate presents the lower part of the reactor (the lower bottom, plate no. 1, sheet no. 1). This could be explained taking into account that in this area the thermal stresses are greater, here occurring the ammonium carbamate synthesis, a strongly exothermal reaction according to equation [4]:

$$2NH_{3\ (g)} + CO_{2\ (g)} = NH_2COONH_4$$

$$\Delta H = -100.5\ \mathrm{kJ/mol}\ \text{(at 14 MPa and 440 K)}$$

Table 2
Average Penetration Index Values in the Urea Synthesis Reactor

Part of reactor	Average penetration index mm/year
plates	0.0651
rolled sheets	0.1477
lower bottom	0.2015

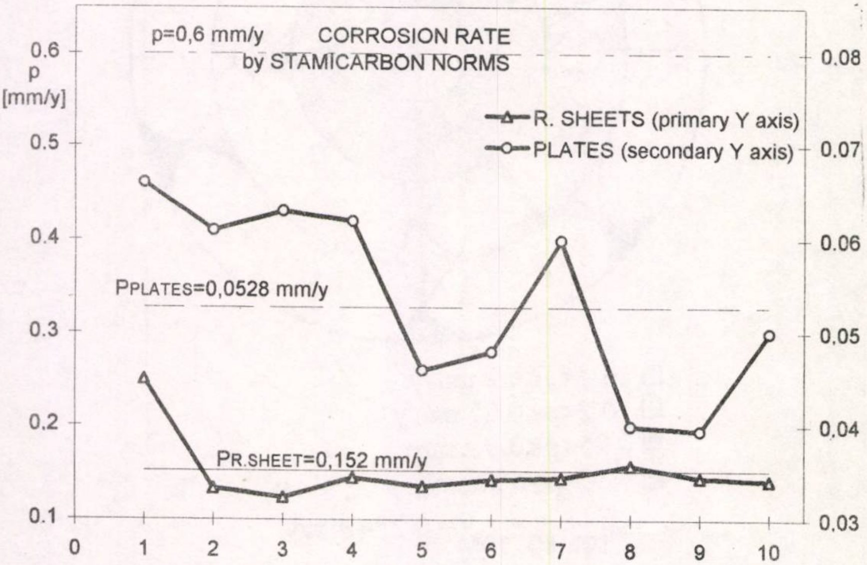

Fig. 6.- Variation of average penetration index on the height of the urea synthesis reactor.

Hydrodynamical conditions are also tougher in this zone of intensive mixing of the reaction mass.

It seems to be apparently unaccountable the different corrosion rates of plates 2 to 10 comparing to the corresponding rolled sheets. An in-depth analyse of the corrosion effects shows that corrosion rates are greater at the peripherical areas of the plates than in their central area. This could be explained taking into account that over the corrosion effects produced by environment composition, temperature and pressure, are overlapped the errosion and abrasion processes, that are acting mainly at walls, where friction forces are more powerful. We can also mention that the sheets are affected by radial forces generated by the internal pressure from the reactor, that may multiply the errosion and the abrasion. On the contrary, the pressure that acts on plates is equally distributed on their both faces, so that the forces acting axially on the plates are reciprocally annulated. In fact, from design, the plates thickness was established at 6 mm, comparatively with 10 mm, the design value of the reactor lining thickness.

Fig. 7 represents the time variation of the yearly corrosion rate for rolled sheets, plates and the bottom of the urea synthesis reactor. Analysing these variations it was observed that corrosion rate varied, with maximal tendencies in 1988–89 for rolled sheets and reactor bottom, respectively in 1989–90 for the plates.

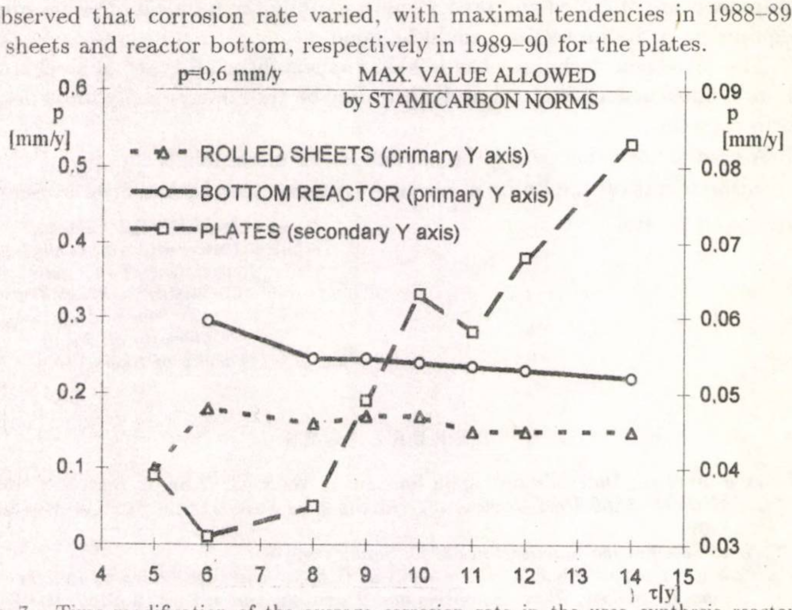

Fig. 7.– Time modification of the average corrosion rate in the urea synthesis reactor.

The growth of the annual corrosion rate denotes an unappropriate operation of the urea plant for the considered periods: an oxygen concentration in the reaction mass uncorrelated with plant loading (oxygen in small concentrations serves as corrosion inhibitor), plant operation below the minimal designed capacity, frequently shut downs and restarts, operation in transient systems, far away from optimal values of operating parameters. An unappropriate operation of the plant leads to the shortening of the equipments life span, the corrosion processes being accelerated.

4. Conclusions

1° Comparatively with other undestructive testing methods used as unconventional methods for corrosion studies, the ultrasonic technique provides quantitative informations, allowing to establish the corrosion rate of metallic materials expressed as the penetration index.

2° The ultrasonic technique is able to build corrosion curves in the coordinates corrosion rate – time, based on directly measured values, more accurate than the ones obtained by classical measurements. By interpreting the corrosion curves, the behaviour of different metallic systems in corrosive environments may be estimated.

3° The method is able to outline the abrasion and errosion processes that may occur at the metal/environment interface.

4° Corrosion monitoring by ultrasonic techniques gives useful informations regarding plants operation in a definite time period. Informations concerning life span of equipments are obtained and predictions regarding the moment of replacement (of the equipment or its protection) could be done.

5° The ultrasonic technique has a wide applicability: all types of steels (carbon steel, mild alloyed steel, high alloyed steel) may be tested, especially for general and uniform corrosion.

6° A case history concerning the application of ultrasonic technique in corrosion rate measurements on the lining of an urea synthesis reactor has been presented.

Received, April 18, 1995

**SOFERT S.A., Bacău,
Technical University "Gh.Asachi", Jassy,
Department of Inorganic
Chemistry Technology
and
**University of Bacău,
Faculty of Engineering*

REFERENCES

1. Voicu S. *et al.*, ***Materials Testing*** (in Romanian). Vol.**3**, Ed. Tehnică, Bucharest, 1986.
2. * * * *SANDVIK 3R60 Urea Grade-Austenitic Stainless Steel.* 51.843, Sandvik AB, February 1987.
3. * * * *Urea Specification Stamicarbon 53930, Stamicarbon BV.*
4. Kaasenbrood P.K.C., Chermin H.A.G., *The Urea Stripping Process - Stripping Technology, Phase Equilibria and Thermodynamics.* Proc. no. *166*, The Fertilizer Society, London, 1977.

METODE NECONVENŢIONALE UTILIZATE PENTRU MĂSURAREA VITEZEI DE COROZIUNE A SISTEMELOR METALICE

(Rezumat)

Se prezintă rezultatele obţinute la măsurarea vitezei de coroziune a placajului anticoroziv din oţel austenitic W1.4435.2 al unui reactor de sinteză a ureei dintr-o instalaţie de uree de tip Stripping–Stamicarbon.

Viteza de coroziune s-a determinat din pierderile de grosime ale materialului de protecţie, măsurate ultrasonic. Măsurătorile au relevat că viteza de coroziune este mai mare la partea inferioară a reactorului, acolo unde şi condiţiile termice şi hidrodinamice sunt mai severe. Virolele reactorului sunt atacate mai puternic decât talerele corespunzătoare, datorită unor fenomene suplimentare de eroziune şi abraziune. În timp, viteza de coroziune a fost maximă în perioada 1988-1990, perioadă în care instalaţia de uree a fost exploatată în mod necorespunzător.

BULETINUL INSTITUTULUI POLITEHNIC DIN IAŞI
Tomul XLIII (XLVII), Fasc. 3–4, 1997
Secţia II
CHIMIE şi INGINERIE CHIMICĂ

D.C. 661.522

ON AMMONIUM SULFATE MANUFACTURE

I. OPERATING PARAMETERS OF THE TECHNOLOGICAL PROCESS

BY

AL. SZÉP, CAROLINA HAGIU and GH. MIHĂILĂ

The results of a quantitative and qualitative analyses of the ammonium sulfate manufacture by neutralization of 70...94% content sulfuric acid with different ammonia sources, like ammonia water and gaseous ammonia with variable concentration are presented. Simultaneous solving of mass and thermal balances models of the auto-thermal ammonium sulfate manufacturing process allowed the determination of the sulfuric acid concentration and the temperature of recycled solution influence upon the recycling number. Imposing the equilibrium concentrations of the solutions in complete recycling cycle and the amount of removed water in an auto-thermal process was established the technological parameters and performance indicators of the cyclic process, respectively: the recycling number of mother liquor, with at least 323 K temperature, between 5...7; concentration of sulfuric acid solution between 70...94% and the transformation degree in water vaporization and sulfate crystallization processes about 100%.

1. Introduction

The technical or agricultural grade ammonium sulfate can be manufactured by both neutralization of different ammonia sources such as ammonia waters, gases with variable content of ammonia and synthetic ammonia from the Haber process with solution of sulfuric acid or hydrogen ammonium sulfate and procedures of double exchange [1]. The actual technologies especially apply the neutralization procedure, using technical grade sulfuric acid or different waste acids and ammonia or ammonia waters.

To implement a manufacturing technology into an existent plant the following steps are necessary to perform: a) definition of the quality and quantity of the requested products; b) definition of the nature of the possible raw material to be used; c) choice of the operating parameters; d) chemical engineering analysis of the component processes; e) design of the technological process; f) elaboration and solving of the mathematical models in order to define the real operating parameters.

All the above stages do not necessitate to operate only with a series of quantifiable scientific and technical information but also with many others, difficult to be quantified, that represent in fact the obtained experience of the designer along his activity. Taking into account the typical steps requested by the synthesis of technological process [2] and mathematical models of mass and heat balance [3], in what follows are presented the results of theoretical analysis in the stage of a technology design for ammonia sulfate manufacture by neutralization of sulfuric acids with ammonia in a plant during retroset.

2. The Block Diagram of the Process

Manufacture of the technical or agricultural grade ammonium sulfate can be described by the acid–base reaction:

$$\begin{aligned} &[H_2SO_4 + H_2O + A_1'']_l + [NH_3 + H_2O + A_2'']_{fl} \longrightarrow [A_2'' + H_2O]_{fl} + \\ &\qquad + [(NH_4)_2SO_4]_s + [(NH_4)_2SO_4 + H_2O + A_1'']_l \end{aligned} \tag{1}$$

and stoichiometric equations:

$$(2)\quad 2NH_{3aq} + H_2SO_{4aq} = (NH_4)_2SO_{4aq} \qquad (3)\quad (NH_4)_2SO_{4aq} \rightleftharpoons (NH_4)_2SO_{4[]s}$$

Depending on the quality of fluid phase (fl), the reaction (2) can be preceded by the ammonia dissolution, namely the elementary process:

$$NH_{3[]g} \rightleftharpoons NH_{3[]l} \tag{2'}$$

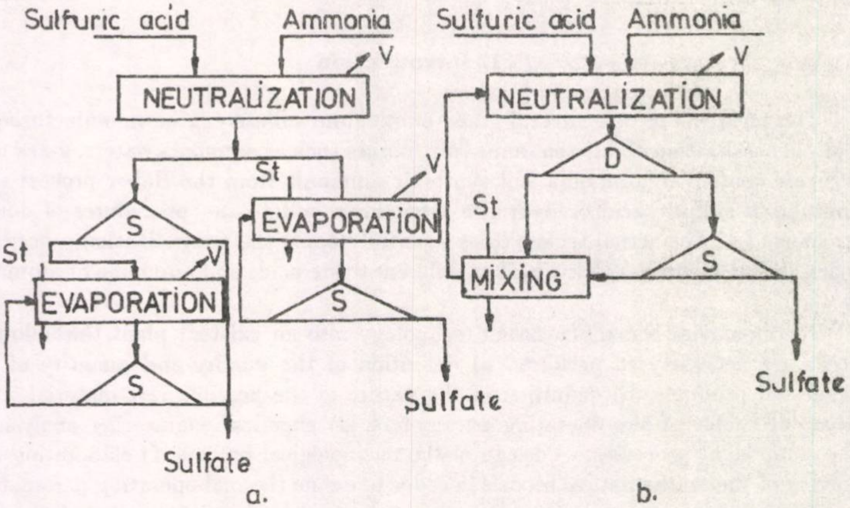
Sulfuric acid
Ammonia
V
NEUTRALIZATION
St
V
S
EVAPORATION
St
V
EVAPORATION
S
S
Sulfate
Sulfate
a.
Sulfuric acid
Ammonia
V
NEUTRALIZATION
D
St
S
MIXING
Sulfate
b.

Fig. 1.– The block diagram of the ammonium sulfate manufacture:
a - process with evaporation; *b* - autothermic cyclic process.

Also depending on the composition of the reactant phases and thermal conditions, neutralization can be accompanied by water vaporization and/or ammonium sulfate crystallization. Depending on the manner in which the water entered by the reactant phases is removed, two block diagram can be imagined. In the block diagram represented in Fig.1 *a*, the water entered with the two phases is eliminated not only autothermally but also by evaporation from the ammonium sulfate solution. The ammonium sulfate can be separated by isotherm or adiabatic crystallization.

In Fig.1 *b* the reaction heat is utilized as energy source for water removal. The ammonium sulfate generated in the neutralization step is removed from solution, as a crystalline form, in both neutralization and suspension cooling. In this variant, the external heat source is not employed, the caloric excess of the system being eliminated as warm water.

Adoption of one of these variant is conditioned by a series of factors such as: the nature and quality of ammonia and sulfate sources, the energetic availability and, not in the last turn, the technological endowment of the plant under retroset.

3. Analysis of the Neutralization Process

The neutralization process, presented in both variants, can be achieved, depending on the nature and quality of ammonia source, either as a process of the molecular mixing with/or without simultaneous crystallization of ammonia sulfate. If the elementary process preceding the neutralization is defined at the same time with choice of ammonia source, the nature of the elementary process that succeed the neutralization is difficult to estimate. To define the nature of elementary process that follows neutralization, a thermodynamic and thermal study of the process has been performed.

In the thermodynamic study of compounds stability, the real system was simplified at only two ternary systems, i.e. H_2SO_4–NH_3–H_2O and $(NH_4)_2SO_4$–H_2SO_4–H_2O. Taking into account that neutralization is a total reaction, it can be represented on a ternary diagram by a reaction line [4]. Thus, in the diagram plotted in Fig. 2, there are represented by P_0, the sulfuric acid solution and by P_i, the gaseous or liquid water ammonia mixtures.

The reaction lines, drawn through the limit points of the saturated equilibrium curves in ammonium sulfate at different temperatures, P_0P_i, mark two domains of the binary NH_3-H_2O mixtures. In the first domain, under lines, the ammonium sulfate does not crystallize because the ammonia content is not enough so that the reaction lines to intersect that of the ammonium sulfate separation domain. In the second case the high ammonia content makes possible the separation of solid phase simultaneously with the neutralization. Knowing the high value of the thermal effect of neutralization process (227.38 kJ/mol), is necessary to be elucidated the conditions under which the energy taken over by evaporated water does not induce the sulfate crystallization and, if does, in what amount. For this reason, we have performed a discussion by means of mathematical mass and heat balance models of the adiabatic neutralization:

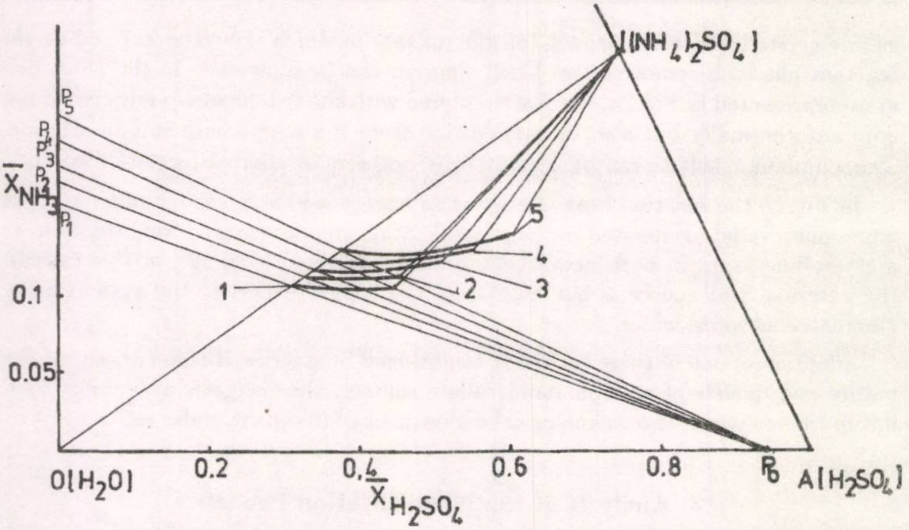

Fig. 2.– Representation of the limit reaction lines in the process of sulfuric acid neutralization with ammonia for the NH_3–H_2SO_4–H_2O ternary system at different temperatures: *1* – 283; *2* – 303; *3* – 323; *4* – 343; *5* – 363 K.

$$\begin{aligned} &m_l^0 Cp_l^0(T_l^0-273) + \tfrac{34 m_l^0 X^0 Cp^0 (T_{\mathrm{Am}}^0-273)}{98 X_{\mathrm{Am}}^0} + \tfrac{m_l^0 X^0 \Delta_R H_T^0}{0.098} = m_l Cp_l(T_l-273) + \\ &+ m_{\mathrm{ev}} I_{\mathrm{H_2O}} + m_G Cp_G(T_f-273) + m_l \tfrac{X_{\mathrm{TSU}}-X_{\mathrm{SU}}}{1-X_{\mathrm{TSU}}}\left[\tfrac{-\Delta H_{\mathrm{Cr}}}{0.132} + Cp_{\mathrm{SU}}(T_f-273)\right], \end{aligned} \tag{4}$$

where:

$$X_{\mathrm{TSU}} = \frac{m_l^0 X^0 M_{\mathrm{SU}}}{M_{\mathrm{H_2SO_4}}(m_l+m_S)},$$

$$X_{\mathrm{SU}} = 0.3173 - 7.41\times10^{-5} T_f + 1.545\times10^{-6} T_f^2, \tag{5}$$

$$m_l = m_l^0 \frac{1 - X^0 + \frac{34}{98} X^0 (1 - X_{\mathrm{Am}}^0)}{1 - X_{\mathrm{SU}}} + \frac{m_{\mathrm{ev}}}{1 - X_{\mathrm{SU}}}$$

for ammonia waters, and

$$m_l = \frac{m_l^0(1 - X^0) - m_{\mathrm{ev}}}{1 - X_{\mathrm{SU}}}$$

for gases with different ammonia content.

The model was solved for the case when using a sulfuric acid solution over 70% H_2SO_4 and different ammonia sources, finding that:

a) when ammonia waters with over 20% NH_3 were used, the water evaporation and sulfate crystallization do accompany the neutralization;

b) when gases with under 13% NH_3 were used, the present inert ensures the neutralization heat elimination, the reaction being accompanied by sulfate crystallization;

c) if the ammonia content in gases is higher than 13%, the neutralization is accompanied by water evaporation and sulfate crystallization.

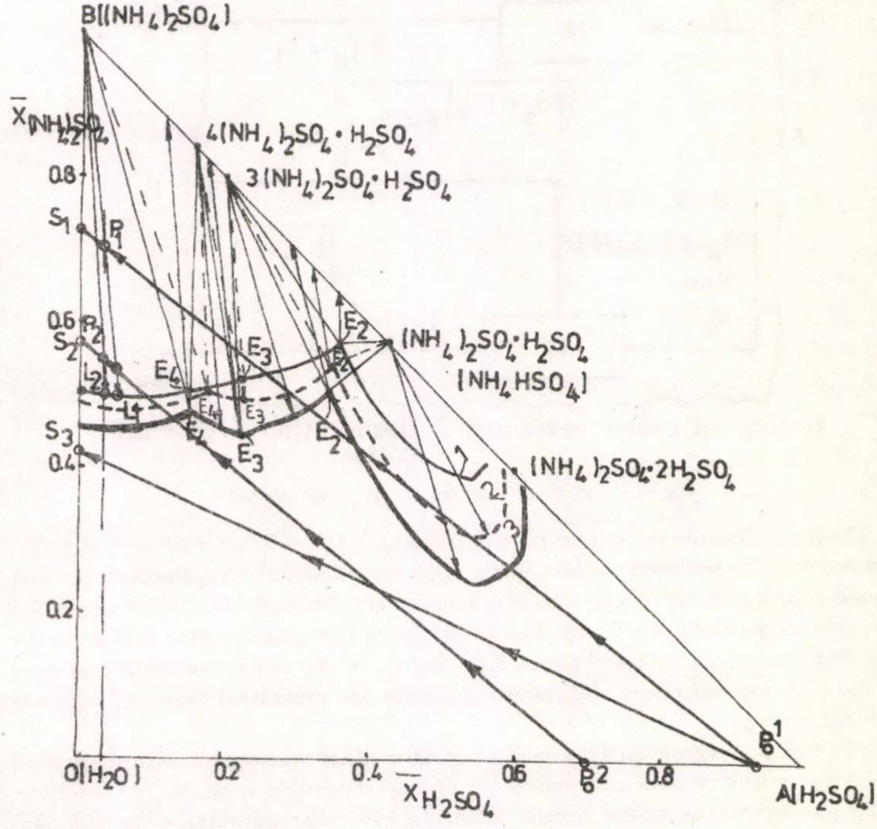
B[(NH4)2SO4]
$\bar{x}_{(NH_4)_2SO_4}$
4(NH4)2SO4 · H2SO4
3(NH4)2SO4 · H2SO4
0.8
S1
P1
0.6
P2
S2
L2
E4
E3
E2
(NH4)2SO4 · H2SO4
(NH4HSO4)
L1
S3
0.4
(NH4)2SO4 · 2H2SO4
2
3
0.2
O(H2O)
0.2
0.4
$\bar{x}_{H_2SO_4}$
0.6
P0 2
0.8
P0 1
A(H2SO4)

Fig. 3.- Representation of the neutralization process of sulfuric acid with ammonia in the $(NH_4)_2SO_4$–H_2SO_4–H_2O ternary system at different temperatures: *1* - 363; *2* - 343; *3* - 323 K.

Analyzing the equilibrium in the OAF triangle of the H_2SO_4–$(NH_4)_2SO_4$–H_2O ternary system (Fig. 3) one finds that at higher concentrations of sulfuric acid, the reaction lines $P_{0i}S_i$ intersect the domains of some compounds such as NH_4HSO_4, $3[(NH_4)_2SO_4].H_2O$, $4[(NH_4)_2SO_4].H_2SO_4$, compounds that fix an appreciated amount of reactant under solid form.

Elimination of the possibility to diminish the utilization degree of sulfuric acid and, implicitly, the contamination of the separated solid, imply the avoidance of the initial concentrations that generate the reaction lines without intersecting the respective domains. This condition can be easily achieved by dilution of the 94...96% sulfuric acid. When use the ternary mother liqueur, obtained after removal of ammonium sulfate from suspension, in dilution result the cyclic process set out in Fig. 4.

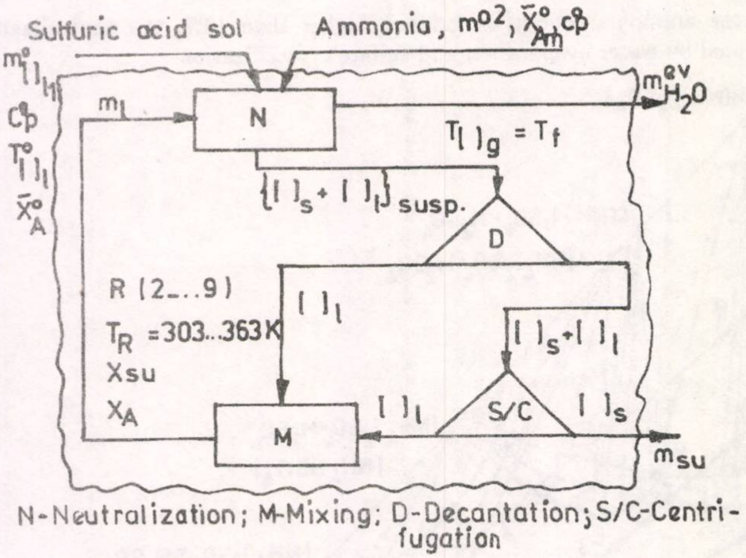

Fig. 4.- The block diagram of the cyclic process.

The block diagram shows that the sulfuric acid of 94...96%, after its neutralization is mixed with the returned mother liqueur (L_2). By ammonia absorption a suspension of solid ammonium sulfate and a ternary solution are obtained. After solid separation the cycle is repeated many times. The advantage of this cyclic process consists in the fact that even at an excess of about 3.5% H_2SO_4 of the ternary solution necessary for complete neutralization of dissolved ammonia, the separation degree of sulfate is still high enough.

The thermodynamic analysis performed shows that when gases with more then 13% NH_3 are used as ammonia source, the process is possible to be realized autothermally, having even an excess of heat. Utilization of ammonia water, even with 35% NH_3, does not ensure the crystallization of the entire quantity of sulfate without external energetic contribution. For this reason we investigated the variant of one cyclic process, determining its operating parameters.

4. Analysis of the Cyclic Process with Complete Recycling

In order to establish the correct parameters of the cyclic process of ammonium sulfate manufacture by neutralization, we have discussed the model of mass and heat balance elaborated on the basis of material flow [6] sat up in Fig. 4. Sectioning the cycle and taking into account that the separation processes are total ones, the balance model, summarized in Table 1, was obtained. The solution of this model was obtained considering as variables the initial concentration of sulfuric acid (X^0), the ammonia content of source (X^0_{Am}), the remaining concentration of sulfuric acid (X_{A}), the returned mother liqueur temperatures (T^0_R) and the recycling ratio (R). To solve the model we have considered that the ternary solution, in equilibrium with the separated salt, is saturated at boiling temperature (T_f). The obtained results are presented in Figs. 5,...,8.

Table 1

Mass and Heat Balance

Process	Mathematical relations
Mass balance	
Neutralization $2NH_3+H_2SO_4=(NH_4)_2SO_4$	$m^0_G = 2M_{\mathrm{Am}}m^0_l X^0/M_{\mathrm{Ac}}/X^0_{\mathrm{Am}}$ $m^0_R = Rm^0_l$ $X^0_{\mathrm{SU}} = 0.317 - 7.416 \times 10^{-5}T^0_R + 1.545 \times 10^{-6}T^{0^2}_R$ $m_{T(s+l)} = m^0_l + m^0_R + 34m^0_l X^0/98 - m_{\mathrm{ev}}$ $m_G = m^0_G(1 - X^0_{\mathrm{Am}}) + m_{\mathrm{ev}}$ $m_{\mathrm{TSU}} = 134m^0_l X^0/98 + m^0_R X^0_{\mathrm{SU}}$ $X_{\mathrm{TSU}} = m_{\mathrm{TSU}}/m_{T(s+l)}$
Crystallization $(NH_4)_2SO_{4[]l} \rightleftharpoons (NH_4)_2SO_{4[]s}$	$X_{\mathrm{SU}} = 0.3173 - 7.416 \times 10^{-5}T_f + 1.545 \times 10^{-6}T^2_f$ $m_l = [m^0_R(1 - X^0_{\mathrm{SU}}) + m^0_l(1 - X^0) - m_{\mathrm{ev}}]/(1 - X_{\mathrm{SU}})$ $m_{\mathrm{SU}} = m_l(X_{\mathrm{TSU}} - X_{\mathrm{SU}})/(1 - X_{\mathrm{TSU}})$
Heat balance	
Cyclic	$Q^0_l + Q^0_G + Q_N + Q^0_R = Q_l + Q_G + Q_s + Q_{\mathrm{Cr}} + Q_{\mathrm{sch}}$ $Q^0_l = m^0_l Cp^0_l(T^0_{\mathrm{Ac}} - 273)$ $Q^0_G = m^0_G X^0_{\mathrm{Am}} Cp^0_{\mathrm{Am}}(T^0_G - 273) + m^0_G(1 - X^0_{\mathrm{Am}})I_{\mathrm{H_2O}}$ $Q^0_R = m^0_R(3,328.5 - 1.25T^0_R)(T^0_R - 273)$ $Q_N = m^0_l X^0 \Delta_R H/132$ $Q_l = m_l(3,328.75 - 1.25T_f)(T_f - 273)$ $Q_G = [m^0_G(1 - X^0_{\mathrm{Am}}) + m_{\mathrm{ev}}]I_{\mathrm{H_2O}}$ $Q_{\mathrm{Cr}} = m_{\mathrm{SU}}\Delta H_{\mathrm{Cr}}/132$ $Q_s = m_{\mathrm{SU}}Cp_{\mathrm{SU}}(T_f - 273)$ $Q_{\mathrm{ch}} = 0.05(Q^0_l + Q^0_G + Q_N + Q^0_R)$

In the Figs. 5 and 6 is pointed out the influence of the recycling ratio, R, temperature of the returned mother liqueur, T^0_R, against the amount of water necessary to eliminate the neutralization heat in two cases, for sulfuric acid of 70% and 90%, respectively. It can be seen that as the ratio increases and temperature decreases, the amount of water decreases.

Taking into account the fact that in a cyclic process the evaporated water is determined, being equal to that entered with the sulfuric acid, the parameters influence in this case is more significant. Fig. 7 indicates how the sulfuric acid concentration and temperature of returned mother liqueur influence the value of recycling ratio. It can be seen that for the process heat removal the recycling ratio must be increased for both high acid concentration and high temperature of the returned solution.

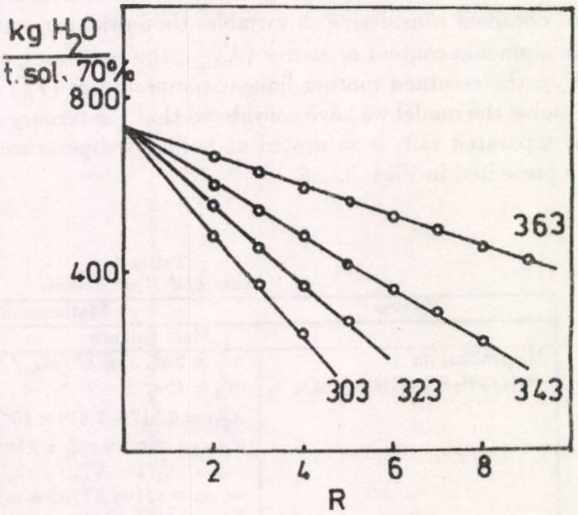

Fig. 5.- Influence of the recycling ratio and temperature on the amount of water necessary to eliminate the neutralization heat of the 70% H_2SO_4 solution.

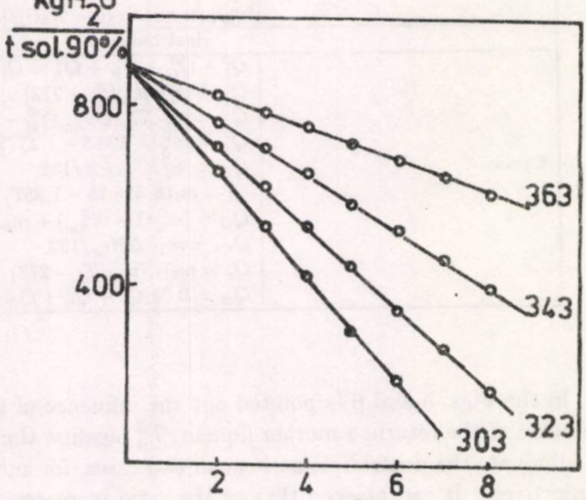

Fig. 6.- Influence of the recycling ratio and temperature on the amount of water necessary to eliminate the neutralization heat of the 90% H_2SO_4 solution.

Dependence of the recycling ratio and the amount of separated sulfate on the temperature of returned liqueur and initial concentration of sulfuric acid is shown in Fig. 8. It can be observed that the recycling ratio, *R*, increases exponentially with temperature increasing, irrespective of the concentration of the used sulfuric acid solution. The temperature dependence on the amount of separated sulfate exhibits a minimum at about 313 K, after which increases exponentially.

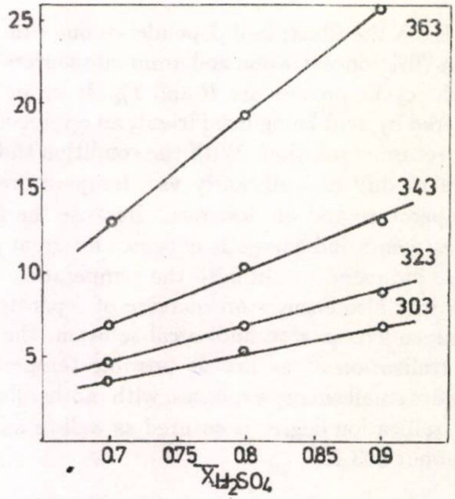

Fig. 7.- Dependence of the recycling ratio on the initial concentration of sulfuric acid and the returned solution temperature.

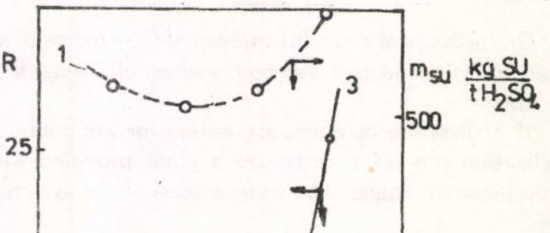

Fig. 8.- Variation of the recycling ratio and the amount of separated ammonium sulfate vs. returned solution for different concentration of sulfuric acid: *1* - 70; *2* - 80; *3* - 90% H_2SO_4.

From the illustrated dependence one can see that using sulfuric acid with more than 70% concentration and ammonia sources with minimum 13% NH_3, the variables of the cyclic process are R and T_R^0. In order to remove the process heat, the water entered by acid being insufficient, an appreciable part of heat must be eliminated by the returned solution. With the condition that the specific heat of returned solution does modify insignificantly vs. temperature, the eliminated heat depends on its temperature and on flow rate. Because the flow rate increases needs great specific investments and energetic expenses for great chemicals amounts transportation it is more indicated to diminish the temperature of the returned solution. Particularly, this way also ensures an increase of separated sulfate yields. Consequently we recommended, as a technological solution, the cooling of the resulted suspension by neutralization at as low as possible temperature, preferable below 323 K. Thus, besides small energy expenses, with mother liqueur recirculation, an advanced sulfate crystallization degree is ensured as well as an energetic excess useful as warm water of about 363 K.

5. Conclusions

On the basis of a careful analysis of the process of ammonium sulfate manufacture from sulfuric acid and different sources of ammonia the following conclusions may be drawn:

1° Utilization of ammonia waters for ammonium sulfate manufacture by neutralization process necessitates a plant provided with an isothermal or adiabatic crystallization stage. The water excess of the system excludes an autothermal process.

2° Utilization of sulfuric acid and gases with minimum 13% NH_3 ensures the obtainment of an autothermal process for the ammonium sulfate manufacture.

3° To eliminate the excess heat a recirculation number between 5 and 7 is imposed.

4° To ensure the crystallization of ammonium sulfate stoichiometric amount, compulsory condition for a symmetric cycle implementation, the cooling of suspension or the mother liqueur, from the boiling temperature at least 323 K is imposed. This technological variant ensures an economically supported recirculation number.

Notations and Symbols

m_l^0, m_l – initial and final solution mass, [kg];
Cp_l^0, Cp_l – initial and final specific heat of liquids, [J/kgK];
T_l^0, T_l – initial and final temperature of liquid, [K];
X^0, X_{Am}^0 – initial content of sulfuric acid and ammonia source, [kg/kg];
Cp^0 – initial specific heat of the ammonia source, [J/kgK];
T_{Am}^0 – initial temperature of the ammonia source, [K];
T_f – final temperature of the reaction mass, [K];
$\Delta_R H_T$, ΔH_{Cr} – thermal effect of the neutralization process and of the crystallization, [J/mol];
Cp_{SU} – specific heat of the ammonium sulfate, [J/mol K];
m_{ev}, I_{H_2O} – mass and enthalpy of the evaporated water, [kg], [J/kg];
$m_{T(s+l)}$ – total suspension mass , [kg];
m_g, Cp_g – mass and specific heat of the final gas, [kg], [J/kgK];
X_{TSU}, X_{SU} – sulfate fraction of suspension and solution, [kg/kg];

m_g^0, m_R^0 - initial mass of the gaseous ammonia source and mass of the returned solution, [kg];
M_{Am}, M_{ac} - molar mass of ammonia and sulfuric acid, [kg/kmol];
X_{SU}^0 - sulfate mass fraction of initial solution, [kg/kg];
T_R^0 - returned solution temperature, [K];
R - recycling ratio, [kg returned solution/kg initial solution];
Q_{ch} - environment exchanged heat, [J];
Q^0, Q - initial and final heat, [J];
g, R, l, s, V, St, Cr, S, D, N - symbols for gas, returned solution, liquid, solid, vapors (water steam), steam, crystallization, separation, decantation and neutralization processes.

Received, November 8, 1996
Revised, September 25, 1997

Technical University "Gh.Asachi", Jassy,
Department of Inorganic
Substances Technology

REFERENCES

1. Calistru C., Leonte C., Siminiceanu I., Hagiu C., Popa O., *Tehnologia îngrăşămintelor minerale.* Vol. **I**, Ed. Tehnică, Bucureşti, 1984, 233.
2. Fonyo Zs., Rév E., Tegyei A., Magyar Kémikusok Lapja, **39**, 1 (1984).
3. Leonte C., Szép Al., Balasanian I., Ifrim L., Calistru C., *Tehnologie chimică anorganică.* Vol.**I**, Univ. Tehn. „Gh.Asachi", Iaşi, 1992, 37.
4. Calistru C., Leonte C., *Tehnologia substanţelor anorganice.* Ed.Did. şi Ped., Bucureşti, 1972, 551.
5. * * * *Spravočnik eksperimentalnyi dannyh po rostvorimosti mnogokomponentnyh vodno solevyh sistem.* T. **I**, Goshimizdat, Moskva, 1953, 607.
6. Vasilescu I., Székely Gh., Secreteanu A., Ihoş A., Rev. Chim. (Bucharest), **46**, 33 (1995).

OBŢINEREA SULFATULUI DE AMONIU PRIN SINTEZA DIRECTĂ
I. Stabilirea regimului tehnologic

(Rezumat)

S-a efectuat o analiză calitativă şi cantitativă a procesului de obţinere a sulfatului de amoniu prin neutralizarea soluţiilor de acid sulfuric de 70...94% H_2SO_4 cu diferite surse de amoniac, ca apa amoniacală şi gaze cu conţinut variabil de amoniac.

Rezolvarea simultană a modelului de bilanţ masic şi termic al procesului de obţinere autotermă a sulfatului de amoniu, în condiţiile concentraţiilor de echilibru ale soluţiilor ciclului cu recirculare completă, a permis determinarea influenţei concentraţiei acidului sulfuric şi a temperaturii soluţiei recirculate asupra numărului de recirculare. Prin impunerea cantităţii de apă ce trebuie îndepărtată într-un proces autoterm au rezultat parametrii tehnologici şi indicatorii de performanţă ai ciclului simetric, respectiv: numărul de recirculare al soluţiei mume, cu temperatura de cel puţin 323 K, cuprins între 5 şi 7; concentraţia acidului sulfuric de 70...94%; gradul de îndepărtare a apei prin autoevaporare şi gradul de transformare a sulfatului în cele două procese de cristalizare de 100%.

BULETINUL INSTITUTULUI POLITEHNIC DIN IAŞI
Tomul XLIII (XLVII), Fasc. 3–4, 1997
Secţia II
CHIMIE şi INGINERIE CHIMICĂ

D.C. 551.51

MODEL FOR THE AIR DISPERSION OF A POLLUTANT

BY

VALERIU NAGACEVSCHI, MATEI MACOVEANU and N. PEIU

An improved Gaussian-type mathematical model for the dispersion pollutant in the air is proposed. The values of the parameters which intervene in the model are specified for its validation.

1. Introduction

Nowadays, when the ambient air pollution is studied, one uses a series of mathematical models [1], based on the dispersion of a pollutant in the air, under various meteorological condition; these models are generally of the Gaussian type. In these models the pollutant dispersion under given conditions is well approximated by the normal distribution function (Gauss).

Computer programmes for simulation of the air pollution from a pollutant source (sources) have been developed on the basis of these models.

2. Proposed Mathematical Model

A Gaussian mathematical model for the dispersion of a pollutant, drafted by us in 1978 [2], [3], and being based on the Sutton equation [4], has been used to determine the displacement area of a pollutant that contains lead in the industrial zone of Jassy. We have encountered some difficulties in using this model for the evaluation of some parameters from the model equation, due to the absence of the experimental data at the moment.

The initially adopted model is:

$$\Psi_{xyz} = \frac{2Q}{\pi u c_y c_z x^{2-n}} \exp\left\{-\frac{1}{x^{2-n}}\left[\frac{y^2}{c_y^2} + \frac{(z-H)^2}{c_z^2}\right]\right\}, \tag{1}$$

where: Ψ_{xyz} is the pollutant concentration in the air at the x, y, z coordinates point, [kg/m^3]; x, y, z – coordinates (x – in the direction of the wind, y – perpendicular on x and z – in the vertical direction), [m]; Q – pollutant emission rate, [kg/s]; u – mean speed of the wind at the plume level, [m/s]; H – effective stack height,

[m]; n – number characteristic for the meteorological conditions; c_y, c_z – parameters depending on the atmospheric stability.

Initially, there were no complete indications to evaluate the n, c_y and c_z parameters.

Taking into account recent bibliographical information [1], this paper presents an *improved variant* of the adopted model and specifies the values of the mentioned parameters.

In its improved variant, this model needs a computation of the plume rise, according to the Briggs method [5], [1].

The experimental data published by Briggs and Pasquill [6] allow the determination of the standard deviations on the y and z directions, noted σ_y, σ_z, as functions of the x distance and the atmospheric stability class. The establishing of the classification for the atmospheric stability is done according to the meteorological conditions (wind speed, solar heating, moment of the day) as follows: A – most unstable, B – unstable, C – slighty unstable, D – neutral, E – stable, F – most stable.

For the presented model we have found, in the first approximation, the correlations between the parameters of the model, c_y, c_z and n, and the standard deviations

$$\sigma_y = \sqrt{0.5}c_y x^{1-n_1/2}, \qquad \sigma_z = \sqrt{0.5}c_z x^{1-n_2/2}, \tag{2}$$

where n_1, n_2 are supplementary parameters (similar to the n parameter).

The values of the model parameters c_y, c_z, n_1 and n_2, deduced from the correlation, are given in Table 1 (rural aria) and Table 2 (urban area). Their validity is limited to the range 100 m...10,000 m.

Table 1

Rural Area, Distances Greater than 100 m

	A	B	C	D	E	F
n_1	0.214	0.163	0.144	0.129	0.149	0.150
c_y	0.64094	0.40646	0.24559	0.15336	0.11831	0.0853
n_2	–0.8646	–0.022	0.153	0.512	0.628	0.651
c_z	0.024678	0.13609	0.15171	0.22533	0.22726	0.15643

Table 2

Urban Area, Distances Greater than 100 m

	$A-B$	C	D	$E-F$
n_1	0.30	0.321	0.302	0.307
c_y	0.93652	0.080793	0.46293	0.31792
n_2	–0.28	–0.035	0.323	0.546
c_z	0.20626	0.26565	0.45847	0.40506

For the range 0.1...100 m the existing experimental data are extrapolated and similar results (Tables 3 and 4) are obtained.

The model (1) will be rewritten in this case as follows:

$$\Psi_{xyz} = \frac{Q}{\pi u c_y c_z x^{2-\frac{n_1+n_2}{2}}} \exp\left\{-\left[\frac{y^2}{c_y^2 x^{2-n_1}} + \frac{(z-H)^2}{c_x^2 x^{2-n_2}}\right]\right\}, \tag{3}$$

Table 3

Rural Area, Distances Greater than 100 m

	A	B	C	D	E	F
n_1	-0.2949	-0.1970	-0.0638	0.06253	0.1510	0.2465
c_y	0.19859	0.17743	0.15220	0.13160	0.11886	0.10648
n_2	-0.07107	-0.00354	0.08167	0.20646	0.28133	0.40480
c_z	0.153480	0.14200	0.12873	0.11150	0.10229	0.08874

Table 4

Urban Area, Distances Greater than 100 m

	$A-B$	C	D	$E-F$
n_1	-0.34736	-0.29056	-0.142	-0.02987
c_y	0.21095	0.19760	0.16654	0.14637
n_2	-0.29593	-0.20586	-0.12520	0.05933
c_z	0.19883	0.17925	0.16335	0.13208

or

$$\Psi_{xyz} = \frac{Q}{\pi u c_y c_z x^{2-n}} \exp\left\{-\frac{1}{x^{2-n}}\left[\alpha(x)\frac{y^2}{c_y^2} + \frac{1}{\alpha(x)}\cdot\frac{(z-H)^2}{c_z^2}\right]\right\}, \tag{4}$$

where: n is the average value between n_1 and n_2;

$$n = \frac{n_1 + n_2}{2}; \tag{5}$$

$\alpha(x)$ – correction factor according to the experimental data:

$$\alpha(x) = x^{\frac{n_1 - n_2}{2}}. \tag{6}$$

The dispersion model given by the relation (4) represents an improvement of the model (1) due to: a) the introduction of a correction factor $\alpha(x)$, according to the existing experimental data; b) specification of the values for the c_y, c_z and n parameters.

The theory of the Gaussian model [1] mentions the fact that the relations (1) and (4) are applied in the case when the plume trace does not reach the ground, existing only as a simple dispersion of the pollutant. From the moment when the ground is reached ($H \approx 3\sigma_z$) appears a ground reflection of the plume trace, determining an increase in the pollutant concentration on the air. The increased concentration of the pollutant in the reflection zone is computed by means of the relation:

$$\begin{aligned}\Psi_{xyz} = {} & \frac{Q}{\pi u c_y c_z x^{2-n}} \exp\left[-\frac{\alpha(x)}{x^{2-n}}\cdot\frac{y^2}{c_y^2}\right]\left\{\exp\left[-\frac{1}{c^{2-n}}\cdot\frac{1}{\alpha(x)}\cdot\frac{(z-H)^2}{c_z^2}\right] + \right. \\ & \left. + \exp\left[-\frac{1}{x^{2-n}}\cdot\frac{1}{\alpha(x)}\cdot\frac{(z+H)^2}{c_z^2}\right]\right\}.\end{aligned} \tag{7}$$

3. Results and Discussions

The obtained results using the improved model, given by the relations (4) and (7) respectively, are close to the results obtained with other variants of the Gaussian-type model for the pollutant dispersion on the air.

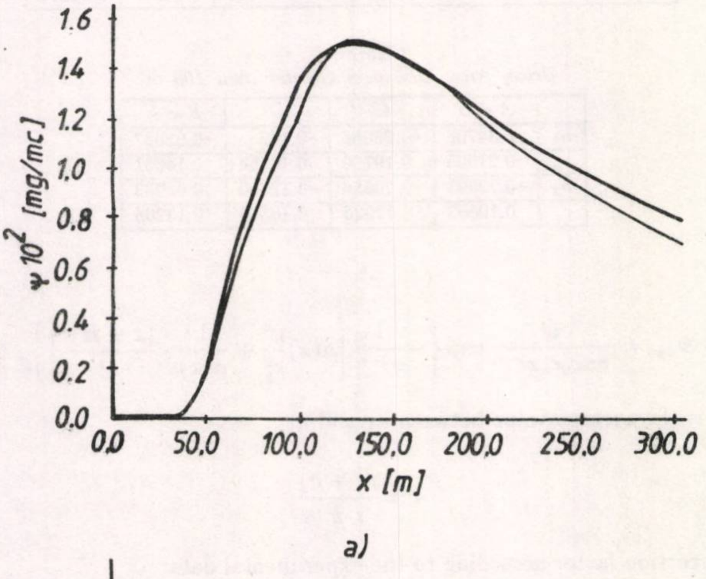

Fig. 1.– a – concentration profile in the horizontal plane, at $z=0$ and $y=0$; b – isoconcentration $\Psi=10^{-2}$ mg/m^3 in the horizontal plane at $z=0$; thin line – classic Gaussian model; thick line – opposed model.

For exemplification, we present in Figs.1 *a* and 1 *b* the comparative results for the dispersion in the air of the stiren pollutant obtained on the extrusion section of the ABS plates, using the above mentioned improved model and the classic Gaussian model [1]:

$$\begin{aligned}\text{Data}:\ & Q = 65\ \text{mg/s}; & Q_s = 0.9306\ \text{m}^3/\text{s}; & \ h_{\text{st}} = 15\ \text{m}; \qquad z = 0\ \text{m};\\ & u = 1.0\ \text{m/s}; & \text{terrain} - \text{urban}; & \ \text{atm.cond.} - \text{neutral},\ (D);\\ & T_s = 32°\text{C}; & T_a = 20°\text{C}; & \ \Psi_{\text{lim}} = 0.8\ \text{mg/m}^3/24\ \text{hrs},\end{aligned}$$

where: Q_s is the flowrate of the stack gas, [m^3/s]; h_{st} – stack height, [m]; T_s – stack gas temperature, [°C]; T_a – ambient temperature, [°C]; Ψ_{lim} – the maximum admissible pollutant concentration, [mg/m^3/24 hrs].

4. Conclusions

1° The advantage of the proposed model as compared with other Gauss-type ones consists in the direct dependence of the pollutant concentration on downwind distance from the polluting source, x.

2° There were made some specifications on choosing the c_y, c_z and n parameters from the presented mathematical model, according to the actual experimental data.

3° It was also extended the valability domain of the mathematical model from the range 0.1...100 m, an active zone for the small power pollution sources or with a small height of the stack.

4° Some improvements were made to the existing mathematical model [2], thus introducing a correction factor according to the atmospheric stability.

5° The initial mathematical model was improved for the case of the ground reflection of the plume.

6° The comparison of the improved model with other mathematical models for the pollutant dispersion indicates the like results for different cases of pollution with the at ground concentration measurement.

Received, April 30, 1996
Revised, June 18, 1997

Technical University "Gh.Asachi", Jassy,
Department of Environement Engineering

REFERENCES

1. Finch R.N., Serth R.W., Hydrocarbon Processing, 75 (1990).
2. Hâncu I., Macoveanu M., Mazilu V., Bul. Inst. polit., Iaşi, **XXIII (XXVII)**, *3-4*, s.II, 15-20 (1977).
3. Hâncu I., Macoveanu M., Nagacevschi V., Bul. Inst. polit., Iaşi, **XXIV (XXVIII)**, *3-4*, s.II, 51-55 (1978).
4. Sutton O.G., *Atmospheric Turbulence*. Methuen, London, 1955.
5. Briggs G.A., *Plume Rise Predictions*, Ch. **3** in *Lectures on Air Pollution and Environmental. Impact Analysys* (ed. D.A. Hargen). Amer. Meteorol. Soc., Boston, Ma, 1975.
6. Pasquill F., *Atmospheric Dispersion Parameters in Gaussian Plume Modeling* (II). *Possible Requirements for Change in the Turner Workbook Value.* EPA-600/4-76-030b, Res. Triangle Park, No.27711, US, Environmental Protection Agency, 1976.

MODEL PENTRU DISPERSIA UNUI POLUANT ÎN ATMOSFERĂ

(Rezumat)

Este prezentat un model matematic perfecţionat, de tip gaussian, pentru dispersia în atmosferă a unui poluant gazos. Sunt indicate valorile parametrilor din modelul adoptat. Rezultatele obţinute pentru un studiu de caz cu modelul perfecţionat sunt comparate cu cele date de un model existent.

BULETINUL INSTITUTULUI POLITEHNIC DIN IAŞI
Tomul XLIII (XLVII), Fasc. 3–4, 1997
Secţia II
CHIMIE şi INGINERIE CHIMICĂ

C.D. 615-012

RECHERCHES CONCERNANT LA SYNTHÈSE ET LA PURIFICATION DU SULBACTAME-PIVOXYLE

PAR
CRISTINA VLASE, CORNELIU ONISCU,
EUGEN DIACONU et AUREL VLASE

La sulbactame est un inhibiteur de β-lactamase ayant une biodisponibilité réduite à l'administration orale. Son double-ester lipophilique permet l'augmentation significative de l'absorbtion orale.

On présente les résultats des recherches expérimentales effectuées pour établir un procédé efficace de la synthèse du sulbactame-pivoxyle. L'étude réalisée a permis d'obtenir du sulbactame-pivoxyle de pureté pharmaceutique (contenu 92...95% déterminé par HPLC) est avec de bons rendements (80...92%) en réalisant l'esterification du sulbactame-acide avec chlorométhyl-pivoxyle, dans l'acétate d'éthyle, à 60°... 65°C, pendant 8 h et purification du produit brut ainsi préparé par recristallisation fractionée dans l'acétate d'éthyle-hexane.

1. Introduction

Compte tenu que le sel de sodium de sulbactame présente une faible biodisponibilité à l'administration orale, on a synthétisé de nombreuses prodrugs, facile à hydrolyser *in vivo*; ces substances présentent des désavantages liés à leur faible solubilité dans l'eau, à leur stabilité limitée *in vitro* et aux difficultés concernant la réalisation des formules pharmaceutiques (la plupart de ces esters se présentent comme des huiles).

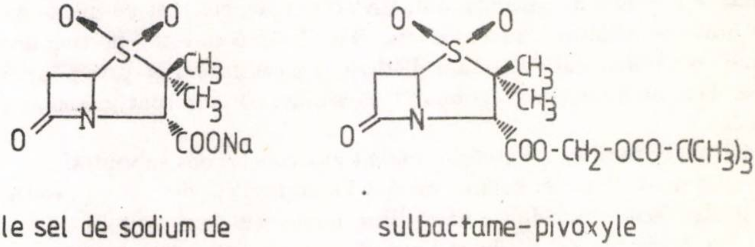

le sel de sodium de sulbactame

sulbactame-pivoxyle

Fig. 1.– Les structures de sulbactame et sulbactame-pivoxyle.

Les recherches effectués par Pfizer ont conduit à la selection de l'ester pivaloyloxyméthylique de sulbactame (sulbactame-pivoxyle) (Fig. 1) qui présente la plus favorable stabilité *in vitro* et plusieurs possibilités d'obtenir des formules pharmaceutiques (tablettes, capsules, poudres, sirops, suspensions, etc.), puisque cet ester est une substance solide stabile [1], [2].

Dans ce qui suit on présente les résultats des recherches effectuées en vue d'établir une méthode de synthèse du sulbactame-pivoxyle et les possibilités de purification de cet ester pour obtenir un produit de pureté pharmaceutique.

2. Préparation du sulbactame-pivoxyle de pureté pharmaceutique

Bien que le prodrug pivaloyloxyméthylique de sulbactame n'est pas prévu dans aucune Pharmacopée, on a convenu, en conformité avec les connaissances antérieures liées aux prodrugs des pénicillines (pivampicilline, pivmécilliname, etc.), que pour l'utilisation thérapéutique le principe actif doit avoir une pureté de minimum 90%.

La littérature [3],...,[5] présente comme méthode générale de synthèse l'estérification du sulbactame avec chlorométhylpivalate (or d'autres halogénures de pivaloyloxyméthyle) obtenues *in situ* en présences des catalyseurs de transfert entre-phases), dans des solvants polaires anhydres, à des températures de 20°...25°C, pendant 24...66 heures. Pour l'isolation de l'ester on dilue le mélange de réaction avec de l'eau et de l'acétate d'éthyle et on sépare la phase organique; l'ester est obtenu par évaporation du solvant sous pression réduite. Rendement: 78...80%. Les produits obtenus conformément à ces procédés sont impurs (contenu 70...75% déterminé par HPLC) et ne peuvent pas être utilisés dans la thérapie. Pour obtenir un produit ayant une plus grande pureté on a étudié les conditions de réaction et isolation–purification qui doivent être utilisées pour préparer le sulbactame-pivoxyle avec de bons rendements et une pureté satisfaisante pour l'utilisation pharmaceutique.

2.1. L'étude des conditions de réaction dans la synthèse du sulbactame-pivoxyle

On a étudié l'estérification du sulbactame acide (contenu HPLC: 95...98%) avec iodométhylpivalate préparé *in situ* par le traitement du chlorométhylpivalate avec des iodures alcalines en présence d'amines tertiaires comme catalyseurs de transfert entre-phases.

L'estérification est réalisée dans les solvants aprotiques dipolaires précisés dans la littérature (diméthylformamide, diméthylacétamide, etc.) et de même dans des solvants protiques polaires ou nonpolaires. Dans les expériments effectués on a isolé l'ester par extraction dans l'acétate d'éthyle, concentration et précipitation avec *n*.hexane. Les conditions de réaction et les résultats obtenus sont présentés dans le Tableau 1.

L'étude expérimentale effectuée a conduit aux conclusions suivantes:

a) Il est mieux d'utiliser comme solvant l'acétate d'éthyle, cas où l'isolation de l'ester est plus facile et conduit à un meilleur rendement.

b) Il est favorable de conduire l'estérification à 60°...65°C, ce qui permet à diminuer le temps de réaction et d'obtenir un produit de plus grande pureté. Le sulbactame-pivoxyle ainsi obtenu doit être purifié jusqu'à un contenu de minimum 90%.

Tableau 1

Les conditions de réaction et les résultats obtenus expérimentalement dans la synthèse du sulbactame-pivoxyle

No.	Solvant	*t* °C	Temps h	Rendement %	Pureté %
1	DMF	20...22	24	75...77	75...86
2	DMA	50...65	6...8	72...77	72...82
3	acétone	reflux	3	75	73...75
4	acétone	reflux	5	66	70
5	acétate d'éthyle	reflux	6	78	80...82
6	acétate d'éthyle	60...65	12	72	82...83
7	acétate d'éthyle	60...65	8	75...78	83...85
8	acétate d'éthyle	60...65	8	72	80...82
9	acétate d'éthyle	20...25	24	90	66...68

2.2. Purification du sulbactame-pivoxyle

a) *Purification par recristallisation*

La purification a été réalisées dans diverses systèmes en utilisant comme solvants: acétate d'éthyle, chlorure de méthylène, acétone, tetrahydrofurane et comme non-solvants: benzène, hexane ou des mélanges de ces solvants. Les produits les plus pures ont été obtenus par recristallisation fractionnée dans les systèmes: acétate d'éthyle–hexane, acétate d'éthyle–benzène en mélange avec hexane. On a suivi le degré de purification par chromatographie en couche-mince[1]). Conformément à ce procédé on obtient le sulbactame-pivoxyle de pureté 92...95% (HPLC). Rendements: 80...82%.

b) *Purification par chromatographie sur colonne*

Pour éloigner les impuretés du produit brut on a utilisé aussi la chromatographie sur colonne de silice et élution simple ou en étapes. On a utilisé comme éluants: hexane, toluène et benzène et aussi leurs mélanges avec acétate d'éthyle, chlorure de methylène et acétone. La plus bonne purification a été réalisée en utilisant comme éluant *n*.hexane:acétate d'éthyle 7:3 et 8:2, conditions dans lesquelles on obtient l'ester pivaloyloxyméthylique ayant un degré de pureté de 92...94% (HPLC) et des rendements de 70...75%.

Le procédé de purification du sulbactame-pivoxyle par chromatographie sur colonne assure un produit similaire à celui obtenu par recristallisation, mais les rendements sont diminués (par rapport au procédé de purification par recristallisation) et les conditions technologiques réclamés par ce procédé sont plus sévères. En conséquence on a opté pour le procédé de purification par recristallisation qui assure des rendements globaux (par rapport au sulbactame acide) de 62...63%.

---

[1]) Phase stationnaire: Kieselgel 60 F 254; phase mobile: benzène-acétonitrile 3:1; développant: UV, $\lambda = 254$ nm.

3. Mode de préparation

3.1. Préparation du sulbactame-pivoxyle

On introduit 12 g sulbactame acide (51,5 mmoles) dans 120 ml d'acétate d'éthyle anhydre. On agite 5 min. et puis on ajoute goutte à goutte, à 5°C, sous vive agitation, 7,88 ml triéthylamine. Puis on ajoute 4,5 g KI et 9,7 ml chlorométhylpivalate (64,5 mmoles). On chauffe le mélange a 60°...65°C pendant 8 h. Après le refroidissement sur bain de glace à 5°...10°C on ajoute 60 ml d'eau et on corrige le pH à 6,5...7 avec une solution 1 N NaOH. On sépare les phases. On lave la solution organique avec 60 ml d'eau. On sèche ensuite la solution sur du sulfate de sodium, tout en l'agitant avec charbon décolorant sous refroidissement sur bain de glace. On filtre le solide et on le lave avec d'acétate d'éthyle. On le concentre à 30°C sous pression réduite pour obtenir une huile, puis on ajoute l'huile goutte à goutte à 400 ml de hexane, sous refroidissement sur bain de glace.

On recueille le produit par filtration, on le lave avec hexane. Après séchage sous vide poussé, pendant 4 h, on obtient 13,9 g ester brut. Rendement: 77,7%, pureté: 83...85%.

3.2. Purification du sulbactame-pivoxyle

La purification de l'ester a été réalisée dans les conditions ci-dessous.

On dissout 13,9 g ester brut (obtenu selon le procédé décrit plus haut) dans 100 ml d'acétate d'éthyle, on ajoute sous vive agitation 100 ml n.hexane et on conserve à froid pendant 3 h. On recueille, par filtration, les cristaux qui se sont formés, contenant surtout des impuretés, puis on ajoute à la solution filtrée 200 ml n.hexane. On conserve à froid pendant 8 h, puis on recueille par filtration les cristaux qui se sont formés et on les lave avec du hexane. Rendement: 62,6%; pureté: 94...95% (HPLC).

Spectre infrarouge (KBr): 1 805, 1 785, 1 773, 1 754 cm^{-1}.

Les analyses ont été effectuées on utilisant comme phase stationnaire chromossile $NH_2/10\mu$; phase mobile: acétate d'ammonium 0,2%-acétonitrile 1:1; détection: UV, $\lambda = 230$ nm.

4. Conclusions

1° On a établi une méthode de synthèse pour le sulbactame-pivoxyle par l'estérification du sulbactame avec du chlorométhylpivalate en présence de KI dans l'acétate d'éthyle, à 60°...65°C, pendant 8 h.

2° On a établi une méthode de purification de l'ester par recristallisation dans l'acétate d'éthyle-hexane, qui assure un produit de pureté pharmaceutique.

Reçue le 20 mai 1996

Université Technique „Gh.Asachi“, Jassy,
Chaire d'Industries Organiques

BIBLIOGRAPHIE

1. Haempel B., Bruckner G., Lode H., Koeppe P., *Comparative Pharmacokinetics of Sulbactam/Ampicillin and Clavulanic Acid/Amoxicillin in Human Volunteers.* 5-ème Congrès méditerranéen de Chémoterapie, Athens, 1986.
2. Schmalreck A.F., Wildfeuer A., Arzneim-Forsch/Drug Res. **40**(II), *10*, 1145-1155 (1990).
3. * * * Patent USA *4,234,579* (1981).
4. Setti L.E., Mascaretti O.A., J. Chem. Soc. Perkin Trans. I, **8**, 2059-2060 (1988).
5. English A.R., Girard D., Yasys U.V., Martingano R., Kellog M.S., J. Med. Chem., **33**, 344-347 (1990).

CERCETĂRI PRIVIND SINTEZA ŞI PURIFICAREA SULBACTAMEI-PIVOXIL

(Rezumat)

Sulbactama este un inhibitor de beta-lactamază cu biodisponibilitate redusă la administrarea orală. Esterul său lipofilic pivaloiloximetilic permite creşterea apreciabilă a absorbţiei orale.

Se prezintă rezultatele cercetărilor experimentale efectuate în vederea stabilirii unui procedeu eficient de sinteză a sulbactamei-pivoxil de puritate farmaceutică (conţinut 92...95% determinat prin HPLC) cu bune randamente (80...82%), prin realizarea esterificării sulbactamei acid cu clorometilpivalat, în acetat de etil, la 60°...65°C timp de 8 ore şi purificarea produsului brut astfel obţinut prin recristalizare fracţionată în acetat de etil-hexan.

BULETINUL INSTITUTULUI POLITEHNIC DIN IAŞI
Tomul XLIII (XLVII), Fasc. 3–4, 1997
Secţia II
CHIMIE şi INGINERIE CHIMICĂ

D.C. 678.84

POLYSILANES

1. COUPLING REACTION OF DICHLOROMETHYLPHENYLSILANE IN THE PRESENCE OF ALKALI METAL/CROWN ETHER SYSTEMS

BY

VALERIA HARABAGIU, MARIANA PINTEALĂ, CORNELIA COTZUR,
*CRISTINA IOJOIU and *BOGDAN C. SIMIONESCU

The present work deals with the reductive coupling of dichloromethylphenylsilane (DCMPS) in the presence of alkali metal/complexing agent systems, using two different pathways: the reaction of DCMPS with stoechiometric amounts of Na/K alloy/18-C-6 soluble complexed species and the coupling reaction of DCMPS in phase transfer conditions.

Reductive coupling of DCMPS in the presence of stoechiometric amounts of Na/K alloy/18-C-6 complexed species gives rise to a low molecular weight, nearly monodisperse polymer, while the reaction performed in the presence of sodium and in phase transfer conditions yields higher molecular weight polymers with larger polydispersity; however, the molecular weight distribution is broader and lower amounts – as compared to the "classical" coupling processes – of linear and cyclic silane oligomers are formed.

1. Introduction

Polysilanes were found to possess interesting photo- and electrochemical behaviour related to the conjugation of the σ electrons in the Si–Si backbone [1]. The properties of polysilanes are function of their degree of polymerization [2]. Their synthesis was achieved by the reductive coupling of diorganodihalogensilanes in the presence of alkali metals [3], [4], by sonochemically assisted reductive coupling [5], by the polymerization of "masked" disilylenes [6] or of strained cyclosilanes [7] and by dehydrogenative coupling of hydrosilanes [8].

The reductive coupling takes place at high temperature (more than 100°C) in the presence of sodium dispersions. A two electron transfer process was supposed to be implied in the mechanism and radical, anion or silylene species were proposed to act as propagating centers [9],...,[11]. A polydisperse polymer, containing high and low molecular weight fractions as well as cyclosilanes, is usually obtained. This is a logical consequence of the heterogeneous character of the synthetic process and of the possible competition between a few reaction mechanisms.

The introduction of complexing agents in the reaction medium determines the increase of both system reactivity and polymer yield, while their influence upon polymer molecular weight and polydispersity is contradictory [12], [13].

The temperature controls both the polymer yield and the distribution of the molecular weight. Generally, temperature rise is accompanied by higher monomer conversions, but the extent of high polymer fraction is lowered and the polydispersity is increased. The temperature effect depends on monomer nature and is related to the exothermicity of the coupling reaction. Highly reactive aryl substituted monomers undergo reductive coupling with important heat release and kinetic studies demonstrated low induction periods and a very rapid monomer consumption. The large number of generated active species determines the decrease of polymer molecular weight [14]. Sterically hindered monomers, such as dichlorodi(n-hexyl)silane, present a low thermal effect and both induction period and polymer molecular weight are higher [13].

Aryl substituted monomers are reactive at temperatures lower than 100°C and yield polymers with high, monomodal molecular weights in lower conversions [13]. On the contrary, the dialkyl substituted monomers do not react below 100°C, unless complexing agents [13] or ultrasounds [5] are used. However, monomer conversion is low but it increases for copolymerization reactions with phenylchlorosilanes [5], [15].

In this context, the present paper is intended to be the first in a series of studies on the reductive coupling of dichlorosilanes in the presence of alkali metal/complexing agent systems. The complexing agent performs the transfer of the alkali metal to the organic solution, thus shifting the heterogeneous system to a homogeneous one. Since a higher reactivity of complexed species is to be expected, the number of the participating mechanisms should decrease and a more precise kinetic approach could be envisaged.

2. Experimental

2.1. Materials

Dichloromethylphenylsilane (DCMPS) was distilled just before use. 1,4,7,10,13,16-hexaoxacyclooctadecane (18-C-6) was dried by heating at 40°C under high vacuum for 48 h. The obtained colourless viscous liquid was kept under argon. Toluene was treated with concentrated sulfuric acid, washed with water until neutral pH was attained and dried over sodium wire in the presence of benzophenone. THF was refluxed over KOH for 24 h and dried by refluxing over sodium wire.

2.2. Synthesis of Intermediates and of Polysilanes

a) *The preparation of the blue solution* was performed according to a procedure previously described [16]. The required amount of liquid Na/K alloy was introduced into a special device, degased and dried under high vacuum. The vacuum was then cut off and a 0.23 M solution of 18-C-6 in THF was introduced into the apparatus (metal/18-C-6 = 2.1/1.0 molar ratio). The solution becomes dark blue. After exactly 15 min. of ultrasonic mixing the blue solution was filtered off directly into a dropping funnel and was used immediately.

The concentration of alkali metals was determined by titration with HCl 0.1 N.

b) *Synthesis of polymethylphenylsilanes (PMPS) by the reaction between stoechiometric amounts of blue solution and DCMPS.* Into a previously dried reaction vessel provided with magnetic stirring, external cooling and a dropping funnel a calculated amount of DCMPS as 20% solution in THF was cooled at 0°C. The blue solution (alkali metal/DCMPS = 2/1) was added dropwise through the dropping funnel. Once the addition of blue solution was completed, the temperature of the reaction mixture was allowed to increase to 20°C and the stirring was continued for 1 h. The reaction was deactivated with methanol. The obtained colourless solution was filtered, concentrated and the polysilane was recovered by precipitation in isopropanol.

c) *The preparation of PMPS in phase transfer conditions* was performed by coupling of DCMPS in the presence of sodium metal and catalytic amounts of 18-C-6. The technique implies the preparation of metal mirror. The apparatus used for this purpose is presented in Fig.1. The reaction vessel (*2*) is provided with mechanical stirring, a dropping funnel (*3*), a reflux condenser (*4*) and a three-way stopcock that can be switched between argon (*a*) and vacuum (*b*) connections. Small pieces of sodium metal were put under argon into the tube (*1*). The distillation was carried out in high vacuum and the wall of the reaction vessel (*2*) was covered with the sodium mirror. A 0.3 M solution of 18-C-6 in toluene was added over sodium mirror and the mixture was warmed at the reaction temperature. A 10% solution of DCMPS in toluene was then added through the dropping funnel and the mixture was stirred at the reaction temperature for established periods of time. The 18-C-6/DCMPS molar ratio was varied between 0.1 and 0.3 and Na/DCMPS molar ratio was kept close to 3.0 in all experiments (Table 1). The purification of silane polymer was performed in a similar manner as for PMPS obtained with the blue solution.

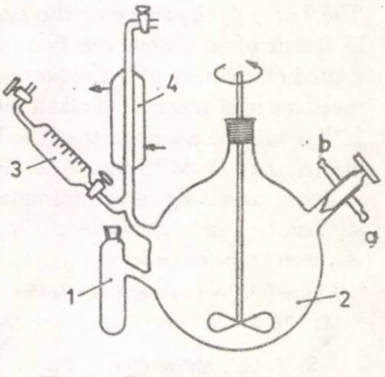

Fig. 1.- Experimental apparatus for the reductive coupling reaction.

2.3. Analysis

The molecular weights of polysilanes were determined by gel permeation chromatography (GPC) on a Waters Associated 440 apparatus (polystyrene standards) and UV absorptions were established on an Unicam spectrometer.

3. Results and Discussion

Polymethylphenylsilanes (PMPS) were obtained by reductive coupling of DCMPS in the presence of alkali metal/18-C-6 systems, using two different pathways: the reaction of DCMPS with stoechiometric amounts of Na/K alloy/18-C-6 soluble complexed species and the coupling reaction of DCMPS in phase transfer conditions.

Due to its multipolar structure a crown ether can draw near the metallic surface, complexing and transfering the cation from the solid state to the organic solution. When metal/crown ether molar ratio was higher than one, metal anions were detected in the organic phase [17]. They are formed through the reaction of metal atoms and solved electrons at the organic solution – solid metal contact surface (Scheme 1). The ^{39}K-NMR spectrum of a K/18-C-6 (2/1 molar ratio) complex solution in THF [17] contains two resonance peaks of nearly identical integrals. The large one at about −107 ppm was attributed to K^+/18-C-6 complex, while the sharp peak at −100 ppm was assigned to K anion.

$$K_{(s)} + 18\text{-C-}6_{(org)} \leftrightarrow K^+/18\text{-C-}6_{(org)} + e^-_{(org)}$$

$$e^-_{(org)} + K_{(s)} \leftrightarrow K^-_{(org)},$$

where: (s) – solid phase; (org) – organic solution phase.

Scheme 1

By adding the Na/K alloy/18-C-6 blue solution over a stoechiometric amount of DCMPS (see experimental part for reaction conditions) a polysilane with $M_n \cong 11{,}000$ was obtained. The GPC curve was monomodal and no cyclic silanes were evidenced. The low polydispersity of the synthesized PMPS ($M_w/M_n \cong 1.1$) strongly argues in favour of an unique reaction mechanism (Scheme 2). Based on the generally accepted mechanism of the reductive coupling of halogenosilanes [18],...,[20] and on the mechanism of reaction of alkali metal/crown ether complexes with different reagents [21], it may be assumed that the K/Na alloy/18-C-6 complex is able to transfer two electrons to DCMPS molecule. The silyl anion species react with another DCMPS molecule resulting in the formation of a Si–Si bond. In the propagating step, the silyl anions undergo nucleophilic substitution of other DCMPS molecules or a two electron transfer process.

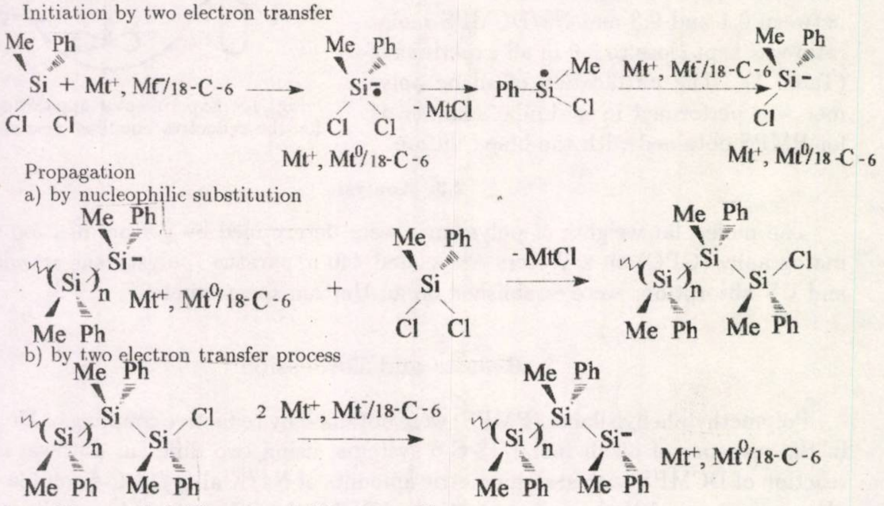
Initiation by two electron transfer
Me Ph
Si + Mt⁺, Mt⁻/18-C-6
Cl Cl
Me Ph
Si
Cl Cl
Mt⁺, Mt⁰/18-C-6
- MtCl
Ph-Si
Me
Cl
Mt⁺, Mt⁻/18-C-6
Me Ph
Si⁻
Cl
Mt⁺, Mt⁰/18-C-6
Propagation
a) by nucleophilic substitution
Me Ph
Si⁻
(Si)n
Mt⁺, Mt⁰/18-C-6
Me Ph
+
Me Ph
Si
Cl Cl
- MtCl
Me Ph
Si
(Si)n
Si
Cl
Me Ph
Me Ph
b) by two electron transfer process
Me Ph
Si
(Si)n
Si
Cl
Me Ph
Me Ph
2 Mt⁺, Mt⁻/18-C-6
Me Ph
Si
(Si)n
Si⁻
Mt⁺, Mt⁰/18-C-6
Me Ph
Me Ph

where: Me – methyl; Ph – phenyl; Mt – Na or K.

Scheme 2

The propagating rate must be higher than the rate of possible side reactions of silyl anions with complexed metal counterions (back bitting reactions on the polysilane chains with the formation of cyclic oligomers) so that the resulting product is nearly monodisperse.

Table 1

Data on the Reductive Coupling Reaction of DCMPS in Phase Transfer Conditions

Initial mixture[a]							Polysilane				
Crt. no.	DCMPS		18-C-6	18-C-6/ DCMPS	Duration	Temp.	Sample code	Yield	Oligomers content	Mn[b]	Mw/ Mn[b]
	g	mol	g	molar	h	°C		%	%	GPC	GPC
1	1.91	0.01	0.0264	0.01	4	65	PMPS-1	35.7	20.1	74,800	2.3
2	3.82	0.02	0.0528	0.01	8	50	PMPS-2	53.2	10.2	95,700	2.8
3	1.91	0.01	0.0528	0.02	4	65	PMPS-3	47.4	19.7	83,200	1.9
4	1.91	0.01	0.0528	0.02	6	50	PMPS-4	52.1	16.4	98,100	2.1
5	3.82	0.02	0.1056	0.02	8	45	PMPS-5	60.4	11.3	120,400	1.9
6	3.82	0.02	0.1584	0.03	4	60	PMPS-6	51.8	10.9	89,500	1.7
7	3.82	0.02	0.1584	0.03	6	60	PMPS-7	73.8	11.5	115,600	1.8
8	3.82	0.02	0.1584	0.03	8	60	PMPS-8	78.3	11.7	135,800	1.9

[a] Solvent, toluene; $[DCMPS]_0=10\%$ by weight; SiCl/Na=1.0/1.5 molar ratio.

[b] High molecular weight fraction.

When the complexing agent is used in strictly catalytic amounts, it plays a phase transfer catalyst role and realises the transfer of alkali metal atoms from the solid state to the organic solution containing the monomer. The reductive coupling of DCMPS (Table 1) in phase transfer conditions was performed in the presence of sodium metal mirror complexed with 18-C-6 in toluene solution. Following the complexation, the reaction temperature was increased to a preestablished value and DCMPS was dropped as a 10% solution in toluene. As revealed by GPC analysis (Fig. 2), the resulted polysilanes present bimodal molecular weight distribution. The content in low molecular weight fractions (oligomers with M_n <10,000) in the final product varies between 10% and 20% and is lower for the samples obtained in the presence of higher amounts of complexing agent. The molecular weight of high polymer fraction increases with both reaction duration and crown ether amount. The polymer yield increases with rising the reaction temperature from 45° to 65°C, with increasing reaction duration and with the amount of crown ether.

The resulting PMPS present characteristic UV spectra with absorption maxima depending on polymer molecular weight. Fig. 3 shows a typical UV spectrum. The absorption at 341 nm is attributed to the high molecular weight polymer fraction, while that at cca 275 nm characterizes the oligosilanes.

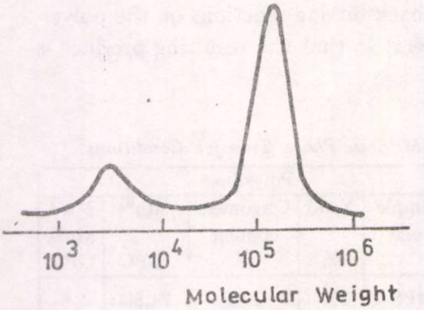

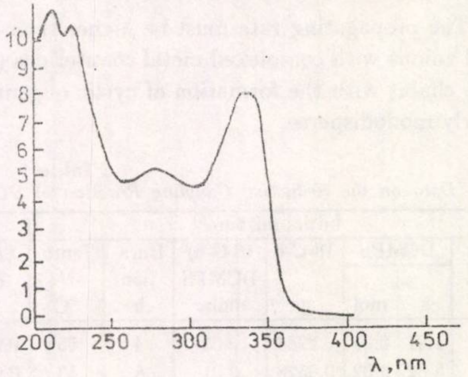

Fig. 2.- GPC curve of PMPS-8 (Table 1). Fig. 3.- UV spectrum of PMPS-8 (Table 1).

4. Conclusions

Polymethylphenylsilane was synthesized in the presence of alkali metal/complexing agent system by two different approaches. Reductive coupling of DCMPS in the presence of stoechiometric amounts of Na/K alloy/18-C-6 complexed species gives rise to a low molecular weight, nearly monodisperse polymer. Reductive coupling in the presence of sodium and in phase transfer conditions yields higher molecular weight polymers; however, the molecular weight distribution is broader and lower amounts – as compared to the "classical" coupling processes – of linear and cyclic silane oligomers are also formed.

Acknowledgements. This work has been supported by a grant of the Ministry of Research and Technology (2040 GR/1996). The reaction between DCMPS and K/Na alloy/18-C-6 blue solution was performed in the Institute of Polymer Chemistry of the Polish Academy of Sciences, Zabrze, Poland. We are grateful to Professor Zbigniew Jedlinski for the fellowship offered to V.H. and for his valuable suggestions.

Received, August 20, 1997

Institute of Macromolecular
Chemistry "P.Poni", Jassy
and
** Technical University "Gh.Asachi", Jassy,*
Department of Macromolecules

REFERENCES

1. West R., Miller R.D., Hofer D., J. Polym. Sci., Polym. Lett. Ed., **21**, 283 (1983).
2. West R., J. Organomet. Chem., **300**, 327 (1986).
3. Trefonas III P., West R., J. Polym. Sci., Polym. Lett. Ed., **23**, 469 (1985).
4. Zeigler J.M., Harrah L.A., Johnson A.W., Polym. Prepr., **28**, *1*, 424 (1987).
5. Kim H.K., Matyjaszewski K., Polym. Prepr., **31**, *2*, 278 (1990).
6. Sakamoto K., Obata K., Hirata H., Nakajima M., Sakurai H., J. Am. Chem. Soc., **111**, 7641 (1989).
7. Matyjaszewski K., Chen Y.L., Kim H.K., ACS Symp. Ser., **360**, 78 (1988).
8. Tilley T.D., Radu N.S., Walzer J.F., Woo H.G., Polym. Prepr., **33**, *1*, 1237 (1992).
9. Matyjaszewski K., Polym. Prepr., **30**, *2*, 224 (1989).

10. Zeigler J.M., Polym. Prepr., **27**, *1*, 109 (1986).
11. Kim H.K., Matyjaszewski K., Polym. Prepr., **30**, *2*, 119 (1989).
12. Jones R.G., Webb S.J., Polym. Prepr., **34**, *1*, 280 (1993).
13. Miller R.D., Thompson D., Sooriyakumaran R., Fickes G.N., J. Polym. Sci., Part A, Polym. Chem., **29**, 813 (1991).
14. Worsfold D.J., ACS Symp. Ser., **360**, ch.9 (1988).
15. Miller R.D., Hofer D., Rabolt J., Sooriyakumaran R., Wilson G.G., Fickes G.N., Guillet J.E., Moore J., ACS Symp. Ser., **346**, ch.15 (1987).
16. Jedlinski Z., Sokol M., Pure Appl. Chem., **67**, 587 (1995).
17. Jedlinski Z., Kurcok P., Kowalczuk M., Macromolecules, **18**, 2679 (1985).
18. Matyjaszewski K., Cypryk M., Frey H., Hrkach J.S., Kim H.K., Moeller M., Ruehl K., White M., J. Macromol. Sci. - Chem., **A28**, 1151 (1991).
19. Gauthier S., Worsfold D.J., Macromolecules, **22**, 2213 (1989).
20. Reyx D., NatarioMartins J.M., Campistron I., Noireaux P., Macromol. Chem. Phys., **196**, 915 (1995).
21. Jedlinski Z., Czech A., Janeczek H., Kowalczuk M., J. Am. Chem. Soc., **117**, 8678 (1995).

POLISILANI

1. Reacţia de cuplare a diclormetilfenilsilanului în prezenţa sistemelor metale alcaline/eter coroană

(Rezumat)

Se studiază cuplarea reductivă a diclormetilfenilsilanului în prezenţa sistemelor metale alcaline/eter coroană. Eterii coroană, în speţă 18-C-6, au fost utilizaţi pentru transportul metalului alcalin de la interfaţa solid/lichid în soluţia organică. S-a constatat o influenţă puternică a raportului molar 18-C-6/metal alcalin asupra caracteristicilor polisilanilor rezultaţi.

BULETINUL INSTITUTULUI POLITEHNIC DIN IAŞI
Tomul XLIII (XLVII), Fasc. 3–4, 1997
Secţia II
CHIMIE şi INGINERIE CHIMICĂ

D.C. 547.538.141; 66.095.2

FREE RADICAL POLYMERIZATION OF STYRENE
MODELLING AND SIMULATION

BY

*MIRCEA CONSTANTINESCU,
VICTOR BULACOVSCHI and SILVIA CURTEANU

A model for batch free-radical polymerization of styrene including initiation by thermal decay of an initiator, propagation, chain transfer to monomer, termination by recombination, is proposed. For the high conversion range, the gel and glass effects are also considered. The simulation results are compared with the experimental data. In order to obtain a better agreement between model and experiment, the minimum of the relative differences between the experimental data and those obtained by simulation was sought by manipulating the parameter θ_t^0.

1. Introduction

Free radical polymerization in concentrated systems has been investigated by many researchers for more than four decades. It is known, from the numerous data published in the literature, that the classic kinetics of the free radical polymerization at lower conversions can not be applied over the whole range of conversion for polymerization systems with high concentration. Even under isothermal conditions, most of such systems showed an important acceleration of the polymerization rate and an increase with 20...30% in the molecular weight of the polymer. This autoacceleration, known as the gel effect or Trommsdorf effect, is caused by the drastic decrease in the termination rate due to diffusional constraints. In addition to the gel effect, a glass effect is also exhibited for high monomer conversions. It is the result of the decrease in the propagation rate constant, k_p, as the temperature of the bulk of reaction crosses below its glass transition point, forcing the polymerization to stop before the complete monomer conversion.

The knowledge on polymers diffusion has considerably advanced in the last years. Many researchers have tried to explain the experimental data by taking into account the gel and glass effects in the kinetic models. Many of the models tried to quantify these effects with empirical equations in which the rate constants depend on several parameters of the system such as conversion, temperature, and free volume of reaction [1],...,[3]. In contrast with these models that involve difussional constraints on the rate constants leading to interruption points, Chiu and coworkers [4] developed a simple continuous model starting from a molecular approach. They considered the effect of temperature, concentration, and molecular weight on diffusion. Thanks to its simplicity and its results, the model has become widely accepted, being successfully used for engineering studies requiring simulation, optimization, control and parametric sensitivity. The drawback of the model consists in the numerical values proposed for its parameters. Thus, the correlations suggested by Baillagou and Soong [5], [6], Louie and co-workers [7], Carrat and co-workers [8] and Gupta and co-workers [9] are not in accordance with the experimental data. Gupta and co-workers [10] proposed an optimization technique for the model parameters based on seeking of the minimum square average error between the predictions of the model and the experimental data.

2. Kinetic Model for Styrene Polymerization

The mathematical model for free radical chain growth polymerization of styrene in the presence of an initiator uses the following kinetic diagram:

a) Initiation: $I \xrightarrow{k_d} 2R^*,$

$$R^* + M \xrightarrow{k_i} P_1.$$

b) Propagation: $P_n + M \xrightarrow{k_p} P_{n+1}.$

c) Chain transfer to monomer: $P_n + M \xrightarrow{k_{tm}} D_n + P_1.$

d) Termination by recombination: $P_n + P_m \xrightarrow{k_{tc}} D_{n+m}.$

The initiation consists in the homolitic dissociation of the initiator molecules (I), followed by the addition of the molecules of monomer (M), to the formed radicals (R^*), having as a result the initiating species of the chain (P_1). For high temperatures, the thermal initiation of the monomer might occur, but it is neglected in this study.

The successive addition of the monomer molecules during propagation leads to the development of some long radicals (P_n).

The chain transfer to monomer and termination by recombination lead to the formation of dead polymer chains (D_n).

From the kinetic diagram one can write the balance equations for the monomer conversion (x), for the concentration of the initiator and for the distributions moments of macroradicals (λ_i), and of dead polymer (μ_i), (i=0,1,2):

$$(1) \qquad \frac{\mathrm{d}I}{\mathrm{d}t} = -k_d I + I\frac{\varepsilon(1-x)}{1+\varepsilon x}\lambda_0(k_p + k_{tm}), \qquad (2) \qquad \frac{\mathrm{d}x}{\mathrm{d}t} = \lambda_0(1-x)(k_p + k_{tm}),$$

$$(3) \qquad \frac{\mathrm{d}\lambda_0}{\mathrm{d}t} = 2fk_d I - k_t\lambda_0^2 + \lambda_0^2\frac{\varepsilon(1-x)}{1+\varepsilon x}(k_p + k_{tm}),$$

$$\frac{\mathrm{d}\lambda_1}{\mathrm{d}t} = k_p M_0 \frac{1-x}{1+\varepsilon x}\lambda_0 - k_t \lambda_1 \lambda_0 - k_{tm} M_0 \frac{1-x}{1+\varepsilon x}(\lambda_1 - \lambda_0) + \lambda_0 \lambda_1 \frac{\varepsilon(1-x)}{1+\varepsilon x}(k_p + k_{tm}), \tag{4}$$

$$\frac{\mathrm{d}\lambda_2}{\mathrm{d}t} = k_p M_0 \frac{1-x}{1+\varepsilon x}(2\lambda_1 + \lambda_0) - k_{tc}\lambda_0\lambda_2 - k_{tm}\frac{M_0(1-x)}{1+\varepsilon x}(\lambda_2 - \lambda_0) + \lambda_2 \lambda_0 \frac{\varepsilon(1-x)}{1+\varepsilon x}(k_p + k_{tm}), \tag{5}$$

$$\frac{\mathrm{d}\mu_0}{\mathrm{d}t} = \frac{1}{2}k_{tc}\lambda_0 + k_{tm} M_0 \frac{1-x}{1+\varepsilon x}\lambda_0 + \mu_0 \lambda_0 \frac{\varepsilon(1-x)}{1+\varepsilon x}(k_p + k_{tm}), \tag{6}$$

$$\frac{\mathrm{d}\mu_1}{\mathrm{d}t} = k_{tc}\lambda_0\lambda_1 + k_{tm} M_0 \frac{1-x}{1+\varepsilon x}\lambda_1 + \mu_1 \lambda_0 \frac{\varepsilon(1-x)}{1+\varepsilon x}(k_p + k_{tm}), \tag{7}$$

$$\frac{\mathrm{d}\mu_2}{\mathrm{d}t} = k_{tc}\lambda_0\lambda_2 + k_{tm} M_0 \frac{1-x}{1+\varepsilon x}\lambda_2 + \mu_2 \lambda_0 \frac{\varepsilon(1-x)}{1+\varepsilon x}(k_p + k_{tm}). \tag{8}$$

ε is a parameter which takes into account the variation of the volume during polymerization.

The kinetic equations (1),...,(8) were written assuming that no monomer is consumed for initiation and considering the quasi-steady state approximation (QSSA).

As the polymerization advances, the rate constants k_{tc} and k_p decrease due to difussional constraints. Therefore, the apparent rate constants depend on the physical properties of the system, which determine the rate of diffusion of macroradicals. Chiu and co-workers proposed for these constants the following model:

$$\frac{1}{k_t} = \frac{1}{k_{t0}} + \theta_t(T, I_0)\frac{\lambda_0}{\exp\left[\frac{2.303\Phi_m}{A(T)+B\Phi_m}\right]}, \tag{9}$$

$$\frac{1}{k_p} = \frac{1}{k_{p0}} + \theta_p(T)\frac{\lambda_0}{\exp\left[\frac{2.303\Phi_m}{A(T)+B\Phi_m}\right]}, \tag{10}$$

$$\Phi_m = \frac{1-x}{1+\varepsilon x}, \tag{11}$$

$$\theta_t = \frac{\theta_t^0}{I_0}\exp\left(\frac{E_{\theta t}}{RT}\right), \tag{12}$$

$$\theta_p = \theta_p^0 \exp\left(\frac{E_{\theta p}}{RT}\right), \tag{13}$$

$$A(T) = C_1 - C_2(T - T_{gp})^2, \tag{14}$$

$$k_{tm} = k_{tm0}\frac{k_p}{k_{p0}}. \tag{15}$$

For the rate constant of the chain transfer to monomer a similar decrease to that of the propagation rate constant (eq.(15)) was proposed. The reason was that both reactions involve the same diffusion mechanism, the monomer molecules migrating toward the growing macroradicals.

The numerical values used in the model (s. Table 1), were also used by Duerksen [11], Kim and Choi [12], and also by Brandrup and Immergut [13].

Table 1

Parameters used for Polystyrene

k_d^0=2.67×10^{15} s^{-1} (for initiation with AIBN); k_{p0}^0=1.051×10^4 $m^3/(mol\ s)$;

k_{tc0}^0=1.26×10^6 $m^3/(mol\ s)$; k_{tm0}^0=2.31×10^3 $m^3/(mol\ s)$;

E_d=1.303×10^5 J/mol; E_p=2.958×10^4 J/mol;

E_{tc}=7.04×10^3 J/mol; E_{tm}=5.275×10^4 J/mol;

$B=0.02;\quad T_{gp}=373.16\ \mathrm{K};\quad \varepsilon = \dfrac{-(160.8+0.233T[°\mathrm{C}])}{1084.8-0.685T[°\mathrm{C}]};$

$k_d = k_d^0\exp[-E_d/(RT)];\quad k_{tc0} = k_{tc0}^0\exp[-E_t/(RT)];$

$k_{p0} = k_{p0}^0\exp[-E_p/(RT)];\quad k_{tm0} = k_{tm0}^0\exp[-E_{tm}/(RT)];$

$DP_n = \dfrac{\lambda_1+\mu_1}{\lambda_0+\mu_0};\quad DP_w = \dfrac{\lambda_2+\mu_2}{\lambda_1+\mu_1};\quad Q = \dfrac{DP_w}{DP_n}.$

In this case, for an efficiency factor of the initiator f=0.66 (AIBN), the model predictions were not in accordance with the experimental data, not even for the begining of the polymerization when the gel effect is insignificant. Gupta and co-workers [10] applied an optimization technique for f and, also, for θ_p, θ_t, A, with a view to obtain a better agreement between simulation and Tobolsky's experimental data [14]. Their results are shown in Table 2.

Table 2

Optimal Parameters for Polystyrene

$f = -12.342396 + 9,577.287/T[\mathrm{K}] - 1,743,120.6/T^2[\mathrm{K}];$

$C_1 = 0.091678;\quad C_2 = 1.142\times10^{-5}K^{-2};$

$\theta_p^0 = 7.4053\times10^{-3}\ \mathrm{s};\quad E_{\theta p} = 4.634\times10^4\ \mathrm{J/mol};$

$\theta_t^0 = 1.6886\times10^{-9}\ (\mathrm{mol\ s})/\mathrm{m}^3;\quad E_{\theta t} = 9.5722\times10^4\ \mathrm{J/mol}.$

3. Results and Discussion

Using's software program for solving differential equations of Stiff type, many simulations were made under different temperature conditions and initial concentrations of monomer and initiator. For each simulation a time spell of 0...2,000 min. was considered, and the variable step was computed within the solving alghoritm of the differential equations system.

Three aspects were followed:

1° The validation of the proposed model for polymerization of styrene through its predictions of the temporal conversion and molecular weight profiles under different conditions of simulation, as well as by their comparison with the experimental data.

2° Justification of the choice of kinetic diagram.

3° Manipulation in the model of several adjustable parameters that considers the gel effect, so that its predictions to be closer to the experimental data.

1°. The results obtained by simulation are plotted in Figs. 1,...,6.

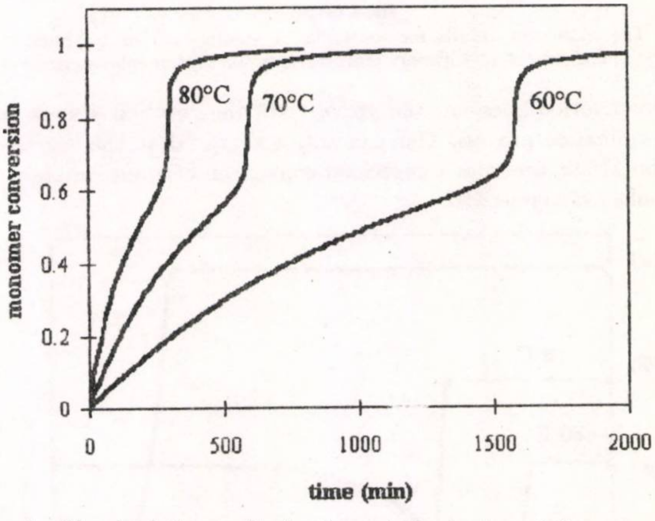

Fig. 1.- The simulation results for the variation in time of the monomer conversion at different temperatures for styrene polymerization.

As shown in Fig. 1, at 70°C the monomer conversion has a dramatic increase, fact specific to a polymerization process accompanied by gel effect (in this case it occurs at about 60%). The reaction is almost completed in 600 min. when the monomer conversion exceeds 95%. According to Fig. 2, for the temperature of 70°C the molecular weight increases of about five times in the same time period.

The temporal variation of the numerical average degree of polymerization, at 70°C, can be seen in Fig. 3. The high values of the degree of polymerization registered at the begining of the reaction are the result of recombination, which is the predominant mechanism of termination.

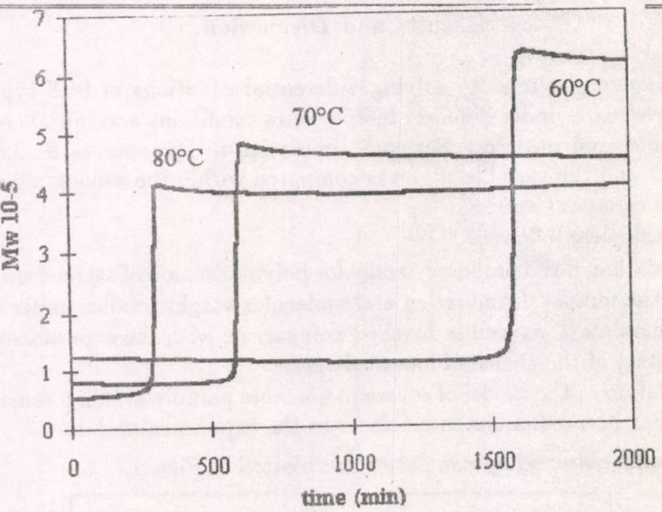

Fig. 2.- The simulation results for the variation in time of the gravimetric average molecular weight at different temperatures for styrene polymerization.

As the polymerization goes on, the viscosity of the reaction system increases hindering the termination process. One can note a sharp fall in the degree of polymerization of about four times, at a monomer conversion of approximately 60%, as soon as the gel effect is manifested.

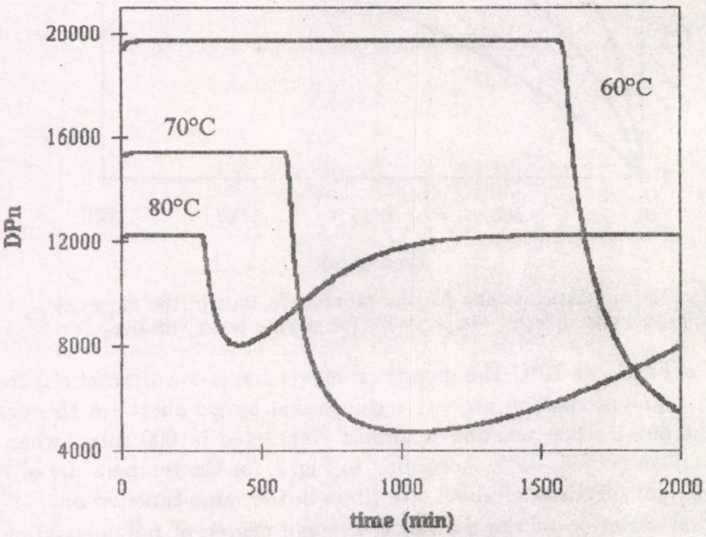

Fig. 3.- The simulation results for the variation in time of the numerical average polymerization degree at different temperatures for styrene polymerization.

The variation of the polydispersity index at 70°C (Fig. 4) is the result of the variation of the numerical average degree of polymerization (Fig. 3) and of the gravimetric average degree of polymerization (it can be inferred from Fig. 2). The degrees of polymerization show a plateau up to 600 min., resulting in constant values of the polydispersity. When the point corresponding to the gel effect that hinders the recombination is reached, the sharp drop in the degree of polymerization is denoted by formation of short chains of different lengths increasing so the polydispersity index.

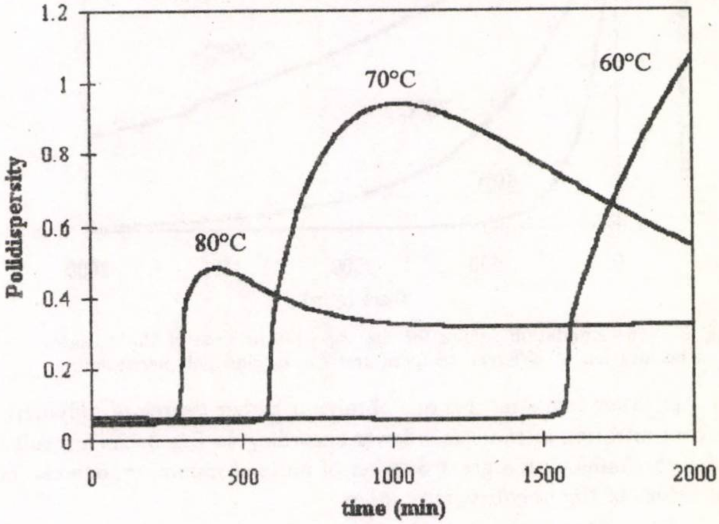

Fig. 4.– The simulation results for the variation in time of the polidispersity index at different temperatures for styrene polymerization.

The curve describing the variation of concentration at 70°C (Fig. 5) shows that in the first 600 min. the initiator is consumed in a proportion of 75%, and after 2,000 min. it is completely consumed.

Finally, as can be seen in Fig. 6 (the curve corresponding to a temperature of 70°C), the rate of the reaction reaches a peak of about 6 mol/(m^3 s).

These statements are also numerically sustained by the date from Table 3. The termination reaction is controlled by diffusion over the whole range of conversion. The decrease in the rate constant, k_{tc}, is relatively slow up to a monomer conversion of about 60%. Beyond this conversion value, k_{tc} swiftly decreases and the k_p also starts to decrease, when the reaction temperature declines below T_{gp} (glass effect). Thus, in a time range of 33,120...36,480 s, the monomer conversion varies from 0.606 to 0.884, k_{tc} decreases from 14,640 to 0.01662 m^3/(mol s), and k_p also decreases from 0.327 to 0.00581 m^3/(mol s).

The curves in Figs. 1,...,6 show the same trend and shape for the different temperatures (60°, 70°, 80°C), whereas the quantitative differences are substantial.

The reduction of temperature delays the autoacceleration. This might be explained by the fact that the viscosity increases directly proportional with a decrease in temperature. Moreover, the lower the temperature the more accentuated the sud-

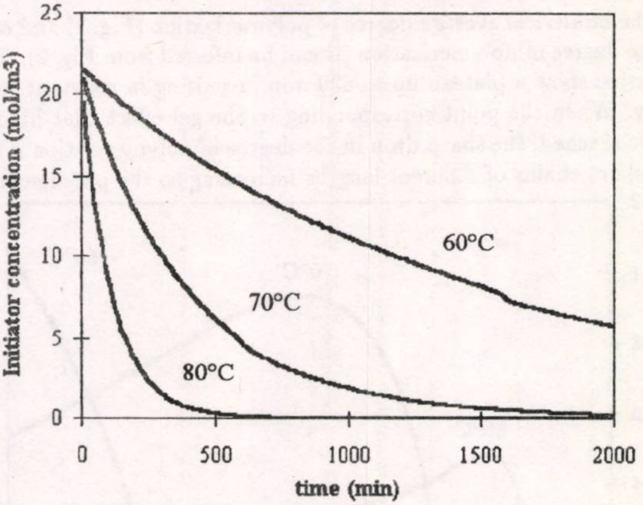

Fig. 5.- The simulation results for the variation in time of the initiator concentration at different temperatures for styrene polymerization.

den increase. At lower temperatures one obtains a higher degree of polymerization because the concentration of radicals is lower according to Fig. 3. As a result of the formation of such chains with a great number of units of monomer, one can note in Fig. 4 higher values of the polydispersity index.

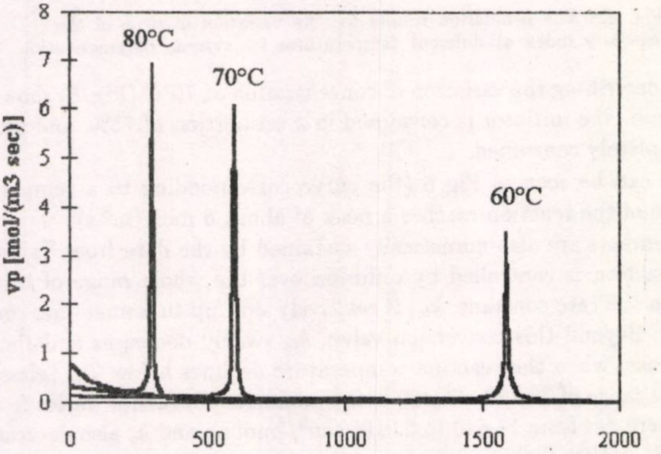

Fig. 6.- The simulation results for the variation in time of the polymerization rate at different temperatures for styrene polymerization.

Finally, Figs. 5 and 6 show that the initiator is faster consumed at higher temperatures and that the maximum value of the reaction rate is higher for higher

Table 3

The Values of the Rate Constants at 70° C and I_0*=21.4 mol/*m^3

Time sec.	x	k_p $m^3/(mol\ s)$	$k_{tm} \times 10^3$ $m^3/(mol\ s)$	k_{tc} $m^3/(mol\ s)$
480	0.017	0.327	0.0212	106,600
12,000	0.31	0.327	0.0212	105,900
15,840	0.38	0.327	0.0212	104,200
19,200	0.43	0.327	0.0212	100,600
25,440	0.51	0.327	0.0212	81,150
27,360	0.53	0.327	0.0212	69,360
30,720	0.57	0.327	0.0212	39,710
32,640	0.60	0.327	0.0212	19,410
33,600	0.62	0.327	0.0212	10,280
34,080	0.63	0.327	0.02119	6,501
34,560	0.64	0.327	0.02119	3,502
35,040	0.66	0.3268	0.02118	1,400
35,520	0.70	0.3259	0.02113	268.4
36,000	0.81	0.1545	0.01	0.8224
36,480	0.88	0.005814	3.76×10^{-4}	0.01662

temperatures.

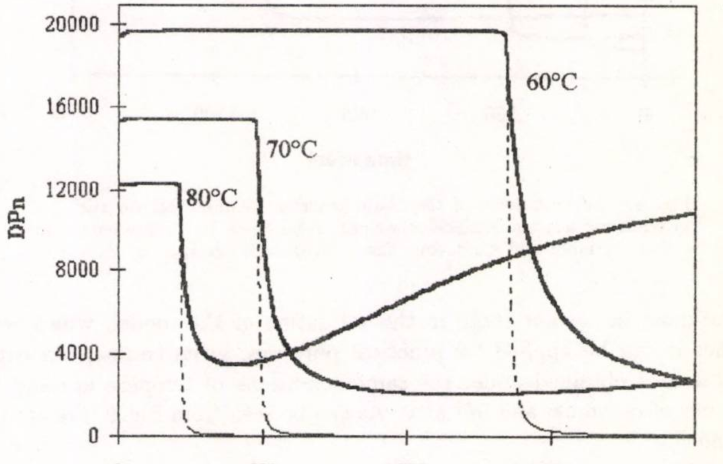

Fig. 7.- The influence of the chain transfer to monomer on the numerical average degree of polymerization; solid line represents k_{tm} variable and dashed line coresponds to k_{tm}=0.

2°. It is compulsory to consider the chain transfer to monomer in the case of the free-radical polymerization of styrene. Figs. 7 and 8 show the influence of the chain transfer to monomer on the degree of polymerization and on the molecular weight at different temperatures. If the chain transfer to monomer were neglected, the decrease in the degree of polymerization specific to the gel effect would be greater than the real one (Fig. 7, the dashed line). The molecular weight would also reach a lower maximum value than that one when the chain transfer to monomer is considered in the kinetic diagram (Fig. 8, the thin line).

The influence of the chain transfer to monomer on the conversion variation is not important.

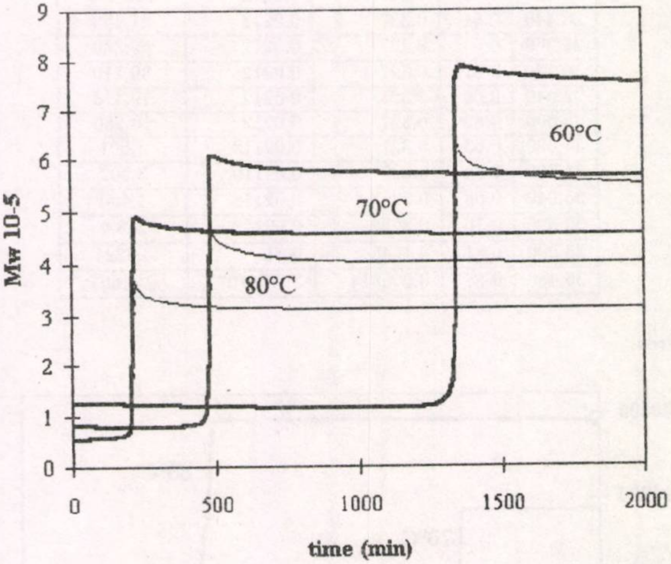

Fig. 8.– The influence of the chain transfer to monomer on the gravimetric average molecular weight; solid thick line represents k_{tm} variable and solid thin line corrresponds to $k_{tm} = 0$.

3°. The most important stage in the validation of the model, which will decide whether it can be applied for practical purposes, is its comparison with the experimental data obtained under the same conditions of temperature and initial concentrations of monomer and initiator. As can be seen from Fig. 9, the agreement is not too good.

In order to obtain a better agreement between the model and experimental data, the minimum of the relative differences between the 26 experimental data and those obtained by simulation at 60°, 70°, 80°C was sought. If we are just changing θ_t^0 from 1.6889×10^{-9} to 0.53598×10^{-8} the model follows fairly well the experimental trend (Fig. 10).

The flexibility of the model is conferred by parameters such as: $C1, C2, \theta_p^0, \theta_t^0, E_{\theta_p}$, E_{θ_t}, or by the coefficients from the dependence of efficiency (f) vs. temperature. These parameters can be modified without restrictions to obtain the best consensus model–experiment.

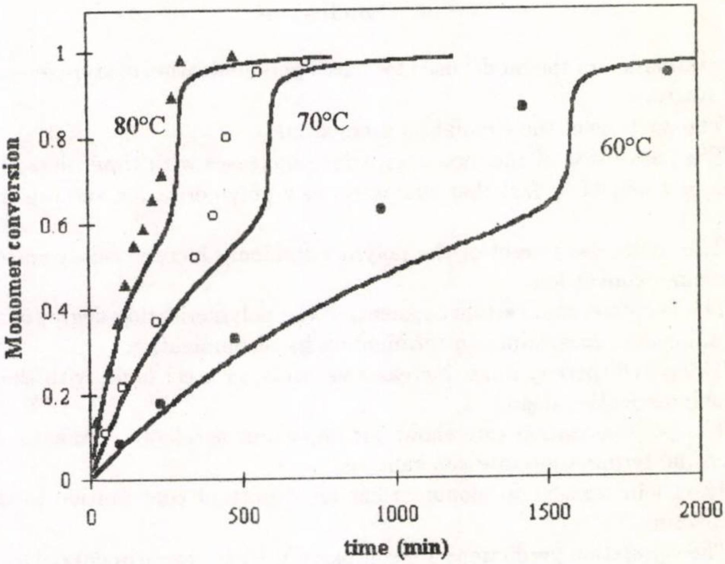

Fig. 9.- Comparison between simulation results (solid line) and experimental data for monomer conversion at different temperatures: 50°C (•), 70°C (○), 90°C (▲).

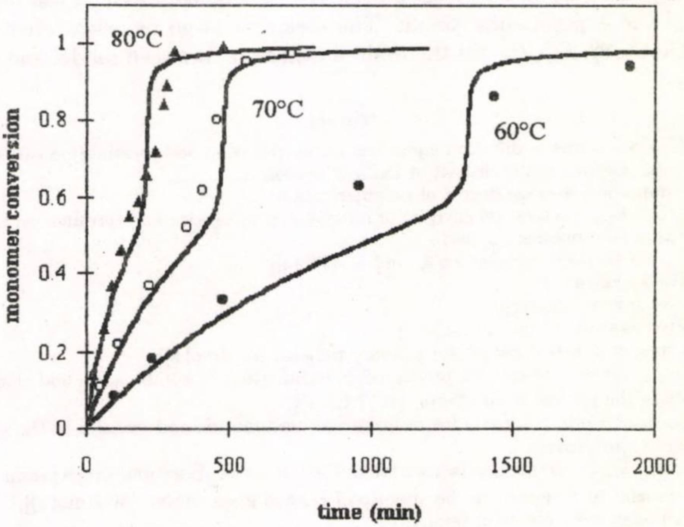

Fig. 10.- Comparison between simulation results (solid line) and experimental data for monomer conversion at different temperatures: 50°C (•), 70°C (○), 90°C (▲) after optimization of parameter θ_t^0.

4. Conclusions

The validation of the model used for batch polymerization of styrene was achieved in two stages:

1. The analysis of the simulation predictions:

a) The conversion of the monomer, which increases with time, showed a sudden increase at about 60%, fact that characterizes a polymerization accompanied by gel effect.

b) The molecular weight of the polymer suddenly increases concomitently with the monomer conversion.

c) The decrease, at a certain moment, in the polymerization degree is attributed to the diffusional constraints on termination by recombination.

d) The polydispersity index increases vs. time, in accordance with the variation of the polymerization degree.

e) The polymerization rate shows an important acceleration thanks to the decrease in the termination rate constant.

f) The chain transfer to monomer has an important contribution to the kinetic of the reaction.

2. The simulation predictions are compared with the experimental data obtained under the same conditions of temperature and initial concentrations. In order to eliminate the unsatisfactory concordance with the experimental data, the optimal values for several parameters that quantify the gel and glass effects in the model were sought. By changing just θ_t^0 from 1.6889×10^{-9} to 0.53598×10^{-8}, the model follows fairly well the experimental trend. The seeking can go on with other parameters such as $C_1, C_2, \theta_p^0, E_{\theta_p}, E_{\theta_t}$ till the desired consensus between model and experiment is achieved.

Notations

A, B, C_1, C_2 – terms in diffusion equations for propagation and termination rate constants;
D_n – dead polymer molecule with n units of monomer;
DP_n – numerical average degree of polymerization;
E_d, E_p, E_{tc}, E_{tm} – activation energies of initiation, propagation and termination by recombination and trasfer to monomer, [J/mol];
$E_{\theta_p}, E_{\theta_t}$ – activation energies for θ_p and θ_t, [J/mol];
f – initiator efficiency;
I – initiator concentration;
k_d – rate constant for initiation, [s^{-1}];
k_i – propagation rate constant for primary radical, [$m^3/(mol\,s)$];
k_p, k_{tc}, k_{tm} – rate constants for propagation, termination by combination and chain transfer in the presence of the gel and glass effects, [$m^3/(mol\,s)$];
k_{p0}, k_{tc0}, k_{tm0} – rate constants for propagation, termination and transfer in the absence of gel and glass effect, [$m^3/(mol\,s)$];
$k_d^0, k_{p0}^0, k_{tc0}^0, k_{tm0}^0$ – frequency factors for rate constant of initiation, propagation, termination and chain transfer to monomer in the absence of gel and glass effects, [$m^3/(mol\,s)$];
M – monomer concentration, [mol/m^3];
M_w – gravimetric average molecular weight;
P_n – macroradical with n units of monomer;
R^* – primary radical;
R – universal gas constant, [J/(mol K)];
Q – polydispersity;

T - temperature, [K];
T_{gp} - glass transition temperature of polymer, [K];
t - time, [s];
v_p - polymerization rate, [mol/(m^3 s)];
x - monomer conversion.

Greek Letters

θ_t, θ_p - characteristic migration times, [s];
θ_t^0, θ_p^0 - pre-exponential factors for θ_t, [(mol s)/m^3] and θ_p, [s];
ε - volume contraction factor;
μ_k - k-th moment of all dead polymer species, [mol/m^3];
Φ_m - volume fraction of monomer;
λ_k - k-th moment of all polymer radicals, [mol/m^3].

Subscripts

0 - inlet value or value in absence of gel and glass effects.

Superscripts

0 - pre-exponential value.

Received, June 9, 1997

* *University "Al.I.Cuza", Jassy,*
Department of Physical Chemistry
and
Technical University "Gh.Asachi", Jassy,
Department of Macromolecules

REFERENCES

1. Cardenas J., O'Driscoll K.F., J. Polym. Sci., Polym. Chem. Ed., **14**, 883 (1976).
2. Früs N., Hamielec A.E., Am. Chem. Soc. Div. Polym. Che., Polym. Prepr., **16**, 192 (1975).
3. Ross R.T., Laurence R.L., AlChESymp. Ser., *160*, 74 (1976).
4. Chiu W.Y., Carratt G.M., Soong D.S., Macromolecules, **16**, 348 (1983).
5. Baillagou P.E., Soong D.S., Chem. Eng. Sci., **40**, 75 (1985).
6. Baillagou P.E., Soong D.S., Chem. Eng. Sci., **40**, 87 (1985).
7. Louie B.M., Carratt G.M., Soong D.S., J. Appl. Polym. Sci., **30**, 3985 (1985).
8. Carratt G.M., Shervin C.R., Soong D.S., Polym. Eng. Sci., **24**, 442 (1984).
9. Kapoor B., Gupta S.K., Varma A., Polym. Eng. Sci., **29**, 1246 (1989).
10. Kumar R.V., Gupta S.K., Polymer, **32**, *17*, 3233 (1991).
11. Duerksen J.H., Hamielec A.E., Hodgins J.W., AIChEJ, **13**, 1081 (1967).
12. Kim K.J., Choi K.Y., Chem. Eng. Sci., **43**, 965 (1988).
13. Brandrup J., Immergut E.H. (Eds.), *Polymer Handbook.* 3rd Ed., J. Wiley, New York, 1989.
14. Tobolsky A.V., J. Am. Chem. Soc., **80**, 5927 (1958); *Ibid.*, **82**, 1277 (1960).

POLIMERIZAREA RADICALĂ A STIRENULUI
Modelare şi simulare

(Rezumat)

Se consideră, pentru polimarizarea radicalică discontinuă a stirenului, un model care include: iniţierea prin descompunerea unui iniţiator, propagarea, transferul de lanţ la monomer, terminarea prin recombinare şi efectele de gel şi vitrifiere pentru domeniul conversiilor mari. Se analizează rezultatele obţinute prin simulare pe model şi se compară cu datele experimentale. Prin minimizarea diferenţelor relative între punctele experimentale şi cele de simulare se modifică valoarea parametrului θ_t^0 realizându-se astfel o apropiere a rezultatelor obţinute prin modelare de cele relevate prin experiment.

BULETINUL INSTITUTULUI POLITEHNIC DIN IAŞI
Tomul XLIII (XLVII), Fasc. 3–4, 1997
Secţia II
CHIMIE şi INGINERIE CHIMICĂ

D.C. 678.746.22; 547.538.141; 547.315.2

ON PARTICLE SIZE DISTRIBUTION OF STYRENE–DIVINYLBENZENE COPOLYMERS PREPARED BY SUSPENSION POLYMERIZATION

BY

Z. BENCHEIKH, B. BELAZOUZ and I. RABIA

Suspension polymerization of styrene–divinylbenzene copolymer was done using a conventional tank reactor with methyl cellulose 1,000 as a suspending agent. The effect of four different stirrer shapes on styrene–divinylbenzene particles was investigated. The finale particle size distribution and uniformity are measured as function of stirring speed and stabilizer concentration. Expressions correlating mean droplet diameter to these parameters are derived.

1. Introduction

In the process of suspension polymerization, a monomer or a mixture of monomers relatively insoluble in water are dispersed as a liquid droplet by continuous agitation in an aqueous phase containing suspending agents. This substance prevents the coalescence of monomer droplets, the adhesion of partially polymerized particles during the course of polymerization and can be a polymer soluble in water or inorganic compounds as water – insoluble powders or precipitates. The polymerization reaction is catalyzed by an initiator soluble in the monomer [1], [2].

The main important issue in suspension polymerization is the control of the uniformity and size distribution of final polymer beads. Several works claimed that particle size is influenced by physical conditions and operating conditions.

In the suspension polymerization process, the particle size of polymers is defined by a balance between break-up and coalescence. The main cause of droplet breakage and coalescence is due to the turbulence produced by energy dissipation induced through the agitation system.

In the stirred tank reactor, coalescence and breakage of the monomer droplets take place in different regions [3]. Coalescence is predominant in the region of circulating flow, where the shearing process is not very strong. Breakage takes place in mostly at the high shear region (breakage region).

According to Park [4], beyond a certain distance from the impeller of about 1/6 impeller diameter, droplet break-up is virtually non-existent.

Different expressions correlating mean droplet diameter to operating conditions were reported by several workers. The most extensive studies were carried out by

Hoff and co-workers [5] and by Hedden [6] for conventional reactor and by Tanaka [7] for circular loop reactor.

The purpose of this investigation is to determine the effect of stirrer shape, stirring speed and concentration of suspending agent on particle size of styrene-divinylbenzene (S-DVB) copolymer beads.

2. Experimental

2.1. Materials

The commercial styrene and divinylbenzene (DVB) (technical grade BDH) monomers were freed from inhibitor with 2N NaOH, washed with distilled water to neutral pH and purified by vacuum distillation before use. Practical-grade DVB had the following chemical composition (measured by gas chromatography): 55.4% DVB isomers, the mainly constituent of the rest was ethylvinylbenzene. The S-DVB copolymer beads were obtained by free radical suspension polymerization. The polymerization process was conducted in a 500 ml spherical bottom reactor. Its diameter is 102 mm. The reaction volume used for the preparation of the copolymer was 250 ml. The reactor was fitted with a mechanical stirrer and a condenser reflex. All reactions were carried out at 80°C for 16 hrs. Benzoyl peroxide (1% by wt in relation to the monomers) was dissolved in the selected S-DVB mixture that was added to the continuous phase. After polymerization, the copolymer beads were washed with water and afterwards with acetone. The beads were Soxhlet extracted with methanol for 16 hrs and dried in vacuum at 60°C for 24 hrs.

2.2. Experimental Conditions

Continuous phase: bi-distilled water.
Stabilizer: methyl cellulose 1,000.
Stabilizer concentration C_T: 0.05...0.8% wt of continuous phase.
Dispersed phase: styrene + divinylbenzene (10%).
Dispersed volume fraction: 0.2.
Stirring speed: 3.3...8.33 s^{-1}.

2.3. Test Method

For sieve analysis the S-DVB beads were subjected to a mechanical wet classification with a constant flow rate of water. The polymer droplets were characterized by Sauter mean particle diameter (d_s).

The viscosity of the aqueous phase was performed using a Cannon-Fenske viscosimeter according to ASTM D 446-74.

3. Results and Discussion

3.1. Effect of Stirrer Geometry

The effect of four different agitator shapes (Fig. 1) on polymer beads was determined. To evaluate visually the effect of stirrer geometry on flow distribution in the

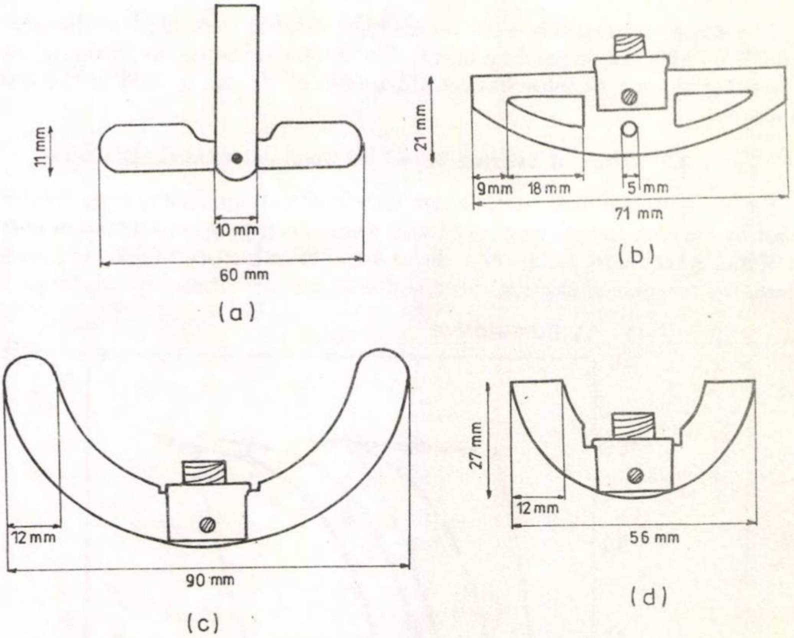

Fig. 1.- Stirrer geometry.

reactor, water (450 ml) was used as an aqueous phase and oil (50 ml) as a dispersed one. The agitator was located 10 mm from the bottom of the reactor.

The dispersion behaviour observed for the oil – water system is summarized as follows. Vortex formation is observed for the four stirrers. A non-uniform distribution of dispersed phase in the whole reactor and for different stirring speed (3.3...11.66 s^{-1}) was observed for agitator (*a*).

The same observations are noticed when agitator (*b*) was used; however, oil agglomeration is reduced at 6.66 s^{-1}.

The dispersion of oil is improved with agitator (*c*), but is mainly located at the top of the stirrer. Agitator (*d*), an anchor shaped form favor a more uniform dispersion in the reactor and agglomeration of dispersed phase was not noticed.

Table 1

Influence of Agitator Geometry on Styrene-Divinylbenzene Copolymer

Agitator	C_T, [% by wt]	ϕ	N_r, [s^{-1}]	Product
d	2	0.25	5	White spherical beads
b	2	0.25	5	White lump
c	1.5	0.25	5	White lump
b	1.5	0.25	5	White lump
b	1.5	0.33	3.33	White lump
a	1.5	0.33	3.33	White lump
d	2	0.25	3.33	White spherical beads
c	2	0.25	3.33	White lump

The same observations were noted when S-DVB were used as dispersed phase and PVA 72,000 as suspending agent. The obtained results are given in Table 1.

Anchor shaped agitator having a diameter of 56 mm is used in the rest of this paper.

3.2. Effect of Stirring Speed on Copolymer Beads Diameter

Fig. 2 shows the final particle size distribution (cumulative mass fraction) measured by varying the stirring speed and using a constant concentration of 0.32% by wt of methyl cellulose 1,000 and a dispersed volume fraction of 0.2. As seen from this figure, the increase of stirring speed shifted the distribution towards large diameter.

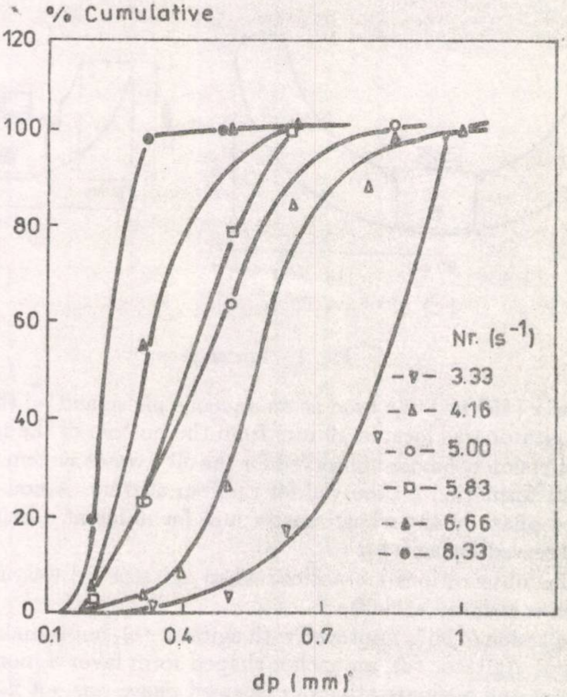

Fig. 2.– Final particle diameter distribution as function of stirring speed.

In suspension polymerization the final particle size is obtained when the rate of coalescence is equal to that of break-up. High stirring speed increases the turbulence of the continuous phase ($\Re e = 13,645...34,115$ according to the corresponding stirring speed) and this leeds to narrow diameters for the monomer droplets.

Fig. 3 illustrates the dependence of the final Sauter mean diameter on stirring speed and can be expressed as follows:

$$\text{(1)} \qquad \text{Ln}\, d_s = \text{Ln}\, A + b_n \text{Ln}\, N_r,$$

where: $A = 3.01 \times 10^{-3}$, $b_n = -1.117$, $3.3 < N_r < 8.33\ \text{s}^{-1}$.

The exponent b_n depends on the type of reactor, agitator and polymerization system. In general, the dependence of mean size on the stirrer speed is reported to be between –0.3 and –3.3. Using basket stirrer, Winslow and co-worker [8] found the value of b_n to be –1.7 for S-DVB suspension polymerization. Tanaka [7], using a circular loop reactor, found the value of b_n equal to –0.6 at $N_r < 30$ s^{-1}.

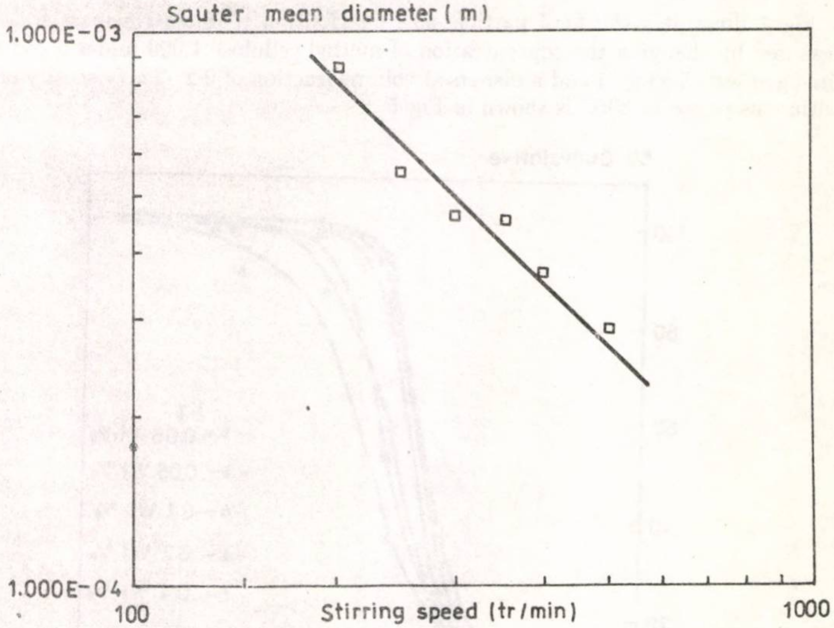

Fig. 3.– Dependence of Sauter mean diameter on stirring speed.

Table 2
Effect of Stirring Speed
on the Relative Distribution Width

N_r, [s^{-1}]	C_T, [% by wt]	ϕ	δ/d
3.33	0.32	0.2	0.43
4.16	0.32	0.2	0.43
5.00	0.32	0.2	0.41
5.30	0.32	0.2	0.40
6.66	0.32	0.2	0.39
8.33	0.32	0.2	0.38

The dispersity coefficient of particle size distribution for different stirring speed is listed in Table 2. The dispersity coefficient is evaluated according to the equation:

$$\frac{\delta}{d_m} = \frac{1}{d_m}\sqrt{\frac{\sum(d_i - d_m)^2}{N-1}}. \tag{2}$$

The smaller the value of the dispersity, the higher the degree of uniformity of final particle diameter.

According to the operating conditions and polymerization system, we found an uniform size distribution to that reported by Tanaka [7] when conventional reactor is used.

3.3. Effect of Stabilizer Concentration

Fig. 4 illustrates the final particle size distribution (cumulative mass fraction) measured by changing the concentration of methyl cellulose 1,000 under a constant stirring speed ($5.83\ \mathrm{s}^{-1}$) and a dispersed volume fraction of 0.2. The viscosity of the continuous phase at 80°C is shown in Fig. 5.

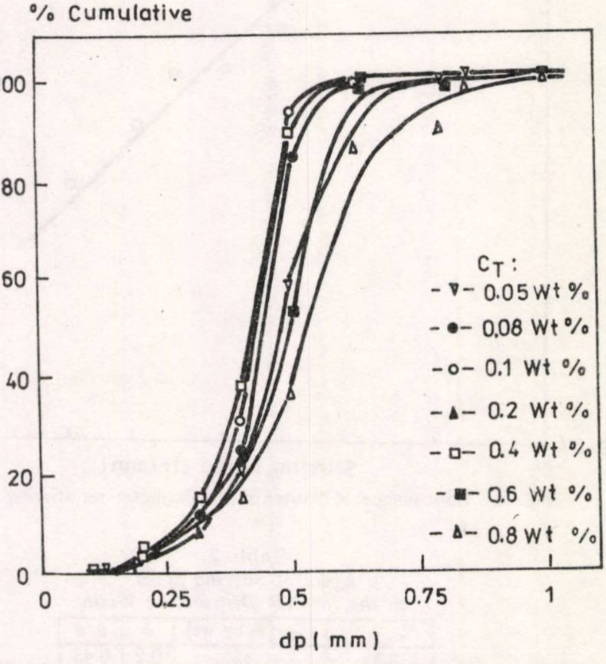

Fig. 4.– Final particle diameter distribution as function of methyl cellulose concentration.

From these figures it can be seen that, for investigated stabilizer concentration, i.e., 0.05...0.8% by wt, a small shift towards large diameter is observed. The small shift can be correlated to the increase in viscosity of continuous phase that reduce the break-up of monomer droplets for high concentration of methyl cellulose.

The effect of stabilizer concentration on Sauter mean diameter is shown in Fig. 6, and can be correlated by equation:

$$\mathrm{Ln}\, d_s = \mathrm{Ln}\, B + c\, \mathrm{Ln}\, C_T, \tag{3}$$

where: $B = 3.82 \times 10^{-4}$, $c = -0.06$, $0.05 < C_T < 0.8\%$ by wt.

The dispersity coefficient remains practically constant under the effect of stabilizer concentration (Table 3).

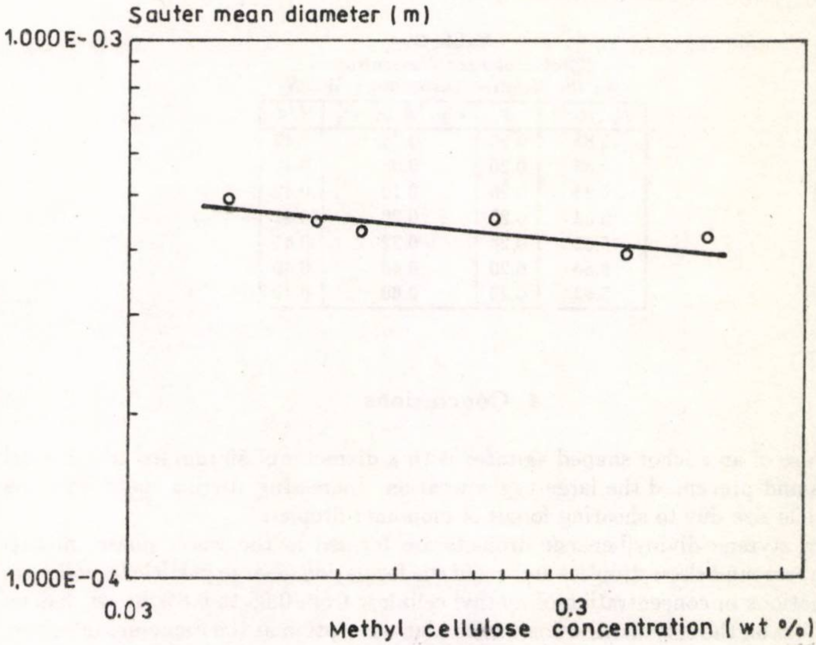

Fig. 5.- Dependence of Sauter mean diameter on methyl cellulose concentration.

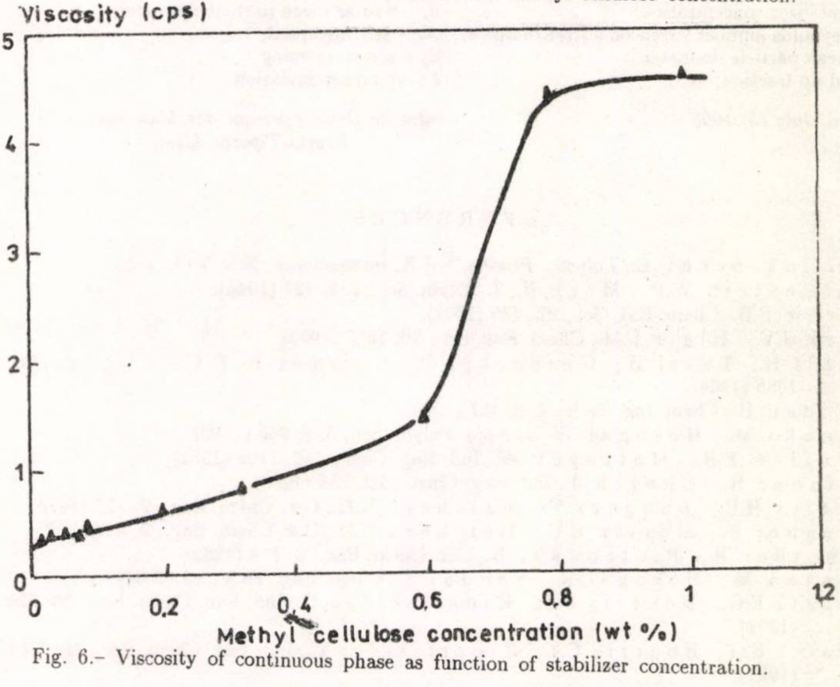

Fig. 6.- Viscosity of continuous phase as function of stabilizer concentration.

Table 3
Effect Stabilizer Concentration on the Relative Distribution Width

N_r, [s^{-1}]	ϕ	C_T, [% by wt]	δ/d
5.83	0.20	0.05	0.42
5.83	0.20	0.08	0.42
5.83	0.20	0.10	0.42
5.83	0.20	0.20	0.42
5.83	0.20	0.32	0.41
5.83	0.20	0.40	0.40
5.83	0.20	0.60	0.42

4. Conclusions

The use of an anchor shaped agitator with a diameter of 56 mm led to spherical particles and prevented the large agglomeration. Increasing stirring speed decrease the particle size due to shearing forces of monomer droplets.

When styrene–divinylbenzene droplets are formed in the water phase, methyl cellulose surround these droplets and avoid the formation of large particle by collision. The variations in concentration of methyl cellulose from 0.05 to 0.8% by wt, has no major effect on the size distribution due to high adsorption at the monomer interface.

Notations

C_T – stabilizer concentration;
$\Re e$ – Reynolds number based on stirrer diameter;
d_m – mean particle diameter;
ϕ – hold up fraction;
d_s – Sauter mean particle diameter;
N_r – stirring speed;
d_p – screen opening;
δ – standard deviation.

Received, July 15, 1996

Centre de Développement des Matériaux/LTP,
Draria-Tipaza, Algeria

REFERENCES

1. Shilidkenecht E., *Polymer Process.* Vol.**X**, Interescience, New York, 1956.
2. Hohenstein W.P., Mark H., J. Polym. Sci., **1**, *2*, 127 (1946).
3. Sprow F.B., Chem. Eng. Sci., **22**, 435 (1967).
4. Park J.Y., Blair L.M., Chem. Eng. Sci., **30**, 1057 (1975).
5. Hopff H., Lussi H., Gespacker P., Hammer H., E. Chem. Ing-Tech., **36**, 1085 (1964).
6. Hedden H., Chem. Ing. Tech., **4**, *2*, 457 (1970).
7. Tanaka M., Hosogai W., J. Appl. Polym. Sci., **3**, *9*, 955 (1990).
8. Winslow F.H., Matreyek W., Ind. Eng. Chem., **43**, 1108 (1951).
9. Shinnar R., Church J., Ind. Eng. Chem., **22**, 253 (1960).
10. Moritz H.U., Langner F., Reichert K.H., Ger. Chem. Eng., **2**, 112 (1979).
11. Langner F., Moritz H.U., Reichert K.H., Ger. Chem. Eng., **2**, 329 (1979).
12. Schorder R., Piotrowski B., Ger. Chem. Eng., **5**, 139 (1982).
13. Tanaka M., Hosogai K., Sendai T., Chem. Eng. Tech., **12** (1989).
14. Chazti E.G., Boutris C.J., Kiparissides C., Ind. Eng. Chem. Res., **30**, 536 (1991).
15. Chatzi E.G., Boutris C.J., Kiparissides C., Ind. Eng. Chem. Res., **30**, 1307 (1991).

DISTRIBUŢIA DIMENSIUNII PARTICULELOR DE COPOLIMERI STIREN-DIVINILBENZEN PREPARAŢI PRIN POLIMERIZARE ÎN SUSPENSIE

(Rezumat)

S-a efectuat polimerizarea în suspensie a sistemului stiren–divinilbenzen folosind un reactor convenţional şi metil celuloză 1000 drept agent de suspendare. S-a investigat efectul a patru tipuri diferite de agitatoare asupra particulelor de stiren–divinilbenzen. Distribuţia finală a mărimii particulelor şi uniformitatea sunt măsurate în funcţie de viteza de agitare şi concentraţia stabilizatorului. S-au dedus expresii ce corelează diametrul mediu al picăturilor cu parametrii de mai sus.

BULETINUL INSTITUTULUI POLITEHNIC DIN IAŞI
Tomul XLIII (XLVII), Fasc. 3–4, 1997
Secţia II
CHIMIE şi INGINERIE CHIMICĂ

C.D. 151-3

LES CRITÈRES DES TECHNIQUES D'INVESTIGATION PSYCHO-SOCIALE

PAR

CARMEN-CĂTĂLINA IOAN

In the context of the present tendency to substitute the traditional methods based on intuitive and subjective elements with the investigative methods and techniques inspired by those used in exact sciences, focused on rigour and objectivity, a brief analysis of the cryteria on which depends the value of a psychosocial inquest technique is presented.

1. L'une des exigences de premier ordre qu'une science doit accomplir pour être reconnue comme telle, c'est de disposer d'un ensemble spécifique de méthodes qui soient capables à pénétrer au delà de la couche superficielle du domaine étudié et arriver au niveau de profondeur, à l'essence des phénomènes abordés. On a dit même, à juste titre, que le progrès scientifique est étroitement lié au perfectionnement des méthodes de recherche.

Dans le domaine des sciences dites positives, comme la physique et la chimie, on utilise depuis longtemps des instruments et des méthodes qui ont pleinement prouvé leur efficacité.

Quant aux sciences sociales ce n'est que depuis peu de temps qu'on a posé d'une façon sérieuse le problème de l'élaboration et du perfectionnement des techniques en vue de collecter des informations, de mesurer et de quantifier les données à l'état brut, de les interpréter, etc.

2. On a cru autrefois que, en ce qui concerne les sciences sociales, l'observation (plus ou moins directe) et le mesurage seraient suffisants. Le psychologue, le sociologue ou bien l'anthropologue se sont basés, il n'y a pas longtemps, sur les rapports des individus concernant leur expérience personelle. A présent, par contre, ces spécialistes considèrent comme decisifs les contacts directs avec les sujets respectifs pour pouvoir examiner, à l'état brut, les attitudes, les perceptions, les intérêts et les aspirations de ceux-ci. Il est toujours vrai que de tels contacts ont constamment caractérisé l'activité des spécialistes du domaine des sciences sociales. Mais le problème important qui se pose aujourd'hui c'est de remplacer les procédés subjectifs et intuitifs traditionnels par des techniques et méthodes d'investigation qui puissent se rapprocher davantage aux méthodes objectives des sciences psycho-chimiques. La condition fondamentale qui s'impose à ces techniques et à ces méthodes c'est de donner la possibilité d'un mesurage scientifique des faits et des phénomènes étudiés.

Ce n'est pas par hasard que les premiers psychologues qui ont utilisé des techniques correspondant à ces exigences avaient initialement travaillé dans le domaine de la physique, de la physiologie ou bien de la chimie [1], ce qui a conduit à des conséquences positives (le transfert massif de la rigueur scientifique dans la méthodologie des sciences sociales), mais aussi à des conséquences négatives (l'excès de quantification, etc.).

3. La valeur d'une technique d'investigation psycho-sociale est établie, en général, selon trois critères à savoir:

a) *Le critère de la validité*, qui exige que le mesurage soit lié par une relation significative, à l'objet investigué, respectivement aux faits et aux phénomènes sociaux qu'on a en vue. Plus exactement, on exige que la technique respective puisse présenter la garantie que son utilisation répond vraiment a ce qu'on se propose de mesurer.

b) *Le critère de la fidelité*, selon lequel toute répétition du même fait du phénomène doit aboutir à des résultats identiques, les variations n'étant admises qu'entre des limites réduites et prévisibles.

c) *Le critère de l'opération*, qui a en vue le caractère spécifique des phénomènes psycho-sociaux, particulièrement leur modification durant l'investigation parce que „l'objet" est dans ce cas toujours „le sujet" et par cela même il peut savoir qu'il est investigué. Une technique d'investigation est opérationnelle si elle peut être appliquée sans déclencher de la part des investigués des comportements et des attitudes qui dénaturent le phénomène poursuivi, en lui imprimant une autre direction que celle „naturelle".

Les deux premiers critères s'appliquent tant aux instruments utilisés pour obtenir des informations, qu'aux techniques liées à l'emploi de ces instruments et à l'interprétation des données. Le deuxième critère a en vue surtout le premier aspect: le protocole de la technique, la manière dont nous utilisons les instruments, l'application de la technique proprement dite, etc.

d) *Le critère de la simplicité et de l'expeditivité.* A la différence des phénomènes qui ont lieu dans la nature, les *phénomènes sociaux* se définissent par une mobilité accentuée et même par leur caractère périssable. Une technique d'investigation, n'importe combien d'efficiente soit elle, si elle s'avère être trop compliquée et si elle nécessite trop de temps pour son application, devient inutilisable pour le simple motif que, au moment de l'obtention des conclusions, le phénomène étudié peut avoir déjà une autre physionomie. Un bon exemple peut nous servir le phénomène du *navéttisme* qui a déclenché il n'y a pas longtemps tant d'investigations psychosociales et qui à présent est en cours de disparition ou, de toute façon, un phénomène marginal, sans importance, ne pouvant plus justifier l'intérêt des psychosociologues.

Reçue le 3 avril 1997

Université Technique „Gh.Asachi", Iassy,
Chaire de Chimie de l'Environnement

BIBLIOGRAPHIE

1. Bartlett F.C., *Remembering - A Study in Experimental and Social Psychology.* London, 1982.

CRITERIILE TEHNICILOR DE ANCHETĂ PSIHOSOCIALĂ

(Rezumat)

In contextul tendinţei actuale de substituire a procedeelor tradiţionale, axate pe elemente intuitive şi subiective, cu tehnici şi metode de investigaţie inspirate de cele folosite in ştiinţele exacte, centrate pe rigoare şi obiectivitate, se prezintă o succintă analiză a criteriilor de care depinde valoarea unei tehnici de anchetă psihosocială.

BULETINUL INSTITUTULUI POLITEHNIC DIN IAŞI
Tomul XLIII (XLVII), Fasc. 3–4, 1997
Secţia II
CHIMIE şi INGINERIE CHIMICĂ

Professor Alexandru Duca at His Eighties

Professor Alexandru Duca was born on October 25, 1917, in Gherla, Someş (Cluj) district, where he attends primary and high school. His first two years of faculty (Chemistry) were in Cluj (1938-1940) and the next years in Timişoara (1940-1942). After graduation he was appointed junior assistant at Inorganic and Analytical Department (professor Raluca Ripan). Between 1943-1947 he is in Reservist Officer School in Galaţi, on the front and prisoner in USSR.

He returns at Inorganic Department at the Faculty of Chemistry in Cluj in November 1947 (professor Raluca Ripan). He is continuing his doctor's degree and obtains it on November 24, 1948. The thesis title was *Contributions to the Study of Periodide Acids Structure and the Corresponding Heteropolycombinations.* The doctor's degree was obtained with the mention "Exceptional".

In 1950 he is appointed lecturer and confirmed by the Superior Diplomas Comission (1956).

Since 1949 he's employed with half norm at the Academy Institute of Chemistry in Cluj.

In 1965 he is transferred at the Polytechnic Institute "Gh.Asachi" in Jassy, the Faculty of Industrial Chemistry, Department of Analytical Chemistry, as professor, head of department. Since 1968 he is "docent doctor" and scientific coordinator for doctor's degree.

With professor Alexandru Duca's arrival in this department, the Analytical Chemistry discipline knew a new development stage. The analytical chemistry courses were systematized and considered thoroughly. Instrumental analyse was introduced; this has an important role in the analytical chemistry courses and in laboratory practical experiments.

He worked in the same department until 1983 when he retired. Since 1983 he is professor emeritus and scientific coordinator for doctor's degree.

In 1970 he was elected member of the Science Academy in New York.

Besides didactical activity (seven lithographed courses (two as singular author and five as a joint author) and joint author at a printed course at the Didactic and Pedagogic Publishing House 1983) he has a large scientific activity (140 published papers, 10 inventor certificates, 24 finalized doctor's degrees; at present he coordinates 5 doctor's degrees, he has many conferences in the country, Bulgaria and Canada, many scientific dissertations, one book in press, *Modified Electrodes Electroanalysis*, by Al. Duca, M. Gaburici and M. Ivănoiu, 500 pages and so on).

His scientific activity can be systematised in the following domains:

1. Contributions to the iso- and hetero-polycombinations class (36 papers; Academy prize in 1966).

2. The separation, concentration and determination of rhenium in molibdenite concentrates (8 papers; the posibility of obtaining rhenium concentrates).

3. The preparation of metallic molibden and amonium molibdate $(NH_4)Mo_7O_{24}$ from Romanian MoS_2 concentrates (2 papers; Academy prize in 1953).

4. The study of some microelements from Transilvanian soil, polarographically and photocolorimetrically (4 papers, colaboration with the Agronomic Institute, Cluj).

5. The determination of small ionic concentrations (simple and complex ions), combinations in B_{12} vitamin family and so on using stripping voltammetry (SV) and stripping titration (6 papers; SV with SME, FME and ME).

6. Analytical contributions in the class of some antibiotics and in B_{12} vitamin family (19 papers, 3 doctor's degrees, 4 inventor certificates).

7. Chemical analyses using kinetic methods (14 papers, one doctor's degree, scientific dissertations and so on).

8. The voltammetry and potentiometry of some polymer conductors (colaboration with the Macromolecules Department, 3 papers, many conferences and scientific dissertations; Academy prize in 1994).

9. Modified electrodes electroanalyse (ME) (4 published papers, 3 papers in press, conferences, scientific dissertations, one book in press).

10. Miscellaneous (conductometry, polarography, separation and concentration by ionic flotation, studies of some catalysators, ion exchange resins, ion exchange membranes, ionic exchange, studies of analytical methods for the technological control of some alcaloids, intermediaries and semisynthesis products used in therapeutics and so on (54 papers, 20 doctor's degrees, 6 inventor certificates).

Professor Alexandru Duca had an important contribution in the teaching and researching sphere of the Romanian analytical chemistry, extending its sphere and contents, from the chemical aspects (volumetry and gravimetry) with specific inorganic character to instrumental analysis and combined methods, automatization and miniaturization, for inorganic and organic substances, polymers and biopolymers.

At present, analytical chemistry gives an increasing attention to the investigation of electrodic surfaces, ISE, analytical sensors, biosensors *in vivo*, ecological and cosmical problems.

Technical University "Gh.Asachi", Jassy,
Department of Analytical Chemistry

BULETINUL INSTITUTULUI POLITEHNIC DIN IAŞI
Tomul XLIII (XLVII), Fasc. 3–4, 1997
Secţia II
CHIMIE şi INGINERIE CHIMICĂ

RECENZII BOOK REVIEWS

ISAC V., ONU A., TUDOREANU C., NEMŢOI GH., *Chimie fizică – Lucrări practice*. Ed. Ştiinţa, Chişinău, Moldova, 1995.

In the chemical literature landscape, the presence of the physical chemistry book is rare enough felt. But, in the last time, at the "Ştiinţa" publishing house, the Republic of Moldova, begined to make one's appearance the efforts of some joint groups of physical chemical investigators, from Chişinău and Iaşi. On this line, one notes the appearance of the book *Physical Chemistry – Practical Works*, having as authors the professors: V. Isac and Ana Onu and the associate professors Cornelia Tudoreanu and Gh. Nemţoi, the first in each group from Chişinău, and the last ones from Iaşi.

The book, based on a large and actual bibliographical information, one constitutes as a guide-book treating the practical experimental methods of research in physical chemistry, the methods which, in fact, are used in the whole investigation of the chemical field.

The book addresses oneself to the disciples in the laboratories, to the teaching staff, to the conductors of industrial chemical processes, to the physicists, to the biologists and to the medical researchers using in the investigations the methods of physical chemistry for solve the own specifically problems.

The structure of the book is made from four big sections, in fact, the most important branches of the physical chemistry, namely: the chemical thermodynamics, the chemical kinetics and the catalysis, the electrochemistry and the colloidal chemistry. Each of the sections, in his turn, is formed from a well balanced structure of the affiliated chapters. The chapter, as an entity, contains a succinct but substantial theoretical treatment of the phenomenon to be pursued, following, after that, the through elaborate details of an appreciable numbers of practical works. In this way one aims at the presentation of an image as complete as possible of the distinct variants in which may be tackled the phenomenon in species. We appreciate the inclusion of some practical works resulting from the own research of the authors, a fact which points out the modernity of the guide-book, realised also by the proposal of the other works as those comprised in the guide-book.

The illustrative presentation of the apparatus, of the auxiliary devices, of the equipment and of the required materials for the practical work facilitate the accomplishing of the carrying out of the research because each of the practical works represents a research on a small scale. The diagrams for the complex chemical processes, as well as the indication of the construction of the graphical behaviour of the phenomena, contributes to the engagement of the thinking of the researcher in clearing up of the pursued process. The use of the literature data necessary for the effectuation of a practical work and the suggestion of the making up of the data tables places the interested person in the situation to economise time in the solving of the investigation. The recommendation of the use of some varied methods in the clarifying of the pursued experimental work stimulate the thinking and the judgement of that who undertakes the research, placing him in the position of obtaining comparable results on different ways.

The addition of the four annexes comes, also, in the support of the facility of the interpretation of the research results.

For those situated between the Prut and the Nistru, the guide-book presents also a benefice, namely that of the correct expression in the Romanian language.

It is obvious that we can assert, without fear to be wrong, that the guide-book *Physical Chem-*

istry – Practical Works (*Chimie fizică – Lucrări practice*) must occupy a well established place in the library or on the desk of each person who bases the own investigations on the physical chemistry methods.

V. Macovei

HAASE B., *Bauteilreinigung – Alternativen zum Einsatz von Halogenkohlenwasserstoffen.* Expert Verlag, Renningen, Germany, 1997, 104 S., ISBN 3-8169-1467-5.

Das Buch: a) liefert eine kurze, verständliche Einführung in die Grundlagen der Oberflächenreinigung; b) diskutiert die Verfahren zur Bestimmung des Reinheitsgrades der Oberfläche und der Oberflächenanalytik; c) erläutert die grundlegenden Unterschiede zwischen Lösenmittelreinigern und wäßrigen Tensidreinigern; d) bietet Handlungsanleitungen für die Neubeschaffung oder den Umbau einer Reinigungsanlage; e) bietet Lösungen für Probleme beim Betrieb einer Reinigungsanlage.

Es wendet sich an alle, die mit der Reinigung von metallischen Oberflächen zu tun haben, insbesondere an: a) die Praktiker an den Reinigungsanlagen; b) diejenigen, die über die Beschaffung einer Reinigungsanlage zu entscheiden oder die Reinigungsmittel auszuwählen haben; c) diejenigen, die in der betrieblichen Praxis für den Erfolg und die Qualität einer Beschichtung oder Wärmebehandlung verantwortlich sind, weil diese Qualität direkt vom Reinigungsergebnis einer vorgeschalteten Bauteilreinigung abhängig ist.

Inhalt: Grundlagen der Reinigung metallischer Oberflächen – Reinheitsanforderungen – Reinigen mit Tensidreinigern – Reinigen mit Kohlenwasserstoff-Lösemitteln – Reinigerauswahl und Anlagentechnik – Trouble-Shooting – Badkontrolle und Badrecycling – Arbeitssicherheit – Arbeitshygiene – Abluft, Abwasser und Abfall – Reinigungsanlagen und Verfahrenstechnik – Rechtliche Grundlagen für Abwasserprobleme in metallbearbeitenden Betrieben.

SCHIK J.P. (Hrs.), *Korrosionsschutz mit wäßrigen Lacksystemen.* Expert Verlag, Renningen, Germany, 1997, 192 S., ISBN 3-8169-1462-4.

Das Buch stellt einen Beitrag zur Gesamtreduzierung von Emissionen dar. Hier geht es um den Ersatz von Lösemitteln durch Wasser.

Eine umfangreiche Zusammenstellung der derzeitigen, ausgereiften wäßrigen Lacksysteme wird angeboten. Sie haben Eingang bei verschiedenen Anwendungen und jetzt immer mehr auf dem Beschichtungssektor und beim Korrosionsschutz gefunden. Vorurteile gegen „Wasser" in diesem Zusammenhang werden abgebaut.

Die Entwicklung der wäßrigen Lacksysteme für den Korrosionsschutz, die Verarbeitung und ihr unterschiedliches Eigenschaftsbild, auch im Vergleich zu konventionellen Lacken, werden ausführlich beschrieben. Einen breiten Rahmen nehmen Hinweise auf die Lackzusammensetzung, Berichte über Praxiserfahrungen und Vorschläge für Problemlösungen ein.

Deutlich kommt heraus, daß die wäßrigen Lacksysteme heute einen hohen technischen Stand erreicht haben.

Inhalt. Die naßchemische Vorbehandlung von Metallen vor der Lackierung – Grundlagen der wäßrigen 2K-Systeme – Wäßrige 1K-Systeme für den Korrosionsschutz – Spezielle Hinweise zu wasserverdünnbaren 2K-Epoxidsystemen für den Korrosionsschutz – Aktive Korrosionsschutzpigmente auf Basis von Phosphaten – Die Eigenschaften von Füllstoffen in wäßrigen Beschichtungssystemen – Einsatz von Lackadditiven in wäßrigen Korrosionsschutz-Systemen – Wasserverdünnbare Beschichtungen für den Korrosionsschutz – Praxiserfahrungen mit wäßrigen 1K- und 2K-Lackierungen im Industriebereich – Applikationstechnik für Wasserlacke.

Data apariției: aprilie 1998, Comanda: 108
Coli tipar: 7,7, Tiraj: 325 exemplare

UNIVERSITATEA TEHNICA „GH. ASACHI"
IASI
TIPOGRAFIA

Str. Lascăr Catargi Nr. 38

ORSZÁGOS MŰSZAKI INFORMÁCIÓS KÖZPONT ÉS KÖNYVTÁR
1883

ISSN 0254-7104